UNIVERSITY OF IOANNINA
SCHOOL OF SCIENCES
DEPARTMENT OF PHYSICS

Predictions in Cosmology and Particle Physics from effective models of String Theory origin

Tavellaris Ilias

Ph.D. Thesis

IOANNINA 2024

ΠΑΝΕΠΙΣΤΗΜΙΟ ΙΩΑΝΝΙΝΩΝ
ΣΧΟΛΗ ΘΕΤΙΚΩΝ ΕΠΙΣΤΗΜΩΝ
ΤΜΗΜΑ ΦΥΣΙΚΗΣ

Προβλέψεις στην Κοσμολογία και Σωματιδιακή φυσική ενεργών προτύπων από την Θεωρία Χορδών

Ταβελλάρης Ηλίας

Διδακτορική διατριβή

ΙΩΑΝΝΙΝΑ 2024

Doctoral Committee

Three-Member Advisory Committee

George Leontaris (Advisor) - Emeritus Professor, Department of Physics, Ioannina U.

Panagiota Kanti - Professor, Department of Physics, Ioannina U.

Leandros Perivolaropoulos - Professor, Department of Physics, Ioannina U.

Seven-Member Ph.D. Examination Committee

George Leontaris (Advisor) - Emeritus Professor, Department of Physics, Ioannina U.

Panagiota Kanti - Professor, Department of Physics, Ioannina U.

Leandros Perivolaropoulos - Professor, Department of Physics, Ioannina U.

Athanasios Dedes - Professor, Department of Physics, Ioannina U.

Ioannis Florakis - Assistant Professor, Department of Physics, Ioannina U.

Ioannis Vergados - Emeritus Professor, Department of Physics, Ioannina U.

Nicholas Vlachos - Emeritus Professor, Department of Physics, Aristotle U. of Thessaloniki

Acknowledgments

I would like to express my deepest gratitude to my supervisor, George Leontaris, for his invaluable guidance, unwavering support, and motivation throughout my academic journey. His mentorship has been instrumental in shaping not only my research but also my personal growth, instilling in me the confidence to pursue my academic aspirations with diligence and passion.

I am also profoundly grateful to my friends and collaborators, Athanasios Karozas and Waqas Ahmed, for their continuous support, insightful discussions, and fruitful collaboration. Working alongside you has enriched this journey and made it all the more rewarding. Our shared experiences have created lasting memories that I will cherish.

A special thank you goes to my friends—both old and new—who have been an integral part of my life during my time in Ioannina and beyond: Diamantis A., Dimitris A., Stelios P., Tasos G., Thodoris N., Manos K., Aggelos L., Lavrentis K., and Thanos K.. Thank you for the countless memories we've created together and the exciting years we shared. Your solidarity and friendship have been a source of joy and strength, making the challenges of this journey more manageable.

I would like to express my heartfelt gratitude to Marina for your unwavering patience and understanding during my ups and downs. Your support has been invaluable, providing me with the strength and encouragement needed to navigate the challenges of this journey. I am deeply appreciative of all that you have done for me.

Finally, to my family, especially my parents, Dimitris and Maria: thank you for your unwavering support, encouragement, and belief in me. Your love and guidance have been my anchor, and without your sacrifices and understanding, none of this would have been possible. You have always been there for me, cheering me on every step of the way.

Ευρωπαϊκή Ένωση
Ευρωπαϊκό Κοινωνικό Ταμείο

Επιχειρησιακό Πρόγραμμα
Ανάπτυξη Ανθρώπινου Δυναμικού,
Εκπαίδευση και Διά Βίου Μάθηση
Ειδική Υπηρεσία Διαχείρισης
Με τη συγχρηματοδότηση της Ελλάδας και της Ευρωπαϊκής Ένωσης

ΕΣΠΑ 2014-2020
ανάπτυξη - εργασία - αλληλεγγύη

Part of the research presented in this doctoral dissertation has been funded by the ESPA 2014-2020 program:
"Grand Unified Models from String Theory: Theoretical Predictions and Modern Particle Physics Experiments" (MIS 5047638 and project code 82634) under the action "Supporting researchers with an emphasis on young researchers – Cycle B'" of the Operational Program "Human Resource Development, Education, and Lifelong Learning."

Μέρος της έρευνας που παρουσιάζεται στην παρούσα διδακτορική διατριβή έχει χρηματοδοτηθεί από το πρόγραμμα ΕΣΠΑ 2014-2020:
"Μεγαλοενοποιημένα Πρότυπα από τη Θεωρία Υπερχορδών: Θεωρητικές προβλέψεις και Σύγχρονα Πειράματα Σωματιδιακής Φυσικής" (MIS 5047638 και κωδικό 82634) της πράξης "Υποστήριξη ερευνητών με έμφαση στους νέους ερευνητές – κύκλος Β΄" του Επιχειρησιακού Προγράμματος "Ανάπτυξη Ανθρώπινου Δυναμικού, Εκπαίδευση και Διά Βίου Μάθηση."

Dedicated to my friends and family
who supported me throughout this journey.
Thank you for everything.

Abstract

This doctoral dissertation's center is on investigating various aspects of particle physics and cosmology, initially through the lens of supersymmetry and subsequently through F-theory. Throughout this study, we construct and analyze various models, aiming to provide solutions to a range of experimental data in both the fields of inflation and particle physics.

Initially, a realistic SO(10) supersymmetric model is constructed within the context of supersymmetry. In this model, fermion families are organized into three 16-plets. Remarkably, this model successfully reproduces the low-energy effective Standard Model and effectively implements inflation. The superpotential, which can undergo renormalization, possesses a $U(1)_{\mathscr{R}}$ symmetry, albeit with violations introduced by non-renormalizable terms. The $SO(10)$ symmetry spontaneously breaks down to the Standard Model through the combined action of $16_H + \overline{16}_H$ and two adjoints $(45_H, 45'_H)$. By utilizing vacuum expectation values from two ten-plets, namely 10_H and $10'_H$, we provide masses upon all fermions, including the right-handed neutrinos, while simultaneously inducing the required CKM mixings. This model also inherently incorporates a doublet-triplets mechanism, preventing the Higgs doublets from acquiring excessive mass. In addition, the model predicts a scalar spectral index and an approximate tensor-to-scalar ratio with agreement to the experimental bounds. The investigation of the reheating process is finally examined, which results in the production of two heavy right-handed neutrinos from the inflaton field's dominant decay, yielding an explanation for the observed baryon asymmetry through non-thermal leptogenesis.

Going beyond supersymmetry, we investigate the cosmological implications of an effective field theory model derived from a configuration of D7 brane stacks within the framework of type-IIB string theory. Our examination revolves around a well-suited geometric arrangement where the Kähler moduli fields are stabilized, and we carefully constrain the parametric space to ensure the existence of a de Sitter vacuum. In addition to the moduli fields, we consider the customary Higgs and matter fields included in the effective field theory. Within this framework, we implement the standard hybrid inflation scenario, featuring a singlet scalar field as the inflaton and utilizing the Higgs states as waterfall fields. The realization of a successful inflationary scenario relies on radiative corrections and soft supersymmetry breaking terms, aligning it with current cosmological data. Notably, our model predicts small tensor-to-scalar ratio values that hold promise for future experimental verification. Furthermore, we subject the model's parameters to additional constraints derived from limitations on dark radiation, quantified as a contribution to the effective number of neutrino species, denoted as N_{eff}. Specifically, our analysis reveals an excess of $\Delta N_{\text{eff}} \leq 0.95$ at a 2σ confidence level, with naturally aligned values for the involved couplings.

We now turn our attention to the phenomenology aspect of F-theory models. We delve into the low-energy implications of F-theory Grand Unified Theory models rooted in an extended $SU(5)$ gauge group, augmented by a non-universal $U(1)'$ symmetry that selectively couples to the three distinct families of quarks and leptons. This gauge group naturally emerges from the maximal exceptional gauge symmetry found within an elliptically fibred internal space, specifically at a single point of enhancement, denoted as $E_8 \supset SU(5) \times SU(5)' \supset SU(5) \times U(1)^4$. Within this framework, we guarantee the presence of rank-one fermion mass textures and a tree-level top quark coupling through the imposition of a Z_2 monodromy group, which effectively identifies two abelian factors within the previously mentioned breaking sequence. The $U(1)'$ factor of the gauge symmetry

seamlessly combines with the three remaining abelian symmetries, left unaltered by Z_2, all without introducing any anomalies. This study yields various classes of models, each distinguished by the $U(1)'$ charges associated with their representations, potentially accommodating extra zero modes in vector-like representations. We conduct in-depth research on these models and evaluate whether their predictions correspond with the results of the Large Hadron Collider (LHC) and other relevant experiments. Additionally, we explore specific scenarios that offer interpretations of the B-meson anomalies observed in experiments such as LHCb and BaBar.

In the final step, we extend our previous work by introducing a vector-like complete fermion family into our models. These extensions are motivated by experimental measurements that reveal deviations from Standard Model predictions. Our analysis is grounded in the framework of $SU(5) \times U(1)'$ Grand Unified Theory, embedded within an E_8 covering group associated with the highest geometric singularity of the elliptic fibration. Within this framework, the $U(1)'$ component emerges as a linear combination of four abelian factors, satisfying the necessary anomaly cancellation conditions. We require universal $U(1)'$ charges for the three chiral families while assigning distinct charges to the fields within the vector-like representations. Under these assumptions, our exploration yields a total of 192 models, categorized into five distinct groups based on their specific GUT properties. We provide representative examples for each category, elucidating the superpotential couplings and fermion mass matrices. Our investigation extends to the low-energy phenomenology of these models, where we delve into predictions related to B-meson anomalies. Additionally, we discuss the role of R-parity violating terms within selected models from this construction.

Περίληψη

Η φυσική είναι ο επιστημονικός κλάδος που δημιουργήθηκε στην προσπάθεια του ανθρώπου να κατανοήσει τον τρόπο με τον οποίο λειτουργεί ο κόσμος. Η πρόοδος που έχει σημειωθεί στο πέρασμα του χρόνου μέχρι και σήμερα είναι τεράστια. Το 1900, ο Max Planck εξετάζοντας την ακτινοβολία μέλανος σώματος προτείνει την έννοια των κβάντων ενέργειας για να περιγράψει τη διακριτή φύση της ενέργειας, κάνοντας το πρώτο βήμα γι αυτό που ονομάζουμε Κβαντική Θεωρία Πεδίου (Quantum Field Theory - QFT). Η διατύπωσή της έγινε στις δεκαετίες του 1930 και 1940 από φυσικούς όπως ο Paul Dirac, ο Wolfgang Pauli και ο Richard Feynman και παρείχε ερμηνεία για τις δυνάμεις που διέπουν τα σωματίδια στον υποατομικό κόσμο.

Από την άλλη πλευρά, λίγο νωρίτερα, το 1915, ο Albert Einstein, δημοσιεύει τη διάσημη πλέον στα χρονικά Γενική Θεωρία της Σχετικότητας. Περιγράφει τους νόμους που διέπουν τον μακρόκοσμο και αποδεικνύει τη σχέση μεταξύ μάζας και καμπυλότητας του χώρου-χρόνου.

Στην πορεία, τις δεκαετίες του 1960 και 1970, διαμορφώνεται το 'Καθιερωμένο Πρότυπο' (Standard Model), ένα σημαντικό επίτευγμα στην προσπάθεια να ενοποιηθούν αλληλεπιδράσεις των υποατομικών σωματιδίων. Η θεωρία αυτή προσέφερε μια θεωρητική βάση για την κβαντομηχανική περιγραφή των σωματιδίων και των αλληλεπιδράσεών τους και μέχρι σήμερα αποτελεί την πιο ακριβή περιγραφή του τρόπου που λειτουργεί ο υποατομικός κόσμος. Ένα σημαντικό παράδειγμα για την επιτυχία της θεωρίας αποτελεί η ανακάλυψη του μποζονίου Higgs το 2012 από τον Μεγάλο Επιταχυντή Αδρονίων (LHC) του CERN, παρέχοντας ερμηνεία για την προέλευση των μαζών των φερμιονίων και το σπάσιμο της Ηλεκτρασθενούς Συμμετρίας.

Το 2015, λαμβάνει χώρα για πρώτη φορά η ανακάλυψη των βαρυντικών κυμάτων, ένα αποτέλεσμα συνεργασίας δύο πειραμάτων LIGO (Laser Interferometer Gravitational-Wave Observatory), τα οποία κατέγραψαν τις πρώτες αποδείξεις βαρυντικών κυμάτων οφειλούμενων στη σύγκρουση δύο μαύρων τρυπών. Οι δύο αυτές θεωρίες για τους νόμους της φύσης τόσο στον μακρόκοσμο όσο και στον μικρόκοσμο, έχουν εμφανίσει τρομερές επιτυχίες, ωστόσο παραμένουν ασυμβίβαστες μεταξύ τους. Η ένωση όλων των δυνάμεων είναι μια διαδικασία που δεν μπορεί να απαντηθεί μέχρι και σήμερα. Παράλληλα, το Καθιερωμένο Πρότυπο αδυνατεί να δώσει εξήγηση σε αρκετά ερωτήματα όπως στην αυξανόμενη διαστολή του σύμπαντος και τη σκοτεινή ενέργεια, στο πρόβλημα της ιεραρχείας των δυνάμεων, δηλαδή την απόσταση μεταξύ των ενεργειακών κλιμάκων που παρατηρείται, και σαν απόρροια την ενοποίηση όλων των δυνάμεων. Ταυτόχρονα, αδυνατεί να δώσει ερμηνεία για την μάζα των νετρίνων τα οποία έχουν παρατηρηθεί και η θεωρία τα αντιμετωπίζει ως άμαζα. Αυτά και άλλα προβλήματα οδήγησαν την επιστημονική κοινότητα στην πρόταση της υπερσυμμετρίας.

Η υπερσυμμετρία (SUSY) είναι ένα μοντέλο που ενώνει τα μποζόνια με τα φερμιόνια σε ζεύγη με τους ίδιους κβαντικούς αριθμούς, προσφέροντας μία δυνατή βάση για τη λύση του προβλήματος της ιεραρχίας. Επίσης, μέσω της θεωρίας αυτής, δημιουργήθηκε η θεωρία υπερβαρύτητας (SUGRA), μια επέκταση της υπερσυμμετρίας, ως ένα υποψήφιο πλαίσιο για την περιγραφή της βαρύτητας. Η ιδέα της υπερσυμμετρίας έδωσε το έναυσμα για τη δημιουργία των Μεγαλο-ενοποιημένων Θεωριών (GUTs), μοντέλων αποτελούμενων από μεγαλύτερες συμμετρίες από αυτή του Καθιερωμένου Προτύπου, έχοντάς το όμως ως υπο-ομάδα μέσα στη συμμετρία αυτή στις χαμηλές ενέργειες.

Αν και η υπερσυμμετρία και η υπερβαρύτητα αποτελούν ελκυστικές ιδέες και προσφέρουν απαντήσεις σε διάφορα θέματα που δεν μπορούσαν να απαντηθούν μέχρι τώρα, η πειραματική απόδειξή τους είναι ένα ανοικτό ζήτημα.

Κάπως έτσι φτάνουμε στη Θεωρία Χορδών η οποία προσφέρει ένα εναλλακτικό πλαίσιο για τη συνολική κατανόηση του σύμπαντος. Πρώτη εμφάνιση του όρου 'χορδή' γίνεται τη δεκαετία του 1970 από τους Yoichiro Nambu, Holger Bech Nielsen, και Leonard Susskind, οι οποίοι παρουσίασαν τις πυρηνικές δυνάμεις ως ταλαντούμενες, μονοδιάστατες χορδές. Σύμφωνα με τη θεωρία αυτή, τα σωματίδια δεν είναι σημεία, αλλά αποτελούνται από χορδές που ταλαντώνονται σε επιπλέον διαστάσεις δημιουργόντας με αυτόν το τρόπο τα παρατηρήσιμα σωματίδια αλλά και τις αλληλεπιδράσεις τους, σύμφωνα με την συχνότητα ταλάντωσης τους. Η θεωρία απαιτεί επιπλέον διαστάσεις πέρα από τις γνωστές τρείς χωρικές και τον χρόνο, κάτι που δημιουργεί πολλές δυνατότητες και προκλήσεις στη μαθηματική ανάλυση. Επιπλέον, στο πλαίσιό της περιλαμβάνει τις μεγαλο-ενοποιημένες Θεωρίες και την υπερσυμμετρία, καθιστώντας την αρκετά ελκυστική ως θεωρία για πάρα πολλούς επιστήμονες.

Η διατριβή αυτή εκπονήθηκε στο πλαίσιο μιας εξερεύνησης του σύμπαντος, τόσο για τον τρόπο που διαστέλλεται (inflation), όσο και για τη φαινομενολογική ερμηνεία πειραματικών δεδομένων υπό το πρίσμα της σωματιδιακής φυσικής μέσω της Θεωρίας Χορδών. Κατά τη διάρκεια αυτής της μελέτης, κατασκευάστηκαν και αναλύθηκαν διάφορα μοντέλα, με στόχο την παροχή λύσεων σε μια σειρά πειραματικών δεδομένων στους τομείς της κοσμολογίας και της φυσικής υποατομικών σωματιδίων.

Αρχικά, κατασκευάστηκε ένα ρεαλιστικό υπερσυμμετρικό μοντέλο SO(10) στο πλαίσιο της υπερσυμμετρίας. Σε αυτό το μοντέλο, οι οικογένειες των φερμιονίων οργανώνονται σε τρεις 16-πλέτες. Αποδεικνύεται ότι το μοντέλο αυτό αναπαράγει με επιτυχία το Καθιερωμένο Πρότυπο (ΚΠ) στις χαμηλές ενέργειες και εφαρμόζει αποτελεσματικά τον πληθωρισμό. Η συμμετρία $SO(10)$ σπάει αυθόρμητα στο ΚΠ μέσω της συνδυαστικής δράσης των $16_H + \overline{16}_H$ και δύο παρακείμενων $(45_H, 45'_H)$. Χρησιμοποιώντας τις αναμενόμενες τιμές του κενού από δύο δεκα-πλέτες, 10_H και $10'_H$, παρέχονται μάζες σε όλα τα φερμιόνια, συμπεριλαμβανομένων των δεξιόχειρων νετρίνων, ενώ ταυτόχρονα εισάγονται οι απαιτούμενες μίξεις για τον πίνακα CKM (Cabibbo-Kobayashi-Maskawa matrix). Το μοντέλο περιλαμβάνει επίσης ένα μηχανισμό doublet-triplet splitting, που αποτρέπει τις διπλέτες του Higgs από το να αποκτήσουν υπερβολική μάζα. Το μοντέλο επιτυγχάνει και στον πληθωρισμό, καθώς οι προβλέψεις του για τα παρατηρούμενα δεδομένα από το Planck είναι μέσα στο εύρος αποδεκτών τιμών. Τέλος, εξετάζεται η διαδικασία της επαναθέρμασης (reheating), όπου η κυρίαρχη αποσύνθεση του πεδίου του πληθωρισμού (inflaton field) παράγει ένα ζεύγος βαρέων δεξιόχειρων νετρίνων, παρέχοντας με αυτήν τη διαδικασία μια εξήγηση για την παρατηρούμενη βαρυόνικη ανισορροπία μέσω της μη-θερμικής λεπτογένεσης.

Η εξερεύνηση στην πορεία επεκτείνεται στη Θεωρία Χορδών, όπου εξετάστηκαν οι κοσμολογικές συνέπειες ενός αποτελεσματικού μοντέλου θεωρίας πεδίου που προκύπτει από μια διάταξη των D7 βρανών (branes) στο πλαίσιο της θεωρίας τύπου-IIB της Θεωριας Χορδών. Η έρευνα περιστρέφεται γύρω από μια κατάλληλη γεωμετρική διάταξη, όπου τα πεδία καταστάσεων (moduli fields) Kähler σταθεροποιούνται και περιορίζεται προσεκτικά ο παραμετρικός χώρος, ώστε να εξασφαλιστεί η ύπαρξη ενός κενού τύπου de Sitter. Εκτός από τα πεδία moduli, λαμβάνονται υπόψη και τα συνηθισμένα πεδία Higgs και ύλης. Μέσα σε αυτό το πλαίσιο, εφαρμόζεται το κανονικό σενάριο υβριδικού πληθωρισμού (standard hybrid inflation), χρησιμοποιώντας ένα βαθμωτό πεδίο υπεύθυνο για τον πληθωρισμό(inflaton) και τις καταστάσεις Higgs ως πεδία καταρράκτες (waterfall fields). Η έρευνα ολοκληρώνεται με την επίτευξη ενός επιτυχημένου σεναρίου πληθωρισμού με τη βοήθεια των radiative corrections, όπως επίσης και μαλακών όρων (soft-tems) σπασίματος της υπερσυμμετρίας.

Η προσοχή μας στρέφεται στη συνέχεια στη φαινομενολογία μοντέλων της Θεωρίας Χορδών, και συγκεκριμένα της F-theory. Εξετάζονται σε αυτό το πλαίσιο οι επιπτώσεις στις χαμηλές ενέργειες των μοντέλων GUT F-theory που βασίζονται στην ομάδα $SU(5)$, επεκταμένη από μία $U(1)'$ (singlet) συμμετρία, η οποία έχει μη καθολική σύζευξη με τις τρείς διαφορετικές οικογένειες των κουάρκ και των λεπτονίων. Αυτή η ομάδα προκύπτει με φυσικό τρόπο από τη μέγιστη συμμετρία βαθμίδας (maximal exeptional gauge group), $E_8 \supset SU(5) \times SU(5)' \supset SU(5) \times U(1)^4$. Επιπρόσθετα με την επιβολή μίας Z_2 μονοδρομίας (monodromy group) επιτυγχάνεται μη διαταρακτικά (tree-level) η σύζευξη για το top quark (top quark coupling). Η μελέτη αυτή καταλήγει σε διάφορα μοντέλα τα οποία κατηγοριοποιούνται βάσει συγκεκριμένων χαρακτηριστικών σε ομάδες και γίνεται ξεχωριστά η ανάλυση τους. Ολοκληρώνοντας, γίνεται μια αναλυτική αξιολόγηση των μοντέλων αυτών για να ελεγθεί έαν οι προβλέψεις τους ανταποκρίνονται στα αποτελέσματα του Large Hadron Collider (LHC) και άλλων σχετικών πειραμάτων. Επιπλέον, διερευνώνται συγκεκριμένα σενάρια που προσφέρουν ερμηνείες για τις ανωμαλίες των B-μεσονίων που παρατηρούνται σε πειράματα όπως το LHCb και το BaBar.

Στο τελικό βήμα της διατριβής, γίνεται επέκταση της προαναφερθείσας εργασίας για την κατασκευή μοντέλων, εισάγοντας μια επιπρόσθετη ολοκληρωμένη οικογένεια φερμιονίων διανυσματικού τύπου(vector-like family) στα μοντέλα αυτά. Αυτές οι επεκτάσεις ενθαρρύνονται από τις πειραματικές μετρήσεις που αποκαλύπτουν αποκλίσεις από τις προβλέψεις του ΚΠ. Η ανάλυση της εργασίας αυτής βασίζεται στο πλαίσιο της μεγαλο-ενοποιημένης θεωρίας $SU(5) \times U(1)'$, ενσωματωμένης στην ομάδα E_8. Εντός αυτού του πλαισίου, η συμμετρία $U(1)'$, αναδύεται ως γραμμικός συνδυασμός τεσσάρων αβελιανών παραγόντων, ικανοποιώντας τις απαραίτητες συνθήκες για την ακύρωση των ανωμαλιών. Στη συνέχεια, καθορίζονται καθολικά φορτία $U(1)'$ για τις τρείς οικογένειες φερμιονίων, ενώ η επιπλέον οικογένεια διανυσματικού τύπου έχει διαφορετικό φορτίο κάτω από αυτή τη συμμετρία. Με αυτές τις υποθέσεις, η έρευνα οδηγεί σε συνολικά 192 μοντέλα, κατηγοριοποιημένα σε πέντε διακριτές κατηγορίες βάσει των ιδιοτήτων τους. Αντιπροσωπευτικά παραδείγματα για κάθε κατηγορία ερευνώνται μαζί με τους αντίστοιχους πίνακες για τις μάζες των φερμιονίων. Η έρευνα ολοκληρώνεται με την εξέταση ξανά της φαινομενολογίας αυτών των μοντέλων σε χαμηλές ενέργειες, όπου διερευνώνται οι προβλέψεις σχετιζόμενες με τις ανωμαλίες των B-μεσονίων από τα πειράματα LHCb και το BaBar.

List of Publications

The primary findings in this thesis are derived from the subsequent peer-reviewed publications, listed in chronological order. The authors are arranged alphabetically following the convention of particle physics.

[1]. *On the LHC signatures of* $SU(5) \times U(1)'$ *F-theory motivated models,*
A. Karozas, G. K. Leontaris, I. Tavellaris and N. D. Vlachos,
Eur. Phys. J. C **81** (2021) no.1, 35

[2]. $SU(5) \times U(1)'$ *Models with a Vector-Like Fermion Family*,
A. Karozas, G. K. Leontaris and I. Tavellaris,
Universe **7** (2021) no.10, 356

[3]. *Flavor and Lepton Universality Violation Phenomena in F-Theory Inspired GUTs,*
A. Karozas, G. K. Leontaris, I. Tavellaris and N. D. Vlachos,
BSM-2021.13

[4]. *Hybrid inflation, reheating and dark radiation in a IIB perturbative moduli stabilization scenario,*
W. Ahmed, A. Karozas, G. K. Leontaris and I. Tavellaris,
JHEP **07** (2024), 282

5. *Inflation with Supersymmetric SO(10)*
A. Karozas, G. K. Leontaris, Q. Shafi and I. Tavellaris,
To appear

Contents

List of Figures

List of Tables

Chapter 1

Expanding the Frontiers: Theories Beyond the Standard Model

In this preliminary chapter, we will lay out the basics of the Standard Model (SM) which is the fundamental theory of particle physics and through the years has been tested extensively, exhibiting exceptional agreement with the experimental observations. We will provide its main attributes and set the need to go beyond to explain unanswered questions. This search will lead us to the incorporation of Grand Unified Theories (GUTs). Our main focus will be on the inflationary era of the universe and how these theories explain the recent experimental data. Finally, we will take it a step forward with the introduction of string theory and more precisely with the introduction of F−Theory, which is a geometric version of type II-B superstring theory. In this scheme, we will illustrate how GUT models can be perceived and study their intriguing properties.

1.1 The beginning: The Standard Model

Over the past decades, the Standard Model of particle physics [5–9] has undergone throw meticulous scrutiny with various experiments and still, this day provides precision and quality descriptions of low-energy particle physics. It encloses the realization of Quantum Field Theory in its theoretical framework and with the combination of quantum mechanics and special relativity provides the properties as well as the interactions of the elementary particles. The SM encompasses all the non−gravitational forces: the Strong, the Weak, and the electromagnetic. So far, no such theory can unify gravity under a gauged quantum field theory framework.

1.1.1 Gauge group and matter fields

The particle content of the SM and its interactions can be described with a set of few straightforward gauge symmetry groups. These are SU(3), SU(2), and U(1), representing strong, weak, and electromagnetic forces, respectively. The basic principle under the gauge symmetries is the invariance of the theory under local transformations which ensures that the physics stays unchanged whenever the fields undergo a transformation. The full gauge symmetry of the SM is the direct product of the described symmetries and has the following form

$$SU(3)_C \times SU(2)_L \times U(1)_Y. \tag{1.1}$$

Name	Field	Particle	SM representation
Gauge Bosons	G^{α}_{μ}	g	G(**8,1,0**)
	$W^{1,2}_{\mu}$,W^{3}_{μ}	$W^{\pm}$,Z^0	W(**1,3,0**)
	B_{μ}	γ	B(**1,1,0**)
Quarks	Q_i	$\binom{u}{d}_L,\binom{c}{s}_L,\binom{t}{b}_L$	Q(**3,2,1/6**)
	u_{R_i}	$u^{\dagger}_R$,$c^{\dagger}_R$,$t^{\dagger}_R$	u^c(**$\overline{3}$,1,-2/3**)
	d_{R_i}	$d^{\dagger}_R$,$s^{\dagger}_R$,$b^{\dagger}_R$	d^c(**$\overline{3}$,1,1/3**)
Leptons	L_i	$\binom{\nu_e}{e}_L,\binom{\nu_\mu}{\mu}_L,\binom{\nu_\tau}{\tau}_L$	L(**1,2,-1/2**)
	l_{R_i}	$e^{\dagger}_R$,$\mu^{\dagger}_R$,$\tau^{\dagger}_R$	e^c(**1,1,1**)
Higgs field	ϕ	H	(**1,2,1/2**)

Table 1.1: Depiction of all the particles under the gauge group $SU(3)_c \times SU(2)_L \times U(1)_Y$ of the SM.

The $SU(3)_C$ gauge group encloses Quantum Chromodynamics (QCD) which is the theory describing the strong force and its interactions. A key ingredient to a theory is the conservation of charge. In QCD, the associated charge is the color charge and comes in three colors: red, green, and blue. The interaction particles mediating this force are the 8 massless gluons (G^{α}) which carry color charge. Quarks also carry color charge so they interact with gluons and this exchange results in the formation of composite particles known as hadrons, such as protons and neutrons.

The unified $SU(2)_L \times U(1)_Y$ gauge symmetry group describes the electroweak force and its mediated by three massless gauge bosons, namely, $W^{1,2,3}$ and one massless gauge boson B correlated with the hypercharge. More analytically, the $SU(2)_L$ is acting with the left-handed fermions and describes the weak isospin interactions, whereas the $U(1)_Y$ regards the weak hypercharge. The $SU(2)_L \times U(1)_Y$ symmetry undergoes spontaneous breaking below the electroweak scale (∼100 GeV), via the Higgs mechanism [10–13], and during this process, the Higgs field acquires a non-zero vacuum expectation value. As a consequence, three of the four gauge bosons ($W^{\pm}$ and Z) acquire mass, while the remaining boson, the photon, remains massless. This leads to the preservation of the unbroken $U(1)_{em}$ symmetry, which is associated with Quantum Electrodynamics.

At the core of the SM are the fermions, the fundamental particles that compose all known matter. There are two separate classes of fermions, quarks, and leptons. Quarks are color triplets and as so they interact with the strong force, whereas leptons, considered to be color singlets, do not interact. Both quarks and leptons have left-handed and right-handed pairs. The left-handed fermions transform as doublets under the $SU(2)_L$ gauge symmetry and interact with the weak force, while, right-handed fermions are singlets under the $SU(2)_L$ and so they don't participate in weak interactions. Neutrinos, the neutral leptons, come only as left-handed in the theory and are considered massless. Another property of fermions is that they come in three copies better known as *generations* or *families*. These generations only differ from each other in their mass with the third generation being the heaviest. In Table (1.1) we present all the particle content of SM where the last column, depicts each field dimensionality under the gauge groups $SU(3)_C$, $SU(2)_L$ and also their hypercharge under $U(1)_Y$, respectively.

1.1.2 Langragian and mass terms

The theory of SM is renormalizable. This means that any divergences occurring in loop diagrams can be removed by introducing counterterms that adjust the theory's parameters. In this way, the theory is finite and can provide consistent predictions in its framework. An important role in the renormalization of the SM is gauge invariance. This property ensures that the theory remains unchanged under the gauge transformations. It is also the property that forbids fermions to obtain mass terms. The solution to this issue is the introduction of Yukawa couplings, where each fermion's mass is directly related to its corresponding Yukawa coupling.

The Lagrangian density encompasses the fundamental interactions and fields of the SM. It incorporates the kinetic terms for the gauge fields, fermions, and scalar fields, as well as the interaction terms such as gauge interactions, Yukawa couplings, and the Higgs potential. Compactly the Lagrangian has the following form :

$$\begin{aligned}
\mathscr{L}_{SM} = & -\frac{1}{4}G^A_{\mu\nu}G^{A\mu\nu} - \frac{1}{4}W^\alpha_{\mu\nu}W^{\alpha\mu\nu} - \frac{1}{4}B_{\mu\nu}B^{\mu\nu} \\
& + i\left(\overline{Q}\not{D}Q + \overline{u}_R\not{D}u_R + \overline{d}_R\not{D}d_R + \overline{L}\not{D}L + \overline{e}_R\not{D}e_R\right) \\
& - \left[\left(\overline{Q}\mathbf{Y_u}u_R\right)\tilde{H} + \left(\overline{Q}\mathbf{Y_d}d_R\right)H + \left(\overline{L}\mathbf{Y_e}e_R\right)H + h.c.\right] \\
& + \left(D_\mu H\right)^\dagger\left(D^\mu H\right) - V(H)
\end{aligned} \tag{1.2}$$

where we have used the Dirac notation $\not{D} = \gamma^\mu D_\mu$ and the conjugate Higgs doublet $\tilde{H} = i\sigma_2 H^*$. Here, the covariant derivative is given by the following formula :

$$D_\mu \equiv \partial_\mu + ig_3 G^A_\mu T^A + ig_2 W^\alpha_\mu S^\alpha + ig_1 Y B_\mu \tag{1.3}$$

where T^A and S^α are the generators of SU(3) and SU(2), respectively, and Y is the hypercharge. The field-strength tensors for the gauge fields are defined as :

$$\begin{aligned}
G^A_{\mu\nu} &= \partial_\mu G^A_\nu - \partial_\nu G^A_\mu - g_3 f^{ABC}G^B_\mu G^C_\nu \ , \\
W^\alpha_{\mu\nu} &= \partial_\mu W^\alpha_\nu - \partial_\nu W^\alpha_\mu - g_2\epsilon^{abc}W^b_\mu W^c_\nu \ , \\
B_{\mu\nu} &= \partial_\mu B_\nu - \partial_\nu B_\mu .
\end{aligned} \tag{1.4}$$

for the SU(3), SU(2) and U(1) respectively. The expression (1.2) consists of four lines. The first line represents the kinetic term for the gauge bosons. The second line corresponds to the kinetic term for the fermionic fields. The third line pertains to the Yukawa sector, which encompasses the interactions between fermions and the Higgs field facilitating the acquisition of masses by the fermions. Lastly, the final line includes the kinetic term of the Higgs boson and additionally, it incorporates the scalar potential of the Higgs field, which is responsible for the spontaneous symmetry breaking.

1.1.3 Higgs Mechanism

The necessity to provide masses to the gauge bosons motivated the introduction of the concept of Spontaneous Symmetry Breaking (SSB). This notion resulted in the development of what is widely

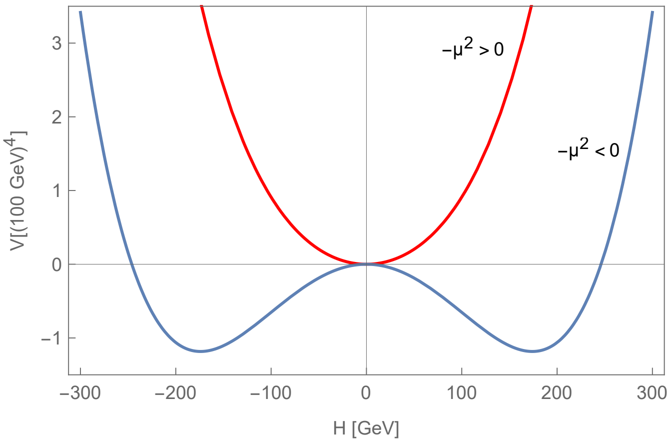

Figure 1.1: Plots of the Higgs potential, as a function of $|H| \equiv \sqrt{H^\dagger H}$, are presented for two cases: $-\mu^2 > 0$ (red line) and $-\mu^2 < 0$ (blue line).

known as the Higgs mechanism. To obtain mass terms in the Lagrangian, the Higgs potential is introduced. This potential is invariant under the $SU(2)_L \times U(1)_Y$ transformations, but its minima, when the Higgs field acquires a non-vanishing vacuum expectation value (VEV), breaks spontaneously the symmetry to the unbroken $U(1)_{em}$. The W and Z bosons, the mediators of the weak force, acquire masses through their interactions with the Higgs field, while the photon, associated with the electromagnetic force, remains massless. The Higgs potential has the following form :

$$V(H) = \mu^2 H^\dagger H + \lambda (H^\dagger H)^2 \tag{1.5}$$

where μ is the mass parameter , and λ is a dimensionless coupling constant. The shape of the potential depends on the signs of these parameters. In the case where λ takes a negative value, the potential energy, denoted as V, becomes unbounded from below. Consequently, the existence of a stable vacuum state is precluded. On the other hand, when both $-\mu^2$ and λ assume positive values, the potential energy function exhibits a minimum at a magnitude of $|H| \equiv \sqrt{H^\dagger H} = 0$, as observed with the red line of Figure (1.1). Within this scenario, the electroweak symmetry remains unbroken within the vacuum state. This is attributed to the fact that performing a gauge transformation on the vacuum state $H = 0$ does not yield any alteration to the vacuum state. Conversely, when $-\mu^2$ is negative and λ is positive, the potential energy function attains a minimum away from $|H| = 0$, as depicted in Figure (1.1) with the blue line. In this particular case, the vacuum state, representing the state of minimum energy, lacks invariance under $SU(2)_L \times U(1)_Y$ transformations. Thus, the gauge symmetry undergoes spontaneous breaking within the vacuum state. The values for the parameters used in these plots are chosen as $|-\mu^2| \approx (88.4GeV)^2$ and $\lambda \approx 0.129$, which were derived from the measured values of $m_h \approx 125$ GeV and $v \approx 246$ GeV. Notably, for the case where $-\mu^2 < 0$ (blue line), the minimum of the potential occurs at $|H| = v/\sqrt{2} = (246/\sqrt{2})$ GeV.

More analytically, in the latter case, the natural component of the Higgs doublet will develop a vacuum expectation value as :

$$\langle H \rangle = \frac{1}{\sqrt{2}} \begin{pmatrix} 0 \\ v \end{pmatrix} \quad , v = \sqrt{\frac{\mu^2}{\lambda}}. \tag{1.6}$$

Expanding now the Higgs field around υ gives :

$$H = \begin{pmatrix} G^+ \\ H^0 \end{pmatrix} = \frac{1}{\sqrt{2}} \begin{pmatrix} G^+ \\ \upsilon + h + iG^0 \end{pmatrix} \tag{1.7}$$

where h is the SM Higgs field and G^+ and G^0 are the Goldstone modes [14–16] which will give masses to the W^+ and Z^0 bosons, respectively. The minimalization of the Higgs potential gives the tree-level relation for the mass of the Higgs field

$$m_h = \upsilon^2 \lambda \tag{1.8}$$

and the interactions of the Higgs field with the massless fields, give the tree-level relations for the masses of the gauge bosons :

$$M_{W^\pm} = \frac{\upsilon g_1}{2} \quad , \quad M_Z = \frac{\upsilon\sqrt{g_1^2 + g_2^2}}{2} \quad , \quad M_A = 0. \tag{1.9}$$

It becomes evident that a disparity exists between the masses of the Z boson and the W gauge bosons. This inequality in the masses of the bosons can be expressed by employing the weak mixing angle (also known as the Weinberg angle). The Weinberg angle can be expressed in terms of the electric charge as :

$$e \equiv g_2 \sin\theta_W = g_1 \cos\theta_W \leftrightarrow \tan\theta_W = \frac{g_1}{g_2} \tag{1.10}$$

In terms of the gauge bosons masses, the Weinberg angle characterizes the relationship between W_μ^3 and B_μ, and the physical mass eigenstates as follows :

$$\cos\theta_W = \frac{M_W}{M_Z}. \tag{1.11}$$

Utilizing the same Higgs doublet, it becomes also possible to generate masses for fermions. This is achieved by incorporating gauge-invariant Yukawa interactions within the framework of $SU(2)_L \times U(1)_Y$. These interactions are established between the Higgs field and the fermions, which can either be singlets or doublets under $SU(2)$. Through the process of spontaneous symmetry breaking of the electroweak symmetry, these Yukawa interactions grant mass terms $m_f^{ij} = Y_f^{ij}\upsilon/\sqrt{2}$ to all fermions, with $f = u, d, e$.[1] These mass terms are 3×3 matrices and consequently, there is mixing between the generations. They can be diagonalized by bi-unitary transformations

$$\begin{aligned} V^{u\dagger} m_u \widetilde{V}^u &= diag\,(m_u, m_c, m_t) \\ V^{d\dagger} m_d \widetilde{V}^d &= diag\,(m_d, m_s, m_b) \\ V^{e\dagger} m_e \widetilde{V}^e &= diag\,(m_e, m_\mu, m_\tau) \end{aligned} \tag{1.12}$$

respecting the property of unitary matrices

$$V \rightarrow V^\dagger V = I.$$

[1]Within the Standard Model (SM) framework, Y_f^{ij} are considered free parameters. Consequently, the model does not impose specific values or constraints on these masses, making it impossible to predict them solely based on theoretical considerations. Instead, we must turn to experimental data to ascertain the actual values of fermion masses, relying on empirical observations to inform our understanding.

Switching from the weak eigenbasis to the mass eigenbasis, one can notice that V^u and V^d are not identical since they are not required to be the same. This discrepancy is confronted with the introduction of the Cabibbo-Kobayashi-Maskawa (CKM) mixing matrix [17–19]

$$V_{CKM} = V^{u\dagger} V_d. \tag{1.13}$$

The CKM matrix is needed to account for the observed flavor mixing and CP (charge conjugation parity symmetry[2] violation in weak decays of quarks. The magnitude of the elements V_{ij} determines the probability of a transition from one quark flavor to another, while the phase of the elements introduces a source of CP violation in the SM. It is often described in terms of three angles and a phase. Initially, we start with a 3×3 complex matrix V, which consists of 9 complex numbers, equivalent to 18 independent real parameters. However, the unitarity condition of V imposes 9 constraints of the form $V^\dagger_{ab} V_{ac} = \delta_{ac}$, effectively reducing the number of independent real parameters to 9. Additionally, we have the freedom to absorb a phase into each left-handed field by redefining $q_L \to e^{i\alpha_{q_L}} q_L$, where q represents either u (up) or d (down) quarks from each of the three generations. This phase absorption allows us to eliminate an arbitrary phase from each row or column of V. However, a common phase redefinition of all the q_L does not affect V, removing only $6 - 1 = 5$ unphysical phases. This leaves us with $9 - 5 = 4$ physically meaningful parameters in V. To understand that these four parameters consist of three angles and a phase, we can observe that a 3×3 real unitary matrix, or an orthogonal matrix, can be described by three independent parameters known as Euler angles. Therefore, since $4 - 3 = 1$, one of the CKM parameters must be a complex phase. This phase is responsible for generating CP violation in the weak interactions of the SM. The standard parametrization of the CKM matrix is as follows:

$$V = \begin{pmatrix} c_{12}c_{13} & s_{12}c_{13} & s_{13}e^{-i\delta} \\ -s_{12}c_{23} - c_{12}s_{23}s_{13}e^{i\delta} & c_{12}c_{23} - s_{12}s_{23}s_{13}e^{i\delta} & s_{23}c_{13} \\ s_{12}s_{23} - c_{12}c_{23}s_{13}e^{i\delta} & -c_{12}s_{23} - s_{12}c_{23}s_{13}e^{i\delta} & c_{23}c_{13} \end{pmatrix} \tag{1.14}$$

where $s_{ij} = \sin\theta_{ij}$ and $c_{ij} = \cos\theta_{ij}$, with θ_{12}, θ_{23}, and θ_{13} representing the three mixing angles, and δ denoting the CP-violating phase. For the lepton sector, there is no equivalent to the CKM matrix since the SM originally treats neutrinos as massless particles. This problem is solved by the introduction of right-handed neutrinos in theories beyond the SM as we will see later.

1.2 Going beyond the Standard Model

The SM has proven to be a remarkable achievement, successfully describing the interactions of elementary particles and their fundamental forces with great precision. However, as our understanding of the universe deepens through groundbreaking experimental discoveries, several critical shortcomings of the SM have emerged. These unresolved phenomena, call for the exploration of physics beyond the SM.

One of the major problems of the theory lies in neutrino physics. While the SM initially considered neutrinos as massless particles, extensive experimental evidence has established that neutrinos possess non-zero masses. As discussed earlier, incorporating neutrino masses by introducing right-handed neutrino fields v_i^c has become imperative to reconcile the theoretical predictions to agree

[2]Charge conjugation parity symmetry states that the laws of physics should remain the same if a particle is interchanged with its antiparticle, while spatial coordinates are inverted (”mirror” or P-symmetry).

with experimental observations. Nevertheless, the SM fails to explain their masses' origin and the intriguing phenomenon of neutrino oscillations [20–26]. These problems can be addressed by the introduction of the Pontecorvo-Maki-Nakagawa-Sakata (PMNS) matrix [27], an equivalent to the CKM matrix, which describes the mixing between neutrino flavor eigenstates $(\nu_e, \nu_\mu, \nu_\tau)$ and the mass eigenstates (ν_1, ν_2, ν_3), as follows:

$$\begin{bmatrix} \nu_e \\ \nu_\mu \\ \nu_\tau \end{bmatrix} = U_{PMNS} \begin{bmatrix} \nu_1 \\ \nu_2 \\ \nu_3 \end{bmatrix} . \tag{1.15}$$

The PMNS matrix is parametrized by three mixing angles (θ_{12}, θ_{13}, θ_{23}) and a CP-violating phase (δ) that are responsible for neutrino oscillations and CP violation. In addition to these parameters, the matrix also includes two Majorana phases (α_1,α_2) when considering Majorana neutrinos[3]. A representation of the matrix is given as follows :

$$U_{\mathrm{PMNS}} = \begin{pmatrix} c_{12}c_{13} & s_{12}c_{13} & s_{13}e^{-i\delta} \\ -s_{12}c_{23} - c_{12}s_{23}s_{13}e^{i\delta} & c_{12}c_{23} - s_{12}s_{23}s_{13}e^{i\delta} & s_{23}c_{13} \\ s_{12}s_{23} - c_{12}c_{23}s_{13}e^{i\delta} & -c_{12}s_{23} - s_{12}c_{23}s_{13}e^{i\delta} & c_{23}c_{13} \end{pmatrix} \begin{pmatrix} e^{i\alpha_1/2} & 0 & 0 \\ 0 & e^{i\alpha_2/2} & 0 \\ 0 & 0 & 1 \end{pmatrix} . \tag{1.16}$$

where the mixing angles $\theta_{ij} \in [0, \frac{\pi}{2}]$, $c_{ij} = \cos\theta_{ij}$,$s_{ij} = \sin\theta_{ij}$, and $\delta \in [0, 2\pi]$, known as the Dirac CP violation phase. The matrix includes two Majorana CP violation (CPV) phases α_1 and α_2. These Majorana phases are represented as a separate diagonal matrix and play a crucial role in understanding the nature of neutrinos as Majorana particles and the violation of lepton number conservation. However, it is essential to note that the Majorana phases do not affect the observable neutrino oscillation phenomena, as they only contribute to the overall phases of the neutrino mass eigenstates. As a result, their values are not directly measurable through neutrino oscillation experiments, and their inclusion in the PMNS matrix emphasizes their theoretical significance rather than their experimental observability.

When constructing a model to describe neutrinos, the key parameters that we focus on are the neutrino masses (m_1, m_2, m_3), the neutrino mixing angles (θ_{12}, θ_{13}, θ_{23}), and the CP-violating phase δ. These parameters are obtained by a global fit of neutrino oscillations and are depicted in Table 1.2. The Table displays two distinct orderings of the neutrino mass eigenstates, termed "normal hierarchy" and "inverted hierarchy," which are determined by the mass differences Δm^2_{21} and Δm^2_{31}. These orderings arise due to the absence of direct measurements for the absolute masses of the three neutrino mass eigenstates through neutrino oscillation experiments. For the case of normal hierarchy, we have $\Delta m^2_{21} > 0$ and $\Delta m^2_{31} > 0$, indicating the ordering $m_1 < m_2 < m_3$. Conversely, for inverted hierarchy, we observe $\Delta m^2_{21} > 0$ and $\Delta m^2_{31} < 0$, corresponding to the mass ordering $m_3 < m_1 < m_2$.

Neutrino masses have emerged as a pivotal subject of investigation also in cosmology, and are recognized to possess masses in the eV range. According to the latest Planck data [29], the bound for the neutrino masses is given by :

$$\sum_i m_i < 0.12 \text{ eV} \tag{1.17}$$

[3]Majorana particles are a type of elementary particle that are their own antiparticles. A Majorana particle is identical to its antiparticle in all respects, including mass, electric charge, and other quantum numbers.

Parameter	Normal Ordering (Best Fit)		Inverted Ordering ($\Delta\chi^2 = 2.7$)	
	BFP $\pm 1\sigma$	3σ Range	BFP $\pm 1\sigma$	3σ Range
$\sin^2\theta_{12}$	$0.304^{+0.013}_{-0.012}$	$0.269 \rightarrow 0.343$	$0.304^{+0.013}_{-0.012}$	$0.269 \rightarrow 0.343$
θ_{12} $(^\circ)$	$33.44^{+0.78}_{-0.75}$	$31.27 \rightarrow 35.86$	$33.45^{+0.78}_{-0.75}$	$31.27 \rightarrow 35.87$
$\sin^2\theta_{23}$	$0.570^{+0.018}_{-0.024}$	$0.407 \rightarrow 0.618$	$0.575^{+0.017}_{-0.021}$	$0.411 \rightarrow 0.621$
θ_{23} $(^\circ)$	$49.0^{+1.1}_{-1.4}$	$39.6 \rightarrow 51.8$	$49.3^{+1.0}_{-1.2}$	$39.9 \rightarrow 52.0$
$\sin^2\theta_{13}$	$0.02221^{+0.00068}_{-0.00062}$	$0.02034 \rightarrow 0.02430$	$0.02240^{+0.00062}_{-0.00062}$	$0.02053 \rightarrow 0.02436$
θ_{13} $(^\circ)$	$8.57^{+0.13}_{-0.12}$	$8.20 \rightarrow 8.97$	$8.61^{+0.12}_{-0.12}$	$8.24 \rightarrow 8.98$
δ_{CP} $(^\circ)$	195^{+51}_{-25}	$107 \rightarrow 403$	286^{+27}_{-32}	$192 \rightarrow 360$
$\Delta m^2_{21} \times 10^{-5}\,\mathrm{eV}^2$	$7.42^{+0.21}_{-0.20}$	$6.82 \rightarrow 8.04$	$7.42^{+0.21}_{-0.20}$	$6.82 \rightarrow 8.04$
$\Delta m^2_{3l} \times 10^{-3}\,\mathrm{eV}^2$	$+2.514^{+0.028}_{-0.027}$	$+2.431 \rightarrow +2.598$	$-2.497^{+0.028}_{-0.028}$	$-2.583 \rightarrow -2.412$

Table 1.2: Best-fit values and allowed ranges of neutrino oscillation parameters obtained from a global fit of current neutrino oscillation data [28]. The table displays the differences in squared masses, denoted as $\Delta m^2_{ij} = m^2_i - m^2_j$, for different neutrino mass eigenstates i and j, for two potential mass hierarchies: normal hierarchy ($m_1 < m_2 < m_3$) and inverted hierarchy ($m_3 < m_1 < m_2$).

exerting considerable influence on the power spectrum of large-scale structures in the universe, and the perturbations observed in the cosmic microwave background (CMB). The CMB, which provides crucial insights into the early universe, can be notably altered by the presence of massive neutrinos. Similarly, the distribution of matter in the cosmos, as captured by the power spectrum of large-scale structures, is intricately intertwined with neutrino masses. Through the incorporation of right-handed neutrinos ν_R into the particle spectrum, we open up the potential for two distinct neutrino mass terms within the system:

$$\mathscr{L} = m_D \bar{\nu}_L \nu_R + M_R \bar{\nu}_R \nu_R^c + \text{h.c.} \tag{1.18}$$

Here, the matrices m_D and M_R are of size 3×3, representing the possible mixing and mass terms, respectively. The first term in the Lagrangian emerges from the conventional Dirac-type coupling, involving the left-handed and right-handed neutrino fields. In contrast, the second term embodies the Majorana mass contribution, taking into account the right-handed neutrinos' inherent Majorana nature. Note that the Yukawa couplings required to generate neutrino masses are exceptionally small. For instance, for a neutrino mass $m_\nu \approx 0.1$ eV, the corresponding neutrino Yukawa coupling would be approximately $y_\nu \approx 4 \times 10^{-13}$. The other possibility is that neutrinos have a Majorana mass. We can construct a Majorana mass for the neutrinos due to their electrically neutral nature, which ensures that this term does not violate electric charge conservation. However, such a mass term is not gauge invariant under $SU(2)_L \times U(1)_Y$. We can generate it after electroweak symmetry breaking by introducing a term involving the Higgs field:

$$\mathscr{L}_{\text{Majorana}} = \lambda_\nu^{ij} \frac{(L_i \bar{H})(\bar{H} L_j)}{\Lambda}, \tag{1.19}$$

where Λ indicates the cutoff scale beyond which a more comprehensive theory must reveal itself, and λ_ν^{ij} are constant couplings coefficients. The dimensionality of the field operator in the numerator

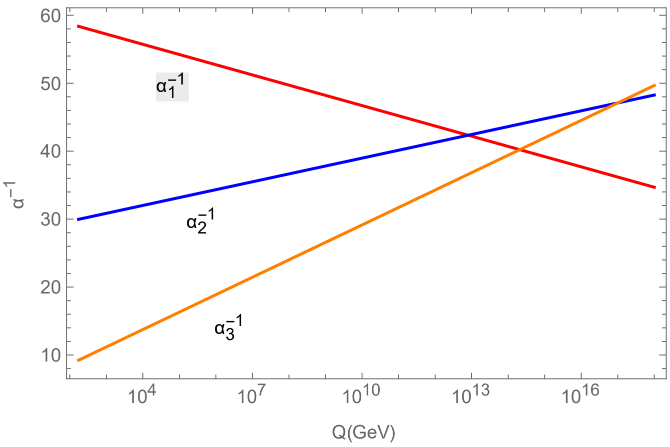

Figure 1.2: Examination of the one-loop level running of the inverse gauge couplings $1/\alpha(Q)$ in the context of the SM. The input scale Q_0 is set at $m_{top} \approx 173.4$ GeV and the gauge couplings are initially defined at this energy scale.

of eq.(1.19) is recognized to be 5, making it a nonrenormalizable interaction with a coefficient of $1/\Lambda$. At tree level, one can introduce such a term through what is known as the see-saw mechanism [30–32]. The Type-I seesaw mechanism introduces right-handed neutrinos (ν_R), also known as sterile neutrinos, to the SM. These right-handed neutrinos are singlets under the SM gauge group and do not participate in the usual weak interactions. In other words, they only interact through gravity and do not have a left-handed counterpart. The neutrino masses are obtained by diagonalizing the combined mass matrix, which is the sum of the Dirac and Majorana mass terms:

$$M_\nu = \begin{pmatrix} 0 & m_D \\ m_D^T & M_R \end{pmatrix} \tag{1.20}$$

Diagonalizing M_ν, leads to three light-mass eigenstates, corresponding to the observed neutrinos, and three heavy-mass eigenstates, corresponding to the right-handed neutrinos. The light neutrino masses are then suppressed by the inverse of the heavy neutrino masses, through the relation:

$$m_\nu \approx -m_D \frac{1}{M_R} m_D^T, \tag{1.21}$$

where M_R is a high scale referred to new physics, resulting in small neutrino masses that are consistent with experimental observations.

Additionally, the concept of dark matter poses another significant challenge to SM [33–40]. Experimental data suggest that dark matter constitutes a substantial portion of the universe's mass but eludes detection through electromagnetic interactions. One can conclude its existence from gravitational effects, yet it remains undetectable within the SM framework. Understanding the nature of dark matter is crucial in realizing the mechanisms of the universe and requires exploring physics beyond the SM to account for this unknown form of matter.

Moreover, SM does not incorporate the force of gravity, described by Einstein's General Theory of Relativity in the early 90's. The inability to incorporate gravity with the other forces leaves a significant gap in the theory, necessitating the exploration of new theoretical frameworks that incorporate these phenomena and surpass current limitations. Efforts to unify the electromagnetic, weak, and strong forces into a grand unified theory, addressing the unification of gauge couplings, have not been successful within the SM, as shown in Figure 1.2. Modifications are needed to obtain a theory in which the gauge couplings are unified around the GUT scale ($M_{GUT} \sim 10^{16}$ GeV). Moreover, the SM's description of CP violation leaves unanswered the mystery of why the universe contains more matter than antimatter without fine-tuning, known as the baryon asymmetry problem or "Strong CP problem" [35, 41–43].

The hierarchy problem [44–46] raises questions about the vast difference between the Planck scale M_P, which characterizes gravity, and the electroweak scale M_W, which relates to the Higgs boson mass. In particular, the mass of the Higgs boson lacks protection from any inherent symmetry, making it vulnerable to radiative corrections that can drive its value toward high-energy scales. The flavor problem [42, 47–49], on the other hand, pertains to the hierarchy of fermion masses and the observed pattern of flavor mixing within the quark and lepton sectors. Despite the SM's ability to accurately predict the masses of these elementary particles, the underlying reasons for the vast differences in their masses remain unsolved. Furthermore, the SM fails to explain the observed flavor-mixing phenomenon, where quarks and leptons change from one type to another through weak interactions.

Charge quantization [50–52] is a fundamental problem in the context of the SM. The theory describes the electromagnetic interactions through the U(1) gauge symmetry, which is associated with the electromagnetic force mediated by photons. According to the SM, particles interact via their electric charges, and these charges are believed to be quantized, meaning they come in discrete units. The charge quantization problem arises because the SM does not provide a theoretical explanation for why all observed elementary particles have electric charges that are quantized in specific integer or fractional multiples of the elementary charge (e). In the SM, the electric charge (Q) is related to the U(1) gauge coupling constant (g) through the formula $Q = n \cdot e$, where n is an integer or fractional number. This equation implies that all charged particles must have electric charges that are integer or fractional multiples of e. While the SM's charge quantization is consistent with experimental observations, its underlying theoretical origin remains unexplained within the framework of the theory. To address this issue, we must seek a more fundamental theory beyond the SM, such as Grand Unified Theories (GUTs) or theories that incorporate supersymmetry.

Finally, cosmic inflation, a rapid expansion phase that shaped the early universe, lacks an explanation within the confines of the SM in which the cosmological constant, responsible for the rapid expansion of the universe, is predicted to be way off the experimental data, known as the "cosmological constant problem" [53–55]. The aforementioned issues and the quest to comprehend the universe on a deeper level motivated physicists and researchers to explore physics beyond the SM.

This exploration encompasses diverse theoretical frameworks, including supersymmetry, Grand Unified Theories (GUTs), and string theory. Advancements in experimental technologies also play a crucial role in probing particles' unknown interactions and behaviors, providing critical insights into phenomena that elude the SM's description. Such insights, guide the development of new theories, aimed at adapting and offering natural explanations for these enigmatic phenomena.

1.3 Supersymmetry

Supersymmetry, known as SUSY [56–65], presents a captivating concept in theoretical physics, although it lacks substantial empirical evidence. Symmetry in physical systems finds representation through specific operators. Within this context, the supercharge operator, represented by $\mathcal{Q}$, takes on the essential role of transforming bosons into fermions and vice versa when it acts upon a state as demonstrated below:

$$\mathcal{Q}|boson\rangle = |fermion\rangle, \quad \mathcal{Q}|fermion\rangle = |boson\rangle. \tag{1.22}$$

This fundamental principle implies the existence of superpartners for each known particle, sharing identical quantum numbers except for a half-unit difference in spin. Crucially, within the framework of SUSY, superpartners are endowed with identical mass, momentum, electric charge, color charge, and weak isospin as their corresponding ordinary particles. However, they distinguish themselves by their spin and the latest defined quantum characteristic known as R-parity [66–69], denoted by:

$$R = (-1)^{3(B-L)+2S} \tag{1.23}$$

Moreover, SUSY stands as a fundamental prediction of String Theory. From a phenomenological standpoint, SUSY elegantly addresses the hierarchy problem under specific conditions and predicts gauge coupling unification. Furthermore, the expanded spectrum of SUSY models offers potential candidates for dark matter. The generators $\mathcal{Q}$ hold a pivotal role in the mathematical foundation of this remarkable symmetry.

The supersymmetric algebra can be expressed through anticommutators of the supercharges, as follows:

$$\begin{aligned} &\{Q_\alpha, \bar{Q}_{\dot{\beta}}\} = 2\sigma^\mu_{\alpha\dot{\beta}} P_\mu, \\ &\{Q_\alpha, Q_\beta\} = \{\bar{Q}_{\dot{\beta}}, \bar{Q}_{\dot{\beta}}\} = 0, \\ &[Q_\alpha, P_\mu] = [\bar{Q}_{\dot{\beta}}, P_\mu] = 0. \end{aligned} \tag{1.24}$$

Here, $\alpha, \beta = 1, ..., N$ denote spinor indices, P_μ represents the momentum operator, and σ_μ stands for the Pauli matrices. Additional terms involving other generators, like R-symmetry charges, can also be included in the supersymmetric algebra. The structure and representations of the supersymmetric algebra are contingent on spacetime's dimensionality, signature, and the value of N. In this context, N corresponds to the number of symmetry's supercharges or independent spinor generators. It can take any positive integer value, leading to different types of supersymmetric theories. For instance:

- N = 1: The simplest and most realistic case with a single supercharge and one superpartner for each particle, famously known as the *Minimal Supersymmetric Standard Model* (MSSM).
- N = 2: A special scenario featuring two supercharges and two superpartners for each particle, with additional symmetries and properties.
- N = 4: The most symmetric case in four dimensions, boasting four supercharges and four superpartners for each particle, resulting in a theory that is finite to all orders of perturbation theory.

In the forthcoming section, we will illustrate the fundamental principles and structure of the simplest case ($N = 1$), renowned as the MSSM. As an extension of the well-established SM, the MSSM presents a profound framework that incorporates supersymmetry and offers a promising resolution to certain unresolved issues encountered within the SM.

1.3.1 The Minimal Supersymmetric Standard Model

The Minimal Supersymmetric Standard Model (MSSM) [36, 70–73] stands as one of the most extensively studied frameworks in theoretical physics, serving as the simplest extension of SM where SUSY is incorporated. Within this framework, every elementary particle from the SM acquires a superpartner, forming supermultiplets where bosons and fermions coexist harmoniously. These superpartners, known as sparticles, possess identical quantum numbers to their ordinary counterparts, except for a half-unit difference in spin. There are two types of supermultiplets in MSSM: chiral supermultiplets and vector supermultiplets. Chiral supermultiplets contain both fermionic (spin-1/2) and bosonic (spin-0) particles, encompassing quarks (squarks), leptons (sleptons), and Higgs bosons (higginos), alongside their corresponding supersymmetric partners. Similarly, vector supermultiplets consist of bosonic (gauge bosons∼ spin-1)and fermionic (gauginos∼ spin 1/2) elements, representing the force-transmitting particles and their supersymmetric counterparts. A detailed particle content of the model is presented in Table 1.3.

Super-multiplets	Super-field	Bosonic Fields	Fermionic Partners	SU(3)	SU(2)	U(1)
gluon/gluino	$\widehat{G}_\alpha$	G_α	$\widetilde{G}_\alpha$	8	1	0
gauge boson/	$\widehat{W}_\alpha$	$W^\pm, W^0$	$\widetilde{W}^\pm, \widetilde{W}^0$	1	3	0
gaugino	$\widehat{B}$	B	$\widetilde{B}$	1	1	0
suark/	$\widehat{Q}$	$(\widetilde{u}_L, \widetilde{d}_L)$	$(u, d)_L$	3	2	1/3
quark	$\hat{u}^c$	$\widetilde{u}^*_R$	u^c_L	$\bar{3}$	1	-2/3
	$\hat{d}^c$	$\widetilde{d}^*_R$	d^c_L	$\bar{3}$	1	1/3
slepton	$\widehat{L}$	$(\widetilde{\nu}_L, \widetilde{e}_L^{\,-})$	$(\nu, e^-)_L$	1	2	-1/2
lepton/	$\hat{e}^c$	$\widetilde{e}^+_R$	e^c_L	1	1	1
Higgs boson	$\widehat{H}_u$	(H^+_u, H^0_u)	$(\widetilde{H}^+_u, \widetilde{H}^0_u)$	1	2	1/2
higgsino	$\widehat{H}_d$	(H^0_d, H^-_d)	$(\widetilde{H}^0_d, \widetilde{H}^-_d)$	1	2	-1/2

Table 1.3: Field content of the MSSM

Adding these additional particles is crucial to maintain quantum consistency and stability in the MSSM. To achieve this, anomaly cancellation conditions must be carefully chosen. Gauge anomalies arise from quantum effects when chiral supermultiplets interact with gauge bosons. A significant aspect of the MSSM is that gauginos possess zero hypercharge (Y=0), indicating they lack any hypercharge quantum number under the U(1) gauge group. This crucial property guarantees the automatic cancellation of gauge anomalies. In addition to gauge anomalies, the Higgs sector of the MSSM can also be subject to various anomalies. There are two Higgs chiral superfields [71, 74], with the two Higgs doublets denoted as H_u and H_d. These doublets are crucial in spontaneous electroweak symmetry breaking, providing mass to gauge bosons (W^+, W^-, and Z^0) and fermions through Yukawa interactions. Remarkably, two Higgs doublets ensure anomaly cancellation, preserving the theory's renormalizability by carefully arranging hypercharge assignments. The necessity for a second Higgs doublet becomes evident from an alternative perspective. In SM, a single Higgs doublet is sufficed to give masses upon both up and down-type quarks by employing both H and its conjugate ($\widetilde{H}$) in the Lagrangian. Nonetheless, in SUSY theories, the superpotential, which governs

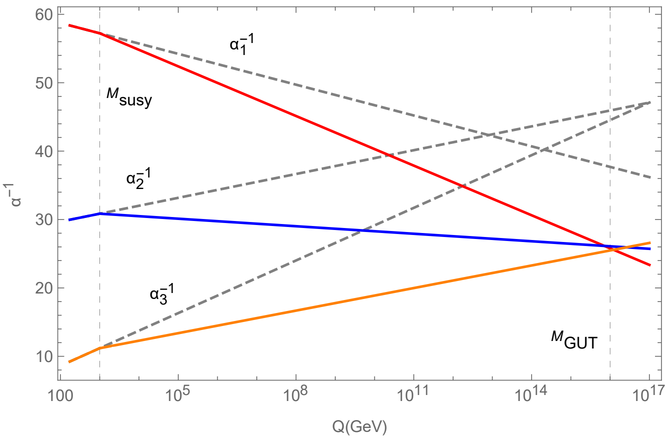

Figure 1.3: The unification of the inverse gauge couplings α^{-1} at the one-loop level in the MSSM, considering a SUSY scale in the TeV range ($M_{\mathrm{SUSY}} = 1\,\mathrm{TeV}$). The three gauge couplings converge at an energy scale with $M_{\mathrm{GUT}} \approx 10^{16}\,\mathrm{GeV}$. For comparison, the evolution of the gauge couplings is also depicted in the case of the SM using dashed lines.

the Yukawa interactions between matter fields and their partners, must be a holomorphic function of the fields. Consequently, the simultaneous inclusion of both H and $\widetilde{H}$ in the superpotential is prohibited. As a result, there arises a demand for two Higgs doublets.

In MSSM, the stabilization of the Higgs boson mass relies on a crucial phenomenon known as supersymmetric cancellation [75–77]. This cancellation predominantly originates from the contributions of scalar partners, including higgsinos and Higgs scalars, to the Higgs boson mass correction. Remarkably, these scalar partners intervene in the quantum corrections in a manner that partially offsets the quadratic divergences arising from the SM fermions and bosons. This partial cancellation effectively resolves the hierarchy problem, which reduces the Higgs boson mass's sensitivity to high energy scales. If SUSY were an exact symmetry of nature, with particle masses being precisely equal to the masses of their superpartners, then the quadratic divergences in the Higgs boson mass would vanish entirely through what is called exact SUSY cancellation. Nonetheless, it is essential to emphasize that exact SUSY cancellation does not manifest in reality, as this scenario would necessitate supersymmetric particles to possess masses very close to those of their Standard Model counterparts. As of now, no evidence supporting such supersymmetric particles has been detected at the energy levels accessible to present-day particle colliders, leading to the conclusion that SUSY must be a broken symmetry in nature.

The incorporation of supersymmetry breaking into the model is achieved through the introduction of soft SUSY-breaking terms into the Lagrangian [57,75,78,79]. These terms are carefully added to avoid the reintroduction of the hierarchy problem and preserve the naturalness. It is important to note that these soft terms are manually inserted and do not stem from any specific underlying mechanism of the theory. However, these terms play a crucial role in regulating the masses of supersymmetric particles, guaranteeing this way deviations from their Standard Model counterparts. Through meticulous control of these masses, the soft terms additionally aid in stabilizing the Higgs boson mass, effectively protecting it from substantial quantum corrections.

Remarkably, these soft terms also intersect with another intriguing aspect of the MSSM, the unification of gauge couplings [78,80,81,83]. With the introduction of superpartners, the evolution of gauge couplings is altered from the non-supersymmetric case, and the theory exhibits a remarkable convergence of these couplings at the GUT scale. The gauge couplings of each fundamental force evolve differently with energy. However, the three gauge couplings converge to a common value when the energy scale is raised to a certain point known as the GUT scale (M_G). Such unification of couplings suggests the potential convergence of fundamental forces at high energy scales, serving as indirect evidence for the presence of supersymmetry at the TeV scale. A depiction of the evolution of the inverse gauge couplings in the MSSM is showcased in Figure 1.3. From the figure, it is evident that a convergence of the three gauge couplings occurs at the GUT scale ($M_G \approx 2 \times 10^{16}$), while SUSY decouples at a scale of $M_{SUSY} \approx 1$ TeV.

For a chiral field, the fundamental expression for the general form of the superpotential stands as follows:

$$W(\Phi) = \frac{1}{2} M_{ij} \Phi_i \Phi_j + \frac{1}{3!} y_{ijk} \Phi_i \Phi_j \Phi_k \tag{1.25}$$

where, M_{ij} embodies the mass matrix, with indices i and j symbolizing the components of the chiral superfields, and y_{ijk} captures the Yukawa couplings, with i, j, and k corresponding to the chiral superfields engaged in the interaction. The first term signifies an interaction influenced by the mass matrix, contributing to how masses combine within these fields. The second term is related to an interaction governed by Yukawa coupling, explaining how these fields can link together. The factor $\frac{1}{3!}$ is used to account for the different permutations of the three fields, as the order of multiplication does not matter for identical particles. Yukawa couplings are responsible for generating fermion masses. Considering now the tree-level scalar potential within the MSSM, this potential emerges as an interplay between F-terms and D-terms, both springing from the scalar components of chiral superfields. The scalar potential V is given by the sum of F-term and D-term contributions:

$$V = V_F + V_D. \tag{1.26}$$

Let's investigate these two contributions more analytically. The F-term of a chiral superfield Φ is given by $F_\Phi = \frac{\partial W}{\partial \Phi}$, where W is the superpotential. The F-term contribution to the scalar potential is obtained by squaring the F-terms and summing over all scalar field components of the chiral superfields:

$$V_F = \sum_i |F_i|^2 = \sum_i \left| \frac{\partial W}{\partial \Phi_i} \right|^2. \tag{1.27}$$

On the other hand, the D-term contribution arises from the interaction between the scalar components of chiral superfields and the gauge fields associated with the gauge group symmetries in the theory. In general, the D-term corresponding to a chiral superfield Φ_i reads as

$$D^a = g^a \sum_i \Phi_i^\dagger T^a \Phi_i, \tag{1.28}$$

where g_a are the gauge coupling corresponding to the gauge group, T^a are the generators of the group, and the sum covers all scalar field components of the chiral fields charged under the gauge group. The D-term's impact on the scalar potential emerges through summation across all gauge group factors:

$$V_D = \frac{1}{2} \sum_a D^a D_a = \frac{1}{2} \sum_a \left(\sum_i g^a \Phi_i^\dagger T^a \Phi_i \right)^2 \tag{1.29}$$

The tree-level scalar potential V is the sum of V_F and V_D:

$$V = \sum_i \left| \frac{\partial W}{\partial \Phi_i} \right|^2 + \frac{1}{2} \sum_a \left(\sum_i g^a \Phi_i^\dagger T^a \Phi_i \right)^2 \tag{1.30}$$

and provides valuable insights into symmetry breaking, which emerges as a consequence of the vacuum structure obtained by the potential.

In the context of the MSSM, the superpotential is formulated as follows :

$$W_{\text{MSSM}} = Y_u^{ij} u_i^c Q_j H_u - Y_d^{ij} d_i^c Q_j H_d - Y_e^{ij} e_i^c L_j H_d + \mu H_u H_d. \tag{1.31}$$

The terms involving the Higgs doublet superfields (H_u and H_d) provide masses to up-type and down-type quarks, respectively, and generate the masses of charged leptons through their interactions with left-handed lepton doublet. The Higgs mixing term, denoted as μ (also referred to as the μ-term), plays a significant role in electroweak symmetry breaking and contributes to the masses of gauge bosons and fermions. It is worth noting that the MSSM itself does not provide a natural explanation for the origin of the μ-term in its superpotential. This has led to the consideration of extensions and mechanisms that could give rise to the μ-term. One such extension is the Next-to-Minimal Supersymmetric Standard Model (NMSSM) [87–91], which incorporates an additional singlet scalar field (S). In the NMSSM, the μ-term can be dynamically generated through the VEV of the singlet field ($\mu = \lambda s$, where λ is a dimensionless coupling constant), thus providing a solution to the μ problem [84, 86, 276] of the MSSM.

In the formula above, Y_u, Y_d, and Y_e represent the Yukawa couplings for up-type, down-type quarks, and charged leptons, respectively. These couplings are related to the masses of quarks and leptons through the following relations :

$$Y_u = \frac{\sqrt{2} m_u}{v \sin\beta}, \quad Y_d = \frac{\sqrt{2} m_d}{v \cos\beta}, \quad Y_e = \frac{\sqrt{2} m_e}{v \cos\beta}, \tag{1.32}$$

where the mixing angle β represents the ratio of the VEVs of the two Higgs doublets, v_u and v_d respectively, and it is defined as $\tan\beta = v_u/v_d$, with a range of $[0, \pi/2)$. Also, the relation $v = \sqrt{v_u^2 + v_d^2}$ connects these VEVs, where v is the vacuum expectation value responsible for breaking the electroweak symmetry.

R-parity in the MSSM

R-parity stands as a fundamental discrete symmetry that exerts a defining influence over interactions within the framework of the MSSM. It embodies a multiplicative quantum attribute, assigning a value of either +1 or -1 to each constituent particle in the theory. Within this context, R-parity's role becomes prominent, serving to differentiate standard particles (with even R-parity) from their supersymmetric counterparts (with odd R-parity). In the realm of the MSSM, R-parity maintains its significance by stipulating that interactions involve an even number of supersymmetric participants. The motivation behind upholding R-parity is driven by empirical considerations, prominently addressing the non-observation of proton decay from the experiments so far. Violation of R-parity would introduce processes contradicting baryon and lepton numbers, inevitably leading to rapid proton decay. Moreover, by maintaining R-parity conservation, an interesting possibility emerges, the identification of a potential dark matter candidate in the shape of the lightest supersymmetric particle (LSP). Matter parity, a concept intertwined with R-parity, parallels its principles. Matter parity is encapsulated by the expression

$$P_M = -1^{3(B-L)}, \tag{1.33}$$

where B and L denote the baryon and lepton numbers, respectively. Notably, within the confines of the MSSM, conserving matter parity seamlessly aligns with the preservation of R-parity. This interrelation holds promise, as matter parity could evolve into an inviolable and essential symmetry, in contrast to the potential vulnerabilities of B and L in the face of non-perturbative electroweak influences. The MSSM Lagrangian incorporates terms that respect the conservation of R-parity, a quantum number defined for each particle as :

$$R_p = (-1)^{3(B-L)+2s} \tag{1.34}$$

where B represents baryon number, L is lepton number, and s denotes the particle's spin. The R-parity conserving terms ensure that the net R-parity of any interaction remains unchanged, resulting in stable particles and prohibiting processes that violate baryon or lepton numbers. The MSSM Lagrangian terms we've introduced so far all respect R-parity. In addition to these terms, there are gauge invariant terms that violate this symmetry, leading to unique phenomena and offering potential solutions to certain puzzles in particle physics. Two kinds of terms can violate R-parity (RPV) [68, 92–95] and these are :

- Bilinear RPV Terms:

$$W_{\not{R}p} = \mu_i L_i H_u + \frac{1}{2}\lambda_{ijk} L_i L_j e^c_k + \lambda'_{ijk} L_i Q_j d^c_k. \tag{1.35}$$

  These terms introduce interactions between lepton doublets (L_i), with up-type Higgs (H_u), and mixing of lepton with quark fields. All of these terms contribute to the lepton number violation.

- Trilinear RPV Terms:

$$W_{\not{R}p} = \frac{1}{2}\lambda''_{ijk} u^c_i d^c_j d^c_k \tag{1.36}$$

  These terms induce interactions involving down-type singlet quarks (d^c_k) and up-type singlet antiquarks (u^c_i). The coupling λ''_{ijk} contributes to baryon number violation, and when combined with λ'_{ijk}, allows processes that convert quarks into leptons.

The violation of baryon and lepton number conservation, induced by the RPV terms in the MSSM, introduces the intriguing possibility of proton decay, a process not allowed in the SM. Specifically, one example of such decay is $p^+ \to e^+\pi^0$, where a proton transforms into a positron and a neutral pion. This decay pathway arises from the interplay of the λ'_{112} and λ''_{112} couplings in the RPV terms. However, experimental observations have set stringent limits on the rate of proton decay. Current experimental data require that the λ' or λ'' couplings associated with proton decay must be extremely small, pushing the proton's lifetime to be exceedingly long ($\sim 10^{34}$ years).

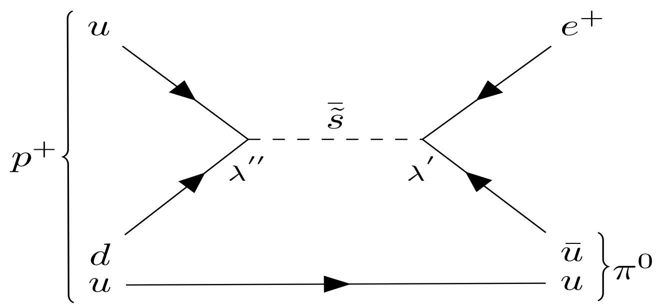

Figure 1.4: Proton decay $p \to \pi^0 + e^+$ with both lepton and baryon violation.

1.4 Unifying Forces: Grand Unified Theories (GUTs)

Although remarkably successful, the SM leaves certain questions unanswered and intriguing features unexplained. In light of this, the emergence of GUTs gains clarity. GUTs arise as a response to the compelling need to unify the fundamental forces of nature into a cohesive framework. While the SM elegantly describes the electromagnetic, weak, and strong forces, it retains a structure of three distinct descriptions rather than embodying a singular unifying principle.

GUTs set out with the aim to construct a grand theoretical structure where these forces are facets of a single, profound entity. This vision extends to energy levels far beyond the reach of current particle accelerators, where GUTs propose the compelling possibility that these forces might harmoniously merge, revealing a previously hidden unity.

GUTs find their motivation rooted in two key objectives. Firstly, they offer a mean to address lingering issues within the SM. This includes resolving aspects such as the seemingly arbitrary values of specific parameters, which currently lack a clear explanation. Secondly, GUTs tackle the SM's limitation in incorporating gravity, a fundamental force not accounted for in the SM. In aiming to unite all forces, GUTs offer a potential framework to connect these forces and incorporate gravity into a comprehensive unified theory.

Central to the GUT framework lies an intricate web of symmetries. They elaborately intertwine the familiar SM gauge group, denoted as $SU(3) \times SU(2) \times U(1)$, within a broader structural context represented by the group G. The investigation of GUTs addresses symmetries, with the SM group as a subgroup. The group G_{SM} is a semisimple Lie Group of rank 4, indicating that G must possess an equal or higher rank. Additionally, group G should honor the chiral structure of the SM, where left-handed and right-handed particles reside in distinct representations of the group.

Among the rank 4 simple groups, only the unitary group SU(5) satisfies these stipulations. While other possibilities like SO(8), SO(9), Sp(8), or F_4 exist, none of them offer complex representations. The SU(5) unified group was first introduced by H. Georgi and S. Glashow [96] and marks the initial effort to construct a GUT. No other rank 4 candidate group, whether simple or non-simple, fulfill the criteria.

Expanding to rank 5, a few potential candidates emerge. However, most of them fail to meet the prerequisite of having complex representations. For instance, SO(11) or Sp(10) are not valid candidates, while SU(6) introduces exotic fields in the same representations as the SM fermions, making decoupling challenging. Consequently, a solitary simple group candidate, Consequently, a solitary simple group candidate, $SO(10)$, remains. Despite being an orthogonal group, it has complex representations, as is the case for groups of the form $SO(4k + 2)$ with $k > 0$. SO(10), initially introduced by H. Fritzsch and P. Minkowski [97] and independently by H. Georgi [98], holds strong appeal as it unifies all SM fermions, including right-handed neutrinos, under a single group representation.

Another enticing approach is the Pati-Salam model [99], known as $SU(4)_C \times SU(2)_L \times SU(2)_R$, which elegantly unifies the fermion content of the SM and explains charge quantization. Conversely, the left-right symmetry group $(SU(3)_C \times SU(2)_L \times SU(2)_R \times U(1)_{\bar{Y}})$ provides a structure where right-handed fields engage with right-handed gauge bosons, mirroring the coupling mechanism observed in the SM for left-handed fields and gauge bosons. Remarkably, $SO(10)$ encompasses both $SU(5) \times U(1)$ and $SU(4)_C \times SU(2)_L \times SU(2)_R$ as maximal subgroups, thus merging the benefits of both scenarios. Incorporating larger groups as potential unification candidates results in extensions of the aforementioned models. For instance, a rank 6 unified theory with E_6 as the gauge group contains $SO(10) \times U(1)$ as a maximal subgroup.

1.4.1 SU(5): Georgi-Glashow Model

Georgi and Glashow were the first to pursue the unification of all forces in one single group. We begin with the SM gauge group $SU(3) \times SU(2) \times U(1)$, encompassing 15 Weyl left-handed fermions distributed across 5 distinct representations. The goal is to identify a group that includes the SM group as a subgroup while incorporating irreducible representations for fermions, aligning with the correct behavior under SM group transformations. Notably, the SM involves a total of $8+3+1=12$ generators[4], with four of them being Cartan generators [5]. This implies that the desired group should possess a rank of at least 4 to accommodate more than 12 generators. The minimal group satisfying these criteria is SU(5), having a rank of 4.

The fundamental SU(5) representation, denoted as 5, is given by:

$$5 \to \left(3, 1, -\frac{1}{3}\right) + \left(1, 2, \frac{1}{2}\right). \tag{1.37}$$

Similarly,

$$\bar{5} \to \left(\bar{3}, 1, \frac{1}{3}\right) + \left(1, 2, -\frac{1}{2}\right) \tag{1.38}$$

Alternatively, as a column matrix:

$$\bar{5} \equiv \begin{bmatrix} d_1^c \\ d_2^c \\ d_3^c \\ e \\ -\nu \end{bmatrix} \tag{1.39}$$

It's notable that d^c and L are placed within $\bar{5}$, while u^c is absent due to the requirement of a traceless hypercharge generator. The remaining SM representations for Q, u^c, and e^c neatly fit into

[4]The property $N^2 - 1$ is used to determine the number of generators for the $SU(N)$ group.

[5]Cartan generators of a Lie algebra are defined by the maximal set of mutually commuting generators within the algebra. They form a basis for the Cartan subalgebra (maximal Abelian subalgebra), and they correspond to conserved quantities (electric charge, hypercharge, or angular momentum components like the third component of isospin in the case of the SM).

the antisymmetric 10 multiplet:

$$10 \rightarrow \left(3, 2, \frac{1}{6}\right) + \left(\bar{3}, 1, -\frac{2}{3}\right) + (1, 1, 1). \tag{1.40}$$

This arrangement accommodates a single generation of quark and lepton fields in the $\bar{5} \oplus 10$ representation of SU(5). Represented as a matrix, the antisymmetric 10 takes the form:

$$10 \equiv \begin{bmatrix} 0 & u_3^c & -u_2^c & u_1 & d_1 \\ -u_3^c & 0 & u_1^c & u_2 & d_2 \\ u_2^c & -u_1^c & 0 & u_3 & d_3 \\ -u_1 & -u_2 & -u_3 & 0 & e^c \\ -d_1 & -d_2 & -d_3 & -e^c & 0 \end{bmatrix}. \tag{1.41}$$

The gauge bosons within the SU(5) model are represented by the adjoint 24-dimensional representation. This representation breaks down under $SU(3) \times SU(2) \times U(1)$ as follows:

$$24 \rightarrow (1, 1, 0) + (8, 1, 0) + (1, 3, 0) + (3, 2, -5/6) + (\overline{3}, 2, 5/6) \tag{1.42}$$

The first three terms pertain to the familiar SM gauge bosons. However, the model introduces two new gauge bosons through the terms $(3, 2, -5/6)$ and $(\overline{3}, 2, 5/6)$. These components represent the X and Y bosons, exclusive to the SU(5) model and distinct from SM particles. Their unique role in GUT predictions and high-energy particle behavior is essential.

Regarding the model's Higgs sector, there's a need for a scalar field Σ. This field is responsible for the shift from SU(5) to G_{SM} and in supersymmetric models, one or perhaps two scalar fields come into play. These fields are responsible for the process of electroweak symmetry breaking. Specifically, the Σ scalar field has to be in the SU(5) model's **24** representation, also known as the adjoint representation. This choice is really important because it keeps the group's rank intact during the breaking phase, making sure the transition to the SM stays consistent. Regarding the Higgs field(s) responsible for the breakdown of electroweak symmetry, a straightforward approach involves utilizing the 5 (and $\bar{5}$) representations as depicted below:

$$5_H \rightarrow (H_u, D), \quad \bar{5}_H \rightarrow (H_d, D^c) \tag{1.43}$$

where D and D^c are vector exotic color triplets [92, 100, 101]. It's important to note that in the context of the MSSM or the 2 Higgs Doublet Model (2HDM), two Higgs fields are required for the process of electroweak symmetry breaking.

For the Yukawa sector, we have two types of independent renormalizable interactions and these are :

$$Y_u = 10_i 10_j 5_H \quad \text{and} \quad Y_{d/e} = 10_i \bar{5}_j \bar{5}_H \tag{1.44}$$

These interactions encompass the corresponding SM interactions:

$$Y_u(Q_i u_j^c H_u) + Y_{d/e}(Q_i d_j^c H_d + L_j e_i^c H_d) \tag{1.45}$$

where i and j (varying from 1 to 3) denote family indices. Consequently, as one can notice, a direct correlation manifests between the Yukawa coupling constants associated with the masses of charged leptons and down-type quarks, resulting in the relation $Y_d = Y_e^T$ at GUT scale. While this correlation holds for the third generation, the lightest two fail. This problem can be overcome by introducing gauge invariant 5-dimensional operators. A different approach to address the issue was proposed by Georgi and Jarlskog [47]. They suggested expanding the Higgs sector by introducing a 45_H representation, resulting in the operator $10_i\bar{5}_j\bar{45}_H$, and lead to the mass relations :

$$m_\tau = m_b \ , \ \ m_\mu = 3m_s \ , \ \ m_e = \frac{1}{3}m_d. \tag{1.46}$$

In the pursuit of a unified understanding of fundamental forces, the exploration of GUTs aims to integrate the electromagnetic, weak, and strong forces. Among these, the SU(5) gauge group offers a framework to investigate the unification of interactions within the SM. However, the minimal form of SU(5) GUT, whether with or without SUSY, presents a range of technical challenges. These include incorrect Yukawa relations, an outcome of placing leptons and quarks within the same irreducible representation of the GUT gauge group. This alignment implies interactions between these particles that can lead to undesired phenomena.

One of the most prominent issue is the prediction of rapid proton decay [102, 103], a topic of paramount importance in GUT construction. In non-SUSY SU(5), rapid proton decay arises mainly from effective dimension-6 operators originating from the exchange of additional SU(5) gauge bosons X and Y. To curb these effects, the X and Y gauge bosons must possess substantial masses, approximately 10^{16} GeV, a value intriguingly close to the predicted unification scale in SUSY models. Yet, even the combination of SUSY and GUTs doesn't eliminate rapid proton decay. In minimal SUSY SU(5), fast proton decay persists through dimension-5 operators generated by exotic colored triplet Higgs supermultiplets (D and D^c). To mitigate these effects, these Higgs triplets must attain substantial mass values [101, 104, 105], on the order of the GUT scale, introducing another technical quandary: the doublet-triplet splitting problem.

Moreover, the minimal SU(5) models fail to incorporate right-handed neutrinos. To account for small neutrino masses, separate additions of SU(5) singlets 1_R or other suitable SU(5) representations become necessary [31, 106–108]. Addressing this, a unification approach that encompasses all fermions, including right-handed neutrinos, within a common representation while encompassing SU(5) and Pati-Salam as subgroups, emerges in the form of the special orthogonal group SO(10).

1.4.2 SO(10) model

The SO(10) group [109–113] exhibits greater structural complexity compared to SU(5) due to its larger size [6]. There exist several ways to break down SO(10) into subgroups, such as $SU(5)\times U(1)$, known as the flipped SU(5) group [114–117], or $SO(4) \times SO(6)$, forming the Pati-Salam group. Notably, unification can be achieved both with and without consideration of supersymmetry. As a minimal grand unified theory, SO(10) integrates all fundamental particles and the forces that govern their interactions, while naturally producing small neutrino masses through the seesaw mechanism. Moreover, the 16-dimensional spinorial representation of SO(10), when decomposed under SU(5), reveals $10 \oplus \bar{5} \oplus 1$, providing unification of a single family's SM matter content alongside the prediction of right-handed neutrinos.

Let's delve into the model building within the SO(10) framework. In SU(5), we aggregated all fermions into two irreducible representations, $\bar{5} \oplus 10$. However, with SO(10), we can encompass a

[6] The special orthogonal groups SO(N) exhibit N(N - 1)/2 generators, yielding 45 gauge bosons in the context of SO(10) GUT.

complete family of SM fermions neatly within a single 16-dimensional irreducible representation. This 16-plet breaks down under SU(5) in the following manner:

$$16_F = 10 + \bar{5} + 1. \tag{1.47}$$

This property yields various constraints on SM Yukawa couplings. Specifically, in the context of SO(10), there exist only three possible Yukawa types: those corresponding to the 10, 120, and 126-dimensional Higgs representations. This arises due to the decomposition of $16 \otimes 16$:

$$16 \otimes 16 \to 10 \oplus 120 \oplus \overline{126} \tag{1.48}$$

In the context of minimal SO(10) constructions, the origins of the two Higgs multiplets within the MSSM are traced back to the fundamental representation of SO(10):

$$10_H = 5_H + \bar{5}_H. \tag{1.49}$$

This transition mirrors our comprehension derived from SU(5) theory, yet introduces a distinction: SO(10) discerns Higgs from matter representations, marking a divergence between the Higgs and the rest.

In order for the SM fermions to obtain masses within a renormalizable framework, the inclusion of a 10_H Higgs field is essential. When considering a lone 10_H, the structure of the Yukawa Lagrangian takes the form:

$$L_Y = Y_{ij} 16_i 16_j 10_H + \text{h.c.} \tag{1.50}$$

This configuration straightforwardly yields a notable outcome: all Yukawa interactions originate from a singular term, leading to the unification of Yukawa couplings at the GUT scale. While this argument applies well to the heaviest generations [118–125], modifications are necessary for the lighter generations. The remedy involves introducing an additional 10_H or 120_H to break the symmetry between the down-quark and charged-lepton sectors.

Turning to neutrinos, the introduction of a Majorana mass to the right-handed (RH) neutrinos necessitates $B - L$, which is the difference between baryon number (B) and lepton number (L), to be broken by two units. This mandates the coupling of the bilinear $16^*_H 16^*_H$ with $16_F 16_F$. The emergence of this coupling arises radiatively, facilitated by the exchange of states within the GUT.

Finally, the breaking of SO(10) down to the SM, can be accomplished in various ways, involving the incorporation of scalar fields from the 45 or 54 representations, coupled with a pair of either **16** and $\overline{\mathbf{16}}$ representations or **126** and $\overline{\mathbf{126}}$ representations. Introducing a non-zero vev for a Higgs field within the **45** representation leads to the breaking of SO(10) into various subgroups such as SU(5), flipped SU(5), $SU(4) \times SU(2) \times U(1)$, $SU(3) \times SU(2)_L \times SU(2)_R$, or $SU(3) \times SU(2)_L \times U(1)^2$. On the other hand, the **54** representation leads to the breaking of SO(10) into the Pati–Salam subgroup. Employing a combination of both the **45** or **54** representations and the **16**+$\overline{\mathbf{16}}$ or 126+$\overline{\mathbf{126}}$ representations leads to the reduction of SO(10) to the structure of SM.

1.4.3 Exceptional groups : E_6 to E_8

E_6 is a gauge group that encompasses both SO(10) and SU(5), constituting an exceptional Lie algebra with complex representations [126–130]. It serves as the minimal embedding of $SO(10) \otimes U(1)$ and incorporates one 78_H representation along with two pairs of $27_H \oplus \overline{27}_H$ chiral superfields.

The exceptional Lie groups, namely G_2, F_4, E_6, E_7, and E_8, stand apart from the classical Lie groups due to their unique mathematical properties and profound implications for physics. Among these exceptional groups, the embedding of SO(10) from E_6 exemplifies the potential to unify a wider range of particle content and interactions within a single comprehensive framework. To realize the embedding of SO(10) into E_6, we consider the following breaking pattern:

$$E_6 \to SO(10) \times U(1)_\psi \to SU(5) \times U(1)_\psi \times U(1)_\chi. \tag{1.51}$$

In the E_6 model, bosons are associated with the adjoint representation **78**, while fermions are attributed to the fundamental representation **27**. These representations further break down within the context of SO(10) as follows:

$$\begin{aligned} 27 &= 16_1 + 10_{-2} + 1_4, \\ 78 &= 45_0 + 16_{-3} + \overline{16}_3 + 1_0, \end{aligned} \tag{1.52}$$

where the subscripts denote the charge under the $U(1)_\psi$. Expanding on this, the subsequent breaking of SO(10) yields the following decomposition:

$$27 \quad \to 10_{1,-1} + \overline{5}_{1,3} + 1_{1,-5} + 5_{-2,2} + \overline{5}_{-2,-2} + 1_{4,0}. \tag{1.53}$$

The second subscript in the equation denotes the charge under the $U(1)_\chi$. It is worth noting that both charges above are un-normalized. In the conventional description, the first three terms accommodate the ordinary quarks, the right-handed electron, the lepton doublets, and the right-handed neutrino. Next, the pair of 5-plets accommodates the Higgs doublets (or exotic doublets) and a pair of exotic color triplets. Finally, there are SO(10) singlets, which serve the purpose of generating large Majorana masses and providing a mechanism for explaining neutrino oscillations and the small masses of the known neutrinos.

In E_6 models, a notable feature emerges, the introduction of an array of novel particles, including extra scalar singlets and exotic vector-like pairs [131]. These newfound constituents exert substantial influence on the model's behavior at lower energy scales. The specific composition of the low-energy particle spectrum in E_6 models hinges significantly on the chosen route of symmetry reduction leading to the SM gauge group. Consequently, it depends on the inherent structure of the model's symmetry-breaking sector. Within the broad range of potential outcomes as the E_6 gauge group evolves into lower energy states, the emergence of U(1) extensions to the MSSM, commonly denoted as UMSSM, presents intriguing theoretical and low-energy implications [132–134]. It's worth noting that the SU(5) subgroup within E_6, already encompasses the entirety of the SM gauge group. A plausible scenario unfolds when E_6 directly breaks down into G_{SM} along with two additional U(1) components ($U(1)_\chi$ and $U(1)_\psi$). These U(1) groups can then be combined into a single $U(1)'$, expressed as a linear combination of the two U(1)s:

$$U(1)' = c_1 U(1)_\chi + c_2 U(1)_\psi \tag{1.54}$$

where the condition $c_1 + c_2 = 1$ must be satisfied. This $U(1)'$ can be linked to a heavy Z' gauge boson, as we will see in the upcoming chapters, the presence of which can hold significant ramifications in both particle physics and cosmology [102, 132, 135].

Applying the same logic thus far, we arrive at E_8 as the maximal singularity, serving as the parent symmetry for all GUT groups so far :

$$E_8 \supset E_7 \supset E_6 \supset SO(10) \supset SU(5) \supset G_{SM}. \tag{1.55}$$

Given the complexities involved in constructing a four-dimensional GUT model starting from E_8, our focus shifts towards the non-perturbative version of IIB superstring theory, commonly known as F-theory. In this framework, at low energy levels, we can develop models based on SU(5) extended by a $U(1)'$ symmetry, featuring non-universal couplings to the three families of quarks and leptons. This gauge group naturally arises from the maximal exceptional gauge symmetry within an elliptically fibred internal space, particularly at a single point of enhancement described as:

$$E8 \supset SU(5) \times SU(5)' \supset SU(5) \times U(1)^4. \tag{1.56}$$

This sequence of symmetry breaking guarantees the presence of rank-one fermion mass patterns and a tree-level top quark coupling. This is achieved by imposing a Z_2 monodromy group, which identifies two abelian factors within the aforementioned breakdown. Furthermore, the $U(1)'$ component of the gauge symmetry represents an anomaly-free linear combination of the three remaining abelian symmetries preserved by Z_2, as we will see in the upcoming sections.

1.5 The concept of Strings

In the pursuit of a unified theory that encompasses elementary particles, various extensions of the successful SM have been explored. GUTs, as discussed earlier, offer certain advantages such as charge quantization, gauge coupling unification, and the possibility of accommodating right-handed neutrino candidates. However, these models often grapple with issues like proton decay effects and the doublet-triplet splitting problem, which conflict with the requirement for gauge coupling unification. To address these challenges, an approach involves extending the GUT group with an additional symmetry, which can be either a continuous U(1) or a discrete symmetry. Many GUT models, accompanied by both continuous and discrete symmetries, have been proposed as realistic extensions of the MSSM. Given the multitude of choices in constructing a GUT model, a coherent and well-informed guide is needed. String Theories provide a compelling solution in this context, showcasing a robust group structure that encompasses both continuous and discrete symmetries simultaneously. Over the past decades, String Theory has demonstrated its potency in describing gravity, which in turn places constraints on particle physics theories. Within the framework of String Theory, we depart from the notion of fundamental point-like particles and instead introduce one-dimensional strings. These strings, whether open or closed, occupy ten space-time dimensions, with six of them compactified to exceedingly small scales. Just as a point particle traces a worldline in Minkowski space, a string sweeps out a “worldsheet”, parameterized by timelike (τ) and spacelike (σ) coordinates. This worldsheet defines a mapping from the worldsheet to Minkowski space, represented as $X^\mu(\sigma, \tau)$. Strings manifest in two forms, “open strings” and “closed strings”, based on whether the σ coordinate is periodic. The strength of interactions between these strings is determined by the string coupling constant, g_s. In this context, Type IIB superstring theory, which encompasses both open and closed strings, becomes relevant, particularly when $g_s \ll 1$. When dealing with open strings, we must account for boundary conditions at their endpoints. Two consistent boundary conditions emerge: Neumann boundary conditions, allowing free movement of string endpoints, and Dirichlet boundary conditions, fixing the endpoints at a specific position $X^\mu = c^\mu$[7]. By choosing suitable boundary conditions, a Dp-brane, a (p+1)-dimensional hypersurface

[7]For the Neumann boundary conditions: $\mu = 0, \dots, p$, and for the Dirichlet boundary conditions: $\mu = p + 1, \dots, D-1$.

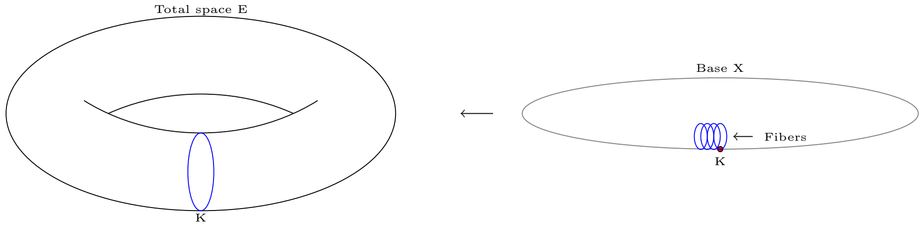

Figure 1.5: Realization of the fibre bundle. The total space E (torus)is constructed from the base space X (gray circle) and the continuously connected fibers (blue circles).

in spacetime, can be defined. In the context of F-Theory, D7-branes are particularly relevant. Particles in our four-dimensional spacetime correspond to strings stretched between these D-branes, with their mass related to the tension T and the distance (d) between the branes in the internal dimensions. This relationship is expressed as $M = T \times d$.

Since all SM particles are effectively massless, the situation corresponds to d = 0, which means we're focusing on scenarios where the endpoints of open strings can overlap in the internal dimensions. When we have N D7 branes occupying the same dimensions, forming a stack of branes, it gives rise to a U(N) gauge theory. In this scenario, the gauge bosons represent strings that start and finish on any of the D7 branes within the same stack. For example, if we have a stack of three D7 branes alongside another stack of two, their intersection occurs in two of the internal dimensions. For this situation, a $U(3) \times U(2)$ gauge group emerges, and massless open strings can originate from the U(3) stack and terminate on the U(2) stack. These strings correspond to states that carry charges under both gauge groups.

These states, often referred to as 'bifundamental' states, constitute the matter fields within the theory. In a simple illustration, these matter fields can be arranged in a 5×5 matrix under a U(5) group, where the gauge fields occupy the 3×3 and 2×2 diagonal blocks, while the matter fields are positioned in the off-diagonal positions. At the intersection of these stacks of branes, we can incorporate all these states into a U(5) group, implying that we can interpret this setup as a U(5) gauge group at the intersection. However, as we move away from the intersection, this U(5) symmetry breaks down into $U(3) \times U(2)$. In cases where there is a triple intersection of D7 branes, further enhancements of the gauge group can occur.

Applying this fundamental logic, we can integrate the SM framework by utilizing perturbative intersecting D-branes within GUT configurations. This leads us to the realization that to manifest the top quarks operator, working within the framework of F-theory is imperative. In doing so, exceptional groups naturally emerge, providing the necessary structural foundation.

1.5.1 GUTs setting from F-theory

F-theory [136–138], a 12-dimensional theoretical framework, emerges as a geometric reinterpretation of type II-B string theory, which is inherently 10-dimensional. Formally, F-theory can be defined on a background spacetime $R^{3,1} \times X$, where $R^{3,1}$ denotes the familiar 4-dimensional spacetime, and X corresponds to a Calabi-Yau (CY) complex fourfold. To understand this theory better, let's delve into some fundamental properties of type II-B superstring theory [139–149].

Type II-B supergravity describes the effective theory and features two primary bosonic field sectors: Ramond-Ramond (R-R fields) and Neveu-Schwarz (NS-NS fields) [161–164]. The NS-NS sector comprises essential elements such as the metric (g_{MN}), the dilaton (ϕ), and a 2-form potential

(B_2). In contrast, the R-R sector includes p-form potentials (C_p) with p values of 0, 2, and 4.

Now, shifting our focus to the geometric aspect of F-theory, consider a Calabi-Yau (CY) fourfold that is elliptically fibered over a three-fold base, denoted as B_3. To understand this concept, let's consider a simple example: the fiber bundle. This bundle incorporates various topological spaces. We have the base space B, which can be any space. At each point K in B ($K \in B$), there is another space (any space) situated above it, known as the fibers over K, which are spread across B. It's important to note that these fibers do not intersect but are continuously connected to form the total space E, thus defining the fiber bundle. This becomes clearer when examining the case of a torus, as depicted in Figure 1.5.

In the context of F-theory, the fibers transform from line segments to two-tori. Each point on the base B_3 is associated with a two-torus, and this base effectively occupies the 6 compactified dimensions of type IIB String Theory. Moreover, the complex modulus of the torus fiber encodes information regarding the axion (C_0) and dilaton (ϕ), two scalar components present in the bosonic spectrum, at every point on the base. This complex modulus, denoted as τ, is defined as

$$\tau = C_0 + ie^{-\phi} = C_0 + \frac{i}{g_s} \tag{1.57}$$

What adds complexity to the scenario is the presence of D7-branes, which extend across 7 spatial dimensions and 1 time dimension. These D7-branes have a significant impact on the complex scalar axio-dilaton field, τ, underscoring the reason F-theory is regarded as a 12-dimensional framework. It achieves this by incorporating two additional geometric dimensions that allow us to track τ's variations across the other ten dimensions.

In our mathematical description of the elliptic fibration, we consider three complex coordinates: (x, y, z), which correspond to the three spatial dimensions of the base space, denoted as B_3. The representation of the elliptic fibration follows a specific equation known as the Weierstrass form:

$$y^2 = x^3 + f(z)x + g(z) \tag{1.58}$$

Here, "f(z)" and "g(z)" are polynomials of the eighth and twelfth degrees in "z". Each point within the base space, B_3, corresponds to a torus defined by the "z" coordinate. Two essential mathematical quantities characterize this elliptic fibration. The first is the discriminant (Δ) of the Weierstrass equation, given by:

$$\Delta(z) = 4f(z)^3 + 27g(z)^2. \tag{1.59}$$

When Δ does not equal zero ($\Delta \neq 0$), the elliptic curve described by our equation remains smooth and non-singular. However, when the Δ vanishes ($\Delta = 0$), it signifies the presence of D7-branes. At these points, the elliptic curve becomes singular, and a two-dimensional subspace within B_3 is affected. The equation $\Delta = 0$ can further break down into irreducible polynomials,$\Delta = \Delta_1 ... \Delta_n = 0$, where each $\Delta_i = 0$ describes the location of a D7-brane. In the context of the torus fiber, it means that the torus degenerates or pinches off at these specific points.

1.5.2 Gauge Groups and Tate's Algorithm

Within the setting of F-theory, the realization of the GUT group occurs through the presence of a 7-brane that wraps a two-complex-dimensional surface known as "S". An interesting aspect of studying the fibration lies in our ability not only to identify the locations of these 7-branes when the discriminant Δ vanishes but also to gain insights into the specific gauge groups they support. This depends on the order in which the discriminant vanishes. Considerable mathematical research has been dedicated to this subject, leading to a systematic classification of singularities connected to gauge groups. Kodaira's work has been instrumental in achieving this classification, relying on the vanishing order of the discriminant Δ and the polynomials "f" and "g" within the Weierstrass equation [150–153]. To describe these singularities, a method called Tate's algorithm is employed [165]. By introducing a coordinate, "z", where "S" is defined as "$z = 0$", we can expand the coefficients "f" and "g" from Equation 1.58 as power series in "z":

$$f(z) = \sum_n f_n z^n, \quad g(z) = \sum_m g_m z^m. \tag{1.60}$$

The general Tate form of the Weierstrass equation then takes the following form:

$$y^2 + a_1 xy + a_3 y = x^3 + a_2 x^2 + a_4 x + a_6. \tag{1.61}$$

Here, the functions a_i, which depend on the complex coordinate 'z' of the base B_3, are connected to the 'f' and 'g' polynomials found in the original Weierstrass equation. Specifically, the polynomials 'f' and 'g,' and consequently, the discriminant Δ, can be represented as functions of the coefficients a_i. To accomplish this, we need to transform Tate's equation (1.61) into the Weierstrass form (1.58). This transformation involves completing the square on the left-hand side and cubing the right-hand side of the equation (1.61), allowing us to compare it with the Weierstrass equation. This process reveals the following relationships:

$$f = -\frac{1}{48}\left(\beta_2^2 - 24\beta_4\right), \quad g = -\frac{1}{864}\left(-\beta_2^3 + 36\beta_2\beta_4 - 216\beta_6\right), \tag{1.62}$$

When we replace 'f' and 'g' in (1.59), the discriminant takes on the following form:

$$\Delta = \frac{1}{8}\left(\beta_8\beta_2^2 - 9\beta_2\beta_4 b\beta_6 + 8\beta_4^3 + 27\beta_6^2\right), \tag{1.63}$$

Here, for brevity, we've introduced the redefined variables:

$$\begin{aligned} \beta_2 &= a_1^2 + 4a_2, \\ \beta_4 &= a_1 a_3 + 2a_4, \\ \beta_6 &= a_3^2 + 4a_6, \\ \beta_8 &= \frac{1}{4}(\beta_2\beta_6 - \beta_4^2). \end{aligned} \tag{1.64}$$

Now, all the symmetry properties of the singularities within the elliptic fibration are encoded in the degree to which the polynomials $a_i \sim b_i z^n$ vanish, alongside the discriminant Δ. The discriminant factorizes, with each factor describing the location of a 7-brane on a divisor "S" in B_3. The summarized results can be found in Table 1.4. As an example, we present the SU(5) case, where the singularity is obtained by the following choice of parameters :

$$a_1 = -b_5\ , \ \ a_2 = b_4 z\ , \ \ a_3 = -b_3 z^2\ , \ \ a_4 = b_2 z^3\ , \ \ a_6 = b_0 z^5 \tag{1.65}$$

where the b_k's are the fibration coefficients and are independent of z. These coefficients, are typically non-zero and can be thought of as sections of line bundles on S. Their homology classes are expressed as

$$[b_k] = \eta - kc_1, \tag{1.66}$$

Group	a_1	a_2	a_3	a_4	a_6	Δ
SU(2n)	0	1	n	n	2n	2n
SU(2n+1)	0	1	n	n+1	2n+1	2n+1
SO(10)	1	1	2	3	5	7
E6	1	2	2	3	5	8
E7	1	2	3	3	5	9
E8	1	2	3	4	5	10

Table 1.4: Classification of singularities obtained from Tate's algorithm. For a more detailed description see [150].

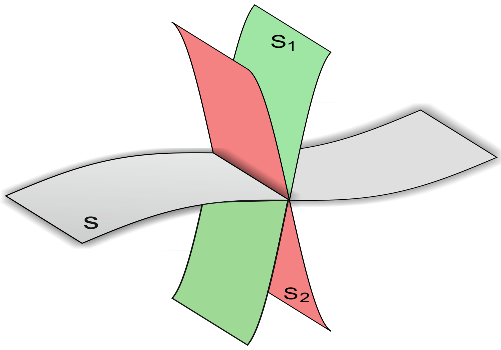

Figure 1.6: Intersecting branes. Matter is located along these intersections and the matter curves are formed.

where c_1 represents the first Chern class of the tangent bundle[8] to S, and -k corresponds to the first Chern class of the normal bundle[9] to S.

This choice for the a_i's leads to the Tate's equation of the form

$$y^2 = x^3 + b_0 z^5 + b_2 x z^3 + b_3 y z^2 + b_4 x^2 z + b_5 x y. \tag{1.67}$$

By referring to Table 1.4, we can observe that this choice indeed corresponds to an SU(5) singularity.

As we've seen so far, the structure of the GUT is elucidated through the reliance of the b_i's on the base coordinates. This dependence characterizes the structure of global F-theory. However, we can work within a framework called semi-local F-theory, where in these models, the intricacies of global F-theory are circumvented by concentrating on regions proximate to the GUT surface, denoted as S.

1.5.3 The semi-local approach

In the context of local F-theory, the primary focus is on the submanifold S, where the GUT symmetry becomes localized. We can examine the intersections between the GUT brane, which wraps around S, and other 7-branes that wrap surfaces S_i and support gauge groups G_i. These intersections serve

[8] A collection of tangent vectors on the manifold S. These vectors describe the direction of possible curves on S at each point.

[9] A collection of vectors at each point on the surface or manifold S. These vectors are perpendicular to S and describe the directions away from the surface.

as the locations where matter resides and are referred to as 'matter curves,' denoted as $\Sigma_i = S \cap S_i$. An example is depicted in Figure 1.6. Along these matter curves, the local symmetry group is enhanced to $G_{\Sigma_i} \supset G_S \times G_i$.

Taking a step further, we can explore the intersections between matter curves at points within S. When matter curves intersect, they induce Yukawa couplings, leading to an additional enhancement of the local symmetry to $G_Y \supset G_{\Sigma_i} G_{\Sigma_j} \times G_{\Sigma_k}$. To study Yukawa couplings within the local framework, we can gain valuable insights by focusing on the local vicinity around the point where these curves intersect on the surface S.

The semi-local approach to F-theory is built upon the assumption of a parent E_8 gauge theory, which undergoes breaking due to a position-dependent VEV for an adjoint Higgs field. In this scenario, all interactions in the theory are assumed to originate from a single point of E_8 enhancement. At this point, all matter curves within the theory converge, and the local symmetry group experiences a complete enhancement to E_8.

1.5.4 Monodromy and the Spectral cover

Among the GUT groups included inside E_8, we are especially drawn to scenarios in which G_S is one of the renowned GUT groups E_6, SO(10), or SU(5). The format in which these groups are embedded within E_8 takes the following form

$$E_8 \supset G_S \times SU(N)_\perp \tag{1.68}$$

where the commutant group is indicated by the subscript "$\perp$" and referred to as the perpendicular group.

Let's consider the case of S(5) as an example ($G_S = SU(5)$). The breaking of E_8 to the GUT group takes place as

$$E_8 \to SU(5)_{GUT} \times SU(5)_\perp \to SU(5)_{GUT} \times U(1)^4. \tag{1.69}$$

The characterization of the matter curves within the theory is determined through the decomposition of E_8's adjoint representation as follows

$$248 \to (24,1) + (1,24) + (5,10) + (\overline{5},\overline{10}) + (10,\overline{5}) + (\overline{10},5) \tag{1.70}$$

From this equation, we can determine that we have 24 singlet curves (denoted as θ_{ij}), five 10 curves, and ten $\bar{5}$ curves.

The equations describing these curves can be expressed in terms of the weights t_i (with $i = 1, ..., 5$ and $\sum t_i = 0$) belonging to the **5** representation of $SU(5)_\perp$ as follows:

$$\begin{aligned} &\Sigma_{10} : t_i = 0 \\ &\Sigma_5 : -t_i - t_j = 0 \quad , \quad \text{for i} \neq \text{j} \\ &\Sigma_1 : \pm(t_i - t_j) = 0 \quad , \quad \text{for i} \neq \text{j} \end{aligned} \tag{1.71}$$

The coefficients b_k in eq.(1.67) are determined by elementary symmetric polynomials[10] of degree k in these weights. These relations are inherently nonlinear, often resulting in connections between

[10]The term "elementary symmetric polynomials of degree i" refers to mathematical expressions that are constructed by taking the sum of all possible products of k distinct elements from a set of variables, which in this case are the t_i weights.

some of the t_i. The specific identification of t_i is contingent upon the "monodromy group" choice since, in our semi-local context, the full Calabi-Yau geometry has been decoupled, necessitating manual selection of the monodromy group.

To ensure the existence of a tree-level top quark Yukawa coupling, a minimum requirement is a Z_2 monodromy, associating two of the weights. This stems from the need for the $10_M \times 10_M \times 5_H$ coupling to remain invariant under perpendicular $U(1)$ symmetries. Since both the top and anti-top quarks originate from the same **10** representation, they share a charge t_i, and the up-type Higgs carries a charge of $-t_j - t_k$. To balance these charges, we must satisfy $2t_i - t_j - t_k = 0$. This condition is only met when $j = k = i$, necessitating the identification of at least two of the weights. Henceforth, we will assume this minimal Z_2 case as a consistent requirement, making the interchange $t_1 \leftrightarrow t_2$.

The spectral cover equation to this configuration is derived by defining the homogeneous coordinates

$$z \to U\ ,\quad x \to V^2\ ,\quad y \to V^3 \tag{1.72}$$

leading to the following Tate equation

$$0 = b_0 U^5 + b_2 V^2 U^3 + b_3 V^3 U^2 + b_4 v^4 U + b_5 V^5. \tag{1.73}$$

Ultimately, by introducing the parameter $s = U/V$, the equation transforms into the following expression:

$$C_5 = \sum_{k=0}^{5} b_k s^{5-k} = b_5 + b_4 s + b_3 s^2 + b_2 s^3 + b_1 s^4 + b_0 s^5. \tag{1.74}$$

This equation constitutes a fifth-degree polynomial and is referred to as the spectral cover equation. Moreover, the solutions to the spectral cover equation correspond to the weights associated with the $SU(5)_\perp$ group [166]. These weights are represented as t_i, where i ranges from 1 to 5. We can express this as follows

$$0 = b_5 + b_4 s + b_3 s^2 + b_2 s^3 + b_0 s^5 \propto \prod_{i=1}^{5} (s + t_i). \tag{1.75}$$

Using the above relation, it becomes a straightforward task to express the coefficients b_k as functions of the roots t_i. Notably, the coefficient b_1 is set to zero since it represents the sum of the roots, which, for SU(N) groups, always equals zero, i.e., $\sum t_i = 0$. Additionally, we observe that the $s = 0$ part of the spectral cover polynomial is equal to the product of the roots, $b_5 = t_1 t_2 t_3 t_4 t_5$. The locations of the corresponding matter multiplets on the Σ_{10} matter curves are defined by the five zeros

$$\Sigma_{10_i}\ ,\quad P_{10} = b_5 = \prod_{i=1}^{5} t_i = 0 \to t_i = 0\ ,\quad i = 1, 2, 3, 4, 5. \tag{1.76}$$

Similarly, we can obtain for the fiveplets of SU(5)

$$\Sigma_{\bar{5}_{ij}}\ ,\quad P_5 = \prod_{t_i \neq t_j} (t_i + t_j) = 0\ , \tag{1.77}$$

and for the 24 singlets curves $\Sigma_{1_{ij}}$

$$\Sigma_{\bar{1}_{ij}}\ ,\quad P_0 = \prod(\pm(t_i - t_j)) = 0. \tag{1.78}$$

Imposing the Z_2 monodromy [167] as stated earlier, corresponds to the splitting of the spectral cover equation in the following manner

$$0 = (a_1 + a_2 s + a_3 s^2)(a_4 + a_5 s)(a_6 + a_7 s)(a_8 + a_9 s) \tag{1.79}$$

where the coefficients denoted as "a_i" are unspecified constants. The initial bracket encompasses the polynomial factor related to the Z_2 monodromy, while the subsequent monomials maintain the integrity of three U(1) symmetries. Expanding this expression now, allows us to establish the homology class for each of the coefficients a_i, which can then be compared with the b_k's. Consequently, we obtain the following results

$$\begin{aligned}
b_0 &= a_3a_5a_7a_9\\
b_1 &= a_3a_5a_7a_8 + a_3a_4a_9a_7 + a_2a_5a_7a_9 + a_3a_5a_6a_9\\
b_2 &= a_3a_5a_6a_8 + a_2a_5a_8a_7 + a_2a_5a_9a_6 + a_1a_5a_9a_7 + a_3a_4a_7a_8 + a_3a_4a_6a_9 + a_2a_4a_7a_9\\
b_3 &= a_3a_4a_8a_6 + a_2a_5a_8a_6 + a_2a_4a_8a_7 + a_1a_7a_8a_5 + a_2a_4a_6a_9 + a_1a_5a_6a_9 + a_1a_4a_7a_9\\
b_4 &= a_2a_4a_8a_6 + a_1a_5a_8a_6 + a_1a_4a_8a_7 + a_1a_4a_6a_9\\
b_5 &= a_1a_4a_6a_8
\end{aligned} \tag{1.80}$$

To begin, we address the $b_1 = 0$ constraint by introducing the following Ansatz:

$$\begin{aligned}
a_2 &= -c(a_5a_7a_8 + a_4a_9a_7 + a_5a_6a_9)\\
a_3 &= ca_5a_7a_9
\end{aligned} \tag{1.81}$$

Upon substitution into the expressions for the coefficients b_k's, we obtain

$$\begin{aligned}
b_0 &= ca_5^2a_7^2a_9^2\\
b_2 &= a_1a_5a_7a_9 - (a_5^2a_7^2a_8^2 + a_5a_7(a_5a_6 + a_4a_7)a_9a_8 + (a_5^2a_6^2 + a_4a_5a_7a_6 + a_4^2a_7^2)a_9^2)c\\
b_3 &= a_1(a_5a_7a_8 + a_5a_6a_9 + a_4a_7a_9) - (a_5a_6 + a_4a_7)(a_5a_8 + a_4a_9)(a_7a_8 + a_6a_9)c\\
b_4 &= a_1(a_5a_6a_8 + a_4a_7a_8 + a_4a_6a_9) - a_4a_6a_8(a_5a_7a_8 + a_5a_6a_9 + a_4a_7a_9)c\\
b_5 &= a_1a_4a_6a_8
\end{aligned} \tag{1.82}$$

Subsequently, we need to establish the homology classes $[a_i]$ for nine variables, a_1 through a_9, in relation to the $[b_k]$ classes $[b_1, ..., b_5]$. By examining eq.(1.80), we can deduce that the latter classes satisfy the general equation $[b_k] = [a_l] + [a_m] + [a_n] + [a_p]$ for k + l + m + n + p = 24. Three classes remain undetermined, and we opt to designate them as $[a_l] = \chi_l$ for l = 5, 7, 9. The remaining classes can be straightforwardly calculated and are summarized in Table 1.5.

The Σ_{10} curves are obtained by setting s = 0 in the polynomial, resulting in

$$b_5 \equiv \Pi_5(0) = a_1a_4a_5a_6 = 0. \tag{1.83}$$

This condition results in $a_1 = 0, a_4 = 0, a_5 = 0$, and $a_6 = 0$. Consequently, after applying the monodromy operation, we are left with four curves (one less due to the monodromy) to accommodate

a_1	a_2	a_3	a_4	a_5	a_6	a_7	a_8	a_9
$\eta - 2c_1 - \chi$	$\eta - c_1 - \chi$	$\eta - \chi$	$-c_1 + x_5$	χ_5	$-c_1 + x_7\ x_7$	χ_7	$-c_1 + \chi_9$	χ_9

Table 1.5: Homology classes associated with the coefficients a_i in the context of a Z_2 monodromy in the SU(5) scenario.

Field	$U(1)_i$	Homology	$U(1)_Y$-flux	$U(1)$-flux
10_1	$t_{1,2}$	$\eta - 2c1 - \chi$	$-N$	M_{10_1}
10_2	t_3	$-c1 + \chi_7$	N_7	M_{10_2}
10_3	t_4	$-c1 + \chi_8$	N_8	M_{10_3}
10_4	t_5	$-c1 + \chi_9$	N_9	M_{10_4}
5_{H_u}	$-2t_{1,2}$	$-c1 + \chi$	N	$M_{5_{H_u}}$
5_1	$-t_{1,2} - t_3$	$\eta - 2c1 - \chi$	$-N$	M_{5_1}
5_2	$-t_{1,2} - t_4$	$\eta - 2c1 - \chi$	$-N$	M_{5_2}
5_3	$-t_{1,2} - t_5$	$\eta - 2c1 - \chi$	$-N$	M_{5_3}
5_4	$-t_3 - t_4$	$-c_1 + \chi - \chi_9$	$N\ -N_9$	M_{5_4}
5_5	$-t_3 - t_5$	$-c_1 + \chi - \chi_8$	$N\ -N_8$	$M_{5_{H_d}}$
5_6	$-t_4 - t_5$	$-c_1 + \chi - \chi_7$	$N\ -N_7$	M_{5_6}

Table 1.6: Representation content of fields within the framework of $SU(5) \times U(1)_{t_i}$, along with their respective homology classes and flux restrictions. It's important to highlight that the $\overline{10}$ and $\overline{5}$ representations feature opposite values of t_i ($t_i \to -t_i$). Furthermore, we should take note that the fluxes adhere to the conditions $N = N_7 + N_8 + N_9$ and $\sum_i M_{10_i} + \sum_j M_{5_j} = 0$, while $\chi = \chi_7 + \chi_8 + \chi_9$.

the necessary components of the three families. The handling of the Σ_5 curves follows a similar approach. The corresponding spectral cover for the fiveplets is a 10-degree polynomial and has the following form

$$\mathscr{P}_{10}(s) = \sum_{n=1}^{10} c_n s^{10-n} = b_0 \prod_{i,l} (s - t_i - t_j) \ , \quad i < j \ , \quad i, j = 1, ..., 5. \tag{1.84}$$

We express the coefficients $c_n = c_n(t_j)$, into functions of $c_n(b_j)$, and by utilizing the equations for $b_k(a_i)$ and the provided Ansatz, we can partition this equation into seven distinct factors, each corresponding to one of the remaining seven fiveplets following the Z_2 monodromy as follows

$$\begin{aligned} P_5 = &(a_1 - ca_4(a_7a_8 + a_6a_9)) \times (a_1 - c(a_5a_6 + a_4a_7)a_8) \times (a_1 - ca_6(a_5a_8 + a_4a_9)) \\ &\times (a_4a_7a_9 + a_5(a_7a_8 + a_6a_9)) \times (a_5a_6 + a_4a_7) \times (a_5a_8 + a_4a_9) \times (a_7a_8 + a_6a_9) \end{aligned} \tag{1.85}$$

Their homologies can be specified using those of a_i. Notice that in the first line of eq.(1.85), the three factors correspond to three fiveplets of the same homology class $[a_1] = \eta - 2c_1 - \chi$. In Table 1.6, we present the complete spectrum.

1.5.5 GUT symmetry breaking

In F-theory constructions, breaking the GUT symmetry often involves introducing fluxes on the worldvolume of the seven-brane supporting the unified gauge group. In scenarios where SU(5) symmetry is present, the symmetry breaking is achieved by introducing a non-trivial hypercharge flux.

This flux leads to the splitting of SU(5) multiplets along certain curves where the flux imposes non-trivial restrictions. Consequently, some components of the SU(5) representation, can be removed due to the flux-induced effects. This mechanism is particularly relevant for eliminating unwanted triplet states within the Higgs fiveplets.

To put this concept into practice within a particular scenario, let's start by how SU(5) fits into E_8. In eq.(1.69) we saw that E_8 breaks to $SU(5)_{GUT} \times U(1)^4$. The chiral matter fields and Higgs particles associated with SU(5) originate from the adjoint representation of the E_8 symmetry and are distributed across various curves known as Σ_{10_j} and $\Sigma_{\bar{5}_i}$. In a given construction, we represent the numbers of 10 and 5 representations as integers, denoted by M_{10_j} and M_{5_i}, respectively. Additionally, we consider the U(1) fluxes (those not part of $SU(5)_{GUT}$) and apply the tracelessness condition [168]. This condition imposes constraints on the numbers of these multiplets

$$\sum_i M_5^i + \sum_j M_{10}^j = 0 \tag{1.86}$$

Now, let's explore a specific scenario where all chiral matter of the 10-type is exclusively located on a single Σ_{10} curve, while all chiral states of the 5-type are confined to a single $\Sigma_{\bar{5}}$ curve. In this particular setup, eq.(1.86) leads to the relationship $M_{10} = -M_5 = M$. We use N_{Y_5} and $N_{Y_{10}}$ to represent the respective units of Y flux, which results in the splitting of SU(5) multiplets as follows

$$\Sigma_{\bar{5}} : \begin{cases} n_{(3,1)_{-1/3}} - n_{(\bar{3},1)_{1/3}} & = M_5 \\ n_{(1,2)_{1/2}} - n_{(1,2)_{-1/2}} & = M_5 + N_{Y_5} \end{cases} \quad \Sigma_{10} \quad : \begin{cases} n_{(3,2)_{1/6}} - n_{(\bar{3},2)_{-1/6}} & = M_{10} \\ n_{(\bar{3},1)_{-2/3}} - n_{(3,1)_{2/3}} & = M_{10} - N_{Y_{10}} \\ n_{(1,1)_1} - n_{(1,1)_{-1}} & = M_{10} + N_{Y_{10}} \end{cases}$$

These formulas essentially quantify the difference between the number of 5-components and the number of $\bar{5}$-components, as well as the difference between the number of 10-components and the number of $\overline{10}$-components. To ensure that the families are present within the $\bar{5}$'s, we need to satisfy the condition where $n_{(\bar{3},1)_{1/3}} > n_{(3,1)_{-1/3}}$, which implies that $M_5 < 0$. Similarly, since the remaining components of fermion generations are hosted within the 10's, we aim to have 10-components remaining after symmetry breaking. This means $M_{10} > 0$. For instance, if we want exactly three generations, we would require $M_{10} = -M_5 = 3$ and $N_{Y_j} = 0$. In practice, different curves belong to distinct homology classes, and flux imposes non-trivial constraints on some of them, leading to $N_{Y_j} \neq 0$ for at least some values of j.

1.6 Inflation: Basics to Grand Unification

1.6.1 Brief History

The foundations of inflationary cosmology began to take shape in the early 1970s with the discovery of several key elements [169–173]. One pivotal realization was the role of the energy density associated with a scalar field, serving as the equivalent of vacuum energy or a cosmological constant. This energy density was observed to change during cosmological phase transitions, often undergoing abrupt alterations through first-order phase transitions from a supercooled vacuum state, known as the false vacuum. In 1978, Gennady Chibisov and Andrei Linde [174] attempted to construct a cosmological model based on the concept of exponential expansion in a supercooled vacuum, intending to provide a source for the universe's entropy. However, they encountered the issue of significant inhomogeneity resulting from collisions between bubble walls. In 1980, Alexei Starobinsky proposed a semi-realistic inflationary model based on conformal anomalies in quantum gravity [175]. This model, though rather intricate, made significant contributions, including the prediction of gravitational waves with a flat spectrum. Alan Guth's "old inflation" model, introduced in 1981, simplified the concept by addressing supercooling during phase transitions. While the original version faced challenges, it laid the groundwork for solving major cosmological issues. New insights emerged in 1981 with the invention of the "new inflationary theory", providing solutions to problems associated with earlier models. It introduced the idea that inflation could begin in an unstable state at the top of the effective potential, with the inflaton field gradually rolling down to the potential's minimum. This marked a significant departure from the false vacuum state and contributed to the homogeneity of the universe. A breakthrough came in 1983 with the chaotic inflation scenario [176], which fundamentally altered the perspective on inflation. It demonstrated that inflation could commence without the necessity of thermal equilibrium in the early universe, even in theories with simple potential functions. Chaotic inflation, underpinned by the existence of a sufficiently flat potential region allowing for the slow-roll regime, offered a more versatile framework for inflationary cosmology. This paradigm shift, occurring decades ago, has since become the dominant perspective, while the outdated idea of exponential expansion during high-temperature phase transitions in grand unified theories has largely been abandoned by many, though it continues to persist in some astrophysics textbooks. The progression of chaotic inflation marked a turning point, redefining the trajectory of cosmology as a theory.

1.6.2 Dynamics of Inflation

Following the formulation of Einstein's General Relativity, the exploration of its applications in understanding the dynamic structure of the entire universe became a focal point for researchers. To delve into the universe's large-scale structure effectively, it proves valuable to conceptualize the cosmos as a fluid, with galaxies serving as the constituent particles.

Beyond this foundational premise, cosmology rests on some core principles. *General Relativity* alone stands as a comprehensive framework for describing the vast-scale characteristics of the universe. The motion of galaxies finds its sole governance in gravitational forces generated by these galaxies themselves. This principle, often referred to as *Weyl's Principle* [177], translates into the idea that the world lines of galaxies form a spacetime-filling network of non-intersecting paths, akin to "fluid lines", all converging toward the past. The universe exhibits homogeneity, meaning it is the same at every point in space, and isotropy, indicating symmetry from any vantage point within space. These combined attributes form the basis of the *cosmological principle*.

Of particular significance, the cosmological principle implies that there exists no privileged observational standpoint within the universe. It further suggests that the universe's structure adheres to a constant curvature space. These foundational ideas lay the groundwork for deriving the line element ds^2 that characterizes an expanding universe, ultimately leading to the renowned Friedmann-Robertson-Walker (FRW) metric [178]:

$$ds^2 = dt^2 - a^2(t)\left[\frac{dr^2}{1-kr^2} + r^2(d\theta^2 + \sin^2\theta d\phi^2)\right] \tag{1.87}$$

Within this metric, (r, θ, ϕ) represent radial coordinates, while the parameter k encapsulates the geometry associated with constant curvature space (where $k = 0$ corresponds to flat space, $k = 1$

to spherical space, and $k = -1$ to hyperbolic space). The function $a(t)$ stands for the scale factor, offering insights into the evolution of spatial components as a function of cosmic time t.

The dynamics of the scale factor can be obtained by solving Einstein's equations under the assumptions of homogeneity and isotropy. The system of equations obtained is given by

$$\begin{aligned} 3\ddot{a} &= -4\pi G(\rho + 3p)a \\ \dot{a}^2 + k &= \frac{8\pi G}{3}\rho a^2 \end{aligned} \tag{1.88}$$

where p is the pressure term and ρ is the energy density. The Friedmann equation can be derived by combining these equations:

$$\dot{a}^2 + k = \frac{8\pi G}{3}\rho a^2. \tag{1.89}$$

Observational evidence suggests that our universe is spatially flat on large scales and can be well described by the Friedmann-Robertson-Walker (FRW) metric with $k = 0$. To better understand the causal structure of the FRW spacetime, it is convenient to write the metric in terms of conformal time τ:

$$ds^2 = a^2(\tau)(d\tau^2 - dx^2) \tag{1.90}$$

where $|dx| = d\tau$ represents the comoving distance that a particle can travel in $\Delta\tau$.

In standard Big Bang cosmology, we introduce the concept of *cosmological horizon* [179–181]. Imagine a signal emitted at the moment of the Big Bang ($t = 0$) that travels at the speed of light since then. We can ask what is the distance $l_H(t)$ that such signal covers from the point of its emission after a time $t > 0$, where $l_H(t)$ represents the size of the region causally connected by time t. This means that an observer living at time t cannot know in principle what has happened outside the sphere of radius $l_H(t)$, and therefore this sphere represents the observable part of the universe at time t. This sphere is called the cosmological horizon, and it increases in time as the horizon opens up.

If we choose coordinates such that we have an initial singularity at $t = 0$, then the maximum comoving distance that a particle can travel at $t > 0$ since that moment, is given by

$$\Delta\tau = \int_0^{t_0} \frac{dt'}{a(t')} = \int_{a(0)}^{a(t)} \frac{da'}{a'^2 H(a')} \tag{1.91}$$

where $H(a') = \dot{a}'/a'$ is the *Hubble parameter*, and it is commonly used to describe a characteristic scale within the expanding universe.

1.6.2.1 Field equations

To grasp the evolution of the metric that characterizes the universe, we turn to the fundamental equations governing it, famously known as the Einstein field equations. These equations stem from the variation of the Einstein-Hilbert action concerning the metric tensor, yielding the expression:

$$G_{\mu\nu} = 8\pi G T_{\mu\nu}. \tag{1.92}$$

Here, $G_{\mu\nu}$ represents the Einstein tensor, $T_{\mu\nu}$ is the energy-momentum tensor of the universe, and G denotes Newton's gravitational constant ($M_{PL} = (8\pi G)^{-1/2}$). For simplicity, we'll set M_P to unity, hence $M_P \equiv 1$. Given the universe's inherent homogeneity and isotropy, the form of the energy-momentum tensor is considerably constrained, taking on the general structure:

$$T_{\mu\nu} = (\rho + p)u_\mu u_\nu + pg_{\mu\nu}. \tag{1.93}$$

Here, $u_\mu \equiv \frac{dx_\mu}{d\tau}$ stands for the timelike 4-vector velocity, particularly in a frame that co-moves with the perfect fluid described by $T_{\mu\nu}$. In this co-moving frame, we can conveniently select $u_\mu = \{1, 0, 0, 0\}$. The terms ρ and p correspond to the (rest) energy density and (principal) pressure of the system, respectively. The conservation of the energy-momentum tensor, often referred to through the Bianchi identity $\nabla_\mu G^{\mu\nu} = 0$, leads to a fundamental equation known as the continuity equation for the fluid:

$$\frac{d\rho}{dt} + 3H(\rho + p) = 0.$$

This equation signifies the change in energy density ρ with respect to cosmic time t along with the influence of the Hubble parameter H in connection with the total energy density $\rho + p$. The conservation of energy-momentum is a critical aspect of understanding the dynamics of the universe.

We now introduce a final equation that establishes a connection between the energy density and the pressure within the perfect fluid. This equation is known as the equation of state:

$$p = w\rho. \tag{1.94}$$

It's important to note that, in general, the proportionality factor w can be a function of time. Using this equation, we can express the conservation of energy in the following manner:

$$\frac{\dot{\rho}}{\rho} = -3(1 + w)\frac{\dot{\alpha}}{\alpha}. \tag{1.95}$$

Solving this equation yields:

$$\rho(t) = \frac{\rho_0}{\alpha^{3(1+w)}}, \tag{1.96}$$

where ρ_0 represents an integration constant.

Let's further explore this concept by examining the time derivative of the Hubble parameter, which we'll denote as ϵ:

$$\epsilon = -\frac{\dot{H}}{H^2}. \tag{1.97}$$

This equation provides valuable insights. If $\epsilon < 1$, it indicates that the universe's expansion rate is accelerating. Conversely, if $\epsilon > 1$, the expansion rate decreases, signifying that the universe's expansion is decelerating.

We can also express Einstein's equations, assuming a flat space ($k = 0$), using equation (1.97):

$$H^2 = \frac{8\pi G}{3}\rho \tag{1.98}$$

and

$$(1 - \epsilon)H^2 = -\frac{4\pi G}{3}(\rho + 3p). \tag{1.99}$$

If we substitute equation (1.96) into equation (1.98), after some calculations we end up with the expression

$$a \sim t^{\frac{2}{3(1+w)}}. \tag{1.100}$$

Now, if we substitute this equation into equation (1.97), we find that ϵ remains constant:

$$\epsilon = \frac{3}{2}(1+w). \tag{1.101}$$

From this equation, we can deduce the following results:

- In the case of a radiation-dominated universe ($w = \frac{1}{3}$), $\epsilon = 2$, indicating decelerated expansion.
- For a matter-dominated universe ($w = 0$), $\epsilon = \frac{3}{2}$, also signifying decelerated expansion.
- In the general case of an inflationary universe, where $w \simeq -1$ and $\epsilon \ll 1$, the expansion is accelerating.

1.6.3 Slow Roll conditions

As demonstrated in the Appendix, in a universe dominated by a homogeneous scalar field, we have the acceleration equation (A.34) :

$$H^2(1-\epsilon) = \frac{\ddot{a}}{a} = -\frac{1}{6}(\rho + 3\phi),$$

where we've simplified the equation by setting $8\pi G = 1$. Additionally, when considering the dynamics of this field within the FRW geometry, we obtain the relation (A.33) :

$$H^2 = \frac{1}{3}\rho$$

which combined with eq.(A.79), we obtain :

$$H^2 = \frac{1}{3}\left(\frac{1}{2}\dot{\phi}^2 + V(\phi)\right). \tag{1.103}$$

Regarding the quantity ϵ (A.36), we can express it differently by using the relationship (1.103) and (A.81), like :

$$\frac{3}{2}(\omega+1) = \frac{3}{2}\left[\frac{\dot{\phi}^2}{\frac{1}{2}\dot{\phi}^2 + V}\right] = \frac{3}{2}\left[\frac{\dot{\phi}^2}{3H^2}\right] \Longrightarrow$$

$$\boxed{\epsilon = \frac{1}{2}\frac{\dot{\phi}^2}{H^2}} \tag{1.104}$$

This is referred to as the slow-roll parameter ϵ. We've observed how it can be connected to the Hubble parameter in eq.(A.32). We can reformulate this relationship by introducing the variable $dN = Hdt$, which leads to:

$$\epsilon = -\frac{\dot{H}}{H^2} = -\frac{1}{H}\frac{d\ln H}{dt} \Longrightarrow$$

$$\epsilon = -\frac{d\ln H}{dN}. \tag{1.105}$$

We observe that for an accelerated expansion to take place, the value of ϵ must adhere to the condition $\epsilon < 1$. In the de Sitter limit, where ϕ tends towards $-\rho$, the value of ϵ approaches zero. This implies that the potential energy surpasses the kinetic energy. However, there's another crucial factor to consider. Sustaining the accelerated expansion over an extended period requires the second time derivative of ϕ to be sufficiently small, expressed as :

$$\mid \ddot{\phi} \mid \ll \mid 3H\dot{\phi} \mid , \quad \mid V_{,\phi} \mid . \tag{1.106}$$

In this point we differentiate eq.(A.77) with respect to time t :

$$\ddot{\phi} + 3H\dot{\phi} = -V_{,\phi}$$

we obtain

$$3\dot{H}\dot{\phi} + 3H\ddot{\phi} = -\frac{d}{dt}\frac{d}{d\phi}V \Longrightarrow$$

we ignore the part $3\dot{H}\dot{\phi}$ and we take

$$3H\ddot{\phi} = -\dot{\phi}V_{,\phi\phi} \Longrightarrow$$

$$-\frac{3H^2\ddot{\phi}}{H\dot{\phi}} = V_{,\phi\phi} \tag{1.107}$$

Now we introduce a second slow-roll parameter :

$$\eta = -\frac{\ddot{\phi}}{H\dot{\phi}} = \epsilon - \frac{1}{2\epsilon}\frac{d\epsilon}{dN}, \tag{1.108}$$

so eq.(1.107) takes the final form (including the unit M_{PL} in order to be dimensionless) :

$$\boxed{\eta_\nu(\phi) \equiv M_{PL}^2 \frac{V_{,\phi\phi}}{V}}. \tag{1.109}$$

With the same way we can re-write eq.(1.104) expressed in terms of the inflationary potential :

$$\boxed{\epsilon_\nu(\phi) \equiv \frac{M_{pl}^2}{2}\left(\frac{V,\phi}{V}\right)^2}. \tag{1.110}$$

The background evolution that we used to arrive at the above relations is

$$\dot{\phi} \approx -\frac{V,\phi}{3H} \tag{1.111}$$

$$H^2 \approx \frac{1}{3}V(\phi) \approx constant. \tag{1.112}$$

Recapitulating, in the slow-roll regime

$$\epsilon_\nu, \mid \eta_\nu \mid \ll 1. \tag{1.113}$$

The initial condition is vital to guarantee an accelerated expansion, while the second condition is essential to maintain a minimal fractional change in ϵ per e-fold[11]. These parameters, denoted as ϵ_ν and η_ν, are referred to as *potential slow-roll parameters*, while ϵ and η are known as *Hubble slow-roll parameters*. The relationship between Hubble and potential slow-roll parameters can be expressed as follows :

$$\epsilon \approx \epsilon_\nu, \quad \eta \approx \eta_\nu - \epsilon_\nu. \tag{1.114}$$

Moreover, the inflation ends when we have a violation of the slow-roll conditions :

$$\epsilon(\phi_{end}) \equiv 1, \quad \epsilon_\nu(\phi_{end}) \approx 1. \tag{1.115}$$

Finally, we write down the number of e-folds before the end of inflation :

[11] An e-fold is defined as the amount of time over which the universe expands by a factor of e (natural logarithm). In other words, if the scale factor of the universe increases by e, it has undergone one e-fold of expansion.

$$N(\phi) \equiv \ln \frac{a_{end}}{a} = \int_t^{t_{end}} H dt$$

We change the variable of integration : $dt = \dfrac{d\phi}{\dot{\phi}}$ and using eq.(1.111) and eq.(1.112), we obtain

$$N(\phi) = \int_{\phi}^{\phi_{end}} \frac{H}{\dot{\phi}} d\phi \approx \int_{\phi_{end}}^{\phi} \frac{V}{V_{,\phi}} d\phi \tag{1.116}$$

This relation can be written in terms of ϵ and ϵ_ν as :

$$N(\phi) = \int_{\phi_{end}}^{\phi} \frac{d\phi}{\sqrt{2\epsilon}} \approx \int_{\phi_{end}}^{\phi} \frac{d\phi}{\sqrt{2\epsilon_\nu}} \tag{1.117}$$

It's important to emphasize that the total number of e-folds needed to address the horizon and flatness problems should exceed 50, meaning that we require N to be greater than or approximately equal to 60. The specific value of N is influenced by the details of reheating after inflation and the energy scale of inflation.

In cosmology, slow-roll parameters play a crucial role in understanding the scalar field dynamics during inflation. They are instrumental in calculating two significant observables: the scalar-to-tensor ratio (r) and the spectral index (n_s). These observables are essential for comparing theoretical models with observational data. The scalar-to-tensor ratio r is a parameter that quantifies the amplitude of tensor perturbations (primordial gravitational waves) relative to the density fluctuations (scalar perturbations) in the early universe, particularly in the cosmic microwave background (CMB). The formula for calculating r is as follows:

$$r = \frac{A_t}{A_s}. \tag{1.118}$$

It is closely connected to the slow-roll parameters through the relation:

$$r = 16\epsilon. \tag{1.119}$$

Typical values for the scalar-to-tensor ratio are constrained by observational data [29], and current measurements indicate that $r < 0.044$, and $\Delta_R^2 = A_s \simeq 2.1 \times 10^{-9}$. The spectral index is another crucial parameter that characterizes the primordial density fluctuations in the cosmic microwave background radiation. It describes the scale dependence of the amplitude of these fluctuations. The formula for calculating n_s is as follows:

$$n_s = 1 + \frac{d \ln A_s}{d \ln k}, \tag{1.120}$$

where $k = aH$ is a reference scale (at horizon exit) and is typically set at $0.02 Mpc^{-1}$. It is linked to the slow-roll parameters through the relation:

$$n_s = 1 - 6\epsilon + 2\eta. \tag{1.121}$$

Typical values for the spectral index are very close to 1, with only small deviations. Observations from the Planck mission, have measured n_s to be approximately 0.96 to 0.97. This indicates a nearly scale-invariant spectrum of density perturbations, with a value of $n_s = 1$ corresponding to perfect scale invariance.

1.6.4 Reheating

During cosmic expansion driven by inflation, the universe's energy is mostly stored as potential energy within a scalar field. To shift from this state to the familiar hot Big Bang cosmology we observe today, a conversion of this potential energy into particles and subsequent thermalization becomes necessary. This transformation, taking the universe from an inflationary phase to a hot and radiation-filled one, is termed as reheating [182–184].

Despite its name, reheating doesn't imply a prior thermal state but rather refers to the process of converting potential energy into thermalized particles. Reheating typically occurs as the scalar field responsible for inflation moves towards the minimum of its potential energy. This journey involves a dynamic interplay between potential and kinetic energy. Initially, the field releases its potential energy, converting it into kinetic energy. This sets the stage for the birth of various particles and the eventual thermalization of the universe.

The mechanisms driving reheating can differ based on the specific inflationary model at play. In single-field models, reheating may arise due to the breakdown of the slow-roll condition, signaling a shift in the field's behavior. In multi-field models, like hybrid inflation models, reheating can be triggered when the inflaton field reaches a critical value. This critical point sparks an instability, kickstarting the reheating process.

During reheating, the inflaton field decays into various particles, and the specific particles involved depend on the inflationary model, making reheating inherently model-dependent. A key parameter in this process is the reheating temperature (T_{RH}), and its general form is given by:

$$T_{RH} \simeq \mathscr{O}(0.1)\sqrt{M_P \Gamma} \tag{1.122}$$

where $M_P \approx 2.4 \times 10^{18} GeV/c^2$ stands for the reduced Planck mass, and Γ denotes the decay rate of the inflaton field, quantifying how quickly the inflaton converts its energy into other particles during reheating. In the forthcoming chapters, we will delve deeper into the analytical calculations and deductions related to this crucial process.

1.6.5 SUGRA vs. SUSY in Inflation

The scalar portion of the SUGRA [185–190] Lagrangian relies on three functions, all of which are functions of chiral superfields. The first of these functions is known as the Kähler potential, denoted as $K(\Phi_i, \Phi_i^*)$. It is composed of real functions of scalar fields and their conjugates but lacks holomorphicity. The second function is the superpotential, represented as $W(\Phi_i)$, while the third function is the gauge kinetic function $f(\Phi_i)$. Both the superpotential and the gauge kinetic function are holomorphic functions of complex scalar fields. The action for complex scalar fields minimally coupled to gravity encompasses both kinetic and potential terms:

$$S = \int d^4x\sqrt{-g}\left(\frac{1}{\sqrt{-g}}L_{\text{kinetic}} - V(\Phi_i, \Phi_i^*)\right) \quad . \tag{1.123}$$

Similar to the previous section on SUSY models, we encounter a potential composed of both an F-term and a D-term, denoted as $V = V_F + V_D$. However, in this case, the F-term is influenced by the superpotential W and the Kähler potential K:

$$V(\phi, \phi^*) = V_F + V_D = e^G\left[G_i(G^{-1})_{i\bar{j}}G_{\bar{j}} - 3\right] + V_D(\phi, \phi^*), \tag{1.124}$$

where $G = K + \ln(WW^*)$, and $G_{i\bar{j}}$ is given by:

$$G_{i\bar{j}}(\phi, \phi^*) \equiv \frac{\partial}{\partial \phi^i} \frac{\partial}{\partial \phi^{*\bar{j}}} K(\phi, \phi^*). \tag{1.125}$$

By substituting G into the above expression, we obtain:

$$V(\phi, \phi^*) = e^K \left[(K^{-1})_{i\bar{j}} (D_i W)(D_{\bar{j}} W^*) - 3WW^* \right] + V_D(\phi, \phi^*), \tag{1.126}$$

where $D_i W$ represents the Kähler covariant derivative of the superpotential W and is defined as:

$$D_i W = \frac{\partial}{\partial \phi^i} W + K_i W. \tag{1.127}$$

Finally, we define K in its canonical form as:

$$K = -3 \ln \left(-\frac{\Omega}{3} \right), \tag{1.128}$$

where Ω is the frame function:

$$\Omega = \phi_i^* \phi_i - 3 \ . \tag{1.129}$$

It's worth noting that the Kähler potential determines the kinetic term of the inflaton field (ϕ), given by $-K_{,\phi\phi^*} \partial\phi\partial\phi^*$, while the superpotential W governs the interactions in the model.

Chapter 2

Inflation with Supersymmetric $SO(10)$

2.1 Introduction

Supersymmetric models endowed with minimal renormalizable superpotentials and canonical Kähler potentials emerge as viable candidates to realize the successful framework of Hybrid Inflation [154]- [159]. In particular, these models allow for the implementation of an inflationary scenario using a minimal superpotential given by $\mathscr{W} = \kappa S(\bar{\phi}\phi - M^2)$, where $\bar{\phi}$ and ϕ represent superfields conjugate to each other, and S is a singlet scalar field. Here, κ stands as a small dimensionless parameter, while M denotes a high mass scale.

In the conventional hybrid inflationary scenario, the scalar field S assumes the role of the inflaton, gradually descending along a suitable scalar potential valley, with the fields ϕ and $\bar{\phi}$ responsible for terminating the inflationary phase. Moreover, a specific choice of the Kähler potential enables the implementation of quartic inflation with non-minimal coupling to gravity [160]. Despite the success of such an inflationary paradigm, a central challenge remains: integrating cosmology with the Standard Model of particle physics into a predictive unified theory. To address this issue, substantial efforts have been devoted to unifying various types of inflationary scenarios with particle physics theories [191]- [208]. In this work, we explore the incorporation of inflation within a realistic $SO(10)$ model, where the roles of ϕ and $\bar{\phi}$ are assumed by the Higgs fields in the representations $\underline{16}_H$ and $\overline{\underline{16}}_{\bar{H}}$. This setup successfully reproduces the MSSM at low energies. The $SO(10)$ GUT boasts several appealing features. Each of the three generations naturally includes the right-handed neutrino within the 16-representation of $SO(10)$, leading to the automatic realization of the seesaw mechanism. The model facilitates the generation of baryon asymmetry through leptogenesis [209, 210], and it effortlessly implements a doublet-triplet splitting mechanism without requiring fine-tuning [211]. The incorporation of a Z_2 matter parity occurs automatically, and the proton decay rate is naturally suppressed beyond current experimental limits [212, 213]. Additionally, intriguing features such as Yukawa unification have been explored in the literature [214, 215].

In the course of this exploration, we introduce an inflationary framework into a viable $SO(10)$ supersymmetric GUT, which reproduces the effective low-energy theory of the MSSM. The tree-level superpotential is endowed with an $\mathscr{R}$-symmetry that can eventually be broken by non-renormalizable terms. In our construction, a pair of $\underline{16}_H + \overline{\underline{16}}_{\bar{H}}$ representations and the $\underline{45}$ adjoint representation break $SO(10)$ GUT spontaneously down to the SM. Furthermore, the VEVs of a pair of $\underline{10}_H$ and $\underline{10}'_H$ representations, along with a second $\underline{45}'$ representation, generate masses for all fermions, including the right-handed neutrinos, and induce the necessary CKM mixing. A doublet-triplet splitting mechanism safeguards the Higgs doublets from acquiring large masses, and the proton decay rate is sufficiently suppressed.

2.2 The Model

We commence by outlining a promising supersymmetric $SO(10)$ model that incorporates an $\mathscr{R}$-symmetry. This symmetry remains intact for renormalizable terms but is assumed to be broken by non-renormalizable interactions. The model accommodates particle content in $\underline{10}, \underline{16}$, and $\underline{45}$ dimensional representations. Although higher-dimensional representations, such as $\underline{120}$ and $\underline{126}$, offer intriguing features, we opt to exclude them for two main reasons. First, we wish to maintain the possibility of embedding the model within a string theory framework, where generating large $SO(10)$ representations can be challenging. Second, a renormalization group analysis involving larger representations leads to large values of the gauge coupling constant at the unification scale (M_{GUT}), causing the breakdown of the perturbative approach [216].

The matter and Higgs content of the model is structured as follows: The fifteen fermions, which fit into $10 + \bar{5}$ representations of $SU(5)$, along with the right-handed neutrino in each generation, are accommodated in the $\underline{16}$ representation of $SO(10)$. The SM Higgs fields, found in $5_H + \bar{5}_{\bar{H}}$ representations of $SU(5)$, constitute the $\underline{10}$ representation of $SO(10)$. The breaking of $SO(10)$ to $SU(5)$ and subsequently to the SM is achieved through a pair of $\underline{16}_H + \overline{\underline{16}}_H$ representations and the $\underline{45}$ adjoint representation. Additionally, we introduce a $\underline{10}'$ representation of $SO(10)$, an extra adjoint represented by $\underline{45}'$, and an $SO(10)$ singlet denoted as S. To describe the decomposition of $SO(10)$ representations under $SU(5) \times U(1)_\chi$, we employ the following charge assignments:

$$\underline{16} \rightarrow 10_{-1} + \bar{5}_3 + 1_{-5}, \tag{2.1}$$
$$\underline{10} \rightarrow 5_2 + \bar{5}_{-2}, \tag{2.2}$$
$$\underline{45} \rightarrow 24_0 + 1_0 + 10_4 + \overline{10}_{-4}. \tag{2.3}$$

Subsequently, we ensure that the renormalizable superpotential maintains its invariance under an $\mathscr{R}$-symmetry by assigning to the fields the $\mathscr{R}$-charges as presented in Table 2.1. These charges are essential for preserving the symmetry of the theory and are a fundamental aspect of our model. It is noteworthy that the superpotential itself carries an $\mathscr{R}$-charge of 1. Table 2.1 provides a compre-

Representation:	$\underline{16}_i$	$\underline{10}_H$	$\underline{10}'_H$	$\underline{16}_H$	$\overline{\underline{16}}_{\bar{H}}$	$\underline{45}$	$\underline{45}'$	S
$\mathscr{R}$-symmetry:	$\frac{1}{2}$	0	1	0	0	1	0	1

Table 2.1: $SO(10)$ superfields along with their corresponding charges under the $\mathscr{R}$-symmetry.

hensive overview of the $\mathscr{R}$-charges assigned to the different $SO(10)$ superfields. Each superfield's $\mathscr{R}$-charge is carefully chosen to ensure the consistency and integrity of the $\mathscr{R}$-symmetry within the model. This symmetry plays a crucial role in governing the dynamics and interactions of the fields, ultimately shaping the physical properties and behavior of the system.

2.2.1 The Superpotential

Within this section, our focus shifts to an in-depth examination of the superpotential terms. A critical element to consider is the tree-level term denoted as $\underline{16}_i \cdot \underline{16}_j \cdot \underline{10}_H$, notable for its invariance under both $\mathscr{R}$-symmetry and $SO(10)$. This term plays a pivotal role as it confers mass upon the three families of charged fermion fields. Additionally, it introduces Dirac masses for the neutrinos, specifically ν_j^c. However, to achieve suitably substantial Majorana masses for ν_j^c and effectively implement the seesaw mechanism, additional terms are deemed necessary. It is essential to highlight that relying solely on the vacuum expectation value (VEV) of a solitary 10-plet proves insufficient for generating the requisite CKM mixing, a point underscored in [216]. To address these challenges effectively, the incorporation of a second 10-plet ($\underline{10}'$) and two instances of the $SO(10)$ adjoint fields, denoted as $\underline{45}_H$ and $\underline{45}'$, becomes imperative. These additions prove instrumental in overcoming the previously mentioned issues. The relevant renormalizable and fourth-order superpotential terms are outlined below:

$$\begin{aligned}\mathscr{W} \supset\, & y\, \underline{16}_i \cdot \underline{16}_j \cdot \underline{10}_H + \frac{1}{M_*}\; \underline{16}_i \cdot \underline{16}_j \cdot \underline{10}'_H \cdot (c_1 \underline{45}_H + c_2 \underline{45}') \\ & + \frac{1}{M_*} \underline{16}_i \cdot \underline{16}_j \cdot \left(\lambda_N\, \overline{\underline{16}}_H \cdot \overline{\underline{16}}_H + \lambda'_N\, \underline{16}_H \cdot \underline{16}_H\right).\end{aligned} \tag{2.4}$$

In the above equation, the symbols y, $c_{1,2}$, λ_N, and λ'_N represent dimensionless coupling constant coefficients, while M_* signifies the cutoff scale of the theory. It is vital to acknowledge that the terms associated with $\underline{10}'_H$ contribute to the charged sector at higher orders and are subject to suppression, typically by a factor of $\frac{\langle 45 \rangle}{M_*} \sim \frac{M_{GUT}}{M_*}$, generally on the order of $\mathscr{O}(10^{-1})$. These contributions, although subleading concerning fermion masses hold substantial importance due to their introduction of a second $\underline{10}'$-plet, a critical element in generating the desired CKM mixings. The relevance of the product $\underline{10}'_H \cdot \underline{45}_H$ is analogous to that of the $\underline{120}_H$, which has been omitted in this work due to previously discussed perturbativity concerns. When this term is decomposed within the framework of the SM gauge symmetry, the ensuing mass terms can be expressed as follows:

$$\underline{16}_i \cdot \underline{16}_j \cdot \underline{10}'_H \cdot \underline{45}_H \to (Q_i u_j^c - 3\ell_i \nu_j^c) h_u + (Q_i d_j^c - 3\ell_i e_j^c) h_d + \cdots .$$

Of note is the introduction of a numeric factor of -3 into the charged lepton and neutrino mass terms, originating from the $\underline{45}_H$ VEV along the $B-L$ direction. This factor assumes paramount importance as it serves to differentiate the down quark mass matrix from the charged leptons, thereby establishing the Georgi-Jarlskog mass relation and ensuring the correct mass relations at low energy scales. Furthermore, the term $\underline{16}_i \underline{16}_j \overline{\underline{16}}_H \overline{\underline{16}}_H / M_*$ takes center stage by providing Majorana masses for the right-handed neutrinos at an order approximately equal to $\frac{\langle 16_H \rangle^2}{M_*} \sim \frac{M_{GUT}^2}{M_*}$. The additional term, $\underline{16}_i \underline{16}_j \underline{16}_H \underline{16}_H / M_*$, plays a crucial role in shaping the CKM matrix. More specifically, in the context of the $SU(5)$ group, the first term leads to the following expressions:

$$\frac{\lambda_N}{M_*} \underline{16}_i \cdot \underline{16}_j \cdot \overline{\underline{16}}_H \cdot \overline{\underline{16}}_H \to \frac{\lambda_N}{M_*} \left(10_i 10_j 5_H \overline{1}_H + 1_i 1_j \overline{1}_H \overline{1}_H\right) + \cdots . \tag{2.5}$$

In this context, the singlets $1_i, 1_j$ are identified as the right-handed neutrinos, $\nu_{i,j}^c$, while the singlets $1_H, \overline{1}_H$ correspond to $\nu_H^c, \overline{\nu}_H^c$, thus, the second term on the right-hand side yields Majorana masses approximately given by:

$$M_{N_i} \approx \lambda_{N_i} \frac{\langle \nu_{\bar{H}} \rangle^2}{M_*} \sim \frac{M_{GUT}^2}{M_*} . \tag{2.6}$$

Throughout the remainder of this work, we adopt the notation $\nu_i^c = N_i$, and we assume a "natural" hierarchy with M_{N_1} being smaller than M_{N_2} and M_{N_3} ($M_{N_1} < M_{N_2} < M_{N_3}$). Consequently, the light Majorana masses can be estimated as:

$$m_{\nu_i} \sim \frac{m_{\nu_D}^2}{M_{N_i}} \sim \lambda_{N_i}^{-1} \frac{m_{\nu_D}^2}{M_{GUT}^2} M_* \,. \tag{2.7}$$

In this equation, m_{ν_D} denotes the Dirac mass of the neutrino, arising from the coupling between the left- and right-handed neutrino fields through interactions with Higgs fields. The light neutrino masses, m_{ν_i}, are inversely proportional to M_{N_i}, illustrating the “seesaw” effect: as the heavy right-handed neutrino masses increase, the resulting masses for the left-handed neutrinos become correspondingly small. This expression, forms the basis for the subsequent analysis of the heavy fields within the model.

Deriving Heavy Majorana Neutrino Masses

To uncover insights into the heavy Majorana neutrino masses, we turn to neutrino oscillation experiments and a chosen neutrino mass spectrum. Latest analyses [217] of experimental data, assuming normal hierarchy, yield the following mass-squared differences for the physical neutrino states:

$$\begin{aligned} \Delta m_{31}^2 &\approx 2.5 \times 10^{-3} eV^2, \\ \Delta m_{21}^2 &\approx 7.39 \times 10^{-5} eV^2. \end{aligned} \tag{2.8}$$

Leveraging equation (2.7) and assuming $m_{\nu_3} > m_{\nu_2} > m_{\nu_1}$, we can deduce:

$$M_{N_3} \approx \frac{m_{\nu_D}^2}{m_{\nu_3}} \approx \frac{m_{top}^2}{\sqrt{\Delta m_{32}^2}} \sim 10^{14}\text{GeV},$$

which represents the mass of the heaviest right-handed neutrino. This estimation is predicated on the assumption that Dirac neutrino masses are roughly equivalent to the corresponding up-type quark masses ($m_{\nu_{Di}} \approx m_{u_i}$). Similarly, we can determine the ratio between M_{N_2} and M_{N_3} based on equation (2.7):

$$\frac{M_{N_2}}{M_{N_3}} \approx \frac{m_{charm}^2}{m_{top}^2} \sqrt{\frac{\Delta m_{32}^2}{\Delta m_{21}^2}} \sim 10^{-4},$$

leading to $M_{N_2} \approx 10^{10}$ GeV. The coupling $\underline{16}_i \underline{16}_j \underline{16}_H \underline{16}_H / M_*$ yields the following terms:

$$\frac{\lambda'_N}{M_*} \underline{16}_i \cdot \underline{16}_j \cdot \underline{16}_H \cdot \underline{16}_H \to \frac{\lambda'_N}{M_*} \left(10_i \bar{5}_j \bar{5}_H 1_H + 10_H \bar{5}_H \bar{5}_i 1_j\right).$$

This term’s significance lies in its contribution to the down quark mass matrix, effectively distinguishing up and down quark contributions [213]. Thus, it serves as a secondary source of CKM mixing within the present model. Shifting our focus to the Higgs sector, we encounter $\mathscr{R}$-symmetry preserving renormalizable terms:

$$\begin{aligned} \mathscr{W}_H \supset\ & \underline{10}_H \cdot \underline{45}' \cdot \underline{10}'_H + M_{10} \underline{10}_H \cdot \underline{10}'_H + M_{45} \underline{45} \cdot \underline{45}' \\ & + (\underline{16}_H \cdot \underline{16}_H - \overline{\underline{16}}_H \cdot \overline{\underline{16}}_H) \underline{10}'_H + \lambda_A \overline{\underline{16}}_H \cdot \underline{45} \cdot \underline{16}_H . \end{aligned} \tag{2.9}$$

It is important to note that tree-level mass terms of the form $M_{10}\underline{10} \cdot \underline{10}$ and $M_{16}\underline{16}_H\underline{16}_H$ are incompatible with the imposed $\mathscr{R}$-symmetry on the superpotential. Additionally, the term $\underline{10}_H \cdot \underline{45} \cdot \underline{10}_H$ does not contribute due to antisymmetry. Furthermore, there exist terms involving the singlet field S, which plays a pivotal role in inflation and will be subject to analysis in upcoming sections. We now delve into the dynamics of the additional heavy fields introduced within the framework of this model.

2.2.2 Masses of Color Triplets and Doublet-Triplet Splitting

In the context of the $SO(10)$ representations outlined earlier, it's crucial to account for various fields that go beyond the MSSM spectrum, particularly those involving color triplets. These triplets have interactions with SM matter and must possess sufficient mass to prevent undesirable processes that violate baryon numbers. Before we proceed, it's necessary to ensure that the low-energy effective model does not contain undesired states. The components 10_H, $\overline{10}_{\bar{H}}$, 5_H, and $\bar{5}_{\bar{H}}$ within $\overline{\underline{16}}_{\bar{H}}$ and $\underline{16}_H$ in $SU(5)$ receive masses from the trilinear term:

$$\lambda_A \overline{\underline{16}}_H \cdot \underline{45} \cdot \underline{16}_H = \lambda_A(\overline{10}_H + 5_H + \bar{1}_H)(24_0 + 1_0 + 10_4 + \overline{10}_{-4})(10_H + \bar{5}_H + 1_H).$$

This term involves VEVs, such as $\langle \bar{\nu}^c_H \rangle$ and $\langle \underline{45} \rangle$, which break $SO(10)$ down to the SM. There's also an additional bilinear gauge-invariant mass term for the 10-plets of $SU(5)$:

$$M_{45}\underline{45} \cdot \underline{45}' \to M_{45}(\overline{10}_{-4} \cdot 10' + \overline{10}'_{-4} \cdot 10).$$

In the basis defined by the $SU(5)$ 10-plet fields $10'_4$, 10_4, and 10_H, we obtain the mass matrix:

$$\mathscr{M}_{10} = \begin{pmatrix} 0 & M_{45} & 0 \\ M_{45} & 0 & \lambda_A \langle \nu^c_H \rangle \\ 0 & \lambda_A \langle \bar{\nu}^c_H \rangle & \lambda_A \langle A \rangle \end{pmatrix},$$

where $\langle 24_0 + 1_0 \rangle = \langle A \rangle$. The eigenmasses M_{10_j} are of order:

$$M_{10_j} \approx \lambda_A \langle A \rangle \text{ and } \pm \sqrt{M_{45}^2 + \lambda_A^2 \langle \nu^c_H \rangle^2}.$$

The masses of $(\overline{10}, 10)$ $SU(5)$-pairs depend on the dimensionless parameter λ_A and the mass scale M_{45}, which will be crucial for the subsequent inflationary analysis. The issue of doublet-triplet splitting in the $5_h, \bar{5}_h \in 10_h$ of $SO(10)$ is elegantly addressed by implementing the mechanism from [212]. In this construction, it's realized using the terms $\underline{10} \cdot \underline{45} \cdot \underline{10}' + M_{10}\underline{10} \cdot \underline{10}'$ and a $\underline{45}$-VEV along a specific direction:

$$\langle 45 \rangle = \begin{pmatrix} \alpha & 0 & 0 & 0 & 0 \\ 0 & \alpha & 0 & 0 & 0 \\ 0 & 0 & \alpha & 0 & 0 \\ 0 & 0 & 0 & \beta & 0 \\ 0 & 0 & 0 & 0 & \beta \end{pmatrix} \otimes \begin{pmatrix} 0 & 1 \\ -1 & 0 \end{pmatrix}.$$

To protect the doublets and keep them light down to the electroweak scale, we must fine-tune the parameter β to be roughly of the same order as M_{10}. Given that M_{10} is on the order of M_{GUT}, the colored triplets acquire superheavy masses, sufficiently suppressing baryon decay-violating processes. As we conclude this section, it's worth noting that the threshold effects associated with the extra color triplets, which attain masses near the GUT scale, have minimal impact on the renormalization group running of the gauge couplings. Thus, after the $SO(10)$ breaking, the gauge coupling running is primarily determined by the MSSM spectrum, achieving unification at a scale around $M_{GUT} \sim 10^{16}$ GeV. One specific threshold effect is related to the masses of the right-handed neutrinos, which, as previously observed, lie in the intermediate range of $\sim 10^{12}$-10^{14} GeV. These right-handed neutrino thresholds have implications for b-τ unification, particularly the prediction of $m_b^0 = m_\tau^0$ at the GUT scale, a well-known feature of $SO(10)$ models. This prediction aligns with the experimentally observed low-energy masses m_b and m_τ. It has been shown that maintaining m_b-m_τ unification at the GUT scale is possible, provided there is sufficient mixing between the second and third generations in the charged lepton mass matrix. This requirement also aligns with the explanation of atmospheric neutrino mixing.

2.3 Inflation

The $SO(10)$ model developed in the previous sections successfully reproduces the MSSM spectrum in the low-energy limit. Moreover, the incorporation of an $\mathscr{R}$-symmetry and the implementation of the doublet-triplet mechanism address several well-known issues of low-energy effective theories derived from GUTs. In this section, we explore how this supersymmetric $SO(10)$ model provides all the essential components for realizing a successful inflationary scenario. The tree-level terms that preserve the $\mathscr{R}$-symmetry and involve the singlet field S, playing a crucial role in inflation, are as follows:

$$\mathscr{W}_S = \kappa\, S\,(\underline{16}_H \cdot \overline{\underline{16}}_H + \lambda\, \underline{45}'\underline{45}' + \lambda_{10}\, \underline{10}_H \cdot \underline{10}_H - M^2).$$

In this model, inflation is driven by the conjugate pair of Higgs fields $\underline{16}_H$ and $\overline{\underline{16}}_{\bar{H}}$, which we denote as:

$$\underline{16}_H \to \phi \;\text{ and }\; \overline{\underline{16}}_H \to \bar{\phi}, \tag{2.10}$$

respectively. Similarly, for the corresponding fields in $\underline{45}$ and $\underline{45}'$, we use the notation:

$$\underline{45} \to a, \;\text{ and }\; \underline{45}' \to b\;. \tag{2.11}$$

To implement non-minimal quartic inflation, following references [160,218], we introduce the Kähler potential:

$$\Phi = 1 - \frac{1}{3}\left(|\phi|^2 + |\bar{\phi}|^2 + |S|^2 + |a|^2 + |b|^2\right) + \frac{1+6\xi}{3}\left(\bar{\phi}\phi + h.c + \cdots\right), \tag{2.12}$$

where the fields are measured in Planck units, $M_{Pl} \approx 2.44 \times 10^{18}$ GeV, and ξ is a dimensionless parameter.

2.3.1 Slow Roll Parameters

To assess the compatibility of the proposed inflationary model with cosmological data [219], we need to compute key inflationary observables, including the slow roll parameters η and ϵ. Here, we provide a brief overview of the fundamental components, following the notation of [220]. The action in the Jordan frame is given by:

$$S = \int d^4x\sqrt{-g}\left(f(\phi)\,R + k(\phi)\frac{1}{2}g^{\mu\nu}\partial_\mu\phi\partial_\nu\varphi - \frac{\lambda_0}{16}\phi^4 - \lambda_N\frac{\phi^2}{M_*}NN\right),$$

where the last term arises from (2.5). For simplicity, we include only one neutrino species for now, which is sufficient to describe the desired inflationary effects. Regarding the functions f and k, in this case, we take:

$$f(\phi) = -\frac{1}{2}(1+\xi\phi^2), \quad k(\phi) = 1.$$

This choice corresponds to the Lagrangian of quartic inflation with a non-minimal gravitational coupling in the Jordan frame [221]. To obtain canonical kinetic energy in the Einstein frame, we introduce a new field σ related to ϕ by:

$$\left(\frac{d\sigma}{d\phi}\right)^2 = \frac{k(\phi)}{f(\phi)} + \frac{3}{2}\left(\frac{f'(\phi)}{f(\phi)}\right)^2 = \frac{1+\xi(1+6\xi)\phi^2}{(1+\xi\phi^2)^2}.$$

The action in the Einstein frame is expressed as:

$$S_E = \int d^4x\sqrt{-g_E}\left(-\frac{1}{2}R_E + \frac{1}{2}(\partial\sigma)^2 - V_E(\sigma(\phi))\right),$$

with the potential given by:

$$V_E = \frac{\lambda_0}{16}\frac{\phi^4}{(1+\xi\phi^2)^2}. \tag{2.13}$$

This particular setup has been successfully realized in supersymmetric $SO(10)$ GUTs [160]. Any modifications due to quantum corrections have also been studied [221]. The slow-roll parameters, expressed in terms of the original scalar field ϕ, are as follows:

$$\begin{aligned}
\epsilon(\phi) &= \frac{1}{2}\left(\frac{V_E'}{V_E\sigma'}\right)^2,\\
\eta(\phi) &= \frac{V_E''}{V_E(\sigma')^2} - \frac{V_E'\sigma''}{V_E(\sigma')^3},\\
\zeta(\phi) &= \left(\frac{V_E'}{V_E\sigma'}\right)\left(\frac{V_E'''}{V_E(\sigma')^3} - 3\frac{V_E''\sigma''}{V_E(\sigma')^4} + 3\frac{V_E'(\sigma'')^2}{V_E(\sigma')^5} - \frac{V_E'\sigma'''}{V_E(\sigma')^4}\right).
\end{aligned} \tag{2.14}$$

In the context of slow-roll inflation, the conditions $\epsilon \ll 1$, $\eta \ll 1$, and $\zeta^2 \ll 1$ must be satisfied. These conditions ensure that inflation occurs smoothly. Key inflationary observables include the scalar spectral index n_s, the tensor-to-scalar ratio r, and the running of the spectral index $\alpha_s = \frac{dn_s}{d\ln k}$. They are calculated as follows:

$$\begin{aligned}
n_s &= 1 - 6\epsilon + 2\eta,\\
r &= 16\epsilon,\\
\alpha_s &= 16\epsilon\eta - 24\epsilon^2 - 2\zeta.
\end{aligned} \tag{2.15}$$

Additionally, we consider the number of e-folds N and the amplitude of the curvature perturbation Δ_R^2:

$$\begin{aligned} N &= \frac{1}{\sqrt{2}} \int_{\phi_f}^{\phi_0} \frac{d\phi}{\sqrt{\epsilon}} \frac{d\sigma}{d\phi}, \\ \Delta_R^2 &= \left. \frac{V_E}{24\pi^2 \epsilon} \right|_{k_0}, \end{aligned} \tag{2.16}$$

where ϕ_0 represents the inflaton value at the horizon exit of the scale corresponding to the pivot scale k_0, and ϕ_f is the value of ϕ at the end of inflation (i.e., when $\epsilon = 1$). The pivot scale is set to $k_0 = 0.002\ \mathrm{Mpc}^{-1}$, and the number of e-folds is taken to be approximately $N \approx 55 - 60$. By satisfying the constraint $\Delta_R^2 = (2.0989 \pm 0.101) \times 10^{-9}$ [219], we can express the predictions of the model in terms of its various parameters.

2.3.2 The Effective Potential

Now, let's delve into the predictions of our model, specifically focusing on the effective potential. We'll begin with the canonical Kähler potential mentioned in (2.12). Using the notation introduced in equations (2.10) and (2.11), and setting $\phi = \bar{\phi} = \varphi/2$, the relevant tree-level superpotential terms for inflation can be expressed as:

$$\mathscr{W} = \kappa s(\bar{\varphi}\varphi/4 + \lambda b^2 - M^2) + M_{45} ab + \frac{\lambda_A}{4} \bar{\varphi} a \varphi. \tag{2.17}$$

To calculate the scalar potential, we require the Kähler matrix, denoted as $\mathscr{M}$, which is given by:

$$\mathscr{M} = 3 \begin{pmatrix} \frac{3(1+\xi\varphi^2)-a^2-b^2-s^2}{3} & -\frac{s}{3} & \xi\varphi & \xi\varphi & -\frac{a}{3} & -\frac{b}{3} \\ -\frac{s}{3} & -\frac{1}{3} & 0 & 0 & 0 & 0 \\ \xi\varphi & 0 & -\frac{1}{3} & 0 & 0 & 0 \\ \xi\varphi & 0 & 0 & -\frac{1}{3} & 0 & 0 \\ -\frac{a}{3} & 0 & 0 & 0 & -\frac{1}{3} & 0 \\ -\frac{b}{3} & 0 & 0 & 0 & 0 & -\frac{1}{3} \end{pmatrix}.$$

For convenience, we also define a "vector" involving the corresponding derivatives of the superpotential:

$$\vec{v}^T = \{3\mathscr{W}, \frac{\partial \mathscr{W}}{\partial s}, \frac{\partial \mathscr{W}}{\partial \varphi}, \frac{\partial \mathscr{W}}{\partial \bar{\varphi}}, \frac{\partial \mathscr{W}}{\partial a}, \frac{\partial \mathscr{W}}{\partial b}\}.$$

The effective potential, denoted as V_{eff}, is then defined as:

$$V_{\mathrm{eff}} = -\vec{v}^T \mathscr{M}^{-1} \vec{v}, \tag{2.18}$$

where $V_E = \frac{V_{\mathrm{eff}}}{\Phi^2}$, and Φ is defined in (2.12). In the subsequent section, we will derive the analytical form of the potential based on (2.18) and explore the conditions on the model's parameters and spectrum to ensure a successful inflationary scenario.

2.4 Analysis

The effective potential, denoted as V_{eff}, relies on the fields φ, s, a, b within the parameter space defined by $\xi, \kappa, \lambda_A, M, M_{45}$. It is conceivable that this potential possesses numerous minima. In a more general context, the non-zero VEVs of the two $SO(10)$ adjoints, namely a and b, are typically expected to align with the GUT scale. To maintain generality, we consider a scenario where these adjoint VEVs are related by an order-one constant, denoted as $\gamma = \mathcal{O}(1)$, which can be absorbed into the unknown coefficients. If the adjoint field a (and, consequently, b) attains GUT-scale values during inflation, it effectively mitigates the monopole problem. Although the exact potential is complex, we can make a reasonable approximation based on the observation that the GUT scale is two orders of magnitude smaller than the Planck mass, allowing us to assume that $a \ll 1$. In this limit, particularly when $s = 0$, the potential can be approximated as follows:

$$
\begin{aligned}
V(\phi) &\approx \frac{\lambda_A^2 \varphi^4 + \kappa^2 \left(4M^2 - \varphi^2\right)^2}{16\left(1+\xi\varphi^2\right)^2} + \frac{\lambda_A\, M_{45}\varphi^2\, a}{2\sqrt{2}\left(1+\xi\varphi^2\right)^2} + O\left(a^2\right) \\
&\approx \frac{\lambda_A^2}{16}\frac{\varphi^4}{\left(1+\xi\varphi^2\right)^2} + \frac{\lambda_A\, M_{45}\varphi^2\, a}{2\sqrt{2}\left(1+\xi\varphi^2\right)^2}\,.
\end{aligned}
\tag{2.19}
$$

The first term mirrors the potential in Eq (2.13) with $\lambda_0 = \lambda_A^2$, while the second term represents the contribution arising from the adjoint fields. This approximation holds when $\lambda_A\varphi^2 \gg 4\sqrt{2}M_{45}a$. It's important to note that both M_{45} and a are significantly smaller than the Planck scale, given their association with the $SO(10)$ breaking scale, where $M_{45} \ll 1$ and $a \ll 1$. Therefore, this approximation is valid, especially in the vicinity of the potential maximum where φ assumes relatively large values. We proceed to employ equations (2.15) and (2.16) to compute the slow-roll parameters and investigate their effects on various model parameters, while considering the latest Planck constraints [219]. To evaluate the inflationary predictions of the model, we focus on the $s = 0$ trajectory at $\varphi = \varphi_0$. This involves a systematic procedure: First, we enforce the constraint arising from the amplitude of the curvature perturbation, $\Delta_R^2 = (2.0989 \pm 0.101) \times 10^{-9}$. Then, while keeping the number of e-folds constant, we express the observables in terms of the model parameters, including λ_A, ξ, κ, and the mass scales a, M, M_{45}. Notably, the model's predictions are relatively insensitive to variations in κ and M. Therefore, we simplify the parameter space by setting $\kappa \sim 10^{-6}$ and $M \sim (10^{-8})M_{PL}$. Consequently, we vary ξ, a, M_{45}, and the coupling constant λ_A. In the scenario discussed previously, the coupling λ_A is the square of the coupling in Eq (2.13), i.e., $\lambda_0 = \lambda_A^2$. In comparison to the highly constrained minimal ϕ^4 model, this particular case offers increased flexibility due to the presence of new degrees of freedom, such as the adjoint VEV denoted as $a = \langle \underline{45} \rangle$ and the mass parameter M_{45}.

Inflationary Predictions and Constraints

The inflationary predictions of our model are visually presented in Figure 2.1. This plot showcases solutions for the tensor-to-scalar ratio r and the spectral index n_s, along with Planck's 1-σ (dark blue) and 2-σ (light blue) data contours. We provide two curves: one on the left in red, corresponding to $N = 55$ e-folds, and the other on the right in orange, representing $N = 60$ e-folds. Each curve features data points for various values of ξ, specifically $\xi = 0, 10^{-3}, 10^{-2}, 0.02, 0.05, 0.3, 0.6, 1, 10, 100, 280$, arranged from top to bottom. For $\xi = 0$, our predictions naturally fall outside the realm of observational data. However, with $N = 55$ e-folds and $\xi \geq 10^{-2}$, we notice the results converging with the

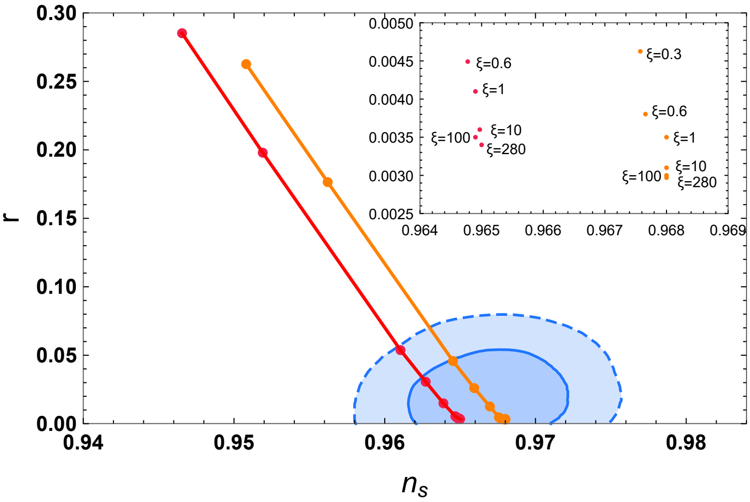

Figure 2.1: Solutions in the (n_s-r) plane for varying ξ values. The number of e-folds was taken as $N = 55$ (red curve) and $N = 60$ (orange). The dots on the curves correspond to $\xi = 0, 10^{-3}, 10^{-2}, 0.02, 0.05, 0.3, 0.6, 1, 10, 100, 280$, top to bottom. The blue solid (dashed) contours correspond to 1-σ (2-σ) Planck's data based on TT, TE, EE+lowE+lensing+BK14+BAO in [219]. For $\xi = 280$, the tensor to scalar ratio is $r_{min} \approx 0.0034$ and $r_{min} \approx 0.0030$ for $N = 55$ and $N = 60$ accordingly.

				N=55				
ξ	ϕ_f/M_{Pl}	ϕ_0/M_{Pl}	n_s	r	$-\alpha_s/10^{-4}$	λ_A	$a = \langle 45\rangle/M_{Pl}$	M_{45}/M_{Pl}
1	0.98	8.1	0.9649	0.0041	2.488	$4.56{\cdot}10^{-5}$	$1.8{\cdot}10^{-3}$	$1.56{\cdot}10^{-4}$
10	0.33	2.74	0.96497	0.0036	5.578	$4.26{\cdot}10^{-4}$	$1.39{\cdot}10^{-3}$	$2.53{\cdot}10^{-4}$
100	0.106	0.875	0.9649	0.0035	1.614	$4.25{\cdot}10^{-3}$	$1.24{\cdot}10^{-4}$	$2.02{\cdot}10^{-3}$
280	0.06	0.51	0.9650	0.0034	2.760	$1.18{\cdot}10^{-2}$	$1.01{\cdot}10^{-2}$	$8.66{\cdot}10^{-5}$
				N=60				
ξ	ϕ_f/M_{Pl}	ϕ_0/M_{Pl}	n_s	r	$-\alpha_s/10^{-4}$	λ_A	$a = \langle 45\rangle/M_{Pl}$	M_{45}/M_{Pl}
1	0.99	8.47	0.968	0.0035	2.002	$4.20{\cdot}10^{-5}$	$1.35{\cdot}10^{-3}$	$1.24{\cdot}10^{-4}$
10	0.32	2.78	0.968	0.0031	4.659	$3.91{\cdot}10^{-4}$	$1.96{\cdot}10^{-4}$	$5.1{\cdot}10^{-3}$
100	0.11	0.91	0.968	0.0030	1.325	$3.89{\cdot}10^{-3}$	$1.24{\cdot}10^{-4}$	$2.03{\cdot}10^{-3}$
280	0.06	0.53	0.968	0.00297	2.263	$1.09{\cdot}10^{-2}$	$1.01{\cdot}10^{-2}$	$8.59{\cdot}10^{-5}$

Table 2.2: A collection of characteristic values of the parameters involved in the analysis along with the corresponding output for the spectral index n_s, the tensor to scalar ratio r and the running of the spectral index α_s.

Planck contours. Furthermore, when $\xi \gtrsim 0.3$, the solutions primarily cluster around a region characterized by $r \sim 0.0035$ and $n_s = 0.965$. Similar trends emerge for $N = 60$, with solutions shifting towards the lower right. Precisely, for $\xi \lesssim 10^{-3}$, our results deviate from the Planck data, but for $1 \lesssim \xi \leqslant 280$, we obtain consistent solutions featuring $r \sim 0.003$ and $n_s \approx 0.968$. This is depicted in the zoom-in plot added to the upper-right corner of Figure 2.1. In this analysis, we maintain certain parameter values: $\lambda_A \sim (10^{-5} - 10^{-2})$, $a \sim (10^{-4} - 10^{-2})$, and $M_{45} \sim (10^{-5} - 10^{-3})$. Within this parameter space, the running of the spectral index is estimated to be $|\alpha_s| \sim 10^{-4}$. Table 2.2 provides a detailed collection of parameter values and corresponding outcomes for spectral index n_s, tensor-to-scalar ratio r, and the running of the spectral index $-\alpha_s/10^{-4}$ for both $N = 55$ and

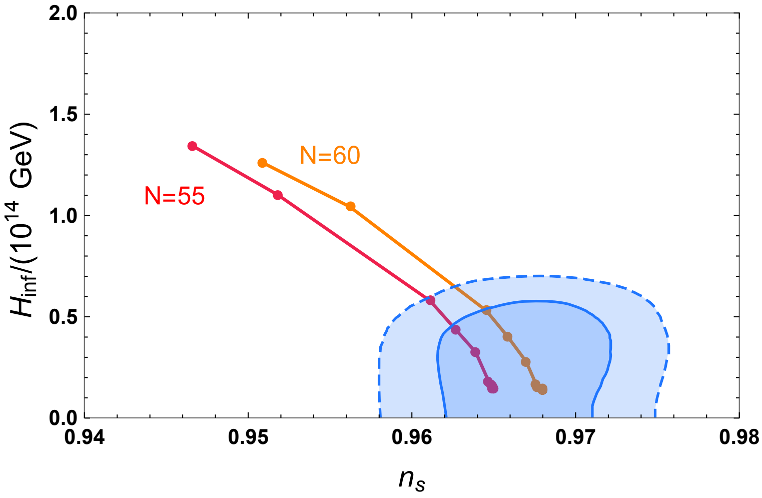

Figure 2.2: Predictions of the model in the (n_s-H_{inf}) plane, superimposed on TT,TE,EE+lowE+lensing+BK14+BAO 1-σ and 2-σ regions taken from [219]. The description of the plot is the same as in Figure 2.1.

$N = 60$. The next aspect we investigate is the VEV of $a = \langle 45 \rangle$. Since $SO(10)$ symmetry breaking through the $\underline{45}$ representation can lead to monopole production, it's crucial to ascertain if the value of $a = \langle \underline{45} \rangle$ is significantly higher than the inflation scale. The inflation scale is characterized by the Hubble parameter H_{inf}, as expressed by:

$$H_{inf}^2 = \frac{V(\phi)}{3M_{Pl}^2}.$$

Here, $V(\phi)$ is the potential outlined in Equation (2.19), and ϕ represents the value of the inflaton field at the pivot scale. Figure 2.2 displays the model's predictions in the $n_s - H_{inf}$ plane, with Planck's 1-σ and 2-σ bounds also included. In most scenarios, we observe that H_{inf} is lower than $a = \langle \underline{45} \rangle$ and tends towards a value of approximately $\sim 1.5 \times 10^{13}$ GeV as ξ increases. Simultaneously, n_s consistently adheres to the Planck data. Since $H_{inf} < a$, this implies that GUT monopoles are inflated away. With these results in mind, we proceed with the study of the reheating process and the gravitino mass, two intriguing topics that establish a significant connection between particle physics and cosmology.

2.5 Reheating, Non-thermal Leptogenesis, and Gravitino Mass

In our proposed model, we offer a plausible explanation for the observed baryon asymmetry of the universe within the framework of leptogenesis [209,210]. The reheating mechanism in our model proceeds via the dominant decay of the inflaton field into a pair of right-handed neutrinos [210] through the $SO(10)$ superpotential term (2.5). Subsequently, the out-of-equilibrium decay of these right-handed neutrinos into Higgs and leptons results in a lepton asymmetry. This lepton asymmetry is then partially converted into the observed baryon asymmetry through non-perturbative electroweak

			N=55			
ξ	$a = \langle 45 \rangle / M_{Pl}$	M_{45}/M_{Pl}	$m_\phi(GeV)$	λ_{N_2}	M_N(GeV)	m_{ν_2}(eV)
1	$1.80{\cdot}10^{-3}$	$1.56{\cdot}10^{-4}$	$7.34{\cdot}10^{12}$	$4.57{\cdot}10^{-4}$	$7.49{\cdot}10^{10}$	$1.36{\cdot}10^{-2}$
10	$1.39{\cdot}10^{-3}$	$2.53{\cdot}10^{-4}$	$2.51{\cdot}10^{13}$	$2.47{\cdot}10^{-4}$	$4.05{\cdot}10^{10}$	$2.51{\cdot}10^{-2}$
100	$1.24{\cdot}10^{-4}$	$2.02{\cdot}10^{-3}$	$6.71{\cdot}10^{13}$	$1.51{\cdot}10^{-4}$	$2.48{\cdot}10^{10}$	$4.04{\cdot}10^{-2}$
280	$1.01{\cdot}10^{-2}$	$8.66{\cdot}10^{-5}$	$2.08{\cdot}10^{14}$	$8.55{\cdot}10^{-5}$	$1.40{\cdot}10^{10}$	$7.19{\cdot}10^{-2}$
			N=60			
ξ	$a = \langle 45 \rangle / M_{Pl}$	M_{45}/M_{Pl}	$m_\phi(GeV)$	λ_{N_2}	M_N(GeV)	m_{ν_2}(eV)
1	$1.35{\cdot}10^{-3}$	$1.24{\cdot}10^{-4}$	$5.44{\cdot}10^{12}$	$5.31{\cdot}10^{-4}$	$8.70{\cdot}10^{10}$	$1.17{\cdot}10^{-2}$
10	$1.96{\cdot}10^{-4}$	$5.1{\cdot}10^{-3}$	$4.06{\cdot}10^{13}$	$1.94{\cdot}10^{-4}$	$3.19{\cdot}10^{10}$	$3.16{\cdot}10^{-2}$
100	$1.24{\cdot}10^{-4}$	$2.03{\cdot}10^{-3}$	$6.42{\cdot}10^{13}$	$1.55{\cdot}10^{-4}$	$2.54{\cdot}10^{10}$	$3.97{\cdot}10^{-2}$
280	$1.01{\cdot}10^{-2}$	$8.59{\cdot}10^{-5}$	$1.99{\cdot}10^{14}$	$8.77{\cdot}10^{-5}$	$1.44{\cdot}10^{10}$	$6.97{\cdot}10^{-2}$

Table 2.3: Inflaton mass and neutrino masses for $T_{RH} = 10^9$ GeV.

processes [209]. For scenarios where $\kappa \ll 1$ and $M \ll 1$, the inflaton mass is well-approximated by:

$$m_\phi^2 \approx \frac{\lambda_A}{\sqrt{2}} M_{45}\, a. \tag{2.20}$$

Remarkably, this expression is independent of the parameter ξ. To ensure successful leptogenesis, a necessary condition is that $m_\phi \gtrsim 2M_N$, implying that at least one of the right-handed neutrinos must have a mass less than half that of the inflaton. We can calculate the reheating temperature using the following formula [222]:

$$T_{RH} \approx \left(\frac{90}{\pi^2 g_*}\right)^{1/4} \sqrt{\Gamma_\phi M_{Pl}}.$$

Here, the decay rate Γ_ϕ is determined by:

$$\Gamma_\phi \approx \frac{1}{16\pi}\left(\frac{M_N}{M_G}\right)^2 m_\phi.$$

The mass of the right-handed neutrino, M_N, is derived from Eq (2.6). In our analysis, we aim to avoid the *gravitino cosmological problem*[1] [223, 224], which places an upper bound on the reheating temperature $T_{RH} \lesssim 10^6 - 10^9$ GeV, resulting in a gravitino mass range of 100 GeV$\lesssim m_{3/2} \lesssim 10$ TeV [225]. To accomplish this, we identify M_N with the mass of the second-generation right-handed neutrino, $M_N = M_{N_2}$, which, as discussed in the previous section, is expected to be around $\sim 10^{10}$ GeV. With Eq (2.20) and the results from Table 2.2, we find that the kinematic condition $m_\phi > 2M_2$ is consistently met. It is important to note that with T_{RH} below M_{N_2}, we are dealing with non-thermal leptogenesis [210]. Table 2.3 presents representative results regarding the reheating temperature and the mass of the second-generation heavy right-handed neutrinos. In this table,

[1]Cosmological problems with gravitinos: the existence of gravitinos in the early universe raises issues with possible overproduction, interruption of nucleosynthesis, and implications for dark matter models.

we have optimized the Majorana neutrino mass M_2 to adhere to the constraints imposed by the reheating temperature and the bounds set by cosmological measurements ($\sum m_\nu < 0.12$ eV) [219]. For analytical simplicity, we have set the reheating temperature to the upper bound of $T_{RH} = 10^9$ GeV and the Dirac neutrino mass $m_{\nu_D} = 1.0$ GeV (approximately equal to the charm quark mass) for both $N = 60$ and $N = 55$ e-folds. An interesting observation is that the VEV $a \equiv \langle 45 \rangle$ of the $SO(10)$ adjoint, related to the GUT breaking scale, consistently exceeds the mass of the inflaton. After the reheating process, we can compute the lepton asymmetry generated by the right-handed neutrino decays using the formula [226]:

$$\frac{n_L}{s} = \sum_i \epsilon_i \mathbf{Br}_i \frac{3T_{RH}}{2m_\phi}.$$

Here, $\mathbf{Br}$ represents the branching ratio into the right-handed neutrino channel, s is the entropy density, and ϵ denotes the lepton asymmetry per right-handed neutrino decay. However, it's important to note that at this stage, the lepton asymmetry is susceptible to washout due to lepton-number-violating processes [227]. These processes can occur through M_{N_1}, which is the lightest right-handed neutrino and could be in thermal equilibrium following the disappearance of M_{N_2} and M_{N_3}. To avoid such washout processes, we ensure that the reheating temperatures adhere to the relation:

$$T_{RH} < M_{N_1}.$$

This ensures that M_{N_1} is not part of the *thermal bath*[2], preserving the lepton asymmetry.

The lepton asymmetry in our model is connected to the baryon asymmetry through the relation [228]:

$$\frac{n_L}{s} \approx -\frac{79}{28}\frac{n_B}{s} \tag{2.21}$$

By combining the relationship above with Eq (2.21), we derive:

$$\frac{n_B}{s} \approx \frac{42}{79} \sum_i \epsilon_i \mathbf{Br}_i \frac{T_{RH}}{m_\phi}.$$

In this expression, we can safely neglect the contribution of the lightest right-handed neutrino (N_1) as it is negligible. The dominant contribution comes from N_2. Assuming the maximal value for the branching ratio $\mathbf{Br_2} = 1/2$ and the upper bound for the reheating temperature ($T_{RH} \sim 10^9$ GeV), we find:

$$\frac{n_B}{s} \approx \frac{2.65 \times 10^8}{m_\phi} \epsilon_2.$$

To satisfy the Planck constraints on the baryon-number-to-entropy density ratio, $n_B/s \simeq 8.7 \times 10^{-10}$, and considering the values of the inflaton mass from Table 2.3, we conclude that ϵ_2 must fall within the range $10^{-6} \lesssim \epsilon_2 \lesssim 10^{-4}$ in order to explain the observed baryon asymmetry of the universe. Moving on to the gravitino mass, it can be calculated using the formula [72]:

$$m_{3/2}^2 = \frac{K^i_j F_i F^{*j}}{3M_{pl}^2}.$$

[2] A state of thermal equilibrium where the particles frequently interact and share a common temperature.

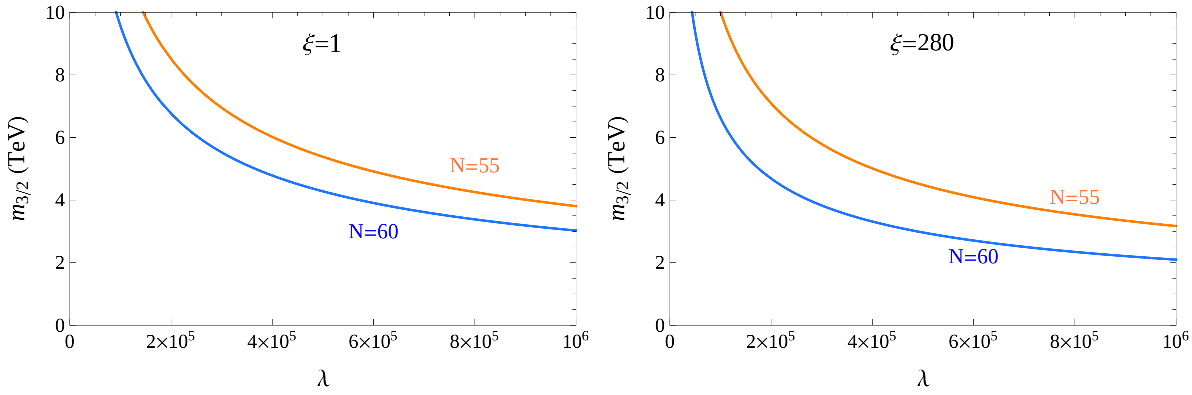

Figure 2.3: Gravitino mass as a function of the Yukawa parameter λ of (2.17), for $\xi = 1$ (left) and $\xi = 280$ (right). The values of M_{45} obtained from Table 2. In the left panel $M = 10^{10}$ GeV for both curves. For the plot in the right panel $M = 10^{10}$ GeV (blue) and $M = 1.5 \times 10^{10}$ GeV (orange).

Here, F_i is determined by the flatness conditions of the superpotential[3]. The gravitino mass can then be expressed as:

$$m_{3/2} = \frac{M M_{45}}{\sqrt{\lambda} M_{pl}}.$$

This mass depends on the parameter λ found in (2.17), which cannot exceed the value of 10^6. This upper bound is established by considering that the product $\kappa\lambda$ defines a typical Yukawa coupling in (2.17), which should remain perturbative, thus leading to $\lambda \lesssim 1/\kappa$. Unlike the reheating temperature and the slow-roll observables, which exhibit less sensitivity to the mass scale M, the gravitino mass shows a clear dependence on this parameter. Consequently, assuming values for M_{45} that align with the inflationary analysis conducted in the previous section, we can employ the constraints on the gravitino mass to derive limitations on both the mass parameter M and the Yukawa coefficient λ. The results of this analysis are depicted in Figure 2.3, where we illustrate the gravitino mass as a function of the parameter λ for $\xi = 1$ (left) and $\xi = 280$ (right). The values of M_{45} are taken from Table 2.2. In the left panel, both curves correspond to $M = 10^{10}$ GeV, while in the right panel, we show results for $M = 10^{10}$ GeV (blue) and $M = 1.5 \times 10^{10}$ GeV (orange). The findings suggest that in order to maintain λ within the $\kappa\lambda < 1$ bound, the mass scale M should be on the order of $\sim 10^{10}$ GeV for both $\xi = 1$ and $\xi = 280$.

2.6 Gauge Coupling Unification

In the previous sections, we discussed the constraints on various heavy particles originating from the $SO(10)$ symmetry breaking and cosmological inflation. These heavy states decouple at scales below the GUT scale, and they affect the renormalization group running of the SM gauge couplings. In this section, we explore the implications of these threshold effects on gauge coupling unification. Recapping the essential elements of the previous analysis, in addition to the spinor $\underline{16}$ representation that houses all the MSSM supermultiplets (including the singlets for RH-neutrinos), the model

[3]These conditions ensure that the scalar potential remains flat along certain directions preventing this way, terms that destabilize the potential or large mass terms which can break supersymmetry.

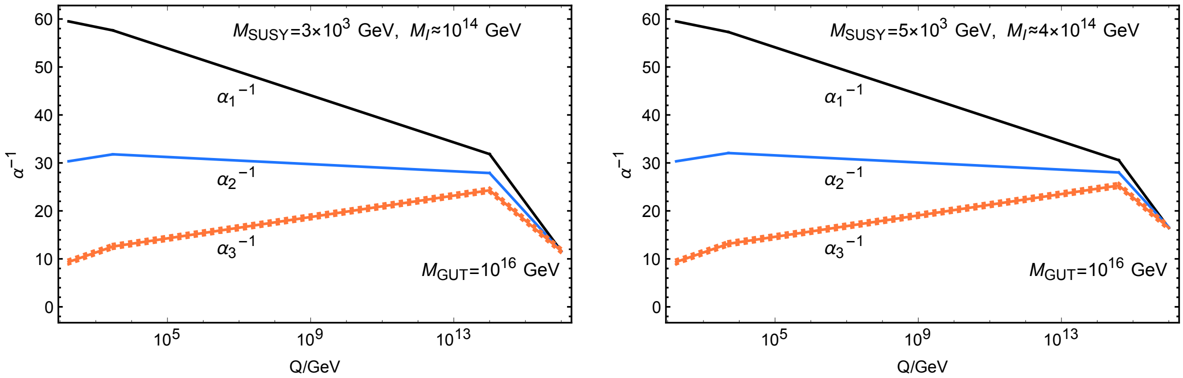

Figure 2.4: Running of the inverse gauge couplings $a_i^{-1}(Q)$ at one-loop for a SUSY scale at the TeV range with $M_{SUSY} = 3$ TeV (left panel) and $M_{SUSY} = 5$ TeV (right panel). The intermediate decouple scale was received at $M_I \approx \times 10^{14}$ GeV (left panel) and $M_I \approx 4 \times 10^{14}$ GeV (right panel). The three gauge couplings unify at an energy scale with $M_{GUT} \approx 10^{16}$ GeV. As input scale we took $Q_0 = m_{top} = 173.4$ GeV and the values of the gauge couplings at this scale was received from [229].

possesses an extended Higgs sector. This sector includes a pair of $\underline{16}_H - \overline{\underline{16}}_{\bar{H}}$, two adjoints $\underline{45}_H$ and $\underline{45}'_H$, and a pair of $\underline{10}_H$ and $\underline{10}'_H$ within $SO(10)$. As mentioned earlier, the Higgs MSSM doublets arise from the $\underline{10}_H$ representations, and the color triplets, which belong to $\underline{10}_H$ and $\underline{10}'_H$, acquire masses at the GUT scale (as discussed previously). Additionally, there are three pairs of $SU(5)$ tenplets. One pair descends from $\underline{16}_H - \overline{\underline{16}}_{\bar{H}}$, and the other two pairs originate from the decomposition of the two $\underline{45}_H$ representations. According to the mass spectrum analysis in Section 2.2.2, the eigenmasses of these states depend on the parameters $\langle \nu^c_H \rangle$, $\langle A \rangle$, M_{45}, and λ_A. The VEVs $\langle \nu^c_H \rangle$ and $\langle A \rangle$ are of $\mathcal{O}(\text{GUT})$, while the values of the parameters M_{45} and λ_A have been determined by the inflationary analysis (see Table 2.2). For large ξ, the derived values of M_{45} and λ_A suggest that the eigenmasses of the $SU(5)$ tenplets are on the order of $\sim \mathcal{O}(10^{14}\ GeV)$. All other heavy states from the $SO(10)$ Higgs content acquire masses at a decoupling scale M_I below the GUT scale. From the previous sections, we infer that M_I is related to the mass scale M_{45}, which has been fixed by the inflationary analysis (see Table 2.2). Below M_I, only the MSSM states contribute to the gauge coupling running. Next, we study the evolution of the SM gauge couplings at the one-loop level, accounting for the appropriate contributions to the beta functions at the following scales: the SUSY scale M_{SUSY}, the intermediate scale $M_I \sim M_{45}$, and the GUT scale $M_{GUT} \sim 10^{16}$. The beta coefficients for the running from $M_I \longrightarrow M_{GUT}$ include those of the MSSM, along with contributions from the additional matter below the GUT scale:

$$\begin{aligned} b_1 &= b_1^{MSSM} + 103/5 \\ b_2 &= b_2^{MSSM} + 21 \\ b_3 &= b_3^{MSSM} + 20 \end{aligned}$$

Here, $(b_1^{MSSM}, b_2^{MSSM}, b_3^{MSSM}) = (33/5, 1, -3)$ represent the beta coefficients of the MSSM spectrum. Figure 2.4 illustrates the evolution of the inverse gauge couplings a_i^{-1} as a function of the energy scale Q at the one-loop level. The left panel shows the case for $M_I \approx 10^{14}$ GeV and $M_{SUSY} = 3$ TeV, while the right panel corresponds to $M_{SUSY} = 5$ TeV with $M_I \approx 4 \times 10^{14}$ GeV. In both scenarios, the three gauge couplings merge at $M_{GUT} \approx 10^{16}$ GeV.

Chapter 3

Hybrid Inflation, Reheating and Dark Radiation in a IIB perturbative moduli stabilization scenario

3.1 Introduction

Cosmological inflation stands out as one of the most successful theoretical frameworks for explaining the evolution of the Universe and its observed large-scale structure today. Over the years, numerous effective quantum field theory models have been developed to bridge the gap between cosmic inflation and particle physics, particularly in describing low-energy observables. An essential criterion for these models is their ability to provide an ultraviolet (UV) completion within a quantum theory of gravity, valid up to the Planck scale (denoted as M_P).

In the current landscape of theoretical physics, String Theory emerges as the most promising candidate for a consistent quantum theory at such high energy scales, while also incorporating the SM and its minimal supersymmetric extension (MSSM). However, string theory operates in a ten-dimensional spacetime framework, necessitating the compactification of six extra dimensions to match the familiar four-dimensional spacetime observed in our universe. This process of reducing higher-dimensional string action to four dimensions results in a vast array of possible string vacua, collectively known as the string landscape. It's important to note that not every successful effective field theory model can seamlessly fit into the framework of string theory [see reviews [233–235] and references therein].

On a parallel note, effective field theory models arising from compactification must meet certain criteria. Among these, they should predict a tiny positive cosmological constant denoted as Λ, approximately on the order of $\Lambda \approx 10^{-122}\, M_P^4$, which can account for dark energy, as indicated by cosmological observations. One way to realize such a scenario is by employing an effective model involving a scalar field ϕ with a potential $V(\phi)$ that exhibits a (potentially metastable) positive minimum equal to the cosmological constant Λ.

In fact, effective field theory models stemming from String Theory compactified on Calabi-Yau (CY) manifolds introduce numerous moduli fields, some of which could potentially serve as the inflaton ϕ. Consequently, the cosmological challenges become intertwined with the well-known problem of moduli stabilization. Moduli stabilization and the presence of (metastable) de Sitter vacua play a pivotal role in successfully implementing the cosmological inflationary scenario in effective field theory (EFT) models with a string origin. Therefore, reconciling these two aspects is crucial in the quest for an appropriate non-vanishing effective potential for a scalar field acting as the inflaton ϕ, enabling the necessary exponential expansion of the universe, given a sufficiently long trajectory length $\sim \Delta\phi$ for the field ϕ to reach its minimum and trigger inflation.

A specific category of models focuses on constructions involving large volume compactification scenarios (LVS) [236–241]. These models incorporate inflatons associated with Kähler moduli fields $T_k = \tau_k + ia_k$. In earlier scenarios [242–245], particularly in the context of type-IIB theory, it was demonstrated that the internal volume modulus $\mathscr{V}$ expressed in terms of the real components of Kähler moduli, $\mathrm{Re}T_k = \tau_k$, could serve as a suitable candidate for the inflaton role ($\phi \propto \log \mathscr{V}$). Radiative corrections, stemming from intersecting space-filling D7 branes, offer a mechanism for stabilizing Kähler moduli and uplifting their scalar potential through universal abelian factors, resulting in a positive cosmological constant [see [246, 247] for more approaches]. Notably, Kähler moduli stabilization is achieved through a non-zero potential generated by α' and radiative (logarithmic) corrections that occur when closed string loops traverse codimension-two bulk regions towards localized gravity sources. Furthermore, the de Sitter vacuum is attained due to positive D-term contributions, as initially proposed in [248].

In the large volume limit, the effective potential induced for the Kähler moduli exhibits a straightforward structure, featuring two local extrema (a minimum and a maximum) and approaching zero as ϕ tends to infinity. The separation between these two local extrema, denoted as $\Delta\phi = \phi_{max} - \phi_{min}$, is proportional to $\log(\mathscr{V}_{max}/\mathscr{V}_{min})$. In the simplest effective model solely comprising moduli fields, this separation can be parametrized with a single non-negative parameter. The largest possible separation $\Delta\phi$ occurs at a critical value of this parameter, beyond which only Anti-de Sitter (AdS) solutions emerge. There exists a non-zero value of this parameter at which a new inflationary small-field scenario is successfully realized. In this novel scenario, the majority of the necessary e-folds N_0 (approximately $N_0 \sim 60$) accumulate in the vicinity of the potential's minimum, resulting in a prediction for the tensor-to-scalar ratio of density fluctuations in the early universe, namely $r \approx 4 \times 10^{-4}$. Despite the successes of this model, it remains incomplete, requiring a waterfall mechanism to terminate inflation and shift the de Sitter vacuum to a lower value consistent with the observed cosmological constant.

It has been demonstrated that when open string states arising in the intersections of D7 branes exhibit appropriate magnetic fluxes and specific brane separations, a charged open string scalar can become tachyonic for certain values of $\mathscr{V}$ less than a critical threshold . This state can serve as a waterfall field [249, 250]. In potential extensions of this scenario, multiple such fields may be included to conclude inflation and establish a deeper vacuum in alignment with the current value of Λ.

In this study, we introduce an alternative scenario that considers not only moduli fields but also ordinary fermion matter and Higgs fields in the effective field theory model. In this variation of the previously described scenario, the Higgs field rolls down a potential hill toward a new, lower minimum. Its initial condition is set in the vicinity of the metastable vacuum of the moduli potential, which is primarily determined by the Kähler moduli and the associated compactification volume $\mathscr{V}$. In this construction, we implement standard hybrid inflation [251] with a singlet scalar field acting as the inflaton and Higgs fields serving as waterfall fields. In this scenario, the vacuum energy is determined by the scalar field and the waterfall fields, with radiative corrections playing a crucial role in shaping the inflationary trajectory. Given the breaking of SUSY during inflation, SUSY soft terms are also incorporated, which are instrumental in achieving spectral index (n_s) values consistent with current experimental constraints. We find small tensor-to-scalar values, which could be tested in future experiments. Additionally, we discuss dark radiation and demonstrate that the changes in the effective number of neutrinos align with a 0.95% confidence level, with natural values for the relevant couplings.

3.2 Description of the model and its constituents

In this study, we delve into the realm of a type-IIB string framework existing in ten dimensions, wherein six of these dimensions are compactified onto a Calabi-Yau threefold denoted as $\mathscr{X}$. Our primary focus centers around the moduli spectrum, which we represent using the following notation: ϕ signifies the dilaton field, while T_i and z_a refer to the Kähler and complex structure (CS) moduli, respectively. Additionally, we introduce the conventional axion-dilaton combination as follows:

$$\tau = C_0 + i\, e^{-\phi} \equiv C_0 + \frac{i}{g_s} \ , \tag{3.0}$$

Here, g_s stands for the string coupling, and C_0 represents a 0-form potential, often referred to as an RR-scalar. We assume the presence of a perturbative superpotential W_0, induced by fluxes and following the form proposed in [253]. At the classical level, W_0 takes on the role of a holomorphic function that depends on the axion-dilaton modulus τ and the CS moduli z_a [1]. Stabilization of τ and z_a occurs in the standard supersymmetric manner, by solving $D_\tau W_0 = 0$ and $D_{z_a} W_0 = 0$, where $D_I = \partial_I W + W \partial_I K$ represents the covariant derivatives.

Our examination involves a geometric configuration of three intersecting D7-brane stacks equipped with magnetic fluxes. Concerning the Kähler potential, we account for α' corrections and the influence of a novel four-dimensional Einstein-Hilbert (EH) term, which is localized within the internal space. This EH term is generated by higher derivative terms in the ten-dimensional string effective action [243]. This setup leads to logarithmic corrections in the scalar potential through loop effects. When these corrections are taken into account, the relevant part of the Kähler potential assumes the following form [243]:

$$K = -2M_P^2 \log(\mathscr{V} + \xi_0 + \eta_0 \log \mathscr{V}) + \cdots \ , \tag{3.1}$$

Here, the ellipsis denotes terms dependent on the complex structure, z_a, and the Kähler moduli, $T_k = \tau_k + i a_k$. The general expression for the volume is given by $\mathscr{V} = \frac{1}{6}\kappa_{ijk} t^i t^j t^k$, where t^i represents the two-cycle Kähler moduli fields, and κ_{ijk} denotes the triple intersection numbers on $\mathscr{X}$.

In our investigation, we consider a specific scenario where three Kähler moduli contribute equally to the volume and are stabilized through perturbative logarithmic loop corrections [254]. Following the framework outlined in [255], we base our model on a Calabi-Yau (CY) threefold corresponding to polytope Id: 249 in the Kreuzer-Skarke CY database [256,257]. This particular CY manifold features three Kähler moduli fields satisfying the simple relation $\tau_i = \mathfrak{a} t^j t^k$, where $\mathfrak{a}$ is a positive constant associated with the intersection number. Consequently, the volume is succinctly represented as [255]:

$$\mathscr{V} = \mathfrak{a}, t^1 t^2 t^3 = \tau_1 t^1 = \tau_2 t^2 = \tau_3 t^3 = \frac{1}{\sqrt{\mathfrak{a}}}\sqrt{\tau_1 \tau_2 \tau_3} \ . \tag{3.2}$$

[1]Non-perturbative corrections, which would also introduce the Kähler moduli through terms like $\mathscr{W}_{NP} \propto e^{-aT_k}$, are omitted here. As explained in the subsequent analysis, T_k can be perturbatively stabilized through one-loop corrected Kähler potential.

Upon dimensional reduction, the effective field theory (EFT) model derived from this setup can manifest as either a Grand Unified Theory (GUT) or directly as the Minimal Supersymmetric Standard Model (MSSM). In these models, the ordinary low-energy (super)-fields appear in appropriate representations of the EFT gauge group. To provide a comprehensive analysis, we also include matter fields in the Kähler potential alongside the previously mentioned quantum corrections. These contributions are crucial for investigating soft supersymmetry breaking effects and cosmological inflation.

In particular, our focus is on the Higgs sector, which plays a pivotal role in scenarios of hybrid inflation and the potential production of dark radiation. For this purpose, we consider a generic set of Higgs pairs, denoted as Φ_i and Φ_j, which are assumed to break the gauge group at a GUT scale significantly lower than the Planck scale, M_P. Additionally, we introduce a field S, representing a gauge singlet superfield responsible for realizing trilinear superpotential couplings of the form $S\Phi_1\Phi_2$. Such singlet fields are ubiquitous in effective string theory models. The relevant terms of the superpotential in this setup can be generically expressed as:

$$W = W_0 + \kappa S(\Phi_1\Phi_2 - M^2) + \cdots \ , \tag{3.3}$$

Here, κ is a coupling constant, M is a high-scale mass parameter whose value is below the string scale, contingent upon the scale at which the Higgs field acquires a VEV, and W_0 represents the flux-induced part introduced earlier. The ellipsis denotes possible additional terms that are not immediately relevant to our current discussion.

Our study of the Kähler metric and the inclusion of matter fields can be compared to the work by Blumenhagen et al. [258], particularly in the examination of chiral matter localized on magnetized D7-branes and the more comprehensively understood fractional D3-branes found at singularities. For the second term within our Kähler metric, we explore soft terms linked to massless open strings concentrated at the intersections between D3 and D7 branes. However, the presence of such massless string states cannot be derived from the Dirac-Born-Infeld (DBI) or Chern-Simons (CS) actions alone.

In the context of hybrid inflation, our framework necessitates incorporating the effects of scalar fields and their fermionic superpartners into the Kähler potential. Typically, these contributions are expressed in a form such as $\tilde{K}_{ij}\Phi_i\bar{\Phi}j$, where $\tilde{K}ij$ depends on moduli like $\tau_k = \frac{T_k+\bar{T}k}{2}$ and S. The detailed form of $\tilde{K}ij$ becomes clear when examining the origin of zero modes, and various scenarios within type IIB theory are possible [259].

In realistic constructions, chiral matter emerges on the world volume of D7-brane stacks or at their intersections with other D7-branes. This is where gauge and scalar fields, such as Φ and $\bar{\Phi}$, manifest on the world volume by configuring D7 branes to wrap suitable divisors. The supermultiplets involving these scalar fields, Φ and $\bar{\Phi}$, exhibit a scaling dependence, with the leading contribution taking the form [260]:

$$\frac{\Phi_i\bar{\Phi}_i}{T_k+\bar{T}_k} \to \frac{\Phi_i\bar{\Phi}_i}{\mathscr{V}^{2/3}}. \tag{3.4}$$

Additionally, there are next-to-leading order α' contributions [258] of the form $\text{Re}(S)/(T_k+\bar{T}_k)$, which are deemed negligible for our analysis and are thus excluded.

Incorporating these matter fields into the Kähler potential (3.2), we obtain the following generic form:

$$\mathscr{K} = -2M_P^2; \log\left[\left(\prod_{k=1}^{3}(T_k+\bar{T}_k)\right)^{\frac{1}{2}} + \mathscr{C}\right] + \sum_{k=1}^{3}\frac{a_k}{T_k+\bar{T}_k}f_k(\Phi_i,\Phi_2,\ldots,S,\bar{S})$$

Here, $\mathscr{C}$ is defined as a function with logarithmic dependence on the moduli fields $T_{1,2,3}$:

$$\mathscr{C} = \xi_0 + \eta_0 \log\left(\prod_{k=1}^{3}(T_k+\bar{T}_k)\right). \tag{3.5}$$

The parameter ξ_0 accounts for α'^3 corrections [261] and is proportional to the Euler characteristic χ_{CY} of the Calabi-Yau manifold:

$$\xi_0 = -\frac{\zeta(3)}{4}\chi_{CY},, \tag{3.6}$$

with η_0 being a coefficient of order one [243]. The functions f_k in Eq. (3.2) describe the Higgs sector contributions. For simplicity, we assume a uniform form for all f_k:

$$f(\Phi,\overline{\Phi},S) = \alpha\Phi_1\Phi_1^\dagger + \beta\Phi_2\Phi_2^\dagger + \gamma SS^\dagger + \lambda(\Phi_1\Phi_2 + h.c.)\ , \tag{3.7}$$

where α, β, γ, and λ are dimensionless couplings. Furthermore, following the approach used in Blumenhagen et al. [258], we express the matter contribution term in (3.2) in terms of the compactification volume (note that $T \propto \mathscr{V}^{2/3}$). Regarding the origin of these fields, we focus on matter fields residing on magnetized D7-branes, as well as chiral fields generated at D7-brane intersections. The general analysis also applies to states associated with the excitations of open strings stretching between D7 and D3 branes or having both ends on the same D3 brane. The choice of the configuration dictates the modular weights in the Kähler potential. For our purposes, we consider the modular weights to be 1 [259]. Thus, in large volume compactifications, the Kähler potential in Eq.(3.2) takes the form [259, 262, 263] [2]:

$$\mathscr{K} = -2\log\left[\mathscr{V} + \xi_0 + \eta_0\log(\mathscr{V})\right] + \frac{3a}{\mathscr{V}^{2/3}}\left[\alpha\Phi_1\Phi_1^\dagger + \beta\Phi_2\Phi_2^\dagger + \gamma SS^\dagger + \lambda(\Phi_1\Phi_2 + h.c.)\right] \tag{3.8}$$

where a is a dimensionless constant and $\mathscr{V}$ is defined as in (3.2). Note that in Eq. (3.8) and from this point onward, we will use $M_P = 1$ units.

At this stage, we have outlined the minimum number of moduli and matter fields that are necessary for our subsequent analysis. We will now proceed to compute the scalar potential, which is crucial for exploring the properties of the model and determining various cosmological and phenomenological observables.

[2] Notice that in our case this formula is identified with the expansion of the warped form of the Kähler potential

$$K = -2\log\left((T+\bar{T})^{3/2} + \xi + \eta\log\mathscr{V} - \frac{a}{2}(T+\bar{T})^{1/2}\varphi_i\bar{\varphi}_i\right) = -2\log\left(\mathscr{V} + \xi + \eta\log\mathscr{V} - \frac{a}{2}\mathscr{V}^{1/3}\varphi_i\bar{\varphi}_i\right)$$

.

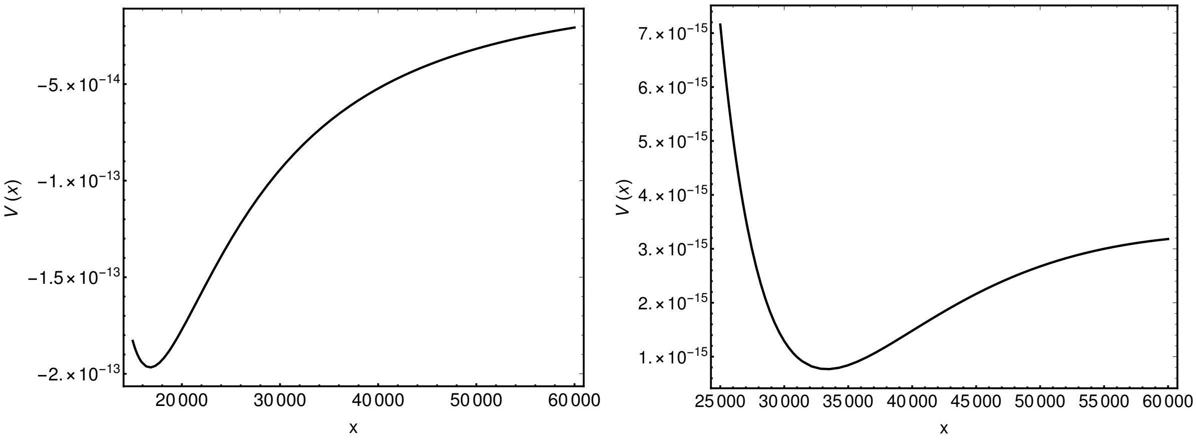

Figure 3.1: Plots of the potential along the volume direction. The left panel shows the F-term potential, while in the right panel, the D-term potential has also been included. We choose $\xi_0 = 10$, $\eta_0 = -0.92$, $S = 0$, $\varphi_{1,o} = \varphi_{2,o} = M$, $\kappa = 0.1$ and $\gamma = 1$. Here x represents the volume, $x \equiv \mathscr{V}$.

3.3 The effective potential

The scalar potential of the effective field theory model consists of various contributions. As we will soon discuss, in the current framework, there are F-terms and D-terms associated with the moduli sector, along with contributions from the EFT matter fields and supersymmetry-breaking terms.

Let's begin with the F-term potential, which is expressed by the generic formula:

$$V_F = e^G \left(G_i G^{-1}_{ij^*} G_{j^*} - 3\right) \ , \tag{3.9}$$

where

$$G = \mathscr{K} + \log|W|^2 \equiv \mathscr{K} + \log W + \log W^*$$

and the indices i, j in the equation above represent derivatives with respect to various moduli and other fields.

When we compute the derivatives and substitute them into Eq (3.9) while retaining only the leading-order terms, the F-term potential simplifies to the following form [3]

$$V_F \simeq \frac{\kappa^2\alpha\beta\left(M^2-\varphi_1\varphi_2\right)^2+\gamma\kappa^2S^2\left(\alpha\varphi_1^2+\beta\varphi_2^2\right)}{3a\alpha\beta\gamma\mathscr{V}^{4/3}} + \frac{3W_0^2(2\eta_0\log\mathscr{V} - 8\eta_0+\xi_0)}{2\mathscr{V}^3}, \tag{3.10}$$

where φ_1 and φ_2 are the bosonic components of the superfields Φ_1 and Φ_2.

At the extrema of the F-term potential, the fields assume the following values [4]

$$S_o = 0, \quad \varphi_{1,o}\varphi_{2,o} = M^2, \quad \mathscr{V}_o = e^{\frac{13}{3}-\frac{\xi_0}{2\eta_0}}. \tag{3.11}$$

[3]The complex field S is generally represented as $S =\mid S \mid e^{i\theta}$, and we choose $\theta = 0$ to align it with the real axis. So, in Eq. (3.10) and the subsequent analysis, S refers to the real part of the field.

[4]In more general EFT backgrounds, it's possible that minimization with respect to the fields S, Φ_i leads to a potential of the form $V \sim \frac{a}{5\mathscr{V}^{4/3}} + \frac{1}{3}\frac{b+\eta\log\mathscr{V}}{\mathscr{V}^3}$. In this case, it's possible to have a dS minimum with the volume acquiring a value $\mathscr{V}_o^{5/3} = \left(\frac{9n}{4a}\right)\mathscr{W}\left(\frac{4a}{9n}\left(e^{\frac{1}{3}-\frac{b}{n}}\right)^{5/3}\right)$, where $\mathscr{W}$ is the product-log (Lambert) function.

Substituting the solution (3.11) into (3.10), we obtain

$$V_F^{extr.} = \frac{3|W_0|^2\eta_0(2\log\mathscr{V}_o - 8 + \frac{\xi_0}{\eta_0})}{2\mathscr{V}_o^3} \equiv \eta_0\,\frac{|W_0|^2}{\mathscr{V}_o^3}\,. \tag{3.12}$$

A simple analysis reveals that this is a minimum of the potential as long as $\eta_0 < 0$. However, since $\frac{|W_0|^2}{\mathscr{V}_o^3} > 0$, the potential (3.12) at the minimum acquires a negative value. Therefore, the F-term potential predicts an anti-de Sitter (AdS) vacuum.

In the left panel of Fig. 3.1, the F-term potential with an AdS minimum is plotted for a specific choice of the parameters ξ_0, η_0, W_0.

Despite the preceding negative F-term contribution, the potential can be elevated to a de Sitter minimum by considering the inclusion of D-term contributions associated with the $U(1)$ symmetries linked to the D7-branes [248, 264] as discussed in [242]. In this scenario, the D-term potential originates from hidden sectors, generated by D7-branes wrapping the 3 divisors with volumes denoted as τ_i. More specifically, in the current geometric configuration, D-term contributions arise from the universal $U(1)$ factors linked to the $D7$ brane stacks. These terms exhibit a general form [242, 264]:

$$V_D = \sum_{i=1}^{3}\frac{g^2_{D7_i}}{2}\left(Q_j\partial_{T_j}K + \sum_{j\neq i} q_i^j|\Theta_i^j|^2\right)^2, \tag{3.13}$$

where $g_{D7_i} = (\mathrm{Re}T_i)^{-1}$ and Q_j, q_i^j denote "charges". We acknowledge that Θ_i^j represent matter fields charged under the $U(1)$ gauge factors. Some aspects regarding strings at $D7$ intersections, in particular, have been recently discussed in [249]. The fields Θ_i^j carry charges under the $U(1)$ factors associated with the D-branes. The question arises about the potential contributions of these fields in the D-term and, consequently, in the scalar potential. One plausible scenario is that non-zero field vevs are chosen to nullify the D-term. In this case, the uplift should be realized through a suitable modification (see footnote 4) or the standard procedure of introducing $\overline{D3}$ branes (see [265]). Here, we simplify the assumption that these singlets have vanishing vevs. Whether the vevs of these fields are zero depends on the specific details of the effective model. One possibility is to assume that in the effective field theory limit, all these fields Θ_i^j are minimized at $\langle\Theta_i^j\rangle = 0$. Alternatively, even in the case of non-zero vevs, there might be accidental cancellations that reduce the significance of their contributions. Some related discussions on these issues can be found in [266].

Here, since the D-term potential is solely employed to uplift the non-supersymmetric AdS vacuum of the F-term potential, following previous works closely (see, for example, [242], [248], and [264]), we reasonably assume that moduli fields dominate over other fields' vevs. Therefore, it is adequate for our purposes to assume that the flux-induced D-term piece $\propto Q_j\partial_{T_j}K$ dominates, and therefore we minimize the potential by setting $\langle\Theta_i^j\rangle$ vevs to zero.

When $\langle\Theta_j\rangle = 0$ ([264] for a more extensive discussion related to D-terms), the second term within the parentheses vanishes. In this case, each component of the D-term takes on a straightforward, model-independent form $V_{D_i} \approx Q_i^2/\tau_i^3$. Consequently, the total D-term potential, which is the sum of three components, is approximated by [242]:

$$V_{\mathscr{D}} = \sum_{i=1}^{3}\frac{d_i}{\tau_i}\left(\frac{\partial\mathscr{K}}{\partial\tau_i}\right)^2 \approx \sum_{i=1}^{3}\frac{d_i}{\tau_i^3} \equiv \frac{d_1}{\tau_1^3} + \frac{d_3}{\tau_3^3} + \frac{d_2\tau_1^3\tau_3^3}{\mathscr{V}^6}\,, \tag{3.14}$$

Here, d_i are positive constants associated with the charges, satisfying $d_i \sim Q_i^2 > 0$. For our computations, we simplified the scenario by focusing on the diagonal terms of the potential. Nonetheless, in more comprehensive models, cross-terms also appear. Our observations indicate that these cross-terms have a similar order of magnitude relative to the expressions involving τ_i. Numerical investigations show that, even with these cross-terms, the potential does exhibit minima in de Sitter (dS) space, albeit with slightly varied coefficient values d_i.

To simplify the calculations, we used the volume formula $\mathscr{V}^2 = \tau_1\tau_2\tau_3$. By substituting τ_2 with $\tau_2 = \mathscr{V}^2/(\tau_1\tau_3)$, we were able to express the total effective potential $V_{\rm eff}$ as the sum of V_F and V_D. This effective potential can then be minimized with respect to the total volume $\mathscr{V}$ and the remaining Kähler moduli τ_1 and τ_3.

We assumed that the F-term of the potential depends on the total volume $\mathscr{V}$, meaning that the explicit dependence of $V_{\rm eff}$ on τ_1 and τ_3 arises solely through the V_D component. It turns out that minimizing with respect to τ_1 and τ_3 determines the ratios between these moduli, i.e., $\left(\frac{\tau_i}{\tau_j}\right)^3 = \frac{d_i}{d_j}$ [267]. In terms of the stabilized total volume $\mathscr{V}$, the conditions for the two τ_i can be expressed as:

$$\tau_i^3 = \left(\frac{d_i^2}{d_k d_j}\right)^{\frac{1}{3}} \mathscr{V}^2 \,,$$

where $i = 1, 3$. In this case, the D-term potential assumes the simplified form:

$$V_D \approx \frac{d}{\mathscr{V}^2} \,, \quad \text{with} \qquad d = 3(d_1 d_2 d_3)^{\frac{1}{3}}. \tag{3.15}$$

At tree level, the potential exhibits two flat directions when the variable S is set to zero. In this situation, one can adjust the values of the variables ϕ_1 and ϕ_2 to create different minima in the potential. However, this principle is valid only when considering the F-term potential alone. The total potential at tree level is composed of both F-term and D-term components. The D-term potential consists of two parts: one arising from the moduli and the other from the matter fields. To cancel the contribution from the matter fields in the D-term potential, we use D-flat directions where $\varphi_1 = \varphi_2 = \varphi$ and $\alpha = \beta$. In this case, the effective potential can be expressed as

$$V_{\rm eff} \;\simeq\; \frac{\kappa^2\alpha\left(M^2 - \varphi^2\right)^2 + 2\gamma\kappa^2 S^2\varphi^2}{3a\alpha\gamma\mathscr{V}^{4/3}} + \frac{3W_0^2(2\eta_0\log(\mathscr{V}) - 8\eta_0 + \xi_0)}{2\mathscr{V}^3} + \frac{d}{\mathscr{V}^2}. \tag{3.16}$$

The right panel of Figure 3.1 exhibits the shape of the potential along the volume modulus $\mathscr{V}$ when both F- and D-terms are incorporated. It is evident that a positive D-term is adequate to raise the potential along the volume direction, resulting in the attainment of a de Sitter minimum.

To locate the extrema of the potential along the φ and S directions, we must set the corresponding derivatives to zero. Consequently, for φ, we impose the condition:

$$\frac{dV_{\rm eff}}{d\varphi} \;=\; 0 \Rightarrow \frac{\kappa^2\left(4\alpha\varphi^3 - 4\alpha M^2\varphi + 4\gamma S^2\varphi\right)}{3a\alpha\gamma\mathscr{V}^{4/3}} = 0 \tag{3.17}$$

which yields three solutions for φ:

$$\varphi = 0, \quad \varphi_\pm = \pm\sqrt{M^2 - \frac{\gamma}{\alpha}S^2}. \tag{3.18}$$

Similarly, along the S direction:

$$\frac{dV_{\text{eff}}}{dS} = 0 \Rightarrow \frac{4\kappa^2 S\varphi^2}{3a\alpha\mathscr{V}^{4/3}} = 0 \tag{3.19}$$

which leads to:

$$S = 0. \tag{3.20}$$

Combining equations (3.18) and (3.20), in the large volume limit, we obtain the following solutions:

$$(S = 0, \varphi = 0), \quad (S = 0, \varphi = \pm M). \tag{3.21}$$

We have previously addressed the minimization of V_F with respect to the volume modulus. However, in the presence of D-terms, the minima along the volume direction experience shifts. Therefore, by requiring the vanishing of the derivative of (3.16) with respect to $\mathscr{V}$, we derive the equation:

$$\begin{aligned}\frac{dV_{\text{eff}}}{d\mathscr{V}} = 0 \quad \Rightarrow \quad & -\frac{4\kappa^2\left(\alpha\varphi^4 + \alpha M^4 - 2\alpha M^2\varphi^2 + 2\gamma S^2\varphi^2\right)}{9a\alpha\gamma\mathscr{V}^{7/3}} - \frac{2d}{\mathscr{V}^3} \\ - \quad & \frac{9\left(2\eta_0 W_0^2\log(\mathscr{V}) - 8\eta_0 W_0^2 + \xi_0 W_0^2\right)}{2\mathscr{V}^4} + \frac{3\eta_0 W_0^2}{\mathscr{V}^4} = 0.\end{aligned} \tag{3.22}$$

In the large volume limit, as a good approximation, the above equation yields the solution:

$$\mathscr{V}_o \approx \frac{9\eta_0 W_0^2}{2d}\mathscr{W}\left(\frac{2de^{\frac{13}{3}-\frac{\xi_0}{2\eta_0}}}{9\eta_0 W_0^2}\right), \tag{3.23}$$

where $\mathscr{W}$ represents the product-log (Lambert) function. The shape of the scalar potential V_{eff} in the φ-S plane is visualized in Figure 3.2. As previously discussed, the D-term contribution in the effective potential guarantees the existence of de Sitter vacua as S approaches zero.

3.3.1 Inflationary phase

We have conducted a comprehensive analysis of the scalar potential within the effective theory and elucidated the roles played by various fields in shaping its form. With this groundwork, we are now well-prepared to explore whether cosmological inflation can be realized in the current model.

In a prior approach, employing the same type-IIB framework and the geometric configuration of intersecting D7-brane stacks, the inflaton field was associated with the logarithm of the compactification volume modulus. Achieving the requisite 60 e-folds for slow-roll inflation led to a lower bound on the minimum vacuum energy [267], although it remained considerably larger than the cosmological constant. Subsequently, a new ”waterfall” field was introduced, introducing an additional direction in the potential. This field rolled down to the new lower minimum, simultaneously ending inflation. This role was demonstrated [249] to be fulfilled by oscillating open string states near the intersections of the D7 stacks.

In the current scenario, where we have incorporated physical states from the effective theory model, new possibilities have emerged. At the minimum along the compactification volume modulus $\mathscr{V}$, the Higgs field φ and the singlet S introduce new directions (perpendicular to that of

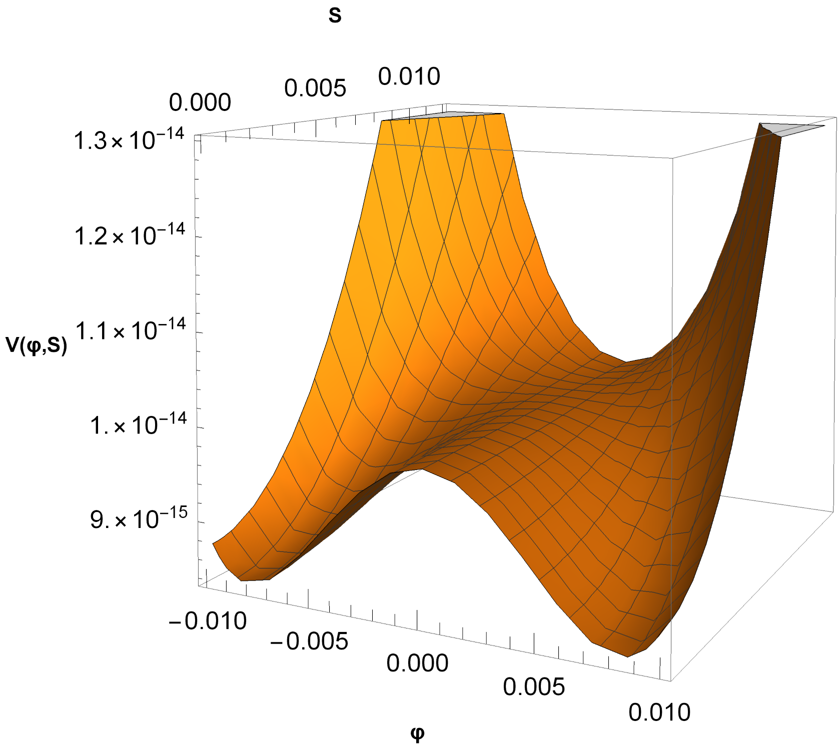

Figure 3.2: The shape of the effective potential in the φ-S plane for the chosen parameters $\xi_0 = 10$, $\eta_0 = -0.92$, $\mathscr{V}_0 = 32000$, $\kappa = 0.1$, $\gamma = 1$, and $d = 10^{-4.52}$.

$\mathscr{V}$), potentially leading to new lower minima in the scalar potential. Consequently, they can be considered as potential candidates for waterfall fields.

In this particular setup, inflation proceeds along the local minimum with $\varphi = 0$ (the inflationary track), starting from large values of S. An instability occurs at the waterfall point $S_c^2 = M^2$, where $S_c = \frac{\partial^2 V}{\partial S^2}\,|_S = 0$. At this point, the field naturally transitions to one of the two SUSY minima at $\varphi = \pm M$. For large values of S, the scalar potential is approximately quadratic in φ, whereas at $S = 0$, equation (3.16) transforms into a Higgs potential. Along the inflationary track, a constant term V_0^{vol} is present at the tree level:

$$V_0^{vol} = \frac{\kappa^2 M^4}{3a\mathscr{V}_o^{4/3}} + \frac{3W_0^2(2\eta_0 \log(\mathscr{V}_o) - 8\eta_0 + \xi_0)}{2\mathscr{V}_o^3} \,,$$

indicating that SUSY is broken during inflation. This breaking of SUSY results in a splitting between fermionic and bosonic mass multiplets and introduces contributions to radiative corrections. Following the work by [268, 269], the soft terms are given by[5]

$$\Delta V_{\text{soft}} = \left[(m_{3/2}^2 + V_0) - \frac{2}{3\mathscr{V}_0^2} W_0^2 + \cdots\right] M^2 y^2 \frac{\mathscr{V}_0^{2/3}}{3a\gamma} = M_{s_c}^2 y^2 \,, \tag{3.24}$$

[5]Note that the factor $\frac{\mathscr{V}_0^{2/3}}{3a\gamma}$ originates from the transition to the canonically normalized field $s = S\sqrt{3a\gamma}/\mathscr{V}_0^{1/3}$. See also Appendix B.1.

where y denotes the ratio $y = s/M$, and

$$M_{s_c} = \left[(m_{3/2}^2 + V_0) - \frac{2}{3\mathscr{V}_0^2} W_0^2 + \cdots \right] M^2 \frac{\mathscr{V}_0^{2/3}}{3a\gamma} \,, \tag{3.25}$$

represents the soft mass parameter for the canonically normalized field y, with V_0 being the minimum of the potential (3.16).[6] For an appropriate set of parameters, V_0 is equivalent to the cosmological constant. The first extremum $(s = 0, \varphi = 0)$ represents a maximum of the potential. For $\varphi = 0$, the trajectory corresponds to the standard hybrid inflation, where $\{\varphi = 0, s > M\}$. When the inflaton reaches $s = M$, the waterfall field takes over, and the inflaton moves towards the minimum at $\varphi = \pm M$. Moreover, SUSY is broken along the inflationary track, and the radiative corrections, along with the soft SUSY-breaking potential V_{soft}, can lift the flatness of the potential while also providing the necessary slope for driving inflation. The effective contribution of the one-loop radiative corrections can be calculated using the Coleman-Weinberg formula [271]:

$$\Delta V_{\text{1-loop}} = \frac{\kappa^4 M^4 y^4}{144\pi^2 a^2 \gamma^2 \mathscr{V}_0^{4/3}} \left[F(y) - \left(\frac{1}{54 a^2 \alpha^2 \gamma^2} - \frac{3}{2} \mathscr{V}_0^{8/3} \right) \right] \,, \tag{3.26}$$

where

$$F(y) = \frac{1}{81 a^2 \alpha^2 \gamma^2} \log \left(\frac{\kappa^2 M^2 y^2}{27 a^2 \alpha \gamma^2 Q^2 \mathscr{V}_0^{2/3}} \right) - \mathscr{V}_0^{8/3} \log \left(\frac{\kappa^2 M^2 y^2 \mathscr{V}_0^{2/3}}{3 a \gamma Q^2} \right) \,. \tag{3.27}$$

Note that the Coleman-Weinberg correction is computed along the inflationary trajectory, where the field s takes a non-zero value while the field φ remains fixed at zero. Furthermore, we set $V_0 = 3.2\times 10^4$ for the volume field[7], and the mass spectrum depends solely on s. Detailed calculations are provided in Appendix B.2.

Including the various contributions computed above, we can write the scalar potential along the inflationary trajectory (i.e., $\varphi_1 = \varphi_2 = 0$) as:

$$\begin{aligned} V &\simeq V_F + V_D + \Delta V_{\text{1-loop}} + \Delta V_{\text{soft}}, \\ &\simeq \kappa^2 M^4 \left(\frac{V_0^{\text{vol}}}{\kappa^2 M^4} + \frac{\kappa^2 y^4 F(y)}{144\pi^2 a^2 \gamma^2 \mathscr{V}_0^{4/3}} - \frac{\kappa^2 y^4}{144\pi^2 a^2 \gamma^2 \mathscr{V}_0^{4/3}} \left(\frac{1}{54 a^2 \alpha^2 \gamma^2} - \frac{3}{2} \mathscr{V}_0^{8/3} \right) + \frac{M_{s_c}^2 y^2}{\kappa^2 M^2} \right) \,, \end{aligned} \tag{3.28}$$

where M_{s_c} is the soft mass parameter of the field s, and $V_0 \approx 0$ due to its extremely small magnitude compared to $m_{3/2}^2$.

To predict various inflationary observables, we employ standard slow-roll parameters:

$$\begin{aligned} \epsilon &= \frac{1}{2} \left(\frac{1}{M} \right)^2 \left(\frac{V'}{V} \right)^2, \quad \eta = \frac{1}{M^2} \left(\frac{V''}{V} \right), \\ \xi^2 &= \frac{1}{M^4} \left(\frac{V' V'''}{V^2} \right), \end{aligned}$$

where prime denotes the derivative with respect to y. Note that the presence of the mass parameter M in the above equations arises from the definition of the field y as the ratio $y = s/M$. In the

[6] The soft mass parameter M_{s_c} depends on both the gravitino mass $m_{3/2}$ and the constant parameter W_0. By choosing W_0 to be very small, the dominant term of the soft masses becomes dependent on the gravitino mass [270].

[7] For a discussion on multifield inflation scenarios in these types of models, see [272].

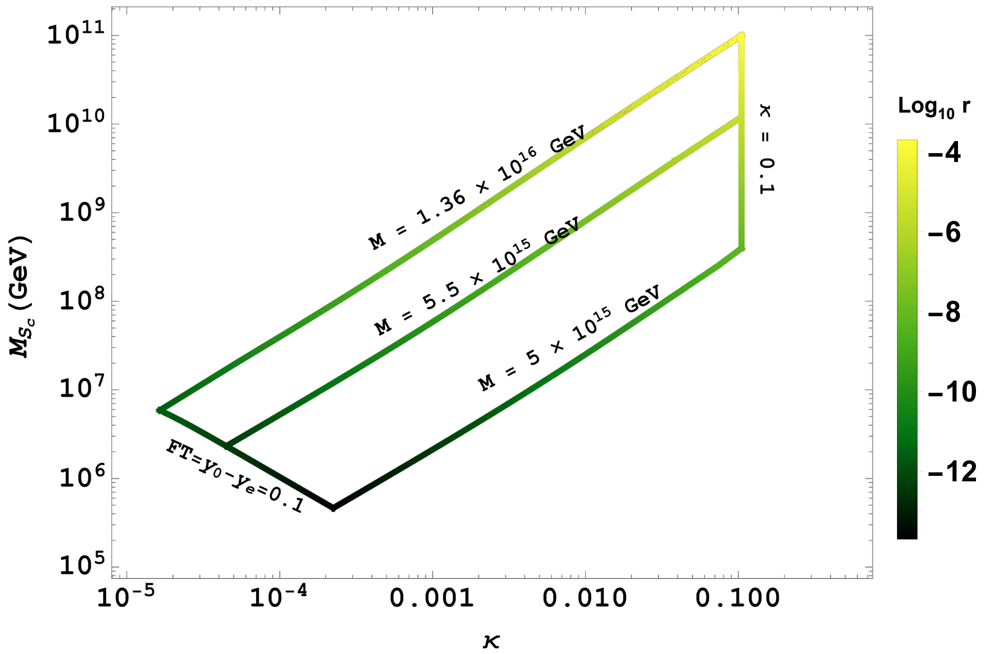

Figure 3.3: Variations of r and M in $\kappa - M_{s_c}$ plane. The upper line has M fixed at a value equal to M_{string}. The other two lines correspond to lower M values, as indicated in the plot.

slow-roll approximation, the scalar spectral index n_s, the tensor-to-scalar ratio r, and the running of the scalar spectral index $\alpha_s \equiv dn_s/d\ln k$ are given by:

$$\begin{aligned} n_s &\simeq 1 + 2\,\eta - 6\,\epsilon, \qquad r \simeq 16\,\epsilon, \\ \alpha_s &\simeq 16\,\epsilon\,\eta - 24\,\epsilon^2 - 2\,\xi^2. \end{aligned}$$

The scalar spectral index n_s in the ΛCDM model is observed to be $n_s = 0.9665 \pm 0.0038$ at the pivot scale $k_0 = 0.05\,\mathrm{Mpc}^{-1}$ [273].

The amplitude of the scalar power spectrum is given by:

$$A_s(k_0) = \frac{1}{24\,\pi^2}\left(\frac{V(y_0)}{\epsilon(y_0)}\right),$$

where $A_s(k_0) = 2.137\times10^{-9}$ at the pivot scale $k_0 = 0.05\,\mathrm{Mpc}^{-1}$ as measured by Planck 2018 [273].

The number of e-folds N_0 before the end of inflation is defined as:

$$N_0 = 2M^2 \int_{y_e}^{y_0} \left(\frac{V}{V'}\right) dy,$$

where $y_0 \equiv y(k_0)$ is the field value at the pivot scale k_0, and y_e is the field value at the end of inflation. The value of y_e is determined either by the breakdown of the slow-roll approximation ($\eta(y_e) = -1$) or by a 'waterfall' destabilization occurring at $y_e = 1$.

3.3.2 Numerical results

The outcomes of our numerical computations are depicted in Fig. 3.3, illustrating the ranges of r, M in the $\kappa - M_{s_c}$ plane. We consider up to the second-order approximation on the slow-roll parameters, setting $\gamma = 1$, $\alpha = 10^{-7}$, $\mathscr{V}_0 = 32000$, and $y_e = 1$. Additionally, we fix the spectral index n_s to the central value ($n_s = 0.96655$) from Planck's data.

Further constraints are imposed, requiring $\kappa \leq 0.1$, the Higgs mass parameter $10^{15} \leq M \leq M_{\text{string}} \sim 1/\mathscr{V}_o^{1/2} = 5.5 \times 10^{-3} M_p = 1.36 \times 10^{16}$ GeV, and FT (defined as the difference of field value at the pivot scale at the end of inflation) to be $FT \equiv y_0 - y_e \lesssim 0.1$. These constraints are illustrated in Fig. 3.3 as the boundaries of the allowed region in the $\kappa - M_{s_c}$ plane. In our analysis, the dominant role in obtaining a parametric space consistent with experimental bounds is played by the soft SUSY contributions, along with the radiative corrections, parametrized by M_{s_c} and a. Additionally, in the entire parameter space, a remains close to the value of 1.

Careful parameter selection in our analysis aims to suppress the contribution of the logarithmic terms in (3.27). However, when $\kappa \geq 0.1$, the logarithmic terms progressively become more dominant compared to the other components of the potential in (3.28). This dominance leads to a deviation of the spectral index (n_s) from the Planck bound.

For the scalar spectral index n_s fixed at Planck's central value ($n_s = 0.96655$), our numerical analysis indicates the following exact range of parameters for acceptable solutions:

$$\begin{gathered}
1.6 \times 10^{-5} \lesssim \kappa \lesssim 0.1, \\
(1 \times 10^{15} \lesssim M \lesssim 1.3 \times 10^{16}) \text{ GeV}, \\
(4.6 \times 10^{5} \lesssim M_{s_c} \lesssim 1 \times 10^{11}) \text{ GeV}, \\
1.9 \times 10^{-14} \lesssim r \lesssim 1.4 \times 10^{-4}, \\
0.86 \lesssim a \lesssim 1.
\end{gathered}$$

Examining these exact solution ranges, our calculations predict a low tensor-to-scalar ratio (r) compared to current experimental bounds. However, ongoing and future gravity waves experiments are expected to reach much smaller ranges of tensor-to-scalar ratio, comparable to our numerical predictions. Note that Fig. 3.3 shows the parametric space where $0.86 \lesssim a \lesssim 1$, aligning with the conditions for dark radiation, as discussed in the following section.

3.4 Reheating and dark radiation

Following the conclusion of inflation, the lightest moduli fields initiate oscillations around their respective minima, accumulating substantial energy density in the process. These modulus fields undergo decay, leading to two distinct categories of decay products. The first category involves decays into the visible sector, specifically particles within the Standard Model (SM) or its extensions, such as the Minimal Supersymmetric Standard Model (MSSM). These decays into visible matter induce a period of reheating, subsequently giving rise to the standard hot Big Bang cosmological evolution.

Additionally, there may be decays into states within the hidden sector. The hidden sector encompasses various candidates for dark radiation, including massless axions or light hidden gauge bosons. Let's consider the case of three Kähler moduli, denoted as $T_k = \tau_k + i a_k$, and $\mathscr{V} = \sqrt{\tau_1 \tau_2 \tau_3}$, where a_k represents the RR-axion.

The decay of the light axion a_k primarily occurs through the supergravity kinetic terms associated with the Kähler moduli, given by:

$$\mathscr{L} \supset K_{i\bar{j}} \partial_\mu T^i \partial^\mu T^{\bar{j}}. \tag{3.29}$$

The tree-level Kähler potential is expressed as:

$$K = -2\log\sqrt{(T_1+\bar{T}_1)(T_2+\bar{T}_2)(T_3+\bar{T}_3)} \; = \; -\log(\tau_1\tau_2\tau_3) + \cdots \tag{3.30}$$

In this equation, the ellipsis represents constant terms that can be disregarded. Consequently, the Kähler matrix is determined as:

$$K_{i\bar{j}} = \frac{1}{4}\mathrm{diag}\left(\frac{1}{\tau_1^2}, \frac{1}{\tau_3^2}, \frac{1}{\tau_3^2}\right). \tag{3.31}$$

As a result, Eq (3.29) can be reformulated as [274],

$$\mathscr{L} \supset \frac{1}{4}\frac{1}{\tau_i^2}\partial_\mu\tau_i\partial^\mu\tau_i$$

It's important to note that we have set the reduced Planck mass $M_p = 1$. To bring this into canonical form, we need to find the transformation $\tau_i(u_i)$ that satisfies:

$$\mathscr{L} \supset \frac{1}{2}\sum_i \partial_\mu u_i\partial^\mu u_i.$$

This implies:

$$\tau_i = e^{\sqrt{2}u_i}$$

The moduli fields for canonical kinetic terms adopt the following expressions:

$$u_k = \frac{1}{\sqrt{2}}\log\tau_k$$

The corresponding volume modulus is:

$$t = \frac{u_1+u_2+u_3}{\sqrt{3}} = \frac{1}{\sqrt{3}}\frac{1}{\sqrt{2}}\sum_k \log\tau_k = \sqrt{\frac{2}{3}}\log\mathscr{V}$$

The transverse directions are:

$$u = \frac{u_1-u_2}{\sqrt{2}} = \frac{1}{2}\log\frac{\tau_1}{\tau_2}, \; v = \frac{u_1+u_2-2u_3}{\sqrt{6}} = \frac{1}{\sqrt{3}}\log\frac{\tau_1\tau_2}{\tau_3^2}$$

We can reverse these relations as follows:

$$\begin{pmatrix} u_1 \\ u_2 \\ u_3 \end{pmatrix} = \begin{pmatrix} \frac{1}{\sqrt{3}} & \frac{1}{\sqrt{2}} & \frac{1}{\sqrt{6}} \\ \frac{1}{\sqrt{3}} & -\frac{1}{\sqrt{2}} & \frac{1}{\sqrt{6}} \\ \frac{1}{\sqrt{3}} & 0 & -\sqrt{\frac{2}{3}} \end{pmatrix} \begin{pmatrix} t \\ u \\ v \end{pmatrix}$$

For the Lagrangian involving the axions, we have [274]:

$$\mathscr{L} \supset -\frac{1}{4}\frac{1}{\tau_i^2}\partial_\mu a_i\partial^\mu a_i = -\frac{1}{4}e^{-2\sqrt{2}u_i}\partial_\mu a_i\partial^\mu a_i \,. \tag{3.32}$$

Expanding this, we obtain:

$$\mathscr{L} \supset -\frac{1}{4}\left[\partial_\mu a_i \partial^\mu a_i - 2\sqrt{2}\left(u_1 \partial_\mu a_1 \partial^\mu a_1 + u_2 \partial_\mu a_2 \partial^\mu a_2 + u_3 \partial_\mu a_3 \partial^\mu a_3\right)\right] , \tag{3.33}$$

where the first term represents the pure kinetic energy for the axions, while the second term represents the interaction terms. For the interaction part, expressing u_1, u_2, and u_3 in terms of u, v, and t, we have:

$$\begin{aligned}\mathscr{L} \supset & \frac{1}{\sqrt{6}} t\left(\partial_\mu a_1 \partial^\mu a_1 + \partial_\mu a_2 \partial^\mu a_2 + \partial_\mu a_3 \partial^\mu a_3\right) \\ & + \frac{1}{2} u\left(\partial_\mu a_1 \partial^\mu a_1 - \partial_\mu a_2 \partial^\mu a_2\right) \\ & + \frac{1}{2\sqrt{3}} v\left(\partial_\mu a_1 \partial^\mu a_1 + \partial_\mu a_2 \partial^\mu a_2 - 2\partial_\mu a_3 \partial^\mu a_3\right) .\end{aligned}$$

The decay rate of the lightest modulus u into axions can be expressed as follows:

$$\Gamma(u \to a_1 a_1) = \frac{1}{64\pi} m_u^3 \tag{3.34}$$

Here, m_u represents the mass of the modulus. In the context of the large volume scenario, a notable hierarchy of mass scales emerges (for further details, refer to [275]). After diagonalization with the Planck mass set to unity, the mass eigenstates can be expressed as:

$$m_t = m_u = m_v \sim \frac{1}{\mathscr{V}_o^{3/2}}, \quad m_{a_i} \sim e^{-2\pi \mathscr{V}_o^{2/3}}, \quad m_{soft} \sim \frac{1}{\mathscr{V}_o^{2/3}}, \quad m_{3/2} \sim \frac{1}{\mathscr{V}_o}, \quad M_{string} \sim \frac{1}{\mathscr{V}_o^{1/2}}.$$

In a similar vein, the primary decay channel in the visible sector is the decay into Higgs bosons. In the case of the Minimal Supersymmetric Standard Model (MSSM), we can make the following identifications: $\Phi_1 = H_u$ and $\Phi_2 = H_d$. Each of these fields consists of two complex components, resulting in eight degrees of freedom. The decay rate can be derived by including the matter contribution to the Kähler potential:

$$\mathscr{L} \supset \frac{3a\lambda}{\sqrt{2}} H_u H_d \Box u + h.c. + \cdots . \tag{3.35}$$

The dominant contribution to the decay of the light moduli u arises from the Giudice-Masiero coupling [276], specifically $3a\lambda H_u H_d \Box u$, as all other couplings are suppressed by mass [277]. Considering that each field is a complex doublet, the partial widths from each of the four decay channels contribute, yielding:

$$\Gamma(u \longrightarrow H_u H_d) = \frac{9a^2\lambda^2}{8\pi} m_u^3. \tag{3.36}$$

The present-day radiation content of the Universe can be characterized by the energy density associated with each relativistic particle species at present. This radiation includes photons and neutrinos, as well as any additional hidden components referred to as dark radiation (DR):

$$\rho_{radiation} = \rho_{photon} + \rho_{neutrino} + \rho_{DR} \tag{3.37}$$

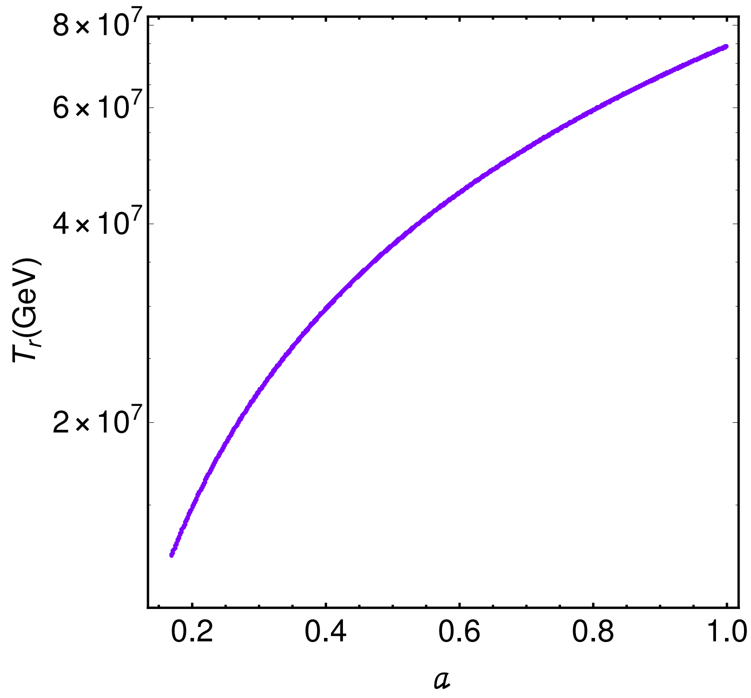

Figure 3.4: Variations of the reheating temperature (T_r) with respect to coefficient a consistent with dark radiation constraint ($\Delta N_{\rm eff} \lesssim 0.95$) at 95% confidence level.

This can be expressed in terms of an effective number of neutrino species, denoted as $N_{\rm eff}$:

$$\rho_{radiation} = \rho_{photon} \left(1 + \frac{7}{8} \left(\frac{4}{11} \right)^{4/3} N_{\rm eff} \right) . \tag{3.38}$$

Any excess radiation can be attributed to the presence of dark radiation (DR), described by:

$$\rho_{DR} = \rho_{photon} \left(\frac{7}{8} \left(\frac{4}{11} \right)^{4/3} \Delta N_{\rm eff} \right) , \tag{3.39}$$

Here, $\Delta N_{\rm eff} = N_{\rm eff} - 3.046$ quantifies the change in the effective number of neutrino species. The value of $N_{\rm eff}$ under the absence of dark radiation is expected to be approximately 3.046, slightly greater than 3 to account for partial reheating due to e^+e^- annihilation. $\Delta N_{\rm eff}$ can also be expressed in terms of decay rate channels:

$$\Delta N_{\rm eff} = \frac{43}{7} \left(\frac{10.75}{g_*(T_r)} \right)^{\frac{1}{3}} \frac{\Gamma_{\tau \to DR}}{\Gamma_{\tau \to SM}} = \frac{43}{7} \left(\frac{10.75}{g_*(T_r)} \right)^{\frac{1}{3}} \frac{1}{72 a^2 \lambda^2} , \tag{3.40}$$

Where $g_*(T_R h)$ represents the effective degree of freedom at the time of reheating the Universe.

The measured values of $N_{\rm eff}$ imply a constraint of $\Delta N_{\rm eff} \lesssim 0.95$ at the 95% confidence level. This translates into a bound on the model's parameters, specifically $a \cdot \lambda \gtrsim 0.1688$. In Fig. 3.3, the parameter space anticipated by the inflationary analysis falls within the range $0.86 \leq a \leq 1$. This interval is consistent with the values predicted by $\Delta N_{\rm eff} \lesssim 0.95$ and aligns with the conditions for dark radiation. Within this parameter range, we derive tensor-to-scalar ratio values of $r \leq 1.4 \times 10^{-4}$, $1 \times 10^{15} \lesssim M \lesssim 1.3 \times 10^{16}$ GeV, and a soft mass parameter $4.6 \times 10^5 \lesssim M_{s_c} \lesssim 1 \times 10^{11}$ GeV.

The isotropy of the Cosmic Microwave Background (CMB) on large scales can be attributed to inflation, followed by a reheating period. During this phase, the Universe's expansion slows down, and energy is transferred to Standard Model (SM) particles, bringing them into local thermal equilibrium. In this scenario, the Universe is reheated by a modulus u decaying into SM particles. The reheating temperature T_r, as determined by Eq. (3.34) and Eq. (3.40), is defined as:

$$T_r = \sqrt{\Gamma_u} = \sqrt{\frac{63}{344\pi}\Delta N_{\text{eff}} \left(\frac{g_*(T_r)}{10.75}\right)^{1/2} a^2\lambda^2 m_u^3}. \tag{3.41}$$

For a SUSY scale within the TeV range, the limitation on the reheating temperature is $T_r \lesssim 1$ GeV, corresponding to $g_*(T_r) = 224/7$, as discussed in Ref [262, 274]. In the current model, where $\mathscr{V}_o \sim 3.2 \times 10^4$ implies a SUSY scale of $m_{soft} > 10$ TeV. Consequently, the restriction on the reheating temperature becomes less stringent in this scenario. For a SUSY scale exceeding 10 TeV, we observe $g_*(T_r) = 106.75$, indicating a reheating temperature of approximately $T_r \sim 10^7$ GeV, as shown in Fig. 3.4.

Chapter 4

On the LHC signatures of $SU(5) \times U(1)'$ F-theory motivated models

4.1 Introduction

Despite its remarkable success, the SM of strong and electroweak interactions leaves numerous theoretical questions unanswered. Over the past few decades, accumulating evidence has indicated the need for new theoretical ingredients to account for various phenomena in particle physics and cosmology. Among its limitations, the minimal SM spectrum lacks a viable candidate for dark matter, and the exceedingly small neutrino masses present a naturalness challenge. Addressing this latter issue elegantly, the seesaw mechanism [32] introduces right-handed neutrinos and a new high-energy scale, offering an explanation for the tiny masses of the three neutrinos and their observed oscillations.

Notably, this framework aligns neatly with the paradigm of (supersymmetric) GUTs, which unify the three fundamental forces at a high GUT scale. Moreover, ongoing neutrino experiments have hinted at the possible existence of a 'sterile' neutrino, which could also serve as a viable dark matter candidate [278, 279]. Many other unresolved questions, such as the presence of remnants of an overarching theory, including leptoquarks, vector-like families, signatures of supersymmetry, and neutral gauge bosons, are anticipated to find answers through experiments conducted at the Large Hadron Collider (LHC).

Remarkably, numerous field theory GUTs incorporate most of these novel fields into larger representations. Furthermore, after spontaneous symmetry breaking occurs, scenarios often emerge in which additional $U(1)$ factors survive down to low energies, implying the existence of neutral gauge bosons with masses accessible to ongoing experiments. However, while GUTs featuring these new characteristics hold significant appeal, they come with trade-offs. Various extra fields, including heavy gauge bosons and other colored states, contribute to phenomena like fast proton decay and other rare processes.

In contrast to conventional field theory GUTs, string theory alternatives are subject to stringent selection rules and other restrictions. However, they also introduce new mechanisms that, under specific conditions, have the potential to mitigate many of the problematic states and undesired features encountered in field theory models. In particular, F-theory models [136, 140, 280] have gained attention for their ability to naturally incorporate such attractive features. These attributes are attributed to the intrinsic geometry of the compactification manifold and the fluxes that traverse matter curves, where various supermultiplets are localized.

To elaborate, the geometric properties and the configuration of fluxes can be chosen in a way that accomplishes several goals simultaneously. They can determine the desired symmetry-breaking patterns, reproduce the known multiplicity of chiral fermion families, and eliminate the presence of colored triplets in Higgs representations. Moreover, in F-theory constructions, the gauge symmetry of the resulting effective field theory model is intricately tied to the geometric structure of the elliptically fibred internal compactification space. Specifically, the non-abelian part of the gauge symmetry is associated with the codimension-one singular fibers, while possible abelian and discrete symmetries are identified in terms of the Mordell-Weil (MW) and Tate-Shafarevish (TS) groups [1].

In the context of elliptically fibred manifolds, the non-abelian gauge symmetry is described by a simply laced algebra, typically belonging to Lie groups of type A, D, or E. Notably, the highest rank corresponds to the exceptional group E_8. Singularities in the fibration correspond to certain divisors wrapped with 7-branes, which are associated with subgroups of E_8 and serve as the GUT group of the effective theory. Additionally, $U(1)$ symmetries may coexist with the non-abelian group. The origin of these $U(1)$ symmetries can either arise from the commutant of the GUT group within E_8 or be rooted in the MW and TS groups mentioned earlier.

Among the myriad possibilities, one particularly intriguing scenario involves the existence of a neutral gauge boson denoted as Z'. This gauge boson is associated with an abelian factor and exhibits non-universal couplings to quarks and leptons. Importantly, this Z' boson acquires mass at the TeV scale. Given that the SM gauge bosons couple universally to quarks and leptons across the three families, the presence of non-universal couplings would introduce deviations from SM predictions. Such deviations could be interpreted as compelling evidence for new physics beyond the SM.

In the context described above, a comprehensive study was introduced in [287], focusing on a generic class of F-theory semi-local models founded upon the E_8 subgroup, specifically $SU(5) \times U(1)'$. Notably, this $U(1)'$ symmetry was chosen to be anomaly-free, allowing for non-universal couplings to the three chiral families of particles, and leading to a low-energy gauge boson with a mass in the range of a few TeV. The work also delved into specific properties of representative models within this framework, particularly concerning new flavor phenomena and, in particular, B-meson physics as explored by the LHCb experiment [290–292].

The current work extends the previous analysis by conducting a systematic investigation into the diverse predictions and constraints that apply to all conceivable classes of viable models emerging from this framework. Initially, models are categorized based on their low-energy spectra and their behavior with respect to the $U(1)'$ symmetry. Two main classes are identified:

- Minimal MSSM Spectrum Models: This class comprises models with the minimum possible MSSM spectrum at low energies. Models within this category are further distinguished by their respective charges under the additional $U(1)'$ symmetry.

- Models with Extra Vector-Like Multiplets: In contrast, this class encompasses effective low-energy models that include additional MSSM multiplets appearing in vector-like pairs.

The current work primarily focuses on analyzing the constraints imposed by various physical processes on the models falling within the first class (i.e., the minimal models). The phenomenological

[1]For a recent survey, see, for example, [149]. For earlier F-theory reviews, refer to [144, 146, 147]. For models involving Mordell-Weil $U(1)$'s and other related topics, consult references [281]- [286].

examination of a representative example that includes extra vector-like states is also presented, while a comprehensive analysis of these models is reserved for future publication.

Within the first category of minimal models, the conditions required for anomaly cancellation lead to non-universal Z' couplings to the three families of fermion fields. Consequently, in most instances, stringent constraints arising from kaon decays suggest a relatively large Z' gauge boson mass, rendering it beyond the reach of present-day experiments. Conversely, models that incorporate extra vector-like pairs provide a spectrum of possibilities. Viable scenarios exist where the fermions of the first two generations share identical Z' couplings. In such cases, the stringent bounds associated with the Kaon oscillation ($K^0 - \overline{K^0}$) system can be circumvented, allowing for a Z' mass as low as a few TeV.

4.2 Non-universal Z' interactions

In the Standard Model, the neutral gauge boson couplings to fermions with the same electric charge are equal, resulting in flavor-diagonal tree-level interactions. However, this universality is not always applicable in models incorporating additional Z' bosons associated with extra $U(1)'$ factors originating from higher symmetries. When the $U(1)'$ charges of some or all of the three fermion families differ, it can give rise to significant flavor mixing effects, even at the tree level. This section delves into the fundamentals of non-universal $U(1)$ symmetries and establishes the necessary formalism for subsequent discussions.

4.2.1 Generalities and Formalism

To lay the foundation, we start by examining the neutral segment of the Lagrangian, which encompasses the interactions of Z' with fermions in the gauge eigenstates basis [135, 293]:

$$-\mathscr{L}_{NC} \supset eJ^{\mu}_{EM}A_{\mu} + \frac{g}{c_W}J^{(0)\,\mu}Z^0_{\mu} + g'J'^{\,\mu}Z'_{\mu}\ , \tag{4.1}$$

Here, A_μ denotes the massless photon field, Z^0 is the neutral gauge boson of the SM, and Z' is the novel boson associated with the additional $U(1)'$ gauge symmetry. Furthermore, g and g' represent the gauge couplings of the weak $SU(2)$ gauge symmetry and the new $U(1)'$ symmetry, respectively. In a compact notation, $\cos\theta_W$ and $\sin\theta_W$ are denoted as c_W and s_W, where θ_W signifies the weak mixing angle with $g = e/\tan\theta_W$. The neutral current linked to the Z' boson can be expressed as:

$$J'^{\,\mu} = \bar{f}^0_L\gamma^\mu q'_{f_L}f^0_L + \bar{f}^0_R\gamma^\mu q'_{f_R}f^0_R\ , \tag{4.2}$$

In this equation, f^0_L (f^0_R) signifies a column vector of left (right) chiral fermions of a specific type (u, d, e, or ν) in the gauge basis, and $q'_{f_{L,R}}$ are diagonal 3×3 matrices representing $U(1)'$ charges. The chiral fermions in the mass eigenstate basis are denoted as f_L, related to gauge eigenstates through unitary transformations:

$$f^0_L = V^\dagger_{f_L}f_L\ , \quad f^0_R = V^\dagger_{f_R}f_R\ \cdot \tag{4.3}$$

The unitary matrices $V_{f_{L,R}}$ are responsible for diagonalizing the Yukawa matrices Y_f:

$$Y^{diag}_f = V_{f_R}Y_fV^\dagger_{f_L}\ , \tag{4.4}$$

and they contribute to the CKM matrix:

$$V_{CKM} = V_{u_L} V_{d_L}^{\dagger} \; . \tag{4.5}$$

In the mass eigenbasis, the neutral current (4.2) takes the form:

$$J^{\mu} = \bar{f}_L \gamma^{\mu} Q'_{f_L} f_L + \bar{f}_R \gamma^{\mu} Q'_{f_R} f_R \; , \tag{4.6}$$

where Q'_{f_L} and Q'_{f_R} are defined as:

$$Q'_{f_L} \equiv V_{f_L} q'_{f_L} V_{f_L}^{\dagger} \; , \quad Q'_{f_R} \equiv V_{f_R} q'_{f_R} V_{f_R}^{\dagger} \; . \tag{4.7}$$

In cases where the $U(1)'$ charges in the q'_{f_L} matrix are equal, q'_{f_L} effectively becomes the unit matrix up to a common charge factor. Due to the unitarity of V_f's, the current in (4.6) remains flavor diagonal. In models featuring family non-universal $U(1)'$ charges, the mixing matrix Q'_{f_L} is non-diagonal, leading to flavor-violating terms in the effective theory.

4.2.2 Quark sector flavor violation

4.2.2.1 $b \to s l^+ l^-$ and R_K anomalies

The potential presence of non-universal Z' couplings to different fermion families can result in deviations from SM predictions, potentially leaving discernible signatures in current or upcoming experiments. The extent of these contributions hinges on several key factors, including the mass $M_{Z'}$ of the Z' gauge boson, the $U(1)'$ gauge coupling g', the $U(1)'$ fermion charges, and the mixing matrices V_f.

An intriguing case brought to attention by LHCb [292] and BaBar [294] collaborations involves anomalies observed in B-meson decays, specifically those related to the transition $b \to s l^+ l^-$, where $l = e, \mu, \tau$. Current LHCb measurements of b decays to different lepton pairs indicate possible deviations from lepton universality. For instance, the analysis of the q^2 invariant mass of the lepton pairs in the range 1.1 GeV$^2 < q^2 <$ 6 GeV^2 for the ratio of the branching ratios $Br(B \to K^{(*)} \ell^+ \ell^-), \ell = \mu, e$ yields [292]:

$$R_K \equiv \frac{Br(B \to K \mu^+ \mu^-)}{Br(B \to K e^+ e^-)} \simeq 0.846^{+0.016\,(\mathrm{stat})}_{-0.014\,(\mathrm{syst})} \; . \tag{4.8}$$

Similar results for $B \to K^*(892) \ell^+ \ell^-$ (where $K^* \to K\pi$), for the same ratio (4.8), are found to be approximately $R_{K^*} \simeq 0.69$. Since the SM strictly predicts $R^{SM}_{K^{(*)}} = 1$, these results strongly suggest the need to explore scenarios of New Physics (NP) where lepton universality is violated. In particular, in the case of $l = \mu$, both experimental and theoretical arguments suggest a potential connection to the muon channel [295–297].

In the SM, the process $B \to K^{(*)} l^+ l^-$ can only occur at the one-loop level, involving $W^{\pm}$ flavor-changing interactions (see the left panel of Figure 4.1. However, the presence of a Z' (neutral) gauge boson with non-universal couplings to fermions can lead to tree-level contributions (right panel of Figure 4.1), which might explain the observed anomalies.

The effective Hamiltonian that describes this interaction is given by [297]:

$$H^{b \to sll}_{eff} = -\frac{4 G_F}{\sqrt{2}} \frac{e^2}{16\pi^2} (V_{tb} V^*_{ts}) \sum_{k=9,10} \left(C^{ll}_k \mathcal{O}^{ll}_k + C'^{ll}_k \mathcal{O}'^{ll}_k \right) \tag{4.9}$$

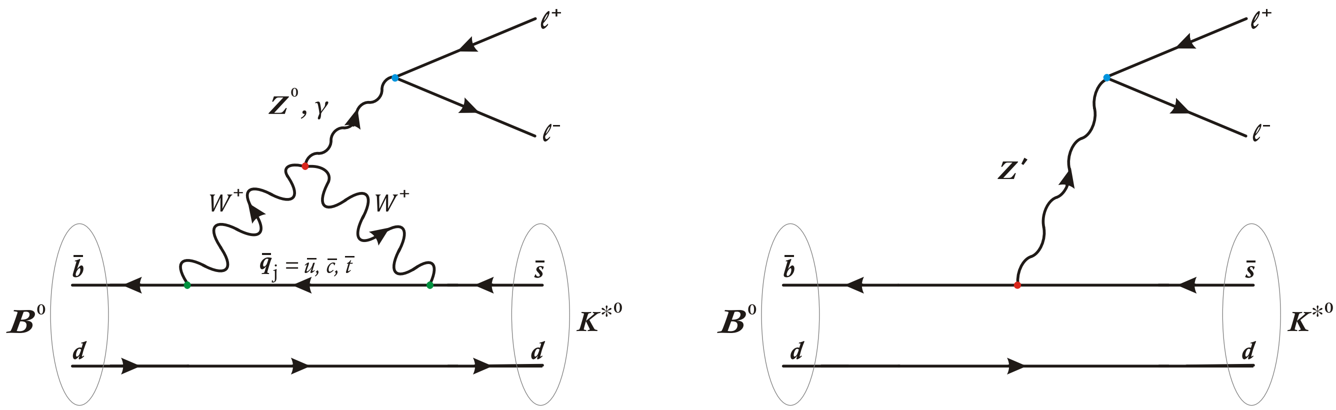

Figure 4.1: Left panel: Example of a Feynman diagram contributing to $B^0 \to K^* l^+ l^-$ in the SM context. Right panel: Tree level contribution in models with non-universal Z''s.

Here, O_n^{xx} represents dimension-6 operators, defined as

$$\mathcal{O}_9^{ll} = (\bar{s}\gamma^\mu P_L b)(\bar{l}\gamma_\mu l), \quad \mathcal{O}_{10}^{ll} = (\bar{s}\gamma^\mu P_L b)(\bar{l}\gamma_\mu l)$$
$$\mathcal{O}_9'^{ll} = (\bar{s}\gamma^\mu P_R b)(\bar{l}\gamma_\mu \gamma_5 l), \quad \mathcal{O}_9'^{ll} = (\bar{s}\gamma^\mu P_R b)(\bar{l}\gamma_\mu \gamma_5 l) \ ,$$

and C_k are Wilson coefficients that quantify the interaction strength. Additionally, G_F denotes the Fermi coupling constant, and V_{tb} and V_{ts}^* are elements of the CKM matrix.

The most recent data on $R_{K^{(*)}}$ ratios can be explained by assuming a negative contribution to the Wilson coefficient $C_9^{\mu\mu}$ while treating all other Wilson coefficients as negligible or vanishing [298]-[302]. The current best-fit value is approximately $C_9^{\mu\mu} \approx -0.95 \pm 0.15$.

In the presence of a non-universal Z' gauge boson, the $C_9^{\mu\mu}$ Wilson coefficient is given by:

$$C_9^{\mu\mu} = -\frac{\sqrt{2}}{4G_F}\frac{16\pi^2}{e^2}\left(\frac{g'}{M_{Z'}}\right)^2 \frac{(Q'_{d_L})_{23}(Q'_{e_L})_{22}}{V_{tb}V_{ts}^*} \ . \tag{4.10}$$

Achieving the desired value for the C_9 coefficient may involve appropriate tuning of the ratio $g'/M_{Z'}$. However, substantial suppressions can arise from the matrices Q'_f. In any case, the predictions must not conflict with well-known constraints stemming from rare processes, such as mixing effects in neutral meson systems.

4.2.2.2 Meson mixing

Flavor-changing Z' interactions within the quark sector can lead to substantial contributions to the mass splitting in a neutral meson system. A representative illustration is provided in Figure 4.2, depicting contributions to $B_s^0[s\bar{b}]$ mixing both in the Standard Model (SM) on the left and at the tree level in non-universal Z' models on the right.

For a meson P^0 characterized by quark structure $[q_i\bar{q}_j]$, the impact of Z' interactions on mass splitting is described by [293]:

$$\Delta M_P \simeq 4\sqrt{2}G_F M_P F_P^2 \left(\frac{M_W}{g \cdot c_w}\right)^2 \left(\frac{g'}{M_{Z'}}\right)^2 \frac{1}{3}\mathrm{Re}[(Q'_{q_L})_{ij}^2] \tag{4.11}$$

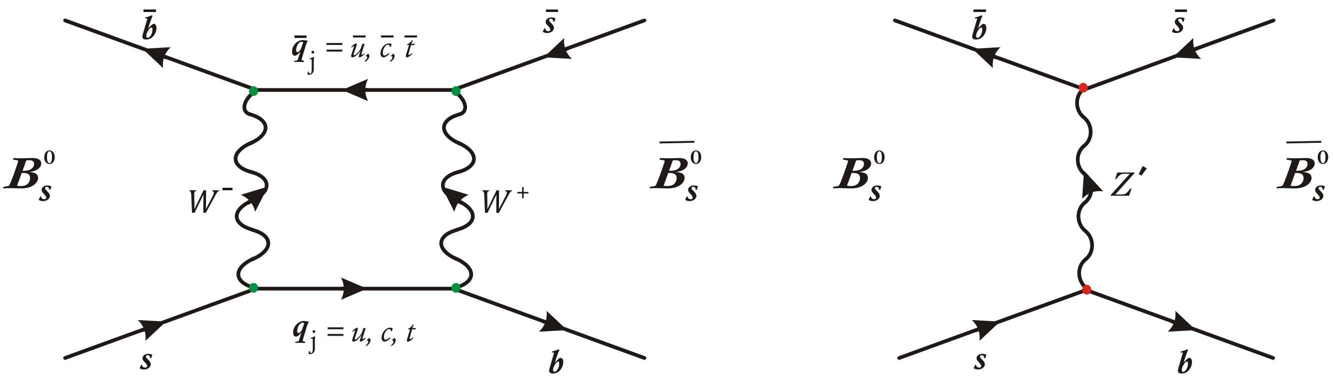

Figure 4.2: Left figure: Representative *box* diagram contribute to $(B_s^0 - \bar{B}_s^0)$ mixing in the SM. Right figure: Tree level contribution in models with non-universal Z' gauge bosons.

Here, M_W represents the mass of the $W^{\pm}$ gauge bosons, while M_P and F_P denote the mass and decay constant of the meson P^0, respectively. Additionally, c_w is defined as $\cos\theta_W$, where θ_W is the Weinberg angle.

It's worth noting that there exist significant uncertainties in the SM calculations of ΔM_P, primarily stemming from QCD factors and the CKM matrix elements. Nevertheless, experimental findings suggest that there might still be room for contributions from New Physics (NP).

We will now proceed to examine both theoretical and experimental constraints on $P^0 - \bar{P}^0$ meson systems, which will be crucial for our subsequent analysis.

- $B_s^0 - \overline{B_s^0}$ mixing:

B_s mixing can be effectively described by the Lagrangian:

$$\mathscr{L}^{NP} = -\frac{4G_F}{\sqrt{2}}(V_{tb}V_{ts}^*)^2[C_{bs}^{LL}(\bar{s}_L\gamma_\mu b_L)^2 + h.c.] \;, \tag{4.12}$$

In this equation, C_{bs}^{LL} represents a Wilson coefficient that alters the Standard Model (SM) prediction, as indicated by the equation below [303]:

$$\Delta M_s^{pred} = |1 + C_{bs}^{LL}/R_{SM}^{loop}|\Delta M_s^{SM} \;, \tag{4.13}$$

where $R_{SM}^{loop} = 1.3397 \times 10^{-3}$.

In the context of models featuring non-universal Z' couplings to fermions, the Wilson coefficient C_{bs}^{LL} is expressed as follows:

$$C_{bs}^{LL} = \frac{\eta^{LL}}{4\sqrt{2}G_F}\left(\frac{g'}{M_{Z'}}\right)^2 \frac{(Q'_{d_L})_{23}^2}{(V_{tb}V_{ts}^*)^2} \tag{4.14}$$

Here, $\eta^{LL} \equiv \eta^{LL}(M_{Z'})$ represents a constant that accounts for renormalization group effects. This constant has a weak dependency on the $M_{Z'}$ scale, and for our analysis, we assume $\eta^{LL} = 0.79$ corresponding to $M_{Z'} = 1\,TeV$.

For the Standard Model contribution ΔM_s^{SM}, we utilize the result obtained in Ref. [305]:

$$\Delta M_s^{SM} = (18.5^{+1.2}_{-1.5})\;ps^{-1} \;,$$

When compared to the experimental limit [306], $\Delta M_s^{exp} = (17.757^{+0.021}_{-0.021})\;ps^{-1}$, this demonstrates that a small positive C_{bs}^{LL} is permissible according to Eq (4.13).

• $K^0-\overline{K^0}$ mixing :

Standard Model computations for the mass splitting in the neutral Kaon system encompass a blend of short-distance and long-distance effects, expressed as [307]:

$$\Delta M_K^{SM}=(0.8\pm 0.1)\Delta M_K^{Exp}\ , \tag{4.15}$$

where experimental data are given by [306]:

$$\Delta M_K^{exp}\simeq 3.482\times 10^{-15}\ \ GeV.$$

This slight deviation between SM computations and experimental observations can be accounted for by introducing New Physics (NP) effects into the analysis. Therefore, following (4.15), the contribution of a non-universal Z' boson to ΔM_K must satisfy the following constraint [308]:

$$\Delta M_K^{NP}\lesssim 0.2\times\Delta M_K^{exp}\ , \tag{4.16}$$

where ΔM_K^{NP} can be calculated directly using the formula (4.11).

• $D^0-\overline{D^0}$ mixing:

Neutral D mesons are composed of up-type quarks, $D^0:\rightarrow[c\bar{u}]$. Experimental measurements for $D^0-\overline{D^0}$ oscillations are sensitive to the ratio:

$$x_D\equiv\frac{\Delta M_D}{\Gamma_D}\ , \tag{4.17}$$

with the observed value for the ratio being $x_D\simeq 0.32$ [309]. Given the substantial theoretical and experimental uncertainties in this process, we will consider NP contributions to x_D less than or equal to the experimental value.

4.2.2.3 Leptonic Meson Decays : $P^0\rightarrow l_i\bar{l}_i$

In the SM, the decay of a neutral meson P^0 into a lepton (l_i) and its anti-lepton ($\bar{l}_i$) occurs at the one-loop level. In the SM, these processes are suppressed due to the Glashow-Iliopoulos-Maiani (GIM) cancellation mechanism [310]. However, in non-universal Z' models, significantly larger tree-level contributions may be permitted. The decay width induced by Z' interactions can be expressed in terms of the SM decay $P^-\rightarrow l_i\bar{\nu}_i$ as [293]:

$$\Gamma(P^0\rightarrow l_i\bar{l}_i)\simeq 8\frac{\Gamma(P^-\rightarrow l_i\bar{\nu}_i)}{|V_{kj}^{CKM}|^2}\frac{M_P^3\sqrt{M_P^2-4m_{l_i}^2}}{(M_P^2-m_{l_i}^2)^2}\left(\frac{g'}{M_{Z'}}\right)^4\left(\frac{M_{Z_0}}{g}\right)^4|(Q'_{q_L})_{mn}(Q'_{e_L})_{ii}|^2\ , \tag{4.18}$$

Here, the indices j,k refer to the quark structure $[q_j\bar{q}_k]$ of the meson P^- involved in the SM interaction. Similarly, the indices m,n are used to denote the quark structure of the neutral meson P^0. For all relevant experimental constraints related to these interactions, you can refer to [306].

4.2.3 Lepton flavour violation

The lepton flavor violation processes involving decays of neutral mesons and radiative lepton decays can be significantly affected by non-universal Z' interactions. Here are the expressions for various processes and their associated constraints:

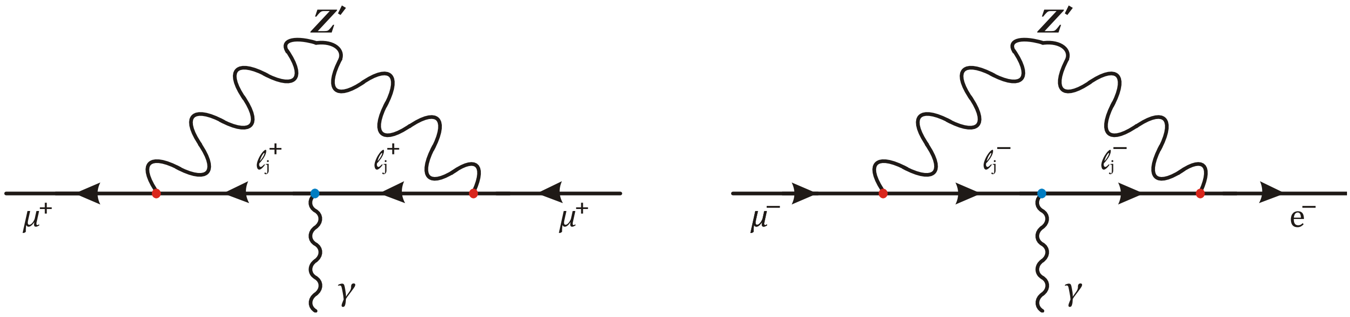

Figure 4.3: Left side: Contribution of a non-universal Z' boson into the magnetic moment of (anti)muon. Right side: Contribution to the decay, $\mu^- \to e^-\gamma$. Any of the three (anti)leptons ($j = e, \mu, \tau$) could run into the loop due to the non-universal charges under the extra $U(1)$ symmetry.

4.2.3.1 $P^0 \to l_i \bar{l}_j$

The decay width due to tree-level Z' contributions is given by:

$$\Gamma(P^0 \to l_i\bar{l}_j) \simeq 4\frac{\Gamma(P^- \to l_i\bar{\nu}_i)}{|V_{kr}^{CKM}|^2}\left(\frac{g'}{M_{Z'}}\right)^4\left(\frac{M_{Z_0}}{g}\right)^4 |(Q'_{u_L})_{mn}(Q'_{e_L})_{ij}|^2 \tag{4.19}$$

As previously mentioned, the indices k, r denotes the quark structure $[q_r\bar{q}_k]$ of the meson involved in the SM interaction, while generation indices m, n refer to the quark structure of P^0.

4.2.3.2 $(g-2)_\mu$

The muon's anomalous magnetic moment, represented as a_μ, is a meticulously measured physical parameter. Nevertheless, an intriguing inconsistency arises when comparing experimental measurements to the precise computations of the Standard Model (SM), as documented in [306]:

$$\Delta a_\mu \equiv a_\mu^{exp} - a_\mu^{SM} = 261(63)(48)\times 10^{-11}, \tag{4.20}$$

where $a_\mu^{SM} = 116591830(1)(40)(26)\times 10^{-11}$. This dissimilarity, referred to as Δa_μ, hints at the potential influence of New Physics (NP). When considering a neutral Z' boson, loop diagrams akin to the one depicted on the left side of Figure 4.3 contribute to the anomalous magnetic moment of the muon, Δa_μ. Collectively, the 1-loop contribution originating from non-universal Z' bosons is articulated in [311] as:

$$\Delta a_\mu^{Z'} = -\frac{m_\mu^2}{8\pi^2}\left(\frac{g'}{M_{Z'}}\right)^2\sum_{j=1}^{3}|(Q'_{e_L})_{2j}|^2 F(x_{l_j}^{Z'}), \tag{4.21}$$

where $x_{l_j}^{Z'} = (m_{l_j}/M_{Z'})^2$, and the loop function $F(x)$ is characterized by:

$$F(x) = \frac{5x^4 - 14x^3 + 39x^2 - 38x - 18x^2\ln(x) + 8}{12(1-x)^4}. \tag{4.22}$$

In our analysis, it is imperative to ensure that $\Delta a_\mu^{Z'}$ remains less than or equal to the experimental value Δa_μ. This comparison's imposed constraints aid in defining the parameter space of the non-universal Z' model while considering its compatibility with experimental observations. For visual reference, Figure 4.3 illustrates the contributions of a non-universal Z' boson to the muon's magnetic moment and the radiative decay $\mu^- \to e^-\gamma$, emphasizing that any of the three leptons ($j = e, \mu, \tau$) could engage in the loop due to non-universal charges under the extra $U(1)$ symmetry.

4.2.3.3 $l_i \to l_j\gamma$

A flavor-violating Z' boson also contributes to radiative decays of the form $l_i \to l_j\gamma$. Figure 4.3 (right) displays the 1-loop diagram for the strongly constrained decay $\mu^- \to e^-\gamma$. When we solely consider contributions from the Z' boson, the branching ratio for these interactions can be expressed using [312]:

$$\mathrm{Br}(l_i \to l_j\gamma) = \frac{e^2}{16\pi\Gamma_{l_i}} \left(m_{l_i} - \frac{m_{l_j}^2}{m_{l_i}}\right)^3 (g')^2 \sum_f \left[y_2(Q'_{e_L})_{fj}(Q'_{e_L})_{fi}\right] \; , \tag{4.23}$$

Here, the index $f = 1, 2, 3$ corresponds to the lepton circulating within the loop, Γ_{l_i} represents the total decay width of the lepton l_i, and y_2 is a loop function that can be found in [312]. The most recent experimental constraints on these processes are:

$$\mathrm{Br}(\mu \to \mathrm{e}\gamma) < 4.2 \times 10^{-13}, \; \mathrm{Br}(\tau \to \mathrm{e}\gamma) < 3.3 \times 10^{-8} \;\; \text{and} \;\; \mathrm{Br}(\tau \to \mu\gamma) < 4.4 \times 10^{-8} \cdot$$

It is expected that the most influential constraints will emerge from the muon decay process.

4.2.3.4 $l_i \to l_j l_k \bar{l}_j$

A lepton-flavor-violating Z' boson facilitates tree-level three-body leptonic decays, characterized by the form $l_i \to l_j l_j \bar{l}_k$. The branching ratio for these decays is described by the following expression [313]:

$$\mathrm{Br}(l_i \to l_j l_j \bar{l}_k) = \frac{m_{l_i}^5}{768\pi^3\Gamma_{l_i}} \left(\frac{g'}{M_{Z'}}\right)^4 |(Q'_{e_L})_{ij}(Q'_{e_L})_{kj}|^2 \; , \tag{4.24}$$

Here, it is important to note that the masses of the produced leptons have been omitted. For decays of the form $l_i \to l_j l_k \bar{l}_j$ with $k \neq j$, the branching ratio is given by the following equation:

$$\mathrm{Br}(l_i \to l_j l_j \bar{l}_k) = \frac{m_{l_i}^5}{1536\pi^3\Gamma_{l_i}} \left(\frac{g'}{M_{Z'}}\right)^4 |(Q'_{e_L})_{ik}(Q'_{e_L})_{jj} + (Q'_{e_L})_{ij}(Q'_{e_L})_{jk}|^2 \; . \tag{4.25}$$

The primary constraint in this context arises from the muon decay process $\mu^- \to e^-e^-e^+$. The branching ratio for this decay is constrained to be less than 10^{-12} at a 90% confidence level [314].

4.3 Non-universal $U(1)'$ models from F-theory

We now shift our focus to the realm of F-theory constructions that accommodate abelian factors bearing non-universal couplings with the three families of the Standard Model. Specifically, we center our attention on constructions based on an elliptically fibred compact space, with E_8 serving as the maximal singularity. Within this framework, we introduce a divisor in the internal manifold where the associated non-abelian gauge symmetry is $SU(5)$. Under this choice, the E_8 decomposition takes the form:

$$E_8 \supset SU(5) \times SU(5)_\perp \ . \tag{4.26}$$

In our analysis, we will focus on local constructions and describe the resultant effective theory utilizing the Higgs bundle picture. This approach relies on adjoint scalars, with only the Cartan generators acquiring non-vanishing vacuum expectation values (VEVs). It's worth noting that for non-diagonal generalizations, known as "T-branes," you can refer to [315].

In the local picture, we work with spectral data, including eigenvalues and eigenvectors. For the $SU(5)$ case, this data corresponds to a fifth-degree polynomial:

$$\mathscr{C}_5 = \sum_{k=0}^{5} b_k t^{5-k} = b_0 t^5 + b_1 t^4 + b_2 t^3 + b_3 t^2 + b_4 t + b_5 = 0 \ . \tag{4.27}$$

This polynomial defines the spectral cover for the fundamental representation of $SU(5)$. Furthermore, as a general property of $SU(n)$ groups, the five roots:

$$Q = \{t_1, t_2, t_3, t_4, t_5\} \ , \tag{4.28}$$

must sum to zero:

$$-b_1 \equiv \sum_{i=1}^{5} t_i = 0 \ . \tag{4.29}$$

The remaining coefficients, generically denoted as b_k for $k = 0, 2, 3, 4, 5$, are typically non-zero and carry information about the geometric properties of the internal manifold. The zero-mode spectrum of the effective low-energy theory arises from the decomposition of the E_8 adjoint with respect to the breaking pattern (4.26), which decomposes as follows:

$$248 \to (24, 1) + \boxed{(1, 24) + (10, 5) + (\overline{5}, 10) + (5, \overline{10})} + (\overline{10}, \overline{5}) \ . \tag{4.30}$$

The ordinary matter and Higgs fields, including the potential presence of singlets in the spectrum, are contained within the box on the right-hand side of (4.30). These fields transform as bi-fundamental representations with respect to the two $SU(5)$ groups.

For our analysis, we work within the limit where the perpendicular symmetry $SU(5)_\perp$ reduces down to the Cartan subalgebra following the breaking pattern $SU(5)_\perp \to U(1)_\perp^4$. In this simplified scenario, the GUT representations are characterized by specific combinations of the five weights given in (4.28). The five 10-plets, in particular, are described by the parameters $t_{1,2,\ldots,5}$, while the five-plets, originally transforming as decuplets under the second $SU(5)_\perp$, are represented by the combinations $t_i + t_j$. In the geometric context, these $SU(5)$ GUT representations reside on Riemann surfaces known as "matter curves," denoted as Σ_a, formed by the intersections of the $SU(5)$ GUT divisor with "perpendicular" 7-branes. These properties are summarized in the following notation:

$$\Sigma_{10_{t_i}} : \ 10_{t_i}, \overline{10}_{-t_i}, \ \ \Sigma_{5_{t_i+t_j}} : \ \overline{5}_{t_i+t_j}, 5_{-t_i-t_j}, \ \ \Sigma_{1_{t_i-t_j}} : \ 1_{t_i-t_j} \ . \tag{4.31}$$

As established earlier, the weights $t_{i=1,2,3,4,5}$ associated with the $SU(5)_\perp$ group are the roots of the polynomial (4.27). Consequently, they can be expressed as functions of the coefficients b_k, which encode the geometric properties of the compactification manifold. In our subsequent analysis, we will leverage topological invariant quantities and flux data to determine the spectrum and parameter space of the effective low-energy models under consideration.

We commence our exploration by identifying the zero-mode spectrum within the context we've outlined. Utilizing the spectral cover description as outlined in equations (4.27-4.31), we can determine the various matter curves within the theory that accommodate the $SU(5)$ GUT multiplets. These matter curves are governed by the following equations:

For $\Sigma_{10_{t_i}}$:

$$P_{10} := b_5 \sim \prod_{i=1}^{5} t_i = 0 \ , \tag{4.32}$$

For $\Sigma_{5_{t_i+t_j}}$:

$$P_5 := b_3^2 b_4 - b_2 b_3 b_5 + b_0 b_5^2 \sim \prod_{i\neq j} (t_i + t_j) = 0 \ . \tag{4.33}$$

In scenarios where all five roots t_i of the polynomial (4.27) are distinct and can be expressed as holomorphic functions of the coefficients b_k, we observe that there can be five matter curves accommodating the tenplets (decuplets) and ten matter curves for the fiveplets (quintuplets). This implies that the polynomial (4.27) could be factored as a product $\prod_{i=1}^{5}(\alpha_i t_i + \beta_i)$, with the coefficients α_i and β_i carrying the topological properties of the manifolds while remaining in the same field as the original b_k.

However, in the generic case, not all five solutions $t_i(b_k)$ belong to the same field as b_k. Consequently, there exist monodromy relations among subsets of the roots t_i, reducing the number of independent matter curves. Depending on the specific geometric properties of the compactification manifold, various factorizations of the spectral cover polynomial $\mathscr{C}_5$ can occur. These factorizations are parametrized by the Cartan subalgebra modulo the Weyl group $W(SU(5)_\perp)$. In essence, generic solutions involve branch cuts, and some roots become indistinguishable.

The simplest case arises when two of these roots are subject to a Z_2 monodromy, given by:

$$Z_2 : \ t_1 = t_2 \ . \tag{4.34}$$

Remarkably, the Z_2 monodromy has immediate implications in the effective field theory model. It allows for the tree-level coupling in the superpotential:

$$10_{t_1} 10_{t_2} 5_{-t_1-t_2} \xrightarrow{Z_2} 10_{t_1} 10_{t_1} 5_{-2t_1} \ , \tag{4.35}$$

which can induce a heavy top-quark mass in line with the requirements of low-energy phenomenology.

Returning to the spectral cover description under the Z_2 monodromy, the polynomial (4.27) factorizes as follows:

$$\mathscr{C}_5 = (a_1 + a_2 t + a_3 t^2)(a_4 + a_7 t)(a_5 + a_8 t)(a_6 + a_9 t) \ , \tag{4.36}$$

a_1	a_2	a_3	a_4	a_5	a_6	a_7	a_8	a_9	c
$\eta-2\mathsf{c}_1-\chi$	$\eta-\mathsf{c}_1-\chi$	$\eta-\chi$	$-\mathsf{c}_1+\chi_7$	$-\mathsf{c}_1+\chi_8$	$-\mathsf{c}_1+\chi_9$	χ_7	χ_8	χ_9	$\eta-2\chi$

Table 4.1: Homology classes of the coefficients a_j and c. Note that $\chi=\chi_5+\chi_7+\chi_9$ where χ_7,χ_8,χ_9 are the unspecified homologies of the coefficients a_5, a_7 and a_9 respectively.

where the existence of the second-degree polynomial is not factorizable as presented earlier, indicating that the corresponding roots t_1 and t_2 are indeed connected by the Z_2 monodromy.

We can establish the relationships between the coefficients b_k and a_j by comparing the spectral polynomial in (4.27). Consequently, we obtain the following relations:

$$\begin{aligned}
b_0 &= a_3a_7a_8a_9 \ ,\\
b_1 &= a_3a_6a_7a_8+a_3a_4a_9a_8+a_2a_7a_9a_8+a_3a_5a_7a_9 \ ,\\
b_2 &= a_3a_5a_6a_7+a_2a_6a_8a_7+a_2a_5a_9a_7+a_1a_8a_9a_7+a_3a_4a_6a_8+a_3a_4a_5a_9+a_2a_4a_8a_9 \ ,\\
b_3 &= a_3a_4a_5a_6+a_2a_5a_7a_6+a_2a_4a_8a_6+a_1a_7a_8a_6+a_2a_4a_5a_9+a_1a_5a_7a_9+a_1a_4a_8a_9 \ ,\\
b_4 &= a_2a_4a_5a_6+a_1a_5a_7a_6+a_1a_4a_8a_6+a_1a_4a_5a_9 \ ,\\
b_5 &= a_1a_4a_5a_6 \quad .
\end{aligned} \tag{4.37}$$

We impose the $SU(5)$ constraint $b_1=0$ under the assumption [167]:

$$a_2=-c(a_6a_7a_8+a_5a_7a_9+a_4a_8a_9),\quad a_3=ca_7a_8a_9, \tag{4.38}$$

where we introduce a new holomorphic section c. Substituting these into (4.37), we obtain:

$$\begin{aligned}
b_0 &= c\, a_7^2a_8^2a_9^2 \ ,\\
b_2 &= a_9\left(a_1a_7a_8-\left(a_5^2a_7^2+a_4a_5a_8a_7+a_4^2a_8^2\right)a_9c\right)-ca_6^2a_7^2a_8^2-ca_6a_7\left(a_5a_7+a_4a_8\right)a_9a_8 \ ,\\
b_3 &= a_1\left(a_6a_7a_8+\left(a_5a_7+a_4a_8\right)a_9\right)-\left(a_5a_7+a_4a_8\right)\left(a_6a_7+a_4a_9\right)\left(a_6a_8+a_5a_9\right)c \ ,\\
b_4 &= a_1\left(a_4a_6a_8+a_5\left(a_6a_7+a_4a_9\right)\right)-a_4a_5a_6\left(a_6a_7a_8+\left(a_5a_7+a_4a_8\right)a_9\right)c \ ,\\
b_5 &= a_1a_4a_5a_6 \quad .
\end{aligned} \tag{4.39}$$

The equations for the tenplets and fiveplets can now be expressed in terms of the holomorphic sections a_j and c. For the tenplets, we end up with four factors:

$$P_{10}=a_1\times a_4\times a_5\times a_6, \tag{4.40}$$

which correspond to four matter curves accommodating the tenplets of $SU(5)$. Substituting (4.39) into P_5 factorizes the equation into seven factors, corresponding to seven distinct fiveplets:

$$\begin{aligned}
P_5 \;=\; & (a_5a_7+a_4a_8)\times(a_6a_7+a_4a_9)\times(a_6a_8+a_5a_9)\\
& \times(a_6a_7a_8+a_4a_9a_8+a_5a_7a_9)\times(a_1-a_5a_6a_7c-a_4a_6a_8c)\\
& \times(a_1-a_5a_6a_7c-a_4a_5a_9c)\times(a_1-a_4a_6a_8c-a_4a_5a_9c) \quad .
\end{aligned} \tag{4.41}$$

Finally, we compute the homologies of the sections a_j's and c, as well as the homologies of each matter curve, by using the known homologies of the b_k coefficients:

$$[b_k]=(6-k)\mathsf{c}_1-t=\eta-k\,\mathsf{c}_1 \tag{4.42}$$

Matter Curve	Σ_{10_1}	Σ_{10_2}	Σ_{10_3}	Σ_{10_4}	Σ_{5_1}	Σ_{5_2}	Σ_{5_3}	Σ_{5_4}	Σ_{5_5}	Σ_{5_6}	Σ_{5_7}
Weights	$\pm t_1$	$\pm t_2$	$\pm t_3$	$\pm t_4$	$\pm 2t_1$	$\pm(t_1+t_3)$	$\pm(t_1+t_4)$	$\pm(t_1+t_5)$	$\pm(t_3+t_4)$	$\pm(t_3+t_5)$	$\pm(t_4+t_5)$
Def. equation	a_1	a_4	a_5	a_6	$a_6a_7a_8+\ldots$	$a_1-\ldots$	$a_1-\ldots$	$a_1-\ldots$	$a_5a_7+\ldots$	$a_6a_7+\ldots$	$a_6a_8+\ldots$
Homology	$\eta-2\mathsf{c}_1-\chi$	$\chi_7-\mathsf{c}_1$	$\chi_8-\mathsf{c}_1$	$\chi_9-\mathsf{c}_1$	$\chi-\mathsf{c}_1$	$\eta-2\mathsf{c}_1-\chi$	$\eta-2\mathsf{c}_1-\chi$	$\eta-2\mathsf{c}_1-\chi$	$\chi_7+\chi_8-\mathsf{c}_1$	$\chi_7+\chi_9-\mathsf{c}_1$	$\chi_8+\chi_9-\mathsf{c}_1$

Table 4.2: Matter curves along with their $U(1)_\perp$ weights ($\pm$ refer to $10/\overline{10}$ and $\bar{5}/5$ respectively), their defining equation and the corresponding homology class.

where c_1 is the first Chern class of the tangent bundle to S_{GUT}, $-t$ is the first Chern class of the normal bundle to S_{GUT}, and $\eta = 6\,\mathsf{c}_1 - t$. There are more a's than b's, so three homologies, $[a_7] = \chi_7$, $[a_8] = \chi_8$, and $[a_9] = \chi_9$, remain unspecified, as presented in Table 4.1.

4.3.1 $SU(5) \times U(1)'$ in the spectral cover description

Our objective is to investigate models based on $SU(5) \times U(1)'$, with a particular focus on the role of the non-universal $U(1)'$ symmetry, which needs to be consistently incorporated into the covering group E_8. Naturally, the $U(1)'$ symmetry should be a linear combination of the abelian factors present in $SU(5)_\perp$. A convenient abelian basis for expressing the desired $U(1)'$ symmetry arises through the following sequence of symmetry breaking:

$$\begin{aligned} E_8 &\supset E_6 \times SU(3)_\perp \supset E_6 \times U(1)_\perp \times U(1)'_\perp \\ &\supset SO(10) \times U(1)_\psi \times U(1)_\perp \times U(1)'_\perp \\ &\supset SU(5)_{GUT} \times U(1)_\chi \times U(1)_\psi \times U(1)_\perp \times U(1)'_\perp . \end{aligned}$$

Subsequently, the Cartan generators corresponding to the four $U(1)$ factors are expressed as:

$$\begin{aligned} Q'_\perp &= \frac{1}{2}\mathrm{diag}(1,-1,0,0,0), \\ Q_\perp &= \frac{1}{2\sqrt{3}}\mathrm{diag}(1,1,-2,0,0), \\ Q_\psi &= \frac{1}{2\sqrt{6}}\mathrm{diag}(1,1,1,-3,0), \\ Q_\chi &= \frac{1}{2\sqrt{10}}\mathrm{diag}(1,1,1,1,-4). \end{aligned}$$

The monodromy $t_1 \leftrightarrow t_2$ imposed in the previous section eliminates the abelian factor corresponding to $Q'_\perp$ when $t_1 \neq t_2$. As a result, we are left with the remaining three $SU(5)_\perp$ generators:

$$Q_\perp,\; Q_\psi,\; Q_\chi\;, \tag{4.43}$$

as given in the above relations. Subsequently, we assume that a low-energy $U(1)'$ is generated by a linear combination of the unbroken $U(1)$'s:

$$Q' = c_1 Q_\perp + c_2 Q_\psi + c_3 Q_\chi\;. \tag{4.44}$$

Concerning the coefficients c_1, c_2, c_3, we adopt the following normalization condition:

$$c_1^2 + c_2^2 + c_3^2 = 1\;, \tag{4.45}$$

while further constraints will be imposed through the application of anomaly cancellation conditions.

Matter Curve	Q'	N_Y	M	SM Content
$\Sigma_{10_{1,\pm t_1}}$	$\frac{10\sqrt{3}c_1+5\sqrt{6}c_2+3\sqrt{10}c_3}{60}$	$-N$	m_1	$m_1Q+(m_1+N)u^c+(m_1-N)e^c$
$\Sigma_{10_{2,\pm t_3}}$	$\frac{-20\sqrt{3}c_1+5\sqrt{6}c_2+3\sqrt{10}c_3}{60}$	N_7	m_2	$m_2Q+(m_2-N_7)u^c+(m_2+N_7)e^c$
$\Sigma_{10_{3,\pm t_4}}$	$\frac{\sqrt{10}c_3-5\sqrt{6}c_2}{20}$	N_8	m_3	$m_3Q+(m_3-N_8)u^c+(m_3+N_8)e^c$
$\Sigma_{10_{4,\pm t_5}}$	$-\sqrt{\frac{2}{5}}c_3$	N_9	m_4	$m_4Q+(m_4-N_9)u^c+(m_4+N_9)e^c$
$\Sigma_{5_{1,(\pm 2t_1)}}$	$-\frac{c_1}{\sqrt{3}}-\frac{c_2}{\sqrt{6}}-\frac{c_3}{\sqrt{10}}$	N	M_1	$M_1\overline{d^c}+(M_1+N)\overline{L}$
$\Sigma_{5_{2,\pm(t_1+t_3)}}$	$\frac{5\sqrt{3}c_1-5\sqrt{6}c_2-3\sqrt{10}c_3}{30}$	$-N$	M_2	$M_2\overline{d^c}+(M_2-N)\overline{L}$
$\Sigma_{5_{3,\pm(t_1+t_4)}}$	$-\frac{c_1}{2\sqrt{3}}+\frac{c_2}{\sqrt{6}}-\frac{c_3}{\sqrt{10}}$	$-N$	M_3	$M_3\overline{d^c}+(M_3-N)\overline{L}$
$\Sigma_{5_{4,\pm(t_1+t_5)}}$	$\frac{-10\sqrt{3}c_1-5\sqrt{6}c_2+9\sqrt{10}c_3}{60}$	$-N$	M_4	$M_4\overline{d^c}+(M_4-N)\overline{L}$
$\Sigma_{5_{5,\pm(t_3+t_4)}}$	$\frac{c_1}{\sqrt{3}}+\frac{c_2}{\sqrt{6}}-\frac{c_3}{\sqrt{10}}$	N_7+N_8	M_5	$M_5\overline{d^c}+(M_5+N_7+N_8)\overline{L}$
$\Sigma_{5_{6,\pm(t_3+t_5)}}$	$\frac{20\sqrt{3}c_1-5\sqrt{6}c_2+9\sqrt{10}c_3}{60}$	N_7+N_9	M_6	$M_6\overline{d^c}+(M_6+N_7+N_9)\overline{L}$
$\Sigma_{5_{7,\pm(t_4+t_5)}}$	$\frac{5\sqrt{6}c_2+3\sqrt{10}c_3}{20}$	N_8+N_9	M_7	$M_7\overline{d^c}+(M_7+N_8+N_9)\overline{L}$

Table 4.3: Matter curves along with their $U(1)'$ charges, flux data and the corresponding SM content. Note that $N=N_7+N_8+N_9$.

4.3.2 The Flux mechanism

Let's now delve into the process of symmetry breaking. In F-theory, the generation of observed chirality in the massless spectrum is achieved through the use of fluxes. More specifically, we can consider two distinct categories of fluxes. Initially, a flux is introduced along a $U(1)_\perp$, and its geometric constraint along a particular matter curve Σ_{n_j} is parameterized by an integer value. Consequently, the chiralities of the $SU(5)$ representations are defined as follows:

$$\begin{aligned} \#10_i-\#\overline{10}_i &= m_i\ , & (4.46)\\ \#5_j-\#\overline{5}_j &= M_j\ . & (4.47)\end{aligned}$$

These integers M_i and m_j are subject to the chirality condition:

$$\sum_i m_i=-\sum_j M_j=3 \tag{4.48}$$

This condition aligns with the anomaly conditions of the SM [316,317].

Next, we introduce a flux in the hypercharge direction, denoted as $\mathcal{F}_Y$, to break $SU(5)_{GUT}$ down to the SM gauge group. This"hyperflux" is also responsible for splitting $SU(5)$ representations. If we use integers $N_{i,j}$ to represent hyperfluxes penetrating certain matter curves, the combined effect of these two types of fluxes on the 10-plets and 5-plets is described as follows

$$10_{t_j}=\begin{cases} n_{(3,2)_{\frac{1}{6}}}-n_{(\bar{3},2)_{-\frac{1}{6}}} &= m_j\\ n_{(\bar{3},1)_{-\frac{2}{3}}}-n_{(3,1)_{\frac{2}{3}}} &= m_j-N_j\\ n_{(1,1)_{+1}}-n_{(1,1)_{-1}} &= m_j+N_j\end{cases}\ , \tag{4.49}$$

$$5_{t_i} = \begin{cases} n_{(3,1)_{-\frac{1}{3}}} - n_{(\bar{3},1)_{+\frac{1}{3}}} & = \; M_i \\ n_{(1,2)_{+\frac{1}{2}}} - n_{(1,2)_{-\frac{1}{2}}} & = \; M_i + N_i \; . \end{cases} \tag{4.50}$$

It's worth noting that the Higgs field resides on a matter curve of the type described in (4.50). This arrangement elegantly resolves the doublet-triplet splitting problem. By imposing $M_i = 0$, we eliminate the color triplet, and by selecting $N_i \neq 0$, we ensure the existence of massless doublets in the low-energy spectrum.

The $U(1)_Y$ flux is subject to specific conditions to prevent a heavy Green-Schwarz mass for the corresponding gauge boson. These conditions are expressed as:

$$\mathcal{F}_Y \cdot \eta = \mathcal{F}_Y \cdot \mathsf{c}_1 = 0 \; ,$$

Additionally, we assume that $\mathcal{F}_Y \cdot \chi_i = N_i$ (with $i = 7, 8, 9$) and correspondingly $\mathcal{F}_Y \cdot \chi = N$, where $N = N_7 + N_8 + N_9$. These conditions allow us to determine the effect of hyperflux on each matter curve. While m_i and M_j are constrained by the chirality condition (4.48), the hyperflux integers $N_{7,8,9}$ remain as free parameters of the theory since they are related to the undetermined homologies $\chi_{7,8,9}$.

Table 5.1 summarizes the flux data and the SM content of each matter curve. It also includes the charges of the remaining $U(1)'$ symmetry, which are functions of the coefficients $c_{1,2,3}$ and can be computed by applying anomaly cancellation conditions.

Additionally, there are singlet fields, as defined in (4.31), which play a crucial role in constructing realistic F-theory models. In this framework, these singlet states are parameterized by the vanishing combination $\pm(t_i - t_j) = 0$, $i \neq j$, due to the Z_2 monodromy. This results in twelve sing

lets denoted as θ_{ij}. Their $U(1)'$ charges and multiplicities are collectively presented in the following table:

Singlet Fields	Weights	Q'_{ij} (Q'_{ji})	Multiplicity
θ_{13}, (θ_{31})	$\pm(t_1 - t_3)$	$\pm\frac{\sqrt{3}c_1}{2}$	M_{13}, (M_{31})
θ_{14}, (θ_{41})	$\pm(t_1 - t_4)$	$\pm\frac{c_1+2\sqrt{2}c_2}{2\sqrt{3}}$	M_{14}, (M_{41})
θ_{15}, (θ_{51})	$\pm(t_1 - t_5)$	$\pm\frac{1}{12}\left(2\sqrt{3}c_1 + \sqrt{6}c_2 + 3\sqrt{10}c_3\right)$	M_{15}, (M_{51})
θ_{34}, (θ_{43})	$\pm(t_3 - t_4)$	$\pm\frac{\sqrt{2}c_2 - c_1}{\sqrt{3}}$	M_{34}, (M_{43})
θ_{35}, (θ_{53})	$\pm(t_3 - t_5)$	$\pm\frac{1}{12}\left(-4\sqrt{3}c_1 + \sqrt{6}c_2 + 3\sqrt{10}c_3\right)$	M_{35}, (M_{53})
θ_{45}, (θ_{54})	$\pm(t_4 - t_5)$	$\pm\frac{1}{4}\left(\sqrt{10}c_3 - \sqrt{6}c_2\right)$	M_{45}, (M_{54})

Table 4.4: Singlet fields θ_{ij} along with their corresponding $U(1)'$ charges and multiplicities M_{ij}. The "$(-)$" sign on the weights and charges refers to the singlets in the parentheses.

4.3.3 Anomaly cancellation conditions

In the preceding sections, we provided a comprehensive exposition of the F-$SU(5)$ GUT augmented with a flavor-dependent $U(1)'$ extension. This additional abelian factor is intricately embedded within the framework of $SU(5)_\perp \supset E_8$. For the effective theory to maintain renormalizability and UV completeness, it is imperative that the $U(1)'$ extension adheres to anomaly-free constraints. These constraints exert considerable influence on the $U(1)'$ charges present in the particle spectrum and consequently on the coefficients c_i defining the linear combination in (4.44).

This section is dedicated to the rigorous derivation of the anomaly cancellation conditions, which will help us ascertain the suitable linear combinations (4.44). These conditions will not only specify the permissible $U(1)'$ charge assignments for the zero-mode spectrum but also distinguish various low-energy models, each capable of making distinct predictions that can be tested against experimental data.

While the well-established MSSM anomaly cancellation conditions align with the chirality condition (4.48), enforced by the fluxes, we must also consider additional contributions to gauge anomalies stemming from the new $U(1)'$ factor. To seamlessly integrate this novel abelian factor into the effective theory, we need to address six distinct anomaly conditions:

$$\mathscr{A}_{331} \;:\; SU(3)_C SU(3)_C U(1)' \tag{4.51}$$
$$\mathscr{A}_{211} \;:\; SU(2)_L SU(2)_L U(1)' \tag{4.52}$$
$$\mathscr{A}_{YY1} \;:\; U(1)_Y U(1)_Y U(1)' \tag{4.53}$$
$$\mathscr{A}_{Y11} \;:\; U(1)_Y U(1)' U(1)' \tag{4.54}$$
$$\mathscr{A}_{111} \;:\; U(1)' U(1)' U(1)' \tag{4.55}$$
$$\mathscr{A}_{G} \;:\; \text{Gauge Gravity Anomaly}\,. \tag{4.56}$$

With the data from Table 5.1, we can straightforwardly compute the anomaly conditions (4.51-4.56). Analytical expressions for these conditions are provided in Appendix D.1. Notably, we find that $\mathscr{A}_{221} = \mathscr{A}_{331} = \mathscr{A}_{YY1} \equiv \mathscr{A}$, where $\mathscr{A}$ is contingent upon M_i, m_j, N_k, and linearly depends on $c_{1,2,3}$. On the other hand, the mixed $\mathscr{A}_{Y11}$ anomaly does not exhibit linearity with respect to $c_{1,2,3}$ and relies solely on the hyperflux integers N_k.

The cubic anomaly ($\mathscr{A}_{111}$) and gravitational anomaly ($\mathscr{A}_G$) hinge exclusively on the $U(1)'$ charges (and flux integers), prompting the involvement of singlet fields. The final terms in (D.3) and (D.2) reveal the contribution stemming from these singlets. To ensure that their contribution to the anomalies consistently cancels out, we can operate under the assumption that singlet fields always manifest in pairs ($M_{ij} = M_{ji}$) due to the property $Q'_{ij} = -Q'_{ji}$.

4.3.4 Solution Strategy

The anomaly conditions presented above involve intricate dependencies on the c_i coefficients, as well as the flux integers m_i, M_j, and N_k. To determine the c_i values, our first task is to address the flux integers. The precise configuration of the particle spectrum in this framework hinges on the specific choices made for these flux parameters. While there is some flexibility in selecting and distributing generations across different matter curves, certain phenomenological considerations can guide our decisions.

For instance, ensuring a tree-level top Yukawa coupling implies that the top quark should be localized on the 10_1 matter curve (as indicated in Table 5.1), and the MSSM up-Higgs doublet should be placed at 5_1. This is due to the Z_2 monodromy, which allows for the only renormalizable top-like operator of the form: $10_{t_1}10_{t_1}5_{-2t_1} \equiv 10_1 10_1 5_1$. Consequently, we arrive at the following conditions for some of the flux integers:

$$m_1 = 1,\; m_1 + N \geq 1,\; M_1 + N \geq 1. \tag{4.57}$$

Furthermore, resolving the doublet-triplet splitting problem necessitates that:

$$|N_7| + |N_8| + |N_9| \neq 0. \tag{4.58}$$

We can introduce additional constraints by demanding specific properties within the effective model and a predefined zero-mode spectrum. In the ensuing exploration, we will divide our search into two primary directions: minimal models that exclusively encompass the MSSM spectrum (without exotics) and models featuring vector-like pairs.

For each of these scenarios, we will impose constraints on the fluxes and subsequently search for all potential combinations of flux integers that satisfy these constraints. Subsequently, each set of flux solutions will be subjected to the anomaly conditions (D.1-D.3), and we will verify whether a viable solution for the c_i coefficients exists. Furthermore, each solution for the c_i coefficients must adhere to the normalization condition (4.45).

4.4 Models with MSSM spectrum

Our exploration begins with a straightforward scenario, focusing on models that incorporate the MSSM spectrum alongside pairs of conjugate singlet fields. It is important to underscore that we ensure the inclusion of three chiral families in the quarks and leptons of the MSSM spectrum by upholding the chirality condition (4.48).

In addition to the conditions (4.57) and (4.58), we introduce the following assumption:

$$M_1 = 0, \; N = 1. \tag{4.59}$$

This strategic choice prevents the introduction of exotic states, as only H_u remains as an MSSM state within the 5_1 matter curve. Furthermore, ensuring the absence of exotics imposes the following conditions:

$$m_i \geq 0, \; -M_j \geq 0. \tag{4.60}$$

Subsequently, we delve into the flux parameter space to identify combinations of m_i, M_j, and N_k that comply with the conditions (4.48), (4.57), (4.58), (4.59), and (4.60). We allow the flux parameters to vary within the range of $[-3, 3]$.

Our comprehensive search reveals fifty-four sets of integer flux values that conform to all the criteria outlined for the MSSM spectrum, including the tree-level top term. Out of these fifty-four flux solutions, only six yield a solution for the coefficients c_i with equal pairs of singlets denoted as $M_{ij} = M_{ji}$. This specific category of solutions is elaborated upon in Table 4.5, and the corresponding spectrum of models is presented in Table 4.6. These models are identified as *Class A*.

Model	m_1	m_2	m_3	m_4	M_1	M_2	M_3	M_4	M_5	M_6	M_7	N_7	N_8	N_9	c_1	c_2	c_3
A1	1	2	0	0	0	-1	0	0	-1	-1	0	1	0	0	0	$-\frac{1}{2}\sqrt{\frac{3}{2}}$	$\frac{1}{2}\sqrt{\frac{5}{2}}$
A2	1	0	2	0	0	0	-1	0	-1	0	-1	0	1	0	$\frac{1}{\sqrt{3}}$	$-\frac{1}{2\sqrt{6}}$	$-\frac{1}{2}\sqrt{\frac{5}{2}}$
A3	1	0	0	2	0	0	0	-1	0	-1	-1	0	0	1	$\frac{1}{\sqrt{3}}$	$-\sqrt{\frac{2}{3}}$	0
A4	1	0	0	2	0	0	0	0	-1	-1	-1	0	0	1	$\frac{1}{\sqrt{3}}$	$-\sqrt{\frac{2}{3}}$	0
A5	1	0	2	0	0	0	0	0	-1	-1	-1	0	1	0	$\frac{1}{\sqrt{3}}$	$-\frac{1}{2\sqrt{6}}$	$-\frac{1}{2}\sqrt{\frac{5}{2}}$
A6	1	2	0	0	0	0	0	0	-1	-1	-1	1	0	0	0	$-\frac{1}{2}\sqrt{\frac{3}{2}}$	$\frac{1}{2}\sqrt{\frac{5}{2}}$

Table 4.5: MSSM flux solutions along with the resulting c_i 's. For this class of models (Class A), singlets come in pairs ($M_{ij} = M_{ji}$).

Model **A1**		Model **A2**		Model **A3**		Model **A4**		Model **A5**		Model **A6**	
Q'	SM	Q'	SM	Q'	SM	Q'	SM	Q'	SM	Q'	SM
0	$Q+2u^c$	0	$Q+2u^c$	0	$Q+2u^c$	0	$Q+2u^c$	0	$Q+2u^c$	0	$Q+2u^c$
0	$2Q+u^c+3e^c$	-1/2	-	-1/2	-	-1/2	-	-1/2	-	0	$2Q+u^c+3e^c$
1/2	-	0	$2Q+u^c+3e^c$	1/2	-	1/2	-	0	$2Q+u^c+3e^c$	1/2	-
-1/2	-	1/2	-	0	$2Q+u^c+3e^c$	0	$2Q+u^c+3e^c$	1/2	-	-1/2	-
0	H_u	0	H_u	0	H_u	0	H_u	0	H_u	0	H_u
0	d^c+2L	-1/2	L	-1/2	L	-1/2	L	-1/2	L	0	L
1/2	L	0	d^c+2L	1/2	L	1/2	L	0	L	1/2	L
-1/2	L	1/2	L	0	d^c+2L	0	L	1/2	L	-1/2	L
1/2	d^c	-1/2	d^c	0	-	0	d^c+L	-1/2	d^c	1/2	d^c
-1/2	d^c	0	-	-1/2	d^c	-1/2	d^c	0	d^c+L	-1/2	d^c
0	-	1/2	d^c	1/2	d^c	1/2	d^c	1/2	d^c	0	d^c+L

Table 4.6: Models with MSSM spectrum plus pairs of singlet fields ($M_{ij} = M_{ji}$).

It's important to note that in all the models discussed above, the SM states share identical charges under the additional $U(1)'$, differing only in how these SM states are distributed across various matter curves. Across all scenarios, we anticipate similar implications at low energy levels.

However, if we relax the constraint of $M_{ij} = M_{ji}$ and allow for more general multiplicities for the singlets, we encounter solutions for an additional forty-eight sets of fluxes. This expansion leads to the emergence of three new classes, designated as *Class B*, *Class C*, and *Class D*, each offering consistent solutions. Notably, each class encompasses various flux and c_i solutions that yield identical Q' charges. The specific models within a class vary in terms of how the SM fields are distributed across the matter curves.

A selection of representative solutions from each class is presented in Table 4.7, while the corresponding models can be found in Table 4.8. For a comprehensive inventory of all the flux solutions, along with their associated charges and singlet spectrum, please refer to Appendix D.2.

Model	m_1	m_2	m_3	m_4	M_1	M_2	M_3	M_4	M_5	M_6	M_7	N_7	N_8	N_9	c_1	c_2	c_3
B7	1	0	1	1	0	-1	0	0	-1	0	-1	0	1	0	$-\frac{\sqrt{5}}{3}$	$\frac{1}{6}\sqrt{\frac{5}{2}}$	$-\frac{1}{2}\sqrt{\frac{3}{2}}$
C8	1	0	0	2	0	0	-1	0	0	-1	-1	0	0	1	$-\frac{\sqrt{5}}{6}$	$\frac{7}{12}\sqrt{\frac{5}{2}}$	$-\frac{1}{4\sqrt{6}}$
D9	1	1	0	1	0	0	0	0	-1	-1	-1	0	0	1	$\frac{1}{2}\sqrt{\frac{5}{6}}$	$\frac{5}{8}\sqrt{\frac{5}{3}}$	$-\frac{3}{8}$

Table 4.7: MSSM flux solutions along with the corresponding c_i 's for a general singlet spectrum.

Curve	Model **B7**		Model **C8**		Model **D9**	
	$\sqrt{15}Q'$	SM	$\sqrt{15}Q'$	SM	$\sqrt{10}Q'$	SM
10_1	-1	$Q + 2u^c$	1/4	$Q + 2u^c$	3/4	$Q + 2u^c$
10_2	3/2	-	3/2	-	-1/2	$Q + u^c + e^c$
10_3	-1	$Q + 2e^c$	-9/4	-	-7/4	-
10_4	3/2	$Q + u^c + e^c$	1/4	$2Q + u^c + 3e^c$	3/4	$Q + 2e^c$
5_1	2	H_u	-1/2	H_u	-3/2	H_u
$\bar{5}_2$	1/2	$d^c + 2L$	7/4	L	1/4	L
$\bar{5}_3$	-2	L	-2	$d^c + 2L$	-1	L
$\bar{5}_4$	1/2	L	1/2	L	3/2	L
$\bar{5}_5$	1/2	d^c	-3/4	-	-9/4	$d^c + L$
$\bar{5}_6$	3	d^c	7/4	d^c	1/4	d^c
$\bar{5}_7$	1/2	-	-2	d^c	-1	d^c

Table 4.8: MSSM like models accompanied by a general singlet spectrum.

Turning our attention to the observed patterns in the previously discussed models, a notable trend emerges. In all these models, one of the tenplets, specifically 10_2, 10_3, or 10_4, consistently acquires an equivalent $U(1)'$ charge as the 10_1 matter curve, which is home to the top quark. Consequently, at least one of the lightest left-handed quarks shares an identical Q' charge with the top quark. This alignment suggests that flavor processes associated with these two quark families are likely to be suppressed.

Moving forward, we explore various aspects of the models' phenomenology. Initially, we list all possible $SU(5) \times U(1)'$ invariant tree-level Yukawa terms:

• For the renormalizable top-Yukawa type operator:

$$10_1 10_1 \bar{5}_1. \tag{4.61}$$

This represents the sole allowable tree-level operator for the top quark, as dictated by the t_i weights (see Tables 4.7 and 4.8), thanks to the presence of the Z_2 monodromy.

• For renormalizable bottom-type quarks operators:

$$10_1\bar{5}_2\bar{5}_7,\ 10_1\bar{5}_3\bar{5}_6,\ 10_1\bar{5}_4\bar{5}_5,\ 10_2\bar{5}_3\bar{5}_4,\ 10_3\bar{5}_2\bar{5}_4,\ 10_4\bar{5}_2\bar{5}_3. \tag{4.62}$$

The presence of tree-level bottom and/or R-parity violation (RPV) terms in the models hinges on the specific distribution of SM states among the various matter curves.

4.4.1 Phenomenological Analysis

Thus far, we have identified a limited number of models that exhibit promising low-energy predictions. In the subsequent part of this section, our focus will be directed toward Model D9. The detailed implications of the remaining models will be explored in the Appendix.

For Model D9, the specifics regarding the fermion sectors can be found in Table 4.8, while additional information about the singlet sector is available in Appendix D.2. In our pursuit of realistic fermion hierarchies, we adopt the following distribution of the MSSM spectrum across various matter curves:

$$10_1 \longrightarrow Q_3+u^c_{2,3},\;\; 10_2 \longrightarrow Q_1+u^c_1+e^c_1,\;\; 10_4 \longrightarrow Q_2+e^c_{2,3}\;,$$

$$5_1 \longrightarrow H_u,\;\; \bar{5}_2 \longrightarrow H_d,\;\; \bar{5}_3 \longrightarrow L_3,\;\; \bar{5}_4 \longrightarrow L_2,\;\; \bar{5}_5 \longrightarrow d^c_1+L_1,\;\; \bar{5}_6 \longrightarrow d^c_2,\;\; \bar{5}_7 \longrightarrow d^c_3\;,$$

where the indices (1, 2, 3) on the SM states denote generation.

Top Sector

The primary contributions to the up-type quarks arise from the following superpotential terms:

$$\begin{aligned} W \supset\, & y_t 10_1 10_1 5_1+\frac{y_1}{\Lambda}10_1 10_2 5_1\theta_{13}+\frac{y_2}{\Lambda}10_1 10_4 5_1\theta_{15}+\frac{y_3}{\Lambda^2}10_2 10_4 5_1\theta_{13}\theta_{15}\\ &+\frac{y_4}{\Lambda^2}10_2 10_2 5_1\theta_{13}^2+\frac{y_5}{\Lambda^2}10_1 10_2 5_1\theta_{15}\theta_{53}+\frac{y_6}{\Lambda^3}10_2 10_2 5_1\theta_{15}\theta_{53}\theta_{13}\;, \end{aligned}$$

where y_i's are coefficients of coupling constants, and Λ represents a characteristic high-energy scale of the theory. These operators result in the following mass texture:

$$M_u = v_u\begin{pmatrix} y_4\vartheta_{13}^2+y_6\vartheta_{15}\vartheta_{53}\vartheta_{13} & y_3\vartheta_{13}\vartheta_{15} & y_1\vartheta_{13}+y_5\vartheta_{15}\vartheta_{53}\\ y_1\vartheta_{13}+y_5\vartheta_{15}\vartheta_{53} & y_2\vartheta_{15} & \varepsilon y_t\\ y_1\vartheta_{13}+y_5\vartheta_{15}\vartheta_{53} & y_2\vartheta_{15} & y_t \end{pmatrix}\,, \tag{4.63}$$

where $v_u=\langle H_u\rangle$, $\vartheta_{ij}=\langle\theta_{ij}\rangle/\Lambda$, and $\varepsilon\ll 1$ serves as a suppression factor. This factor captures local effects of Yukawa couplings stemming from a common tree-level operator [318–320]. The matrix exhibits the appropriate structure to account for the hierarchy observed in the top sector.

Bottom Sector

The down-type quarks in this model receive contributions from both tree-level and non-renormalizable operators. The dominant terms are as follows:

$$\begin{aligned} W \supset\, & y_b 10_1\bar{5}_7\bar{5}_2+\frac{\kappa_1}{\Lambda}10_1\bar{5}_5\bar{5}_2\theta_{53}+\frac{\kappa_2}{\Lambda}10_1\bar{5}_6\bar{5}_2\theta_{43}+\frac{\kappa_3}{\Lambda}10_2\bar{5}_7\bar{5}_2\theta_{13}+\frac{\kappa_4}{\Lambda^2}10_2\bar{5}_6\bar{5}_2\theta_{13}\theta_{43}\\ &+\frac{\kappa_5}{\Lambda^2}10_2\bar{5}_5\bar{5}_2\theta_{13}\theta_{53}+\frac{\kappa_6}{\Lambda^2}10_2\bar{5}_7\bar{5}_2\theta_{15}\theta_{53}+\frac{\kappa_7}{\Lambda^3}10_2\bar{5}_5\bar{5}_2\theta_{15}\theta_{53}^2+\frac{\kappa_8}{\Lambda^3}10_2\bar{5}_6\bar{5}_2\theta_{14}\theta_{43}^2+\frac{\kappa_9}{\Lambda}10_4\bar{5}_7\bar{5}_2\theta_{15}\;,\\ &+\frac{\kappa_{10}}{\Lambda}10_4\bar{5}_5\bar{5}_2\theta_{13}+\frac{\kappa_{11}}{\Lambda^2}10_4\bar{5}_6\bar{5}_2\theta_{13}\theta_{45}+\frac{\kappa_{12}}{\Lambda^2}10_4\bar{5}_5\bar{5}_2\theta_{15}\theta_{53}+\frac{\kappa_{13}}{\Lambda^3}10_4\bar{5}_6\bar{5}_2\theta_{15}\theta_{45}\theta_{53} \end{aligned}$$

where κ_i and y_b represent the coefficients of coupling constants. These operators contribute to the following down quark mass matrix:

$$M_d = v_d\begin{pmatrix} \kappa_5\vartheta_{53}\vartheta_{13}+\kappa_7\vartheta_{15}\vartheta_{53}^2 & \kappa_{10}\vartheta_{13}+\kappa_{12}\vartheta_{15}\vartheta_{53} & \kappa_1\vartheta_{53}\\ \kappa_4\vartheta_{13}\vartheta_{43}+\kappa_8\vartheta_{14}\vartheta_{43}^2 & \kappa_{11}\vartheta_{13}\vartheta_{45}+\kappa_{13}\vartheta_{15}\vartheta_{45}\vartheta_{53} & \kappa_2\vartheta_{43}\\ \kappa_3\vartheta_{13}+\kappa_6\vartheta_{15}\vartheta_{53} & \kappa_9\vartheta_{15} & y_b \end{pmatrix}\,, \tag{4.64}$$

where $v_d=\langle H_d\rangle$ represents the vacuum expectation value of the down-type MSSM Higgs. It's important to note that this matrix is subject to corrections from higher-order terms, and due to the contribution of numerous operators, we anticipate significant mixing effects.

Charged Lepton Sector

In the current model, when flux penetrates the various matter curves, the SM generations are distributed across different matter curves. Consequently, down-type quarks and the charged lepton sectors typically arise from different couplings.

However, in this model, the shared operators between the bottom and charged lepton sectors are those previously listed in (4.64) with couplings κ_5, κ_7, κ_{10}, and κ_{12}. All other contributions originate from the operators:

$$W \supset y_\tau 10_4\bar{5}_3\bar{5}_2 + \frac{\lambda_1}{\Lambda}10_2\bar{5}_4\bar{5}_2\theta_{43} + \frac{\lambda_2}{\Lambda}10_2\bar{5}_3\bar{5}_2\theta_{53} + \frac{\lambda_3}{\Lambda}10_4\bar{5}_4\bar{5}_2\theta_{45} \ , \tag{4.65}$$

where y_τ represents a tree-level Yukawa coefficient, λ_i denotes coupling constants, and $\eta \ll 1$ encapsulates the effects of local tree-level Yukawa couplings. Collectively, these operators contribute to the following mass texture for the charged leptons in the model:

$$M_e = v_d \begin{pmatrix} \kappa_5\vartheta_{53}\vartheta_{13} + \kappa_7\vartheta_{15}\vartheta_{53}^2 & \lambda_1\vartheta_{43} & \lambda_2\vartheta_{53} \\ \kappa_{10}\vartheta_{13} + \kappa_{12}\vartheta_{15}\vartheta_{53} & \lambda_3\vartheta_{45} & \eta y_\tau \\ \kappa_{10}\vartheta_{13} + \kappa_{12}\vartheta_{15}\vartheta_{53} & \lambda_3\vartheta_{45} & y_\tau \end{pmatrix} . \tag{4.66}$$

The μ-term

The bilinear term $5_1\bar{5}_2$ does not possess invariance under the additional $U(1)'$ symmetry. However, the μ-term is generated dynamically through the renormalizable operator:

$$\kappa 5_1\bar{5}_3\theta_{13} \longrightarrow \kappa\langle\theta_{13}\rangle H_u H_d \equiv \mu H_u H_d \ . \tag{4.67}$$

There are no specific constraints imposed on the VEV of the singlet field θ_{13}. Therefore, proper tuning of the values of κ and $\langle\theta_{13}\rangle$ can lead to an acceptable μ-parameter, typically around the TeV scale. Consequently, the singlet field θ_{13}, which also contributes to the quarks and charged lepton sectors, must acquire a VEV at an energy scale near the TeV region.

It's also worth noting that some of the singlet fields couple to the left-handed neutrinos and can potentially serve as their right-handed partners. In particular, as suggested in [280], the six-dimensional massive KK-modes corresponding to the neutral singlets identified by the Z_2 symmetry $\theta_{12} \equiv \theta_{21}$ can be associated with $\theta_{12} \to \nu^c$ and $\theta_{21} \to \bar{\nu}^c$, allowing for a Majorana mass term $M_N\nu^c\bar{\nu}^c$. While further exploration of this concept is beyond the scope of this discussion, related phenomenological analyses can be found in [321].

CKM matrix

The fermion mass matrices obtained thus far can be diagonalized through unitary matrices V_{f_L}. The various coupling constants and VEVs can be adjusted to ensure that the diagonal mass matrices satisfy the appropriate mass relations at the GUT scale. For this analysis, we utilize the Renormalization Group Equation (RGE) results for a large $\tan\beta = v_u/v_d$ scenario as provided in Ref. [322]. Additionally, the combination $V_{u_L}V_{d_L}^\dagger$ must closely resemble the CKM matrix.

Using a set of natural numerical values:

$$\kappa_i \simeq 1,\ y_1 = y_4 = y_5 = y_6 = 25y_2 = 25y_3 \simeq 0.5,\ \epsilon = 10^{-4},\ y_t = 0.5,\ y_b = 0.36 \ ,$$

we fit the singlet VEVs ϑ_{ij} to the following values:

$$\vartheta_{13} \simeq 3.16\times10^{-12}, \vartheta_{14} \simeq 3.98\times10^{-3},\ \vartheta_{15} \simeq 10^{-1},\ \vartheta_{43} \simeq 1.9\times10^{-2},\ \vartheta_{53} \simeq 6.94\times10^{-3},\ \vartheta_{45} \simeq 10^{-2} \ .$$

As a result, for the up and down quark diagonalization matrices, we obtain:

$$V_{u_L} = \begin{pmatrix} -1 & -0.000694 & 0.000694 \\ 0.000694 & -1 & 0.000116 \\ 0.0006939 & 0.000116 & 1 \end{pmatrix}, \; V_{d_L} = \begin{pmatrix} -0.9738 & 0.2273 & 0.00674 \\ -0.2266 & -0.9726 & 0.0519 \\ 0.0183 & 0.04908 & 0.9986 \end{pmatrix} \cdot \quad (4.68)$$

The resulting CKM matrix aligns with experimentally measured values:

$$|V_{CKM}| \simeq \begin{pmatrix} 0.973659 & 0.227932 & 0.00601329 \\ 0.227325 & 0.972437 & 0.0518632 \\ 0.0176688 & 0.04913 & 0.998636 \end{pmatrix}. \quad (4.69)$$

Notably, the CKM matrix is primarily influenced by the bottom sector, while V_{u_L} is nearly diagonal and unimodular.

Furthermore, the unitary matrix V_{e_L} that diagonalizes the charged lepton mass matrix can be computed. The correct Yukawa relations and the charged lepton mass spectrum are achieved with:

$$V_{e_L} = \begin{pmatrix} -0.801463 & 0.597943 & 0.0110641 \\ -0.597877 & -0.801539 & 0.00888511 \\ 0.0141811 & 0.000506117 & 0.999899 \end{pmatrix}, \quad (4.70)$$

where the remaining parameters are fitted as follows: $\lambda_1 = 0.4, \lambda_2 = \lambda_3 = 1, \eta = 10^{-4}$, and $y_\tau =\simeq 0.51$.

R-parity violating terms

In the model we are examining, there are several tree-level as well as bilinear operators that can lead to RPV effects while remaining invariant under all the symmetries of the theory. To be more specific, the following tree-level operators violate both lepton and baryon number:

$$10_1\bar{5}_3\bar{5}_6 \longrightarrow \lambda' Q_3 L_3 d_2^c\,, \quad (4.71)$$

$$10_2\bar{5}_3\bar{5}_4 \longrightarrow \lambda L_3 L_2 e_1^c\,, \quad (4.72)$$

It is important to note, however, that there is an absence of $u^c u^c d^c$ type RPV terms, which, in combination with QLd^c terms, could potentially destabilize the proton.

Additionally, there exist bilinear RPV terms stemming from tree-level operators in the present model:

$$5_1\bar{5}_3\theta_{14}\,, \quad 5_1\bar{5}_4\theta_{15}\,. \quad (4.73)$$

The impact of these terms heavily depends on the dynamics of the singlets, but it is desirable to completely eliminate such operators.

One approach to address this is by introducing an R-symmetry manually [167], or by investigating the geometric origin of discrete Z_N symmetries that can effectively eliminate such operators [323]- [326]. Furthermore, a study of these Yukawa coefficients at a local level shows that they can be suppressed for broad regions of the flux parameter space [327].

Given that the primary focus of this work revolves around Z' flavor-changing effects, we will assume that one of the mechanisms mentioned above safeguards the models against undesirable RPV terms.

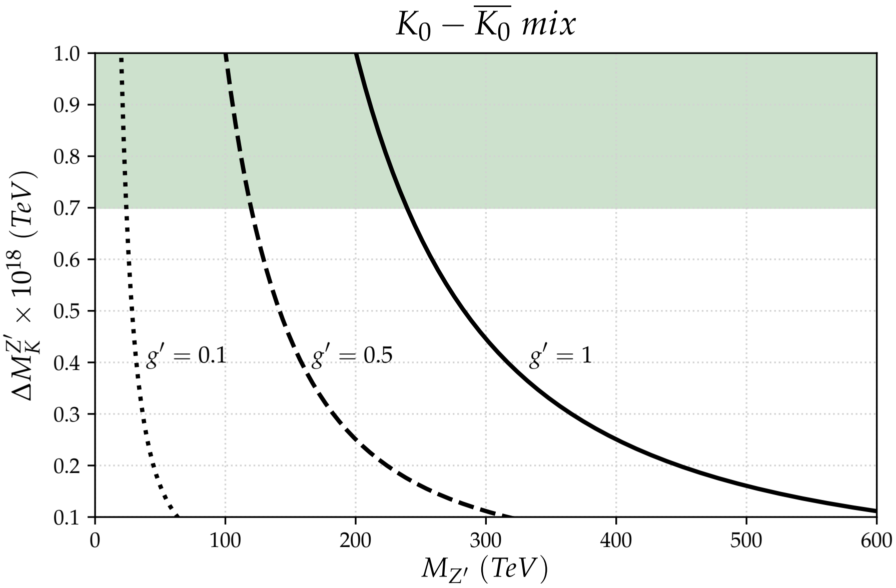

Figure 4.4: Bounds to the neutral gauge boson mass $M_{Z'}$ of Model D9 due to $K_0 - \bar{K}_0$ mixing effects. The vertical axis displays Z' contributions ($\Delta M_K^{Z'}$) to the mass split of the neutral Kaon system. Dotted, dashed and solid black curves correspond to gauge coupling values: $g' = 0.1$, 0.5, and 1 respectively. The shaded region is excluded due the constrain $\Delta M_K^{NP} < 0.2 \Delta M_K^{exp}$.

4.4.2 Z' bounds for Model D9

Having successfully obtained the V_f matrices for both the top/bottom quark and charged lepton sectors, the next step is to straightforwardly calculate the flavor mixing matrices Q'_{f_L} as defined in equation (4.7). These matrices, in conjunction with the Z' mass ($M_{Z'}$) and gauge coupling (g'), play a pivotal role in computing various flavor-violating observables, as elucidated in previous a section Consequently, we can utilize the constraints imposed on these observables to establish limits on the Z' mass and gauge coupling, or more precisely, the ratio $g'/M_{Z'}$.

It is essential to ensure that these derived constraints align with the limitations imposed by the Large Hadron Collider (LHC) findings stemming from dilepton and diquark channels [334–336], especially in the context of heavy Z' searches. It is worth noting that LHC constraints on the masses of neutral gauge bosons vary considerably depending on the specific model. For the majority of GUT-inspired Z' models, masses in the vicinity of $\sim 2-3$ TeV have been excluded.

In the model we are exploring, it is evident that the lightest generations of left-handed quarks possess distinct $U(1)'$ charges. Consequently, we anticipate stringent limitations on the Z' mass, particularly arising from constraints associated with $K - \overline{K}$ mixing. Therefore, our initial focus will be on investigating the neutral Kaon system.

$K^0 - \overline{K^0}$ mixing

By utilizing equation (4.11), we can determine the mass split associated with Kaon oscillations:

$$\Delta M_K^{Z'} \simeq 3.967 \times 10^{-14} \left(\frac{g'}{M_{Z'}} \right)^2 .$$

Our results for the Kaon system are visualized in Figure 4.4. As anticipated, the Kaon system imposes stringent constraints on $M_{Z'}$. To provide an estimate, if $g' \simeq 0.5$, the constraint from the above equation implies that $M_{Z'} \gtrsim 120$ TeV, significantly surpassing the bounds set by recent collider searches.

$B_s^0 - \overline{B_s^0}$ mixing

From equation (4.14), we can approximate:

$$C_{bs}^{LL} \approx 1.9 \times 10^{-5} \left(\frac{g' \text{ TeV}}{M_{Z'}} \right)^2$$

This value is too small to have a substantial impact on ΔM_s, primarily due to the equality in $U(1)'$ charges for b_L and s_L.

$D^0 - \overline{D^0}$ mixing

For $M_D \simeq 1.86483$ GeV [306], and adopting a decay constant value of $f_D \simeq 212$ MeV as determined in [337], equation (4.11) yields:

$$\Delta M_D^{Z'} \simeq 2.71 \times 10^{-18} \left(\frac{g' \text{ TeV}}{M_{Z'}} \right)^2 .$$

Consequently, for $\Gamma_D = 1/\tau_D \simeq 2.43843\ (ps)^{-1}$ [306], we have:

$$x_D := \frac{\Delta M_D}{\Gamma_D} \simeq 0.0017 \left(\frac{g' \ TeV}{M_{Z'}} \right)^2$$

This value consistently satisfies the bound $x_D \leqslant 0.32$.

$P^0 \to l_i \bar{l}_i$ decays

Our findings indicate that all Z' contributions are significantly suppressed when compared to experimental bounds. For instance, let's consider the decay $B_d^0 \to \mu^+\mu^-$. Using equation (4.18), we derive:

$$\text{Br}(B_d^0 \to \mu^+\mu^-) \simeq 5.34 \times 10^{-9} \left(\frac{g' \text{ TeV}}{M_{Z'}} \right)^4$$

This result consistently complies with the experimental bound $\text{Br}(B_d^0 \to \mu^+\mu^-) < 1.6^{+1.6}_{-1.4} \times 10^{-10}$, provided that $g' < 1$ and $M_{Z'} \sim \mathcal{O}(TeV)$. Similar outcomes were obtained for lepton flavor-violating decays of the form $P^0 \to l_i \bar{l}_j$.

Muon anomalous magnetic moment and $\mu \to e\gamma$

Our results indicate that Z' contributions to Δa_μ are consistently smaller than the observed discrepancy. Even in the extreme case where $g' = 1$ and $M_{Z'} = 1$ TeV, our computations yield $\Delta a_\mu^{Z'} \simeq 3 \times 10^{-11}$. This suggests that for small Z' masses, the model may account for the observed $(g-2)_\mu$ anomaly. However, for larger $M_{Z'}$ values as implied by the Kaon system, the results are significantly suppressed.

In LFV radiative decays of the form $l_i \to l_j \gamma$, the muon channel is expected to provide the strongest bounds. For $g' = 1$, the model predicts that $M_{Z'} \gtrsim 1.3$ TeV in order for the predicted $\mu \to e\gamma$ branching ratio to remain consistent with experimental bounds. Conversely, tau decays ($\tau \to e\gamma$, $\tau \to \mu\gamma$) are highly suppressed due to the short lifetime of the tau lepton.

$\mu^- \to e^- e^- e^+$

Although all three-body lepton decays of the form $l_i \to l_j l_j \bar{l}_k$ are heavily suppressed for the tau channel, the model faces stringent constraints from the muon decay $\mu^- \to e^- e^- e^+$. Specifically, the model predicts that

$$\mathrm{Br}(\mu^- \to e^- e^- e^+) \simeq 4.92 \times 10^{-5} \left(\frac{g' \ \mathrm{TeV}}{M_{Z'}} \right)^4 .$$

These predictions are compared with experimental bounds in Figure 4.5. It is apparent that, for $g' = 0.5$ (indicated by the dashed line in the plot), the model necessitates $M_{Z'} \gtrsim 42$ TeV to conform to the existing experimental constraint, $\mathrm{Br}(\mu^- \to e^- e^- e^+) < 10^{-12}$. While the constraints stemming from this decay are more stringent than those from other lepton flavor-violating processes discussed previously, they remain incompatible with the restrictions imposed by the Kaon system.

However, it's important to note that future lepton flavor violation-related experiments, such as the *Mu3e* experiment at PSI, are expected to significantly improve sensitivity. The *Mu3e* experiment aims to reach experimental sensitivities of $\sim 10^{-16}$. In the absence of a signal, three-body LFV muon decays can then be excluded for $\mathrm{Br}(\mu^- \to e^- e^- e^+) < 10^{-16}$. In Figure 4.5, the red horizontal line represents the estimated reach of future $\mu \to 3e$ experiments. For $g' = 0.5$, we find that $M_{Z'} \gtrsim 420$ TeV to satisfy the projected *Mu3e* experimental bounds. Therefore, for this model, the currently dominant constraints from the Kaon system are expected to be surpassed in the near future by the limits of upcoming $\mu^- \to e^- e^- e^+$ experiments.

R_K anomalies

The constraints derived from the Kaon oscillation system and the three-body decay $\mu \to e^- e^- e^+$ effectively rule out the possibility of explaining the observed R_K anomalies within this model. Specifically, for the relevant Wilson coefficient, the model predicts:

$$C_9 \approx -0.079 \left(\frac{g' \ \mathrm{TeV}}{M_{Z'}} \right)^2$$

This coefficient has the desired sign ($C_9 < 0$), but for $M_{Z'} \sim 200$ TeV and $g' \simeq 1$, the resulting value is too small to account for the observed B-meson anomalies.

Similar phenomenological analyses have been conducted for the other models presented earlier, and their flavor violation bounds are discussed in Appendix D.3. In general, the results align closely with those of Model D9. For all the $U(1)'$ models with an MSSM spectrum, the dominant constraints on $M_{Z'}$ originate from the effects of $K^0 - \overline{K^0}$ oscillations and the muon decay $\mu \to e^- e^- e^+$.

The analysis conducted thus far highlights that successfully explaining the LHCb anomalies within the present F-theory framework would require the incorporation of a different mechanism. A commonly explored approach involves addressing the LHCb anomalies through the mixing of conventional SM matter with extra vector-like fermions [340]- [348]. In the next section, we introduce an F-theory model that utilizes such vector-like fermions to potentially account for the LHCb

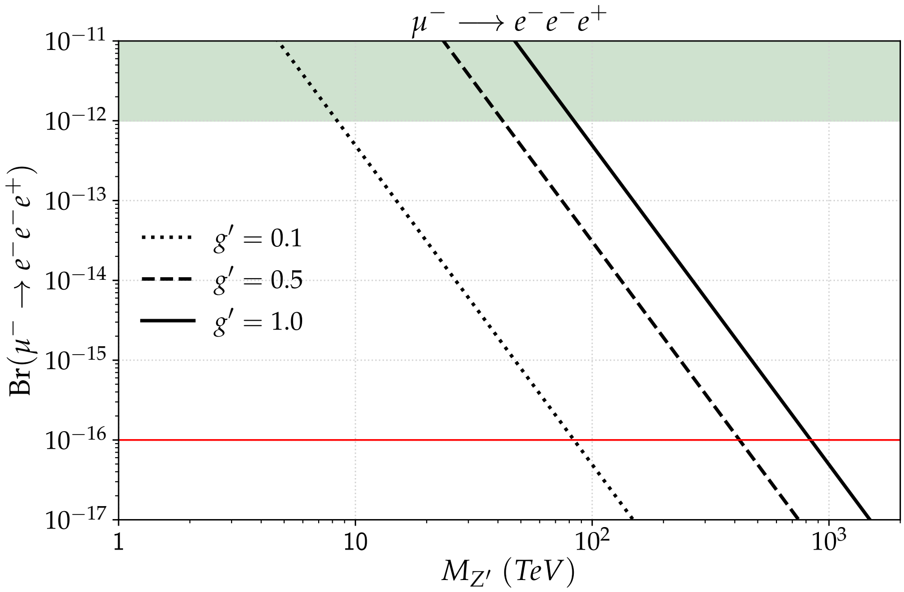

Figure 4.5: Bounds to the neutral gauge boson mass $M_{Z'}$ as predicted in Model D9 from Z' contributions to the lepton flavour violation decay $\mu^- \to e^-e^-e^+$. The plot shows the branching ratio of the decay as a function of the Z' mass for various values of the gauge coupling g'. Both axes are in logarithmic scale. Dotted, dashed and solid black curves correspond to $U(1)'$ gauge couplings: $g' = 0.1$, 0.5 and 1 respectively. The shaded region is excluded due to the current experimental bound: $\mathrm{Br}(\mu^- \to e^-e^-e^+) < 10^{-12}$. The red horizontal line represents the estimated reach of future $\mu \to 3e$ experiments.

anomalies. However, it's worth noting that a comprehensive classification of various F-theory models featuring a complete family of vector-like fermions will be presented in a forthcoming work.

4.5 Models with vector-like exotics

We extend our analysis to models featuring the MSSM spectrum augmented with vector-like (VL) states that form complete $(10+\overline{10})$, $(5+\bar{5})$ pairs under the $SU(5)$ GUT symmetry. As in our previous investigation, we select suitable fluxes, address the anomaly cancellation conditions, and deduce the $U(1)'$ charges for all models with additional vector-like families.

Particular attention is directed towards models where the VL states possess distinct $U(1)'$ charges while maintaining universal $U(1)'$ charges for the SM fermion families. This approach allows us to account for the observed B-meson anomalies arising from the mixing of SM fermions with VL exotics while simultaneously managing other flavor violation observables. A model with these characteristics (initially formulated in [287]) is realized using the following set of fluxes:

$$m_1 = 2\ ,\ \ m_2 = m_3 = -m_4 = 1\ ,\ \ M_1 = M_2 = M_3 = M_7 = 0\ ,\ \ M_4 = -M_6 = 1\ ,\ \ M_5 = -3\ ,$$

This choice of fluxes, satisfying the anomaly cancellation conditions, yields the solution $(c_1,\ c_2,\ c_3) = (\frac{\sqrt{3}}{2},\ -\frac{1}{4}\sqrt{\frac{3}{2}},\ \frac{1}{4}\sqrt{\frac{5}{2}})$. Consequently, the $U(1)'$ charges for the various matter curves are as follows:

$$10_1:\frac{1}{4}\ ,\ \ 10_2:-\frac{1}{2}\ ,\ \ 10_3:\frac{1}{4}\ ,\ \ 10_4:-\frac{1}{4}\ ,$$
$$5_1:-\frac{1}{2}\ ,\ \ 5_2:\frac{1}{4}\ ,\ \ 5_3:-\frac{1}{2}\ ,\ \ 5_4:0\ ,\ \ 5_5:\frac{1}{4}\ ,\ \ 5_6:\frac{3}{4}\ ,\ \ 5_7:0\ .$$

Assuming the following distribution of fermion generations and Higgs fields across matter curves:

$$10_1\longrightarrow Q_{2,3}+u^c_{1,2,3}+e^c_3\ ,\ \ 10_2\longrightarrow Q_4+u^c_4+e^c_4\ ,\ \ 10_3\longrightarrow Q_1+e^c_{1,2}\ ,\ \ \bar{10}_4\longrightarrow\overline{Q_4}+\overline{u^c_4}+\overline{e^c_1}\ ,$$
$$5_1\longrightarrow H_u,\ \ \bar{5}_2\longrightarrow L_1,\ \ \bar{5}_3\longrightarrow H_d,\ \ 5_4\longrightarrow\overline{d^c_4},\ \ \bar{5}_5\longrightarrow d^c_{1,2,3}+L_{2,3},\ \ \bar{5}_6\longrightarrow d^c_4+L_4,\ \ 5_7\longrightarrow\overline{L_4}\ ,$$

we arrive at the desired $U(1)'$ charge assignment. In this assignment, all SM families exhibit a common charge ($Q'_{1,2,3}=1/4$), while those of the VL states are non-uniform.

For clarity, we denote the components of SM doublets as $Q_i=(u_i,d_i)$ and extend this notation to lepton doublets as well, represented as L_i. The components of exotic doublets are expressed as $Q_4\equiv(U',D')$ and $\overline{Q}_4\equiv(\bar{D}',\bar{U}')$. Similarly, we use $u^c_4=\bar{U}$, $\overline{u^c}_4=U$, $e^c_4=\bar{E}$, $\overline{e^c_4}=E$, $d^c_4=\bar{D}$, and $\overline{d^c_4}=D$ to denote the components of the exotic singlets.

The various mass terms can be expressed in a 5×5 notation as $\mathrm{F}_R\mathbf{M_F}\mathrm{F}_L$, where $\mathrm{F}_R=(f^c_i,\bar{F},\bar{F}')$ and $\mathrm{F}_L=(f_i,F',F)^T$, with $f=u,d,e$ and $F=U,D,E$. Our focus will be on the down-type quark sector, although the up-quark sector can be treated similarly by adjusting parameters to ensure the CKM mixing. These invariant operators result in a mass matrix of the form:

$$M_d=\begin{pmatrix} k_0\vartheta_{14}\vartheta_{54}v_d & k\varepsilon^3\vartheta_{54}v_d & k\varepsilon^2\vartheta_{54}v_d & k_4\vartheta_{14}\vartheta_{53}v_d & k_3\vartheta_{14}\theta_{53}\\ k_0\vartheta_{14}\vartheta_{54}v_d & k\varepsilon^2\vartheta_{54}v_d & k\varepsilon\vartheta_{54}v_d & k_4\vartheta_{14}\vartheta_{53}v_d & k_3\vartheta_{14}\theta_{53}\\ k_0\vartheta_{14}\vartheta_{54}v_d & k\varepsilon\vartheta_{54}v_d & k\vartheta_{54}v_d & k_4\vartheta_{14}\vartheta_{53}v_d & k_3\vartheta_{14}\theta_{53}\\ k_2\theta_{14}v_d & k_1\xi v_d & k_1v_d & k_9\vartheta_{13}v_d & k_{10}\theta_{13}\\ k_6\theta_{54}v_d & k_5\xi\theta_{51} & k_5\theta_{51} & k_8\theta_{53} & k_7\vartheta_{14}\vartheta_{53}v_u \end{pmatrix}, \tag{4.74}$$

Here, the k's are coupling constant coefficients, and ε and ξ are small constant parameters encoding local Yukawa effects. The singlet VEVs are represented as $\theta_{ij}=\langle\theta_{ij}\rangle$, while ϑ_{ij} represents the ratio $\langle\theta_{ij}\rangle/\Lambda$.

To simplify the matrix, we consider that some terms are negligible and approximately vanish. Specifically, we assume that $k_2=k_3=k_5\theta_{51}=k_6=k_7\vartheta_{14}\vartheta_{53}\approx0$. Furthermore, we introduce the following simplifications:

$$k\vartheta_{54}v_d=m\ ,\ \ k_0\vartheta_{54}\vartheta_{14}v_d=\alpha m\ ,\ \ k_4\vartheta_{14}\vartheta_{53}=\gamma\xi\ ,\ \ k_9\vartheta_{13}v_d=\beta\mu\ ,\ \ k_{10}\theta_{13}\simeq k_8\theta_{53}=M\ ,\ \varepsilon\approx\xi\ .$$

With these modifications, the matrix takes on the following simplified form:

$$M_d\approx\begin{pmatrix} \alpha m & m\xi^3 & m\xi^2 & \gamma\xi v_d & 0\\ \alpha m & m\xi^2 & m\xi & \gamma\xi v_d & 0\\ \alpha m & m\xi & m & \gamma\xi v_d & 0\\ 0 & k_1\xi v_d & k_1v_d & \beta\mu & M\\ 0 & 0 & 0 & M & 0 \end{pmatrix}. \tag{4.75}$$

In this modified matrix, the local Yukawa parameter ξ establishes a connection between the VL sector and the physics at the electroweak scale. We will use this small parameter to quantify the mixing between the two sectors. To diagonalize the down square mass matrix (M_d^2) perturbatively, we assume $k_1 \approx 0$ and $k_\gamma\, v_d = c\mu$ while retaining terms up to $\mathcal{O}(\xi)$. This results in the mass square matrix being represented as $M_d^2 \approx \mathbf{A} + \xi\,\mathbf{B}$, where:

$$\mathbf{A} = \begin{pmatrix} \alpha^2 m^2 & \alpha^2 m^2 & \alpha^2 m^2 & 0 & 0 \\ \alpha^2 m^2 & \alpha^2 m^2 & \alpha^2 m^2 & 0 & 0 \\ \alpha^2 m^2 & \alpha^2 m^2 & (\alpha^2+1) m^2 & 0 & 0 \\ 0 & 0 & 0 & M^2 & \beta\mu M \\ 0 & 0 & 0 & \beta\mu M & M^2 \end{pmatrix} , \quad \mathbf{B} = \begin{pmatrix} 0 & 0 & 0 & c\beta\mu^2 & c\mu M \\ 0 & 0 & m^2 & c\beta\mu^2 & c\mu M \\ 0 & m^2 & 0 & c\beta\mu^2 & c\mu M \\ c\beta\mu^2 & c\beta\mu^2 & c\beta\mu^2 & 0 & 0 \\ c\mu M & c\mu M & c\mu M & 0 & 0 \end{pmatrix}$$

The block-diagonal matrix $\mathbf{A}$ constitutes the leading-order component of the mass square matrix and can be diagonalized using a unitary matrix $V_{b_L}^0$ as $V_{b_L}^0 \mathbf{A} V_{b_L}^{0T}$. Its mass square eigenvalues are as follows:

$$\begin{aligned} &x_1 = 0\,, \quad x_2 = \frac{m^2}{2}\left(1 + 3\alpha^2 - \sqrt{1 - 2\alpha^2 + 9\alpha^4}\right)\,, \quad x_3 = \frac{m^2}{2}\left(1 + 3\alpha^2 + \sqrt{1 - 2\alpha^2 + 9\alpha^4}\right) \\ &x_4 = M(M - \beta\mu)\,, \quad x_5 = M(M + \beta\mu)\,, \end{aligned}$$

Here, $x_{1,2,3}$ corresponds to the mass squares of the three down-type quark generations $d_{1,2,3}$, respectively. At this stage, we disregard the small mass of the first-generation down quark, which can be generated by high-order corrections. For the second and third generations, we observe that the ratio $\sqrt{x_2/x_3}$ depends solely on the parameter α. Thus, using the known strange-bottom quark mass ratio (m_s/m_b), we estimate that $\alpha \simeq 10^{-2}$.

The corresponding normalized eigenvectors, which form the columns of the diagonalizing matrix, are given by:

$$v_{b1}^0 = \frac{1}{\sqrt{2}}\begin{pmatrix} -1 \\ 1 \\ 0 \\ 0 \\ 0 \end{pmatrix}, \quad v_{b2}^0 = \frac{1}{\sqrt{1+2q^2}}\begin{pmatrix} q \\ q \\ 1 \\ 0 \\ 0 \end{pmatrix}, \quad v_{b3}^0 = \frac{-1}{\sqrt{2(1+2q^2)}}\begin{pmatrix} 1 \\ 1 \\ -2q \\ 0 \\ 0 \end{pmatrix},$$

$$v_{b4}^0 = \frac{1}{\sqrt{2}}\begin{pmatrix} 0 \\ 0 \\ 0 \\ -1 \\ 1 \end{pmatrix}, \quad v_{b5}^0 = \frac{1}{\sqrt{2}}\begin{pmatrix} 0 \\ 0 \\ 0 \\ 1 \\ 1 \end{pmatrix},$$

Here, $q = 1 - \frac{m^2}{x_2}$ depends solely on the parameter α since $x_2 \sim m^2$.

The corrections to the above eigenvectors due to the perturbative part $\xi\mathbf{B}$ can be expressed as follows:

$$v_{b_i} \approx v_{b_i}^0 + \xi \sum_{j\neq i}^{5} \frac{(V_{b_L}^0 \mathbf{B} V_{b_L}^{0\dagger})_{ji}}{x_i - x_j} v_{b_j}^0 \tag{4.76}$$

Here, the second term in the equation represents the $\mathcal{O}(\xi)$ corrections to the fundamental eigenvectors of the leading-order matrix $\mathbf{A}$. The adjusted diagonalizing matrices take on the schematic form $V_{b_L} = V^0_{b_L} + \xi V^1_{b_L}$, and through these matrices, the mixing parameter ξ enters into the computation of various flavor violation observables.

For explaining the LHCb anomalies, we will consider that perturbative corrections are significant for the corresponding bs coupling but almost negligible for other flavor mixing coefficients. In this manner, due to the universal $U(1)'$ charges of the SM matter, most of the flavor violation processes are suppressed.

Assuming that the corresponding lepton contribution is $(Q'_{e_L})_{22} \approx 1$ and for $\alpha = 0.016$, we find that for the $b \to s$ transition matrix element:

$$(Q'_{d_L})_{23} \approx Q'_{1,2,3}\xi^2 - 0.7(c\beta)^2 \left(\frac{m}{M}\right)^2 \left(\frac{\mu}{M}\right)^4 Q'_4\xi^2 \tag{4.77}$$

Where $Q'_{1,2,3} = 1/4$ is the common charge of the MSSM fermions, and $Q'_4 = -1/2$ is the charge of the extra matter originating from the 10_2 matter curve. Note that the corresponding $U(1)'$ charge of the states originating from the 5_4 matter curve is zero and therefore does not contribute to the above formula.

It is evident from equation (4.77) that the first term dominates, as the second term is suppressed due to the large VL mass scale characterized by the parameter M. Therefore, considering only the first term, we have from equation (4.10) that:

$$C_9 \approx -963 \left(\frac{g'}{M_{Z'}}\right)^2 Q'_{1,2,3}\xi^2 \tag{4.78}$$

For $g' \lesssim 1$, $M_{Z'} \gtrsim 4$ TeV, and $\xi^2 \sim \mathcal{O}(10^{-1})$, this predicts $C_9 \approx -1$, which is the desired value for explaining the LHCb anomalies. It is worth noting that this approach is valid in the regime where ξ is small, i.e., $\xi < 1$. If ξ were large, perturbation theory would break down, and a more general treatment would be necessary.

Chapter 5

$SU(5) \times U(1)'$ models with a vector-like fermion family

5.1 Introduction

The pursuit of New Physics (NP) phenomena that go beyond the predictions of the SM is a central and intriguing matter. Many extensions, such as GUTs and effective models derived from String Theory, introduce novel elements into their spectra. These elements could potentially lead to exotic interactions and unique predictions. Among the most eagerly anticipated phenomena is the emergence of additional neutral gauge bosons, leptoquark states that interact with both quarks and leptons, extra neutral states like sterile neutrinos, and vector-like families of particles.

However, the current experimental data from the Large Hadron Collider (LHC) and other sources offer substantial indications of possible new interactions mediated by these exotic states. It's important to note that nothing has been definitively confirmed yet. Notably, some persistent LHCb data discrepancies with SM predictions involve various decay channels of B-mesons. One specific measurement, the ratio of branching ratios $Br(B \to K\mu^+\mu^-)/Br(B \to Ke^+e^-)$, connected to semi-leptonic transitions $b \to s\mu^+\mu^-$ and $b \to se^+e^-$, suggests a violation of lepton flavor universality. Several potential explanations for this effect involve leptoquark states, neutral bosons denoted as Z', with different couplings to the three fermion families, and vector-like generations.

In a prior investigation (see [355], also [287]), we systematically analyzed a class of semi-local F-theory models possessing an $SU(5) \times U(1)'$ gauge symmetry. These models are derived from a covering E_8 gauge group through a series of steps, as expressed by the chain:

$$E_8 \supset SU(5) \times SU(5)' \supset SU(5) \times U(1)^4 \supset SU(5) \times U(1)'. \tag{5.0}$$

Here, $U(1)'$ can represent any linear combination of the four abelian factors present in $SU(5)'$. In this context, we identified all feasible solutions for anomaly-free $U(1)'$ factors and demonstrated that many of these cases lead to non-universal couplings with the three chiral fermion families. We also considered scenarios where the spontaneous breaking of the $U(1)'$ symmetry occurs at a few TeV scale, investigating the implications for low-energy phenomena by calculating observables for various exotic processes in the effective theory.

Despite the intricate structure and diverse non-universal $U(1)'$ factors, stringent lower bounds, primarily from the $K - \bar{K}$ system [356], on the mass of the associated Z' boson greatly outweigh any observable effects in B-meson anomalies. Consequently, the non-universal contributions to

$Br(B \to K\mu^+\mu^-)/Br(B \to Ke^+e^-)$ are entirely depleted. It was demonstrated that in these effective F-theory models, only the presence of additional vector-like families could explain the LHCb data [355].

In this present study, we expand upon previous work [287, 355] concerning F-theory-inspired models with $SU(5) \times U(1)'$ by incorporating vector-like fermion generations into the low-energy spectrum. Specifically, we are interested in models that permit the existence of an entire family of extra fermions in addition to the MSSM particle content. To circumvent severe constraints related to the Kaon system, we seek models where the regular MSSM fermion matter fields acquire universal charges under the additional $U(1)'$ symmetry and are distinct from the corresponding states within the vector-like family. This way, non-universality effects are exclusively induced by the considered vector-like states [341, 346, 357, 358].

5.2 Flux constraints for a spectrum with a complete vector-like family

In this section, we will provide a concise overview of the GUT model, with our primary focus on delineating its fundamental constraints and features stemming from its incorporation within F-theory. For a more comprehensive exposition of the technical intricacies, we refer readers to [355].

Our current investigation revolves around the (semi-local) F-theory construction, which we assume originates from an E_8 singularity following the reduction process outlined in (5.0). At the core of this construction are the Cartan generators denoted as $Q_k = \text{diag}\{t_1, t_2, t_3, t_4, t_5\}$ for $k = 1, 2, 3, 4$. These generators correspond to the four $U(1)$ factors elucidated in (5.0). It is imperative to note that they adhere to the constraint of $SU(5)$ tracelessness, which mandates that $\sum_{i=1}^{5} t_i = 0$. These generators are characterized as follows:

$$Q_a = \frac{1}{2}\text{diag}(1, -1, 0, 0, 0), \qquad Q_b = \frac{1}{2\sqrt{3}}\text{diag}(1, 1, -2, 0, 0),$$
$$Q_\psi = \frac{1}{2\sqrt{6}}\text{diag}(1, 1, 1, -3, 0), \qquad Q_\chi = \frac{1}{2\sqrt{10}}\text{diag}(1, 1, 1, 1, -4). \tag{5.1}$$

In order to establish a tree-level top-quark mass, we introduce a Z_2 monodromy operation, denoted as $t_1 \leftrightarrow t_2$. This operation effectively "breaks" the $U(1)_a$ symmetry while keeping the other three abelian factors unaltered. Moreover, we have the flexibility to introduce specific fluxes [280] along the remaining $U(1)$ factors, allowing us to retain a linear combination known as $U(1)'$ among the abelian factors, which remains unbroken at lower energy scales. Consequently, the gauge symmetry characterizing the effective model under consideration can be expressed as:

$$G_S = SU(5) \times U(1)' \,. \tag{5.2}$$

The $U(1)'$ factor, which is assumed to persist unbroken in the effective model, can be defined as a linear combination of the symmetries that withstand the monodromy operation. Mathematically, this is represented as:

$$Q' = c_1 Q_b + c_2 Q_\psi + c_3 Q_\chi \,, \tag{5.3}$$

where the coefficients c_1, c_2, c_3 must adhere to a normalization constraint:

$$c_1^2 + c_2^2 + c_3^2 = 1 \,. \tag{5.4}$$

These coefficients are also subject to further scrutiny due to anomaly cancellation conditions, which have been exhaustively analyzed in previous research [287, 355].

Once the Z_2 monodromy has been incorporated, the massless fields accommodating the $10, \overline{10}$ and $5, \overline{5}$ representations are distributed across four matter curves, denoted as Σ_{10_j} for $j = 1, 2, 3, 4$, and seven Σ_{5_i} for $i = 1, 2, \ldots, 7$ [167].

The $U(1)$ fluxes previously mentioned also have a direct impact on determining the chiralities of the $SU(5)$ representations. These effects on the representations of the various matter curves denoted as Σ_{10_j} and Σ_{5_i}, can be expressed in terms of integers M_j and m_j as follows:

$$n_{10_j} - n_{\overline{10}_j} = m_j \qquad n_{5_i} - n_{\bar{5}_i} = M_i \ , \tag{5.5}$$

Additionally, to accommodate the three fermion families, a chirality condition must be imposed, stipulating that:

$$\sum_j m_j = -\sum_i M_i = 3$$

Furthermore, by introducing a hypercharge flux denoted as $\mathscr{F}_Y$, the $SU(5)_{GUT}$ symmetry undergoes spontaneous breaking to yield $SU(3)\times SU(2)\times U(1)_Y$. The various multiplicities of the Standard Model (SM) representations can be parametrized with integers N_i and N_j as follows:

$$10_{t_j} = \begin{cases} n_{(3,2)_{\frac{1}{6}}} - n_{(\bar{3},2)_{-\frac{1}{6}}} & = \ m_j \\ n_{(\bar{3},1)_{-\frac{2}{3}}} - n_{(3,1)_{\frac{2}{3}}} & = \ m_j - N_j \\ n_{(1,1)_{+1}} - n_{(1,1)_{-1}} & = \ m_j + N_j \end{cases} ; \quad 5_{t_i} = \begin{cases} n_{(3,1)_{-\frac{1}{3}}} - n_{(\bar{3},1)_{+\frac{1}{3}}} & = \ M_i \\ n_{(1,2)_{+\frac{1}{2}}} - n_{(1,2)_{-\frac{1}{2}}} & = \ M_i + N_i \end{cases} . \tag{5.6}$$

Our starting point involves the flux data and the SM content associated with each matter curve. For a more detailed account of these aspects, we refer readers to our previous work [355]. Here, we present the properties of the complete spectrum as summarized in Table 5.1. To achieve the desired spectrum, the following constraints have been taken into account:

The spectrum of a local F-theory model is determined by selecting a set of integers that satisfy the previously mentioned constraints. To illustrate this, we begin by placing the Higgs doublet H_u on the Σ_{5_1} matter curve. We choose the associated flux integers to be $M_1 = 0$ and $N = 1$. This choice ensures that H_u remains in the massless spectrum while eliminating the down-type color triplet. This mechanism, as discussed in [280], effectively suppresses proton decay.

Moving forward, we focus on the Σ_{10_1} matter curve and allow m_1 to vary within the range $0 < m_1 < 3$. Thanks to the previously mentioned Z_2 monodromy [167, 359], at least one diagonal tree-level up-quark Yukawa coupling, $\lambda_{top}10_1 10_1 5_1$, is generated in the superpotential $\mathscr{W}$. Furthermore, to ensure the presence of exactly one extra family of vector-like fermions, in addition to the constraint $\sum_j m_j = -\sum_i M_i = 3$, which fixes the number of chiral families to three, we impose the following conditions on the various flux integers [287, 355]:

$$\sum_{j=1}^{4} |m_j| = \sum_{i=1}^{7} |M_i| = 5 \ , \tag{5.7}$$

$$|m_1 + 1| + |m_2 - N_7| + |m_3 - N_8| + |m_4 - N_9| = 5 \ , \tag{5.8}$$

Matter Curve	Q'	N_Y	M	SM Content
$\Sigma_{10_{1,\pm t_1}}$	$\frac{10\sqrt{3}c_1+5\sqrt{6}c_2+3\sqrt{10}c_3}{60}$	$-N$	m_1	$m_1Q+(m_1+N)u^c+(m_1-N)e^c$
$\Sigma_{10_{2,\pm t_3}}$	$\frac{-20\sqrt{3}c_1+5\sqrt{6}c_2+3\sqrt{10}c_3}{60}$	N_7	m_2	$m_2Q+(m_2-N_7)u^c+(m_2+N_7)e^c$
$\Sigma_{10_{3,\pm t_4}}$	$\frac{\sqrt{10}c_3-5\sqrt{6}c_2}{20}$	N_8	m_3	$m_3Q+(m_3-N_8)u^c+(m_3+N_8)e^c$
$\Sigma_{10_{4,\pm t_5}}$	$-\sqrt{\frac{2}{5}}c_3$	N_9	m_4	$m_4Q+(m_4-N_9)u^c+(m_4+N_9)e^c$
$\Sigma_{5_{1,(\pm 2t_1)}}$	$-\frac{c_1}{\sqrt{3}}-\frac{c_2}{\sqrt{6}}-\frac{c_3}{\sqrt{10}}$	N	M_1	$M_1\overline{d^c}+(M_1+N)\overline{L}$
$\Sigma_{5_{2,\pm(t_1+t_3)}}$	$\frac{5\sqrt{3}c_1-5\sqrt{6}c_2-3\sqrt{10}c_3}{30}$	$-N$	M_2	$M_2\overline{d^c}+(M_2-N)\overline{L}$
$\Sigma_{5_{3,\pm(t_1+t_4)}}$	$-\frac{c_1}{2\sqrt{3}}+\frac{c_2}{\sqrt{6}}-\frac{c_3}{\sqrt{10}}$	$-N$	M_3	$M_3\overline{d^c}+(M_3-N)\overline{L}$
$\Sigma_{5_{4,\pm(t_1+t_5)}}$	$\frac{-10\sqrt{3}c_1-5\sqrt{6}c_2+9\sqrt{10}c_3}{60}$	$-N$	M_4	$M_4\overline{d^c}+(M_4-N)\overline{L}$
$\Sigma_{5_{5,\pm(t_3+t_4)}}$	$\frac{c_1}{\sqrt{3}}+\frac{c_2}{\sqrt{6}}-\frac{c_3}{\sqrt{10}}$	N_7+N_8	M_5	$M_5\overline{d^c}+(M_5+N_7+N_8)\overline{L}$
$\Sigma_{5_{6,\pm(t_3+t_5)}}$	$\frac{20\sqrt{3}c_1-5\sqrt{6}c_2+9\sqrt{10}c_3}{60}$	N_7+N_9	M_6	$M_6\overline{d^c}+(M_6+N_7+N_9)\overline{L}$
$\Sigma_{5_{7,\pm(t_4+t_5)}}$	$\frac{5\sqrt{6}c_2+3\sqrt{10}c_3}{20}$	N_8+N_9	M_7	$M_7\overline{d^c}+(M_7+N_8+N_9)\overline{L}$

Table 5.1: Matter curves along with their $U(1)'$ charges, flux data and the corresponding SM content. Note that the flux integers satisfy $N=N_7+N_8+N_9$.

$$|m_1-1|+|m_2+N_7|+|m_3+N_8|+|m_4+N_9|=5\ , \tag{5.9}$$

$$1+|M_2-1|+|M_3-1|+|M_4-1|+|M_5+N_7+N_8|+|M_6+N_7+N_9|+|M_7+N_9+N_8|=7\ . \tag{5.10}$$

Apart from m_1, M_1, and $N=N_7+N_8+N_9$, which are subject to the aforementioned conditions, the remaining flux parameters have the following limitations:
The flux integers $m_{2,3,4}$, which characterize the number of Q and $\overline{Q}$ states in the spectrum, are restricted to the range $[-1,2]$. Since the Σ_{10_1} matter curve always hosts at least two u^c's (due to the conditions $M_1=0$, $N=1$, and $0<m_1<3$), we limit the other u^c multiplicities (m_j-N_k with $j=2,3,4$ and $k=7,8,9$) to be in the range $[-1,1]$. Similarly, for the multiplicities of the e^c and $\overline{e^c}$ states, we impose $-1\leq(m_j+N_k)\leq 3$ for $j=2,3,4$ and $k=7,8,9$.
Likewise, for the d^c states, we set the values of the corresponding multiplicities M_i's ($i=2,3,4,5,6,7$) to vary in the range $[-3,1]$, while for the multiplicities of $\overline{L}$ states (see Table 5.1), the relations are set to vary in the range $[-2,1]$. It's worth noting that, in general, we could allow for values in the range $[-3,1]$, but this would lead to the mixing of the vector-like states with the MSSM ones, which is not in line with our intention to search for models with vector-like $U(1)'$ charges different from the MSSM ones.

By implementing all the restrictions described above, we obtain a total of 1728 flux solutions that satisfy the conditions and include one vector-like family in addition to the three standard chiral families of quarks and leptons.

5.3 Classification of the Models

To determine the c_i coefficients and, consequently, the associated $U(1)'$ charges for each model defined by the aforementioned set of fluxes, we employ a systematic approach. We start by applying anomaly cancellation conditions, specifically focusing on the mixed anomalies between the Standard Model (MSSM) particles and the $U(1)'$ gauge boson. These anomalies are denoted as $\mathscr{A}_{331}$, $\mathscr{A}_{221}$, $\mathscr{A}_{YY1}$, and $\mathscr{A}_{Y11}$.

The cubic anomalies associated solely with the $U(1)'$ gauge boson ($\mathscr{A}_{111}$) and gravitational anomalies ($\mathscr{A}_{G}$) are not addressed at this stage. Instead, they will be resolved later by considering the dynamics of the singlet fields typically present in F-theory models.

Furthermore, to focus our search on constructing models that are of potential interest for phenomenology, we impose a constraint. Specifically, we restrict our investigation to scenarios where the three families of particles in the MSSM possess uniform $U(1)'$ charges. In contrast, the charges of the vector-like fields are allowed to differ.

By applying this constraint, we filter down the initial set of 1728 models to a subset of 192 models that exhibit this particular property. These 192 models can be categorized into five distinct classes based on their properties under the $SU(5)\times U(1)'$ symmetry. Each class comprises models that share identical charges under the additional $U(1)'$, differing only in how the Standard Model particles are distributed among various matter curves.

To illustrate the diversity of these classes and to provide a representative example from each, we present one model from each class in Tables 5.2 and 5.3.

Model	m_1	m_2	m_3	m_4	M_1	M_2	M_3	M_4	M_5	M_6	M_7	N_7	N_8	N_9	c_1	c_2	c_3
A	1	2	1	-1	0	-1	0	0	-1	-2	1	1	0	0	0	$\frac{\sqrt{15}}{4}$	$-\frac{1}{4}$
B	1	2	-1	1	0	0	0	0	-1	-3	1	1	0	0	0	$-\frac{1}{2}\sqrt{\frac{15}{34}}$	$-\frac{11}{2\sqrt{34}}$
C	2	1	1	-1	0	0	0	1	-3	-1	0	0	1	0	$\frac{\sqrt{3}}{2}$	$-\frac{1}{4}\sqrt{\frac{3}{2}}$	$\frac{1}{4}\sqrt{\frac{5}{2}}$
D	2	-1	1	1	0	-1	0	1	-1	-2	0	0	0	1	$-\frac{1}{2}\sqrt{\frac{5}{6}}$	$-\frac{5}{8}\sqrt{\frac{5}{3}}$	$\frac{3}{8}$
E	1	-1	2	1	0	0	1	0	0	-1	-3	0	1	0	$2\sqrt{\frac{10}{93}}$	$-\sqrt{\frac{5}{93}}$	$\frac{4}{\sqrt{31}}$

Table 5.2: Representative flux solutions along with the corresponding c_i' s for the five classes of models A, B, C, D and E.

Model **A**		Model **B**		Model **C**		Model **D**		Model **E**	
$\sqrt{10}Q'$	SM	$\sqrt{85}Q'$	SM	Q'	SM	$\sqrt{10}Q'$	SM	$\sqrt{310}Q'$	SM
1/2	$Q+2u^c$	-2	$Q+2u^c$	1/4	$2Q+3u^c+e^c$	-3/4	$2Q+3u^c+e^c$	9/2	$Q+2u^c$
1/2	$2Q+u^c+3e^c$	-2	$2Q+u^c+3e^c$	-1/2	$Q+u^c+e^c$	-1/2	$\overline{Q}+\overline{u^c}+\overline{e^c}$	11/2	$\overline{Q}+\overline{u^c}+\overline{e^c}$
-2	$Q+u^c+e^c$	-1/2	$\overline{Q}+\overline{u^c}+\overline{e^c}$	1/4	$Q+2e^c$	7/4	$Q+u^c+e^c$	9/2	$2Q+u^c+3e^c$
-1/2	$\overline{Q}+\overline{u^c}+\overline{e^c}$	11/2	$Q+u^c+e^c$	1/4	$\overline{Q}+\overline{u^c}+\overline{e^c}$	-3/4	$Q+2e^c$	-8	$Q+u^c+e^c$
-1	H_u	4	H_u	-1/2	H_u	3/2	H_u	-9	H_u
1	d^c+2L	-4	L	-1/4	L	-1/4	d^c+2L	-1	L
-3/2	L	-3/2	L	1/2	L	1	L	-9	$\overline{d^c}$
1	L	7/2	L	0	$\overline{d^c}$	3/2	$\overline{d^c}$	-7/2	L
-3/2	d^c	-3/2	d^c	-1/4	$3d^c+2L$	9/4	d^c+L	1	$\overline{L}$
1	$2d^c+L$	7/2	$3d^c+2L$	-3/4	d^c+L	-1/4	$2d^c+L$	-27/2	d^c+L
3/2	$\overline{d^c}+\overline{L}$	-6	$\overline{d^c}+\overline{L}$	0	$\overline{L}$	-1	$\overline{L}$	-7/2	$3d^c+2L$

Table 5.3: The particle content of models A, B, C, D, and E using the data from Table 5.2.

Table 5.2 displays the flux data alongside the corresponding solution[1] for the coefficients c_i for

[1]It's worth noting that a corresponding "mirror" solution can be obtained by applying the transformation $c_i \to$

each model. You can find the respective $U(1)'$ charges and the particle spectrum for each model in Table 5.3. Notably, models B and C coincide with models 5 and 7, respectively, as previously derived in [287].

In addition to the fields listed in Table 5.3, there are singlet fields with weights corresponding to $(t_i - t_j)$ present in this F-theory construction[2]. For the subsequent analysis, we will refer to these singlet fields using the notation $\theta_{t_i-t_j}$, which we will denote as θ_{ij}.

5.4 Analysis of the Models

In the preceding section, we formulated five distinct classes of models, all of which share a common characteristic. Namely, the $U(1)'$ charges attributed to the vector-like states deviate from the uniform $U(1)'$ charges assigned to the SM chiral families. This particular feature in the models holds the potential to elucidate the observed B-meson anomalies, contingent upon significant mixing between the SM fermions and the vector-like exotics.

Simultaneously, these models uphold lepton universality among the three chiral families and remain within the stringent constraints imposed by the Kaon system and other flavor-violating processes. In the subsequent analysis, we will delve into the models presented in Table 5.3 and formulate the mass matrices for each model.

5.4.1 Model A

In this particular scenario, we have opted for the following set of fluxes:

$$m_1 = m_3 = -m_4 = 1\ ,\quad m_2 = 2\ ,\quad M_1 = M_3 = M_4 = 0\ ,\quad M_2 = M_6 = -2\ ,\quad M_7 = -M_5 = 1\ .$$

The corresponding $U(1)'$ charges assigned to various representations are as follows:

$$\begin{aligned} &10_1 : \frac{1}{2}\ ,\quad 10_2 : \frac{1}{2}\ ,\quad 10_3 : -2\ ,\quad 10_4 : -\frac{1}{2}\ ,\\ &5_1 : -1\ ,\quad 5_2 : -1\ ,\quad 5_3 : \frac{3}{2}\ ,\quad 5_4 : -1\ ,\quad 5_5 : \frac{3}{2}\ ,\quad 5_6 : -1\ ,\quad 5_7 : -\frac{3}{2}\ ,\end{aligned}$$

while the $\overline{10}$ and $\overline{5}$ representations come with the opposite $U(1)'$ charge. We allocate the fermion generations and Higgs fields into matter curves as follows:

$$\begin{aligned} &10_1 \longrightarrow Q_3 + u^c_{2,3}\ ,\quad 10_2 \longrightarrow Q_{1,2} + u^c_1 + e^c_{1,2,3}\ ,\quad 10_3 \longrightarrow Q_4 + u^c_4 + e^c_4\ ,\quad \overline{10}_4 \longrightarrow \overline{Q_4} + \overline{u^c_4} + \overline{e^c_4}\ ,\\ &5_1 \longrightarrow H_u,\ \ \overline{5}_2 \longrightarrow d^c_3 + L_{2,3},\ \ \overline{5}_3 \longrightarrow L_4,\ \ \overline{5}_4 \longrightarrow H_d,\ \ \overline{5}_5 \longrightarrow d^c_4,\ \ \overline{5}_6 \longrightarrow d^c_{1,2} + L_1,\ \ 5_7 \longrightarrow \overline{d^c_4} + \overline{L_4}\ .\end{aligned}$$

Now, we can proceed to formulate the superpotential and, in particular, the various terms contributing to the fermion mass matrices.

We commence with the up-quark sector. The primary contributions to the up-type quark masses stem from the following superpotential terms:

$$\begin{aligned} W \supset\ & y_t 10_1 10_1 5_1 + \tfrac{y_1}{\Lambda} 10_1 10_2 5_1 \theta_{13} + \tfrac{y_2}{\Lambda^2} 10_2 10_2 5_1 \theta_{13}^2 + \tfrac{y_3}{\Lambda} 10_3 10_1 5_1 \theta_{14} + \tfrac{y_4}{\Lambda^2} 10_3 10_2 5_1 \theta_{13}\theta_{14} \\ & + \tfrac{y_5}{\Lambda^2} 10_3 10_3 5_1 \theta_{14}^2 + y_6 10_2 \overline{10}_4 \theta_{53} + y_7 10_1 \overline{10_4} \theta_{51} + y_8 10_3 \overline{10}_4 \theta_{54} + \tfrac{y_9}{\Lambda} \overline{10}_4 \overline{10}_4 \overline{5}_4 \theta_{51}\ , \end{aligned} \tag{5.11}$$

$-c_i$.

[2]For a comprehensive definition of the singlet spectrum within the theory, please refer to [355].

where y_i represents the coupling constant coefficients, and Λ stands for a characteristic high-energy scale within the theory. These operators yield the following mass texture:

$$M_u = \begin{pmatrix} y_2\vartheta_{13}^2 v_u & y_2\vartheta_{13}^2 v_u & y_1\vartheta_{13}v_u & y_4\vartheta_{13}\vartheta_{14}v_u & y_6\theta_{43} \\ y_1\vartheta_{13}v_u & y_1\vartheta_{13}v_u & \epsilon y_t v_u & y_3\vartheta_{14}v_u & y_7\theta_{51} \\ y_1\vartheta_{13}v_u & y_1\vartheta_{13}v_u & y_t v_u & y_3\vartheta_{14}v_u & y_7\theta_{51} \\ y_4\vartheta_{13}\vartheta_{14}v_u & y_4\vartheta_{13}\vartheta_{14}v_u & y_3\vartheta_{14}v_u & y_5\vartheta_{14}^2 v_u & y_8\theta_{54} \\ y_6\theta_{53} & y_6\theta_{53} & y_7\theta_{51} & y_8\theta_{54} & y_9\vartheta_{51}v_d \end{pmatrix}, \tag{5.12}$$

where $v_u = \langle H_u\rangle$, $v_d = \langle H_d\rangle$, $\theta_{ij} = \langle\theta_{ij}\rangle$, $\vartheta_{ij} = \langle\theta_{ij}\rangle/\Lambda$, and $\varepsilon \ll 1$ serves as a suppression factor introduced to account for the local effects of Yukawa couplings stemming from a common operator [318, 360]. We will now examine the interactions in the down-quark and charged lepton sectors.

Within the vector-like portion of the model, there are some common superpotential operators shared between the up and down quark sectors, which are outlined in (5.11) and characterized by the coupling constants y_6, y_7, and y_8. The remaining influential terms that contribute to the down-type quarks are as follows:

$$\begin{aligned} W \supset\ & \tfrac{\kappa_0}{\Lambda}10_1\overline{5}_2\overline{5}_4\theta_{41} + \tfrac{\kappa_1}{\Lambda}10_1\overline{5}_6\overline{5}_4\theta_{45} + \tfrac{\kappa_2}{\Lambda}10_2\overline{5}_2\overline{5}_4\theta_{43} + \tfrac{\kappa_3}{\Lambda^2}10_2\overline{5}_6\overline{5}_4\theta_{13}\theta_{45} + \tfrac{\kappa_4}{\Lambda^2}10_2\overline{5}_6\overline{5}_4\theta_{43}\theta_{15} \\ & +\kappa_5 10_3\overline{5}_2\overline{5}_4 + \tfrac{\kappa_6}{\Lambda}10_3\overline{5}_6\overline{5}_4\theta_{15} + \kappa_7 10_1\overline{5}_5\overline{5}_4 + \tfrac{\kappa_8}{\Lambda}10_2\overline{5}_5\overline{5}_4\theta_{13} + \tfrac{\kappa_9}{\Lambda}10_3\overline{5}_5\overline{5}_4\theta_{14} \\ & + \tfrac{\kappa_{10}}{\Lambda}5_7\overline{5}_2\theta_{41}\theta_{53} + \tfrac{\kappa_{11}}{\Lambda}5_7\overline{5}_2\theta_{51}\theta_{43} + \kappa_{12}5_7\overline{5}_6\theta_{43} + \kappa_{13}5_7\overline{5}_5\theta_{53} + \tfrac{\kappa_{14}}{\Lambda}\overline{10}_4 5_7 5_1\theta_{53}, \end{aligned} \tag{5.13}$$

where κ_i represents the coupling constant coefficients.

Turning to the charged lepton sector, we find common operators shared between the bottom quark and charged leptons, which are described in (5.13) and involve the couplings κ_2, κ_3, κ_4, κ_5, and κ_6. Additionally, there are common operators connecting the up quark and the charged lepton sector as outlined in (5.11) with couplings y_6 and y_8. All other contributions to the charged lepton mass matrix are derived from the operators:

$$\lambda_1 10_2\overline{5}_3\overline{5}_4 + \frac{\lambda_2}{\Lambda}10_3\overline{5}_3\overline{5}_4\theta_{34} + \lambda_3 5_7\overline{5}_6\theta_{43} + \frac{\lambda_4}{\Lambda}5_7\overline{5}_2\theta_{41}\theta_{53} + \frac{\lambda_5}{\Lambda}5_7\overline{5}_2\theta_{51}\theta_{43} + \lambda_6 5_7\overline{5}_3\theta_{51} + \frac{\lambda_7}{\Lambda}\overline{10}_4 5_7 5_1\theta_{53}\ . \tag{5.14}$$

In this scenario, when the various singlet fields θ_{ij} acquire VEV, denoted as $\langle\theta_{ij}\rangle \neq 0$, they induce hierarchical non-zero entries in the mass matrices of quarks and charged leptons. However, these VEVs must adhere to certain phenomenological constraints. Notably, the μ-term, which can potentially originate from the coupling $\theta_{15}5_1\overline{5}_4$, necessitates that $\langle\theta_{15}\rangle \approx 0$ to avoid disconnecting the Higgs doublets from the light spectrum. As a result, we can disregard the mass terms involving θ_{15} for the down quarks and charged leptons.

The down quark mass matrix is expressed as follows:

$$M_d = \begin{pmatrix} \kappa_3\vartheta_{13}\vartheta_{45}v_d & \kappa_3\vartheta_{13}\vartheta_{45}v_d & \kappa_1\vartheta_{45}v_d & 0 & \kappa_{12}\theta_{43} \\ \kappa_3\vartheta_{13}\vartheta_{45}v_d & \kappa_3\vartheta_{13}\vartheta_{45}v_d & \kappa_1\vartheta_{45}v_d & 0 & \kappa_{12}\theta_{43} \\ \kappa_2\vartheta_{43}v_d & \kappa_2\vartheta_{43}v_d & \kappa_0\vartheta_{41}v_d & \kappa_5 v_d & \kappa_{10}\theta_{41}\vartheta_{53} + \kappa_{11}\theta_{51}\vartheta_{43} \\ \kappa_8\vartheta_{13}v_d & \kappa_8\vartheta_{13}v_d & \kappa_7 v_d & \kappa_9\vartheta_{14}v_d & \kappa_{13}\theta_{53} \\ y_6\theta_{53} & y_6\theta_{53} & y_7\theta_{51} & y_8\theta_{54} & \kappa_{14}\vartheta_{53}v_u \end{pmatrix}. \tag{5.15}$$

The mass matrix for the charged leptons is characterized by the following structure:

$$M_e=\begin{pmatrix} \kappa_3\vartheta_{13}\vartheta_{45}v_d & \kappa_2\vartheta_{43}v_d & \kappa_2\vartheta_{43}v_d & \lambda_1 v_d & y_6\theta_{53} \\ \kappa_3\vartheta_{13}\vartheta_{45}v_d & \kappa_2\vartheta_{43}v_d & \kappa_2\vartheta_{43}v_d & \lambda_1 v_d & y_6\theta_{53} \\ \kappa_3\vartheta_{13}\vartheta_{45}v_d & \kappa_2\vartheta_{43}v_d & \kappa_2\vartheta_{43}v_d & \lambda_1 v_d & y_6\theta_{53} \\ 0 & \kappa_5 v_d & \kappa_5 v_d & \lambda_2\vartheta_{34}v_d & y_8\theta_{54} \\ \lambda_3\theta_{43} & \lambda_4\theta_{41}\theta_{53}+\lambda_5\theta_{51}\theta_{43} & \lambda_4\theta_{41}\theta_{53}+\lambda_5\theta_{51}\theta_{43} & \lambda_6\theta_{51} & \lambda_7\vartheta_{53}v_u \end{pmatrix} \tag{5.16}$$

5.4.2 Model B

The second model is generated by employing the following set of flux parameters:

$$m_1=-m_3=m_4=1\ ,\quad m_2=2\ ,\quad M_1=M_2=M_3=M_4=0\ ,\quad M_7=-M_5=1\ ,\quad M_6=-3\ .$$

The corresponding $U(1)'$ charges associated with the various matter curves are as follows:

$$\begin{aligned} &10_1:-2\ ,\quad 10_2:-2\ ,\quad 10_3:-\frac{1}{2}\ ,\quad 10_4:\frac{11}{2}\ ,\\ &5_1:4\ ,\quad 5_2:4\ ,\quad 5_3:\frac{3}{2}\ ,\quad 5_4:-\frac{7}{2}\ ,\quad 5_5:\frac{3}{2}\ ,\quad 5_6:-\frac{7}{2}\ ,\quad 5_7:6\ .\end{aligned}$$

To effectively allocate fermion generations and Higgs fields into matter curves, we propose the following distribution:

$$\begin{aligned} &10_1\longrightarrow Q_3+u^c_{2,3}\ ,\quad 10_2\longrightarrow Q_{1,2}+u^c_1+e^c_{1,2,3}\ ,\quad 1\bar{0}_3\longrightarrow \overline{Q_4}+\overline{u^c_4}+\overline{e^c_4}\ ,\quad 10_4\longrightarrow Q_4+u^c_4+e^c_4\ ,\\ &5_1\longrightarrow H_u,\quad \bar{5}_2\longrightarrow H_d,\quad \bar{5}_3\longrightarrow L_4,\quad \bar{5_4}\longrightarrow L_3,\quad \bar{5}_5\longrightarrow d^c_4,\quad \bar{5}_6\longrightarrow d^c_{1,2,3}+L_{1,2},\quad 5_7\longrightarrow \overline{d^c_4}+\overline{L_4}\ .\end{aligned}$$

In this model, the μ-term is realized through the coupling $\theta_{13}5_1\overline{5_2}$, necessitating that $\langle\theta_{13}\rangle$ is very small compared to the other singlet VEVs. This constraint obliges us to consider high-order terms in some couplings. Let's outline the various terms that contribute to the fermion mass matrices, starting with the up-quark sector.

The dominant contributions to the up-type quark masses arise from the following superpotential terms:

$$\begin{aligned} W\ \supset\ & y_t 10_1 10_1 5_1+\tfrac{y_1}{\Lambda^2}10_1 10_2 5_1\theta_{14}\theta_{43}+\tfrac{y_2}{\Lambda^4}10_2 10_2 5_1\theta_{14}^2\theta_{43}^2+\tfrac{y_3}{\Lambda}10_1 10_4 5_1\theta_{15}+\tfrac{y_4}{\Lambda^2}10_2 10_4 5_1\theta_{13}\theta_{15}\\ &+\tfrac{y_5}{\Lambda^2}10_4 10_4 5_1\theta_{15}^2+y_6 10_1\overline{10}_3\theta_{41}+y_7 10_2\overline{10}_3\theta_{43}+y_8 10_4\overline{10}_3\theta_{45}+\tfrac{y_9}{\Lambda^2}\overline{10}_3\overline{10}_3\overline{5}_2\theta_{41}\theta_{43}\ . \end{aligned} \tag{5.17}$$

These operators give rise to the following mass texture:

$$M_u=\begin{pmatrix} y_2\vartheta_{14}^2\vartheta_{43}^2v_u & y_2\vartheta_{14}^2\vartheta_{43}^2v_u & y_1\vartheta_{14}\vartheta_{43}v_u & 0 & y_7\theta_{53} \\ y_1\vartheta_{14}\vartheta_{43}v_u & y_1\vartheta_{14}\vartheta_{43}v_u & \epsilon y_t v_u & y_3\vartheta_{15}v_u & y_6\theta_{41} \\ y_1\vartheta_{14}\vartheta_{43}v_u & y_1\vartheta_{14}\vartheta_{43}v_u & y_t v_u & y_3\vartheta_{15}v_u & y_6\theta_{41} \\ 0 & 0 & y_3\vartheta_{15}v_u & y_5\vartheta_{15}v_u & y_8\theta_{45} \\ y_7\theta_{43} & y_7\theta_{43} & y_6\theta_{41} & y_8\theta_{45} & y_9\vartheta_{41}\vartheta_{43}v_b \end{pmatrix} \tag{5.18}$$

We now delve into the bottom sector of this model. There are shared operators between the top and bottom sectors, as elucidated in (5.17), featuring couplings denoted by y_6, y_7, and y_8. The remaining paramount terms contributing to the down-type quarks are presented as follows:

$$\begin{aligned} W\ \supset\ & \tfrac{\kappa_0}{\Lambda}10_1\overline{5}_6\overline{5}_2\theta_{43}+\tfrac{\kappa_1}{\Lambda^3}10_2\overline{5}_6\overline{5}_2\theta_{14}\theta_{43}^2+\tfrac{\kappa_2}{\Lambda}10_1\overline{5}_5\overline{5}_2\theta_{53}+\tfrac{\kappa_3}{\Lambda^4}10_2\overline{5}_5\overline{5}_2\theta_{14}\theta_{43}^2\theta_{54}+\tfrac{\kappa_4}{\Lambda^2}10_4\overline{5}_5\overline{5}_2\theta_{14}\theta_{34}\\ &+\tfrac{\kappa_5}{\Lambda^2}10_4\overline{5}_6\overline{5}_2\theta_{43}\theta_{15}+\kappa_6 5_7\overline{5}_6\theta_{43}+\kappa_7 5_7\overline{5}_5\theta_{53}+\tfrac{\kappa_8}{\Lambda}\overline{10}_3 5_7 5_1\theta_{43}\ . \end{aligned} \tag{5.19}$$

From these operators, we derive the subsequent mass matrix that characterizes the down-quark sector:

$$M_d = \begin{pmatrix} \kappa_1\vartheta_{14}\vartheta_{43}^2 v_d & \kappa_1\vartheta_{14}\vartheta_{43}^2 v_d & \epsilon^2\kappa_0 v_d & \kappa_5\vartheta_{43}\vartheta_{15} & \kappa_6\theta_{43} \\ \kappa_1\vartheta_{14}\vartheta_{43}^2 v_d & \kappa_1\vartheta_{14}\vartheta_{43}^2 v_d & \epsilon\kappa_0 v_d & \kappa_5\vartheta_{43}\vartheta_{15} & \kappa_6\theta_{43} \\ \kappa_1\vartheta_{14}\vartheta_{43}^2 v_d & \kappa_1\vartheta_{14}\vartheta_{43}^2 v_d & \kappa_0 v_d & \kappa_5\vartheta_{43}\vartheta_{15} & \kappa_6\theta_{43} \\ \kappa_3\vartheta_{14}\vartheta_{43}^2\vartheta_{54} v_d & \kappa_3\vartheta_{14}\vartheta_{43}^2\vartheta_{54} v_d & \kappa_2\vartheta_{53} v_d & \kappa_4\vartheta_{14}\vartheta_{34} v_d & \kappa_7\theta_{53} \\ y_7\theta_{43} & y_7\theta_{43} & y_6\theta_{41} & y_8\theta_{45} & \kappa_8\vartheta_{43} v_u \end{pmatrix} . \tag{5.20}$$

Concerning the charged lepton sector, there exist shared operators between the bottom sector and charged leptons, as outlined in (5.19), involving couplings κ_1, κ_5, κ_6, and κ_7. Additionally, common operators between the top and charged lepton sectors are delineated in (5.17) with couplings y_7 and y_8. The exclusive contributions for the charged leptons can be attributed to the operators presented below:

$$\frac{\lambda_1}{\Lambda}10_2\overline{5}_4\overline{5}_2\theta_{43} + \frac{\lambda_2}{\Lambda}10_4\overline{5}_4\overline{5}_2\theta_{45} + \frac{\lambda_3}{\Lambda}10_2\overline{5}_3\overline{5}_2\theta_{53} + \lambda_4 10_4\overline{5}_3\overline{5}_2 + \lambda_5 5_7\overline{5}_4\theta_{41} + \lambda_6 5_7\overline{5}_3\theta_{51} + \frac{\lambda_7}{\Lambda}\overline{10}_3 5_7 5_1\theta_{43} \,. \tag{5.21}$$

Collectively, these contributions culminate in the ensuing mass matrix:

$$M_e = \begin{pmatrix} \kappa_1\vartheta_{14}\vartheta_{43}^2 v_d & \kappa_1\vartheta_{14}\vartheta_{43}^2 v_d & \lambda_1\vartheta_{43} v_d & \lambda_3\vartheta_{53} v_d & y_7\theta_{43} \\ \kappa_1\vartheta_{14}\vartheta_{43}^2 v_d & \kappa_1\vartheta_{14}\vartheta_{43}^2 v_d & \lambda_1\vartheta_{43} v_d & \lambda_3\vartheta_{53} v_d & y_7\theta_{43} \\ \kappa_1\vartheta_{14}\vartheta_{43}^2 v_d & \kappa_1\vartheta_{14}\vartheta_{43}^2 v_d & \lambda_1\vartheta_{43} v_d & \lambda_3\vartheta_{53} v_d & y_7\theta_{43} \\ \kappa_5\vartheta_{13}\vartheta_{45} v_d + \kappa_6\vartheta_{43}\vartheta_{15} v_d & \kappa_5\vartheta_{13}\vartheta_{45} v_d + \ kappa_6\vartheta_{43}\vartheta_{15} v_d & \lambda_2\vartheta_{45} v_d & \lambda_4 v_d & y_8\theta_{45} \\ \kappa_7\theta_{43} & \kappa_7\theta_{43} & \lambda_5\theta_{41} & \lambda_6\theta_{51} & \lambda_7\vartheta_{43} v_u \end{pmatrix} . \tag{5.22}$$

5.4.3 Model C

Next, we will examine a representative model from class C. In this analysis, we focus on a particular model from this class, which involves flux integers and corresponding c_i coefficients, as detailed in Table 1. The resulting $U(1)'$ charges assigned to various matter curves are as follows:

$$\begin{aligned} &10_1 : \frac{1}{4}\,, \quad 10_2 : -\frac{1}{2}\,, \quad 10_3 : \frac{1}{4}\,, \quad 10_4 : -\frac{1}{4}\,, \\ &5_1 : -\frac{1}{2}\,, \quad 5_2 : \frac{1}{4}\,, \quad 5_3 : -\frac{1}{2}\,, \quad 5_4 : 0\,, \quad 5_5 : \frac{1}{4}\,, \quad 5_6 : \frac{3}{4}\,, \quad 5_7 : 0\,. \end{aligned}$$

Additionally, we distribute the various fermion and Higgs fields into different matter curves as follows:

$$\begin{aligned} &10_1 \longrightarrow Q_{2,3} + u^c_{1,2,3} + e^c_3\,, \quad 10_2 \longrightarrow Q_4 + u^c_4 + e^c_4\,, \quad 10_3 \longrightarrow Q_1 + e^c_{1,2}\,, \quad \overline{10}_4 \longrightarrow \overline{Q_4} + \overline{u^c_4} + \overline{e^c_4}\,, \\ &5_1 \longrightarrow H_u, \ \ \overline{5}_2 \longrightarrow L_1, \ \ \overline{5}_3 \longrightarrow H_d, \ \ 5_4 \longrightarrow \overline{d^c_4}, \ \ \overline{5}_5 \longrightarrow d^c_{1,2,3} + L_{2,3}, \ \ \overline{5}_6 \longrightarrow d^c_4 + L_4, \ \ 5_7 \longrightarrow \overline{L_4}\,. \end{aligned}$$

In this model, the μ-term arises through the coupling $\theta_{14}5_1\bar{5}_3$, so we require $\langle\theta_{14}\rangle$ to be approximately zero. Furthermore, we will consider high-order terms for certain couplings.

Now, let's describe the various superpotential terms that contribute to the mass matrices for the up, down, and charged lepton sectors. Starting with the up-type quarks, the dominant contributions are given by:

$$\begin{aligned} W \ &\supset y_t 10_1 10_1 5_1 + \tfrac{y_1}{\Lambda^2} 10_1 10_3 5_1 \theta_{13}\theta_{34} + \tfrac{y_2}{\Lambda} 10_1 10_2 5_1 \theta_{13} + \tfrac{y_3}{\Lambda^2} 10_3 10_2 5_1 \theta_{13}\theta_{14} + \tfrac{y_4}{\Lambda^2} 10_2 10_2 5_1 \theta_{13}^2 \\ &+ y_5 10_1 \overline{10}_4 \theta_{51} + y_6 10_2 \overline{10}_4 \theta_{53} + y_7 10_3 \overline{10}_4 \theta_{54} + \tfrac{y_8}{\Lambda^2} \overline{10}_4 \overline{10}_4 \overline{5}_3 \theta_{51}\theta_{54} \ , \end{aligned} \tag{5.23}$$

These terms result in the following mass texture for the up quarks:

$$M_u = \begin{pmatrix} y_1\vartheta_{13}\vartheta_{34}v_u & \eta^3 y_t v_u & \eta^2 y_t v_u & y_2\vartheta_{13}v_u & y_5\theta_{51} \\ y_1\vartheta_{13}\vartheta_{34}v_u & \eta^2 y_t v_u & \eta y_t v_u & y_2\vartheta_{13}v_u & y_5\theta_{51} \\ y_1\vartheta_{13}\vartheta_{34}v_u & \eta y_t v_u & y_t v_u & y_2\vartheta_{13}v_u & y_5\theta_{51} \\ 0 & y_2\vartheta_{13}v_u & y_2\vartheta_{13}v_u & y_4\vartheta_{13}^2 v_u & y_6\theta_{53} \\ y_7\theta_{54} & y_5\theta_{51} & y_5\theta_{51} & y_6\theta_{53} & y_8\vartheta_{51}\vartheta_{54}v_b \end{pmatrix} , \tag{5.24}$$

where η is a small constant parameter describing local Yukawa effects.

There are common operators between the top and bottom sectors with couplings y_5, y_6, and y_7 in Eq (5.23). The remaining operators contributing to the down-type quarks are:

$$\begin{aligned} W \ &\supset \tfrac{k}{\Lambda} 10_1 \bar{5}_5 \bar{5}_3 \theta_{54} + \tfrac{k_0}{\Lambda^3} 10_3 \bar{5}_5 \bar{5}_3 \theta_{13}\theta_{34}\theta_{54} + k_1 10_1 \bar{5}_6 \bar{5}_3 + \tfrac{k_2}{\Lambda} 10_3 \bar{5}_6 \bar{5}_3 \theta_{14} + \tfrac{k_3}{\Lambda} 5_4 \bar{5}_5 \theta_{14}\theta_{53} \\ &+ \tfrac{k_4}{\Lambda^2} 10_2 \bar{5}_5 \bar{5}_3 \theta_{14}\theta_{53} + \tfrac{k_7}{\Lambda^2} \overline{10}_4 5_4 5_1 \theta_{14}\theta_{53} + \tfrac{k_9}{\Lambda} 10_2 \bar{5}_6 \bar{5}_3 \theta_{13} + k_{10} 5_4 \bar{5}_6 \theta_{13}. \end{aligned} \tag{5.25}$$

Combining all these terms results in the following mass matrix describing the down-quark sector:

$$M_d = \begin{pmatrix} k_0\vartheta_{13}\vartheta_{34}\vartheta_{54}v_d & k\varepsilon^3\vartheta_{54}v_d & k\varepsilon^2\vartheta_{54}v_d & 0 & 0 \\ k_0\vartheta_{13}\vartheta_{34}\vartheta_{54}v_d & k\varepsilon^2\vartheta_{54}v_d & k\varepsilon\vartheta_{54}v_d & 0 & 0 \\ k_0\vartheta_{13}\vartheta_{34}\vartheta_{54}v_d & k\varepsilon\vartheta_{54}v_d & k\vartheta_{54}v_d & 0 & 0 \\ 0 & k_1\xi v_d & k_1 v_d & k_9\vartheta_{13}v_d & k_{10}\theta_{13} \\ y_7\theta_{54} & y_5\xi\theta_{51} & y_5\theta_{51} & y_6\theta_{53} & k_7\vartheta_{14}\vartheta_{53}v_u \end{pmatrix} , \tag{5.26}$$

where ϵ and ξ are small constant parameters describing local Yukawa effects.

Moving on to the charged lepton sector, some contributions also descend from terms in Eq (5.25) with couplings y_5, y_6, and y_7. The other leptonic contributions originate from the following operators:

$$\begin{aligned} W \supset & \frac{\lambda_1}{\Lambda} 10_3 \bar{5}_2 \bar{5}_3 \theta_{54} + \frac{\lambda_2}{\Lambda} 10_1 \bar{5}_2 \bar{5}_3 \theta_{51} + \frac{\lambda_3}{\Lambda} 10_2 \bar{5}_2 \bar{5}_3 \theta_{53} \\ & + \frac{\lambda_4}{\Lambda} 5_7 \bar{5}_2 \theta_{41}\theta_{53} + \lambda_5 5_7 \bar{5}_5 \theta_{53} + \lambda_6 5_7 \bar{5}_6 \theta_{43} + \frac{\lambda_7}{\Lambda} \overline{10}_4 5_7 5_1 \theta_{53} \ . \end{aligned}$$

As a result, the mass texture for the charged leptons has the following form:

$$M_e = \begin{pmatrix} \lambda_1\vartheta_{54}v_d & k_0\vartheta_{13}\vartheta_{34}\vartheta_{54}v_d & k_0\vartheta_{13}\vartheta_{34}\vartheta_{54}v_d & 0 & y_7\theta_{54} \\ \lambda_1\vartheta_{54}v_d & k_0\vartheta_{13}\vartheta_{34}\vartheta_{54}v_d & k_0\vartheta_{13}\vartheta_{34}\vartheta_{54}v_d & 0 & y_7\theta_{54} \\ \lambda_2\vartheta_{51}v_d & k\vartheta_{54}v_d & k\vartheta_{54}v_d & k_1 v_d & y_5\theta_{51} \\ \lambda_3\vartheta_{53}v_d & 0 & 0 & k_9\vartheta_{13}v_d & y_6\theta_{53} \\ \lambda_4\vartheta_{41}\theta_{53} & \lambda_5\theta_{53} & \lambda_5\theta_{53} & \lambda_6\theta_{43} & \lambda_7\vartheta_{53}v_u \end{pmatrix} . \tag{5.27}$$

5.4.4 Model D

We will now select a model from the fourth class. In this particular model, the $U(1)'$ charges assigned to different matter curves are as follows:

$$
\begin{aligned}
&10_1:-\frac{3}{4}\,,\quad 10_2:-\frac{1}{2}\,,\quad 10_3:\frac{7}{4}\,,\quad 10_4:-\frac{3}{4}\,,\\
&5_1:\frac{3}{2}\,,\quad 5_2:\frac{1}{4}\,,\quad 5_3:-1\,,\quad 5_4:-\frac{3}{2}\,,\quad 5_5:-\frac{9}{4}\,,\quad 5_6:\frac{1}{4}\,,\quad 5_7:1\,.
\end{aligned}
$$

A promising arrangement of fermion generations and Higgs fields among these matter curves is as follows:

$$
\begin{aligned}
&10_1\longrightarrow Q_{2,3}+u^c_{1,2,3}+e^c_3\,,\ \ \bar{10}_2\longrightarrow\overline{Q_4}+\overline{u^c_4}+\overline{e^c_4}\,,\ \ 10_3\longrightarrow Q_4+u^c_4+e^c_4\,,\ \ 10_4\longrightarrow Q_1+e^c_{1,2}\,,\\
&5_1\longrightarrow H_u,\ \ \bar{5}_2\longrightarrow d^c_1+L_{1,2},\ \ \bar{5}_3\longrightarrow H_d,\ \ 5_4\longrightarrow\overline{d^c_4},\ \ \bar{5}_5\longrightarrow d^c_4+L_4,\ \ \bar{5}_6\longrightarrow d^c_{2,3}+L_3,\ \ 5_7\longrightarrow\overline{L_4}\,.
\end{aligned}
$$

In this configuration, the μ-term arises from the coupling $\theta_{14}5_1\bar{5}_3$, and it is essential that we have $\langle\theta_{14}\rangle$ at approximately zero, as in previous models.

Now, let's outline the various superpotential terms in this model that contribute to the mass matrices for the top and bottom sectors.

The primary contributions to the up-type quarks originate from the following superpotential operators:

$$
\begin{aligned}
W\ \supset\ & y_t10_110_15_1+\tfrac{y_1}{\Lambda}10_110_45_1\theta_{15}+\tfrac{y_2}{\Lambda^2}10_310_15_1\theta_{13}\theta_{34}+\tfrac{y_3}{\Lambda^2}10_310_45_1\theta_{14}\theta_{15}+\tfrac{y_4}{\Lambda^4}10_310_35_1\theta_{13}^2\theta_{34}^2\\
&+y_510_1\overline{10}_2\theta_{31}+y_610_4\overline{10}_2\theta_{35}+y_710_3\overline{10}_2\theta_{34}+\tfrac{y_8}{\Lambda^2}\overline{10}_2\overline{10}_2\bar{5}_3\theta_{31}\theta_{34}\,.
\end{aligned}\tag{5.28}
$$

These operators result in the following mass texture for the up quarks:

$$
M_u=\begin{pmatrix}
y_1\vartheta_{15}v_u & \epsilon^3y_tv_u & \epsilon^2y_tv_u & y_2\vartheta_{13}\vartheta_{34}v_u & y_5\theta_{31}\\
y_1\vartheta_{15}v_u & \epsilon^2y_tv_u & \epsilon y_tv_u & y_2\vartheta_{13}\vartheta_{34}v_u & y_5\theta_{31}\\
y_1\vartheta_{15}v_u & \epsilon y_tv_u & y_tv_u & y_2\vartheta_{13}\vartheta_{34}v_u & y_5\theta_{31}\\
0 & y_2\vartheta_{13}\vartheta_{34}v_u & y_2\vartheta_{13}\vartheta_{34}v_u & y_4\vartheta_{13}^2\vartheta_{34}^2v_u & y_7\theta_{34}\\
y_6\theta_{35} & y_5\theta_{31} & y_5\theta_{31} & y_7\theta_{34} & y_8\vartheta_{31}\vartheta_{34}v_b
\end{pmatrix}.\tag{5.29}
$$

Just as in previous models, the operators with couplings y_5, y_6, and y_7 in Eq 5.28 also contribute to the bottom sector. The remaining dominant terms contributing to the down-type quarks are:

$$
\begin{aligned}
W\ \supset\ & y_b10_1\bar{5}_6\bar{5}_3+\tfrac{\kappa_1}{\Lambda}10_1\bar{5}_2\bar{5}_3\theta_{51}+\tfrac{\kappa_2}{\Lambda}10_4\bar{5}_6\bar{5}_3\theta_{15}+\kappa_310_4\bar{5}_2\bar{5}_3+\tfrac{\kappa_4}{\Lambda^2}10_3\bar{5}_6\bar{5}_3\theta_{13}\theta_{34}\\
&+\tfrac{\kappa_5}{\Lambda}10_3\bar{5}_2\bar{5}_3\theta_{54}+\tfrac{\kappa_6}{\Lambda}10_1\bar{5}_5\bar{5}_3\theta_{54}+\tfrac{\kappa_7}{\Lambda}10_4\bar{5}_5\bar{5}_3\theta_{13}+\tfrac{\kappa_8}{\Lambda^3}10_3\bar{5}_5\bar{5}_3\theta_{13}\theta_{34}\theta_{54}+\kappa_95_4\bar{5}_2\theta_{53}\\
&+\kappa_{10}5_4\bar{5}_6\theta_{13}+\tfrac{\kappa_{11}}{\Lambda}5_4\bar{5}_5\theta_{13}\theta_{54}+\tfrac{\kappa_{12}}{\Lambda^2}\overline{10}_25_45_1\theta_{13}\theta_{34}.
\end{aligned}\tag{5.30}
$$

When we collect all these terms, we obtain the following mass matrix for the down-quark sector of this model:

$$
M_d=\begin{pmatrix}
\kappa_3v_d & \kappa_1\vartheta_{51}v_d & \kappa_1\vartheta_{51}v_d & \kappa_5\vartheta_{54}v_d & \kappa_9\theta_{53}\\
\kappa_2\vartheta_{15}v_d & \epsilon^2y_bv_d & \epsilon y_bv_d & \kappa_4\vartheta_{13}\vartheta_{34}v_d & \kappa_{10}\theta_{13}\\
\kappa_2\vartheta_{15}v_d & \epsilon y_bv_d & y_bv_d & \kappa_4\vartheta_{13}\vartheta_{34}v_d & \kappa_{10}\theta_{13}\\
\kappa_7\vartheta_{13}v_d & \kappa_6\vartheta_{54}v_d & \kappa_6\vartheta_{54}v_d & \kappa_8\vartheta_{13}\vartheta_{34}\vartheta_{54}v_d & \kappa_{11}\theta_{13}\theta_{54}\\
y_6\theta_{35} & y_5\theta_{31} & y_5\theta_{31} & y_7\theta_{34} & \kappa_{12}\vartheta_{13}\vartheta_{34}v_u
\end{pmatrix}.\tag{5.31}
$$

Now, let's shift our focus to the charged lepton sector of the model. The operators with couplings κ_1, κ_2, κ_3, κ_4, κ_5, κ_6, κ_7, and κ_8 from Eq (5.30) also contribute to the charged lepton mass matrix. Additionally, there are common operators between the top and charged lepton sectors outlined in Eq (5.28) with couplings y_5, y_6, and y_7. We also have contributions from the operators:

$$\lambda_1 5_7\overline{5}_2\theta_{41}\theta_{53} + \lambda_2 5_7\overline{5}_2\theta_{51}\theta_{43} + \lambda_3 5_7\overline{5}_6\theta_{43} + \lambda_4 5_7\overline{5}_5\theta_{53} + \lambda_5\overline{10}_2 5_7 5_1\ . \tag{5.32}$$

Taking all these contributions into account, we can write down the mass matrix for the charged leptons in the model as follows:

$$M_e = \begin{pmatrix} \kappa_3 v_d & \kappa_3 v_d & \kappa_2\vartheta_{15}v_d & \kappa_7\vartheta_{13}v_d & y_6\theta_{35} \\ \kappa_3 v_d & \kappa_3 v_d & \kappa_2\vartheta_{15}v_d & \kappa_7\vartheta_{13}v_d & y_6\theta_{35} \\ \kappa_1\vartheta_{51}v_d & \kappa_1\vartheta_{51}v_d & y_\tau v_d & \kappa_6\vartheta_{54}v_d & y_5\theta_{31} \\ \kappa_5\vartheta_{54}v_d & \kappa_5\vartheta_{54}v_d & \kappa_4\vartheta_{14}v_d & \kappa_8\vartheta_{13}\vartheta_{34}\vartheta_{54}v_d & y_7\theta_{34} \\ \lambda_1\theta_{41}\theta_{53}+\lambda_2\theta_{51}\theta_{43} & \lambda_1\theta_{41}\theta_{53}+\lambda_2\theta_{51}\theta_{43} & \lambda_3\theta_{43} & \lambda_4\theta_{53} & \lambda_5 v_u \end{pmatrix} . \tag{5.33}$$

5.4.5 Model E

For our fifth and final Model, we assign $U(1)'$ charges to the different matter curves as follows:

$$\begin{aligned} &10_1 : \frac{9}{2}\ ,\quad 10_2 : \frac{11}{2}\ ,\quad 10_3 : \frac{9}{2}\ ,\quad 10_4 : -8\ , \\ &5_1 : -9\ ,\quad 5_2 : 1\ ,\quad 5_3 : 9\ ,\quad 5_4 : \frac{7}{2}\ ,\quad 5_5 : -1\ ,\quad 5_6 : \frac{27}{2}\ ,\quad 5_7 : \frac{7}{2}\ . \end{aligned}$$

To achieve realistic mass hierarchies, we distribute the fermion generations and Higgs fields among these matter curves in the following manner:

$$\begin{aligned} &10_1 \longrightarrow Q_3 + u^c_{2,3}\ ,\quad \bar{10}_2 \longrightarrow \overline{Q_4} + \overline{u^c_4} + \overline{e^c_4}\ ,\quad 10_3 \longrightarrow Q_{1,2} + u^c_1 + e^c_{1,2,3}\ ,\quad 10_4 \longrightarrow Q_4 + u^c_4 + e^c_4\ , \\ &5_1 \longrightarrow H_u,\ \ \bar{5}_2 \longrightarrow H_d,\ \ 5_3 \longrightarrow \overline{d^c_4},\ \ \bar{5}_4 \longrightarrow L_3,\ \ 5_5 \longrightarrow \overline{L_4},\ \ \bar{5}_6 \longrightarrow d^c_4 + L_4,\ \ \bar{5}_7 \longrightarrow d^c_{1,2,3} + L_{1,2}\ . \end{aligned}$$

In this configuration, the μ-term is generated through the coupling $\theta_{13}5_1\bar{5}_2$, which implies that $\langle\theta_{13}\rangle \approx 0$. With this constraint, we can derive the various superpotential operators for the top and bottom quark sectors.

We begin with the dominant contributions to the up-type quarks, given by:

$$\begin{aligned} W\ \supset\ & y_t 10_1 10_1 5_1 + \tfrac{y_1}{\Lambda}10_1 10_3 5_1\theta_{14} + \tfrac{y_2}{\Lambda^2}10_3 10_3 5_1\theta_{14}^2 + \tfrac{y_3}{\Lambda^2}10_3 10_4 5_1\theta_{14}\theta_{15} + \tfrac{y_4}{\Lambda}10_1 10_4 5_1\theta_{15} \\ & + \tfrac{y_5}{\Lambda^2}10_4 10_4 5_1\theta_{15}^2 + y_6 10_3\overline{10}_2\theta_{34} + y_7 10_1\overline{10}_2\theta_{31} + y_8 10_4\overline{10}_2\theta_{35} + \tfrac{y_9}{\Lambda^2}\overline{10}_2\overline{10}_2\overline{5}_2\theta_{31}^2 \end{aligned} \tag{5.34}$$

These operators lead to the following mass texture for the up-type quarks:

$$M_u = \begin{pmatrix} y_2\vartheta_{14}^2 v_u & y_2\vartheta_{14}^2 v_u & y_1\vartheta_{14}v_u & y_3\vartheta_{14}\vartheta_{15}v_u & y_6\theta_{34} \\ y_1\vartheta_{14}v_u & y_1\vartheta_{14}v_u & \epsilon y_t v_u & y_4\vartheta_{15}v_u & y_7\theta_{31} \\ y_1\vartheta_{14}v_u & y_1\vartheta_{14}v_u & y_t v_u & y_4\vartheta_{15}v_u & y_7\theta_{31} \\ y_3\vartheta_{14}\vartheta_{15}v_u & y_4\vartheta_{15}v_u & y_4\vartheta_{15}v_u & y_5\vartheta_{15}^2 v_u & y_8\theta_{35} \\ y_6\theta_{34} & y_6\theta_{34} & y_7\theta_{31} & y_8\theta_{35} & y_9\vartheta_{31}^2 v_b \end{pmatrix} . \tag{5.35}$$

Some of the operators in Eq (5.34), specifically those with couplings y_6, y_7, and y_8, also contribute to the bottom quark sector. Additionally, the bottom sector receives contributions from the following superpotential terms:

$$\begin{aligned} W \supset\, & y_b 10_1\overline{5}_7\overline{5}_2 + \frac{\kappa_1}{\Lambda}10_3\overline{5}_7\overline{5}_2\theta_{14} + \frac{\kappa_2}{\Lambda}10_4\overline{5}_7\overline{5}_2\theta_{15} + \frac{\kappa_3}{\Lambda}10_3\overline{5}_6\overline{5}_2\theta_{13} + \frac{\kappa_4}{\Lambda}10_1\overline{5}_6\overline{5}_2\theta_{43} \\ & + \kappa_5\overline{5}_7 5_3\theta_{15} + \frac{\kappa_6}{\Lambda}\overline{5}_6 5_3\theta_{13}\theta_{45} + \frac{\kappa_7}{\Lambda}\overline{10}_2 5_3 5_1\theta_{15} + \frac{\kappa_8}{\Lambda^2}10_4\overline{5}_6\overline{5}_2\theta_{13}\theta_{45}\,. \end{aligned}$$

When we compile all these contributions, we obtain the following mass matrix for the down-quark sector:

$$M_d = \begin{pmatrix} \kappa_1\vartheta_{14}v_d & \kappa_1\vartheta_{14}v_d & \epsilon^2 y_b v_d & \kappa_2\vartheta_{15}v_d & \kappa_5\theta_{15} \\ \kappa_1\vartheta_{14}v_d & \kappa_1\vartheta_{14}v_d & \epsilon y_b v_d & \kappa_2\vartheta_{15}v_d & \kappa_5\theta_{15} \\ \kappa_1\vartheta_{14}v_d & \kappa_1\vartheta_{14}v_d & y_b v_d & \kappa_2\vartheta_{15}v_d & \kappa_5\theta_{15} \\ \kappa_3\vartheta_{13}v_d & \kappa_3\vartheta_{13}v_d & \kappa_4\vartheta_{43}v_d & \kappa_8\vartheta_{43}\vartheta_{15}v_d & \kappa_6\vartheta_{13}\theta_{45} \\ y_6\theta_{34} & y_6\theta_{34} & y_7\theta_{31} & y_8\theta_{35} & \kappa_7\vartheta_{15}v_u \end{pmatrix} \tag{5.36}$$

The bottom sector also shares common operators with the charged lepton sector of the model, specifically those with couplings κ_1, κ_2, and κ_8. Furthermore, there are common operators between the top and charged lepton sectors as shown in Eq (5.34), involving couplings y_6 and y_8. All other contributions descend from the operators

$$\begin{aligned} W \supset\, & y_\tau 10_3\overline{5}_4\overline{5}_2 + \frac{\lambda_1}{\Lambda}10_4\overline{5}_4\overline{5}_2\theta_{45} + \frac{\lambda_2}{\Lambda}10_3\overline{5}_6\overline{5}_2\theta_{13} + \lambda_3 5_5\overline{5}_7\theta_{35} + \frac{\lambda_4}{\Lambda}5_5\overline{5}_4\theta_{45}\theta_{31} \\ & + \lambda_5 5_5\overline{5}_6\theta_{45} + \frac{\lambda_6}{\Lambda}\overline{10}_2 5_5 5_1\theta_{35}\,. \end{aligned}$$

Finally, combining the various contributions described so far we end up with the following mass matrix for the charged lepton sector of the model :

$$M_e = \begin{pmatrix} \kappa_1\vartheta_{14}v_d & \kappa_1\vartheta_{14}v_d & \epsilon^2 y_\tau v_d & \lambda_2\vartheta_{13} & y_6\theta_{34} \\ \kappa_1\vartheta_{14}v_d & \kappa_1\vartheta_{14}v_d & \epsilon y_\tau v_d & \lambda_2\vartheta_{13} & y_6\theta_{34} \\ \kappa_1\vartheta_{14}v_d & \kappa_1\vartheta_{14}v_d & y_\tau v_d & \lambda_2\vartheta_{13} & y_6\theta_{34} \\ \kappa_2\vartheta_{15}v_d & \kappa_2\vartheta_{15}v_d & \lambda_1\vartheta_{45}v_d & \kappa_8\vartheta_{15}\vartheta_{43} & y_8\theta_{35} \\ \lambda_3\theta_{35} & \lambda_3\theta_{35} & \lambda_4\theta_{31}\theta_{45} & \lambda_5\theta_{45} & \lambda_6\vartheta_{35}v_u \end{pmatrix}. \tag{5.37}$$

5.5 Flavor violation observables

As the Z' gauge boson interacts differently with the vector-like fields, the introduction of these fields may lead to novel flavor violation phenomena and potentially enhance rare processes, particularly when there is significant mixing between the vector-like fields and the Standard Model matter fields, as discussed in references [341] and [346].

To assess whether the models presented here can explain the observed anomalies at LHCb, we must calculate the unitary transformations required to diagonalize the mass matrices derived in the preceding section. Given the intricate nature of these matrices, we adopt a perturbative approach to diagonalize them, focusing initially on model A. It is worth noting that the analysis for the remaining models closely parallels the one presented here.

5.5.1 Some phenomenological predictions of model A

To proceed with our analysis and explore its phenomenological implications, we begin by deriving the mass matrices and mixing parameters for both quarks and leptons.

Quarks: We initiate our examination with the quark sector of Model A, specifically focusing on the down quark mass matrix. To simplify this matrix (5.15), we assume that certain terms are negligibly small and can be approximated as zero. Specifically, we consider that $\kappa_5=\kappa_{10}=\kappa_{11}=\kappa_{12}=\kappa_{14}=y_6=y_7\approx 0$. We further make the following simplifications

$$\kappa_0\vartheta_{41}v_d=\kappa_1\vartheta_{45}v_d=m\ ,\ \kappa_2\vartheta_{43}v_d=\alpha m\ ,\ \kappa_3\vartheta_{13}\vartheta_{45}v_d=\theta m\ ,\ \kappa_9\vartheta_{14}v_d=c\mu\ ,\ \kappa_8\theta_{13}v_d=bm\ ,$$

$$\kappa_{13}\theta_{53}\simeq y_8\theta_{54}=M,$$

In these approximations, the mass parameters are represented by m, M, and μ, while α, θ, c, b, and ξ are dimensionless coefficients. With these assumptions, the mass matrix takes on a simplified form:

$$M_d=\begin{pmatrix} \theta m\xi^4 & \theta m\xi & m\xi^4 & 0 & 0\\ \theta m\xi & \theta m & m\xi^2 & 0 & 0\\ \alpha m\xi^2 & \alpha m & m & 0 & 0\\ bm & bm\xi & 0 & c\mu & M\\ 0 & 0 & 0 & M & 0 \end{pmatrix}. \tag{5.38}$$

In summary, we have introduced mass parameters m, M, and μ, and dimensionless coefficients α, θ, c, b, and ξ. By retaining terms up to first order in ξ, the mass matrix $M_dM_d^T$ can be approximated as:

$$M_dM_d^T\approx\begin{pmatrix} 0 & \theta^2m^2\xi & \alpha\theta m^2\xi & 0 & 0\\ \theta^2m^2\xi & \theta^2m^2 & \alpha\theta m^2 & 2b\theta m^2\xi & 0\\ \alpha\theta m^2\xi & \alpha\theta m^2 & \alpha^2m^2+m^2 & \alpha bm^2\xi & 0\\ 0 & 2b\theta m^2\xi & \alpha bm^2\xi & b^2m^2+c^2\mu^2+M^2 & c\mu M\\ 0 & 0 & 0 & c\mu M & M^2 \end{pmatrix}. \tag{5.39}$$

Remarkably, we can express (5.39) in the form $M_d^2\approx\mathbf{A}+\xi\,\mathbf{B}$, where:

$$\mathbf{A}=\begin{pmatrix} 0 & 0 & 0 & 0 & 0\\ 0 & \theta^2m^2 & \alpha\theta m^2 & 0 & 0\\ 0 & \alpha\theta m^2 & \alpha^2m^2+m^2 & 0 & 0\\ 0 & 0 & 0 & b^2m^2+c^2\mu^2+M^2 & c\mu M\\ 0 & 0 & 0 & c\mu M & M^2 \end{pmatrix},\quad \mathbf{B}=\begin{pmatrix} 0 & \theta^2m^2 & \alpha\theta m^2 & 0 & 0\\ \theta^2m^2 & 0 & 0 & 2b\theta m^2 & 0\\ \alpha\theta m^2 & 0 & 0 & \alpha bm^2 & 0\\ 0 & 2b\theta m^2 & \alpha bm^2 & 0 & 0\\ 0 & 0 & 0 & 0 & 0 \end{pmatrix}$$

It is important to note that the parameter ξ characterizes the coupling between the electroweak sector and the heavy vector-like component and serves as a perturbative mixing parameter. The leading order part of the matrix, $\mathbf{A}$, can be diagonalized by a unitary matrix $V^0_{b_L}$ to yield $V^0_{b_L}\mathbf{A}V^{0T}_{b_L}$ for small values of the parameter α. The eigenvalues of this matrix are given by:

$$x_1=0,\quad x_2\approx\theta^2\left(m^2-\alpha^2m^2\right),\quad x_3\approx\alpha^2\theta^2m^2+\alpha^2m^2+m^2,\quad x_4\approx M^2,\quad x_5\approx b^2m^2+M^2 \tag{5.40}$$

We observe here that the eigenvalues appear with the desired hierarchy. The corresponding unitary matrix that diagonalizes matrix $\mathbf{A}$ and yields the eigenvalues (5.40) is:

$$V^0_{b_L} = \begin{pmatrix} 1 & 0 & 0 & 0 & 0 \\ 0 & \frac{\alpha^2\theta^2}{2} - 1 & \alpha\theta & 0 & 0 \\ 0 & \alpha\theta & 1 - \frac{\alpha^2\theta^2}{2} & 0 & 0 \\ 0 & 0 & 0 & -\frac{c\mu M}{b^2 m^2} & 1 \\ 0 & 0 & 0 & 1 & \frac{c\mu M}{b^2 m^2} \end{pmatrix} .$$

These columns of this matrix correspond to the unperturbed eigenvectors $v^0_{b_i}$ of the initial matrix.

Now, we consider the corrections to the eigenvectors due to the perturbative part $\xi\mathbf{B}$ using the relation given by the relation :

$$v_{b_i} \approx v^0_{b_i} + \xi \sum_{j\neq i}^{5} \frac{(V^0_{b_L}\mathbf{B}V^{0\dagger}_{b_L})_{ji}}{x_i - x_j} v^0_{b_j} \ , \tag{5.41}$$

where the second term displays the $\mathcal{O}(\xi)$ corrections to the basic eigenvectors of the leading order matrix $\mathbf{A}$. The corrected diagonalizing matrices schematically receive the form $V_{b_L} = V^0_{b_L} + \xi V^1_{b_L}$ and similarly for the up quarks and leptons. This way the mixing parameter ξ enters in the expressions associated with the various flavor violation observables.

Computing the eigenvectors using the formula (5.41), the $\mathcal{O}(\xi)$ corrected unitary matrix is :

$$V_{b_L} \approx \begin{pmatrix} 1 & -\xi & 0 & 0 & 0 \\ -\xi & \frac{\alpha^2\theta^2}{2} - 1 & \alpha\theta & \frac{2b\theta m^2\xi}{M^2} & -\frac{2bc\theta\mu m^2\xi}{M^3} \\ \alpha\theta\xi & \alpha\theta & 1 - \frac{\alpha^2\theta^2}{2} & -\frac{\alpha b m^2\xi}{M^2} & -\frac{\alpha bc\mu m^2\xi}{M^3} \\ 0 & -\frac{2c\theta\mu\xi}{bM} & \frac{\alpha c\mu\xi}{bM} & -\frac{c\mu M}{b^2m^2} & 1 \\ 0 & \frac{2b\theta m^2\xi}{M^2} & \frac{\alpha b m^2\xi}{M^2} & 1 & \frac{c\mu M}{b^2 m^2} \end{pmatrix} .$$

We assume here that the mixing in the top sector is small and that the main mixing descends from the bottom quark sector.

Charged Leptons: Moving on to the charged lepton mass matrix (5.16), we note that certain parameters from the top and bottom sectors also contribute to this matrix. Consequently, we apply the same assumptions to these parameters. Additionally, we assume that $\lambda_1 = \lambda_3 = \lambda_4 = \lambda_5 = \lambda_7 \approx 0$ and introduce the following simplifications:

$$\lambda_2\vartheta_{34}v_d = c\,\mu \ , \lambda_5\vartheta_{51}\vartheta_{43} = qm \ , \ \lambda_6\theta_{51} \approx y_8\theta_{54} = M \ ,$$

Here, the mass parameter M characterizes the scale of the vector-like particles, while q and c are dimensionless parameters.

With these approximations, the matrix takes the following form:

$$M_e \approx \begin{pmatrix} \theta m & \alpha m\xi^4 & \alpha m\xi^4 & 0 & 0 \\ \theta m\xi^3 & \alpha m\xi & \alpha m\xi^2 & 0 & 0 \\ \theta m\xi & \alpha m\xi^2 & \alpha m & 0 & 0 \\ 0 & 0 & 0 & c\mu & M \\ 0 & mq & m\xi q & M & 0 \end{pmatrix} .$$

We proceed by perturbatively diagonalizing the lepton square mass matrix $M_e M_e^T$ (M_e^2 for short), employing ξ as the expansion parameter. Keeping terms up to $\mathcal{O}(\xi)$, we express the mass square matrix in the form $M_e^2 \approx \mathbf{A} + \xi\, \mathbf{B}$, where:

$$\mathbf{A} = \begin{pmatrix} \theta^2 m^2 & 0 & 0 & 0 & 0 \\ 0 & 0 & 0 & 0 & 0 \\ 0 & 0 & \alpha^2 m^2 & 0 & 0 \\ 0 & 0 & 0 & c^2\mu^2 + M^2 & c\mu M \\ 0 & 0 & 0 & c\mu M & m^2 q^2 + M^2 \end{pmatrix},$$

$$\mathbf{B} = \begin{pmatrix} 0 & 0 & \theta^2 m^2 \xi & 0 & 0 \\ 0 & 0 & 0 & 0 & \alpha m^2 \xi q \\ \theta^2 m^2 \xi & 0 & 0 & 0 & \alpha m^2 \xi q \\ 0 & 0 & 0 & 0 & 0 \\ 0 & \alpha m^2 \xi q & \alpha m^2 \xi q & 0 & 0 \end{pmatrix}.$$

The eigenvalues of the dominant part are:

$$x_1 = 0, \quad x_2 = \alpha^2 m^2, \quad x_3 = \theta^2 m^2, \quad x_4 = M^2, \quad x_5 = M^2 + m^2 q^2 \tag{5.42}$$

The unitary matrix $V_{e_L}^0$ that diagonalizes the dominant matrix $\mathbf{A}$ is given by:

$$V_{e_L}^0 = \begin{pmatrix} 0 & 1 & 0 & 0 & 0 \\ 0 & 0 & 1 & 0 & 0 \\ 1 & 0 & 0 & 0 & 0 \\ 0 & 0 & 0 & -1 & \frac{c\mu M}{m^2 q^2} \\ 0 & 0 & 0 & \frac{c\mu M}{m^2 q^2} & 1 \end{pmatrix}.$$

To find the $\mathcal{O}(\xi)$ corrections to the eigenvectors due to the perturbative part $\xi\mathbf{B}$, we apply the relation (5.41). Subsequently, we derive the final unitary matrix:

$$V_{e_L} \approx \begin{pmatrix} 0 & 1 & 0 & \frac{\alpha c\mu m^2 \xi q}{M^3} & \alpha\left(-\frac{c^2\mu^2\xi}{m^2 q^3} - \frac{m^2 \xi q}{M^2}\right) \\ -\frac{\xi\left(\alpha^2+\theta^2\right)}{\theta^2} & 0 & 1 & \frac{\alpha c\mu m^2 \xi q}{M^3} & -\frac{\alpha m^2 \xi q}{M^2} \\ 1 & 0 & \xi & 0 & 0 \\ 0 & \frac{\alpha c\mu\xi}{Mq} & \frac{\alpha c\mu\xi}{Mq} & -1 & \frac{c\mu M}{m^2 q^2} \\ 0 & \frac{\alpha m^2 \xi q}{M^2} & \frac{\alpha m^2 \xi q}{M^2} & \frac{c\mu M}{m^2 q^2} & 1 \end{pmatrix}$$

It's worth noting that, for the sake of simplification, we have assumed series expansions for small α, θ, and c, retaining only the dominant terms in the final result.

B-meson anomalies at LHCb

In the context of a fourth generation, where the $U(1)'$ charge assignments for its constituents differ from those of the SM families, we anticipate the enhancement of several intriguing rare flavor processes. A thorough investigation of these phenomena will be presented in a forthcoming publication. For now, our focus is solely on the B-meson anomaly, specifically the $b \to s\ell\ell$ decay, particularly the ratio $R_{K^{(*)}} = \mathrm{BR}(B \to K^{(*)}\mu\mu)/\mathrm{BR}(K^{(*)}ee)$. This focus arises from the non-universal coupling of the Z' gauge boson with the vector-like fermions, which leads to the Wilson coefficient $C_9^{\mu\mu}$ contributing to the flavor-violating transition $b \to sll$, as expressed by:

$$C_9^{\mu\mu} = -\frac{\sqrt{2}}{4G_F}\frac{16\pi^2}{e^2}\left(\frac{g'}{M_{Z'}}\right)^2 \frac{(Q'_{d_L})_{23}(Q'_{e_L})_{22}}{V_{tb}V_{ts}^*}\,, \tag{5.43}$$

Here, the matrices Q'_{d_L} and Q'_{e_L} are defined as per [293], using:

$$Q'_{f_L} \equiv V_{f_L} q'_{f_L} V_{f_L}^\dagger\,, \tag{5.44}$$

where q'_{f_L} represents 5×5 diagonal matrices of $U(1)'$ charges.[3] The elements $(Q'_{d_L})_{23}$ and $(Q'_{e_L})_{22}$ that contribute to the $C_9^{\mu\mu}$ coefficient can be derived from (5.44), using the diagonalization matrices V_{f_L} computed earlier. This leads to the following approximations:

$$(Q'_{d_L})_{23} \approx -\tfrac{1}{2}\alpha\theta\xi^2 \quad \text{and} \quad (Q'_{e_L})_{22} \approx -1-\xi^2. \tag{5.45}$$

Finally, incorporating the values $G_F \approx 11.66\ TeV^{-2}$, $e \approx 0.303$, $V_{tb} \approx 0.99$, and $V_{ts} \approx 0.0404$, we can estimate:

$$C_9^{\mu\mu} \approx -652.5\ \alpha\theta\xi^2\left(\frac{g'}{M_{Z'}}\right)^2 + 5220\ \alpha b^2\theta\xi^2\left(\frac{g'}{M_{Z'}}\right)^2\left(\frac{m}{M}\right)^4 \tag{5.46}$$

In this equation, the mass parameters m, M, and $M_{Z'}$ are expressed in units of TeV. When using sample values such as $\alpha \approx 0.06$, $\theta \approx 0.27$, $\xi \approx 0.5$, $m \approx 0.1$, $b \approx 0.1$, $M \approx 1.2$, we obtain:

$$C_9^{\mu\mu} \approx -2.64\left(\frac{g'}{M_{Z'}}\right)^2. \tag{5.47}$$

According to the most recent global fits [362], explaining the current experimental data requires $C_9^{\mu\mu} \approx -0.82$. Consequently, in this model, the ratio of the Z' gauge coupling to its mass, $\frac{g'}{(M_{Z'}/\mathrm{TeV})} \approx \frac{1}{2}$, must be at the order of magnitude necessary to account for the observed R_K anomalies. This implies that the Z' mass should be relatively small [363], unless g' is associated with some strong coupling regime. Please note that while we have presented these calculations, a comprehensive analysis encompassing a range of models is required to determine whether the mixing effects can predict the various observed deviations in B-meson decays, which is beyond the scope of this work.

5.6 R-parity violation terms

A noteworthy observation is that certain R-parity violating (RPV) terms, such as $\lambda'_{ijk}L_iQ_jd_k^c$, have the potential to account for the anomalies associated with the $b \to s\ell\ell$ flavor-violating process [331, 364–366].

In this section, our focus is on identifying possible R-parity violating terms (RPV) within the tree-level superpotential (referred to here as W_{tree}^{RPV}) for the models A, B, C, D, E outlined in Table 5.3. We'll briefly discuss their implications. We differentiate between RPV terms that couple

[3] For insights into the effects of complex-valued contributions to the Wilson coefficients, arising from significant CP-violation effects, please refer to [361].

only to the MSSM fields and those that share Yukawa couplings with extra vector-like families. RPV terms in the former category, if present in $W^{RPV}_{\rm tree}$, lead to problematic violations of baryon and/or lepton numbers and must be suppressed. In F-theory constructions, this suppression can be achieved through careful flux restrictions that intersect various matter curves [327], or through additional (discrete) symmetries arising from the background geometry of the theory [286,323,367,368]. Section 4 of [323] provides examples of how such R-parity conservation can be incorporated. However, under certain conditions and restrictions [364], these couplings can contribute to intriguing phenomena such as the B-meson anomalies and other effects like the $(g-2)_\mu$ anomaly [332,333] without exceeding baryon and/or lepton number-violating bounds.

For each of the five classes of models, we identify the RPV terms among all possible superpotential couplings. Given that in all the models presented so far, the up-Higgs doublet is isolated at the 5_1 matter curve, the possible RPV operators in the form of $10 \cdot \overline{5} \cdot \overline{5}$ are as follows:

$$\mathbf{10}_1(\overline{\mathbf{5}}_2\overline{\mathbf{5}}_7 + \overline{\mathbf{5}}_3\overline{\mathbf{5}}_6 + \overline{\mathbf{5}}_4\overline{\mathbf{5}}_5), \quad \mathbf{10}_2\overline{\mathbf{5}}_3\overline{\mathbf{5}}_4, \quad \mathbf{10}_3\overline{\mathbf{5}}_2\overline{\mathbf{5}}_4, \quad \mathbf{10}_4\overline{\mathbf{5}}_2\overline{\mathbf{5}}_3 \,. \tag{5.48}$$

Now, let's discuss each model individually:

Model A. Referring to Table 5.3 and taking into consideration (5.48), we find that the sole RPV term in this model is:

$$\mathbf{10}_1\overline{\mathbf{5}}_3\overline{\mathbf{5}}_6 \longrightarrow L_4 Q_3 d^c_{1,2} \,. \tag{5.49}$$

We observe that R-parity violation occurs only in terms involving the vector-like family, and there are no terms that solely involve the three quark and lepton families of the MSSM. Nonetheless, as recently demonstrated in [331,366], the coupling $L_4Q_3d^c_2$ can make significant contributions to the $b \to s\mu\mu$ process via photonic penguin diagrams.

Model B. Following a similar procedure, we find that this model contains the following RPV terms:

$$W^{RPV}_{tree} \supset \mathbf{10}_1\overline{\mathbf{5}}_4\overline{\mathbf{5}}_5 + \mathbf{10}_2\overline{\mathbf{5}}_3\overline{\mathbf{5}}_4 \longrightarrow L_3Q_3d^c_4 + L_3L_4e^c_{1,2,3} \,. \tag{5.50}$$

The first operator here does not contribute to the $b \to sll$ process due to the absence of the second-generation quark in the coupling. However, the term $L_3L_4e^c_2$, derived from the second operator, leads to non-negligible contributions to the anomalous magnetic moment of the muon [332]. Combining this with non-zero Z' contributions may offer a satisfactory explanation for the $(g-2)_\mu$ anomaly.

Model C, D, and E. None of these models contain renormalizable RPV terms. Therefore, an explanation for the observed experimental discrepancies is expected to arise from Z' interactions and the mixing of SM fermions with the extra vector-like states.

Chapter 6

Summary and conclusions

In this comprehensive exploration, we've embarked on a journey through various Grand Unified Models (GUTs) and string theory-inspired frameworks, unearthing profound insights into particle physics and cosmology. Each model we've examined offers a distinct lens through which to view the fundamental forces of the universe. Our quest has yielded a rich tapestry of knowledge, connecting theoretical concepts to empirical observations. In this concluding chapter, we will recap our findings and emphasize the significance of each model's contributions.

Chapter 2

Unified models with $SO(10)$ gauge symmetry encompass various compelling features and have garnered substantial attention in both field theory and string theory contexts. In this study, we have developed a straightforward $SO(10)$ model, featuring matter and Higgs fields accommodated within lower-dimensional representations. We have conducted a comprehensive analysis of the model's implications, both phenomenological and cosmological in nature.

The Higgs fields, specifically residing in $\underline{16}_H + \overline{\underline{16}}_H$ and in two Adjoints $\underline{45}_H, \underline{45'}_H$, undergo spontaneous symmetry breaking of the $SO(10)$ gauge group, ultimately leading to the Standard Model. Furthermore, the appropriate vacuum expectation values (VEVs) of a pair of tenplets $\underline{10}_h + \underline{10}'_h$ are responsible for fermion masses and the generation of CKM mixing. Consequently, after the $SO(10)$ symmetry breaking, the emergent low-energy effective theory aligns with the minimal supersymmetric standard model.

We have also delved into the cosmological implications of this effective theory, particularly those linked to primordial inflation. Employing the canonical form of the Kähler potential, we have derived the effective scalar potential governing inflation dynamics. Our findings indicate that, for a wide range of parameter values, the slow-roll observables align with observed data.

More broadly, within this model, the effective potential is expressed as a function of an $SO(10)$ singlet S and the Higgs field ϕ, associated with the $\underline{16}_H + \overline{\underline{16}}_H$ and $\underline{45}_H, \underline{45'}_H$ representations. We present scenarios where inflation is driven by the pair of fields $\underline{16}_H + \overline{\underline{16}}_H$, causing the transition from $SO(10)$ to $SU(5)$ and imparting masses to the right-handed neutrinos through a fourth-order non-renormalizable term. The reheating process is considered through the decay of the inflaton field into a pair of heavy right-handed neutrinos, while the observed baryon asymmetry of the universe is accounted for through non-thermal leptogenesis within our model. We have set the reheating temperature at $T_{RH} = 10^9$ GeV and utilized this value to estimate the masses of the heavy Majorana neutrinos, while also considering gravitino constraints to constrain various involved parameters.

In conclusion, our analysis suggests that a scalar spectral index in the range of 0.96-0.97 can be readily accommodated, with a tensor-to-scalar ratio $r \sim 10^{-3}$.

Chapter 3

We have conducted a thorough investigation into the cosmological and low-energy supersymmetry implications of an effective model originating from the geometric arrangement of intersecting three D7-brane stacks within the framework of type-IIB string theory, as detailed in [242]. Within this model, perturbative string loop corrections, which exhibit a logarithmic dependence on the compactification volume $\mathscr{V}$, along with D-terms associated with the universal $U(1)$ factors of D7-brane stacks, collectively generate an effective scalar potential that yields a de Sitter vacuum. This potential also effectively stabilizes all three Kähler moduli fields inherent to the specific geometric configuration.

In our current work, we extended our analysis to account for the effects of ordinary matter contributions within the Kähler potential of the effective model. Specifically, we focused on the pivotal role played by a generic pair of Higgs fields, denoted as Φ_1 and Φ_2 and linked to the gauge group of the effective theory, in shaping low-energy phenomenological predictions and various cosmological observables. This included the incorporation of matter field content, soft-term contributions, and Coleman-Weinberg corrections to the previously derived potential.

We explored the implementation of the standard hybrid inflationary scenario, where a singlet gauge field, sharing common couplings with the Higgs fields in the superpotential, serves as the inflaton, while the Higgs states act as waterfall fields.

With the spectral index fixed at the central value of $n_s = 0.96655$, we presented predictions for the remaining cosmological observables in accordance with the latest Planck data. Notably, we estimated the value of the tensor-to-scalar ratio to be $r \sim 2 \times 10^{-4}$—significantly below current experimental bounds but still within the potential reach of future experiments.

Additionally, we delved into the decay of the lighter Kähler moduli after the conclusion of inflation, including modes that lead to both visible and invisible particles. In the context of an MSSM effective theory and with the presence of a Giudice-Masiero coupling, our calculations indicated that the dominant decay of the lightest modulus is directed towards the Higgs fields, consistent with previous analyses [262].

Furthermore, our investigation extended to predictions regarding dark radiation production. We found that $\Delta N_{\text{eff}} \leq 0.95$ at a 2σ confidence level, which necessitated that model parameters a and λ (associated with couplings proportional to $a\lambda(\Phi_1\Phi_2 + h.c)$ in the Kähler potential) satisfy the bound $a\lambda \gtrsim 0.1688$. For $\lambda \approx 1$, this bound translates into a constraint on a within the perturbative regime.

Concerning other crucial low-energy predictions with a fixed volume at $\mathscr{V}_o \sim 3.2 \times 10^4$, ensuring a de Sitter minimum, our findings indicate a SUSY scale exceeding 10 TeV. Consequently, the constraint on the reheating temperature is alleviated in this scenario. For a SUSY scale (>10 TeV), we calculate $g_*(T_r) = 106.75$ [262], yielding a reheating temperature of approximately $T_r \sim 10^7$ GeV. These results advance our understanding of the model's implications for both particle physics and cosmology.

Chapter 4

In our current research, we have undertaken a comprehensive examination of the low-energy implications arising from F-theory models with $SU(5) \times U(1)'$ GUT symmetry, embedded within the larger structure of $SU(5) \times SU(5)' \supset SU(5) \times U(1)^4$. This particular gauge symmetry naturally emerges from a single point of E_8 enhancement, closely associated with the maximal geometric singularity found in the elliptic fibration of the internal manifold.

To ensure realistic fermion mass textures and a tree-level top quark Yukawa coupling, we have imposed a Z_2 monodromy group, which acts on the geometric configuration of 7-branes and identifies two out of the four abelian factors stemming from the $SU(5)'$ reduction. The $U(1)'$ symmetry in the resulting effective field theory models is a linear combination of the three remaining abelian symmetries originating from $SU(5)'$. Enforcing anomaly cancellation conditions, we systematically constructed all possible $U(1)'$ combinations and discovered a common feature: the appearance of non-universal Z' couplings to the three families of quarks and leptons.

By introducing fluxes consistent with anomaly cancellation conditions and allowing various neutral singlet-fields to acquire non-zero vacuum expectation values, we derived several effective models, each distinguished by its unique low-energy spectrum. Our focus was primarily on exploring viable classes of models emerging from this framework.

We subsequently delved into predictions regarding flavor-changing currents and other processes mediated by the Z' neutral gauge boson associated with the $U(1)'$ symmetry, expected to break at some low energy scale. Using bounds from ongoing investigations at the LHC and related experiments, we converted these predictions into lower bounds on various parameters within the effective theory, notably including the Z' mass.

Our work represents a comprehensive classification of semi-local effective F-theory constructions that reproduce the MSSM spectrum, both with and without vector-like fields. On the phenomenological side, our emphasis lies in the exploration of models featuring the MSSM fields alongside multiple neutral singlets. We have obtained a total of fifty-four (54) MSSM models and classified them based on their predictions regarding the $U(1)'$ charges of the MSSM matter content. In most instances, the $U(1)'$ coupling exhibits non-universal behavior toward the first two fermion families, and the $K_0 - \overline{K_0}$ oscillation system imposes the most stringent constraint on the Z' mass.

For reasonable values of the $U(1)'$ gauge coupling g', we have established lower bounds on $M_{Z'}$ in the few hundred TeV range, significantly surpassing recent LHC searches. Additionally, we have explored various flavor-violation processes that could be tested in ongoing or future experiments. One notable process is the lepton flavor-violating $\mu \to eee$ decay, with the potential for increasing experimental sensitivity by four orders of magnitude compared to current bounds. Such models may provide valuable insights in the event of a positive experimental outcome. Moreover, even in the absence of a signal, anticipated bounds from $\mu \to eee$ searches will remain compatible with, if not dominant compared to, the current bounds obtained in our models from neutral Kaon oscillation effects.

However, we have also observed that models with non-universal Z' couplings solely to the MSSM spectrum are unable to explain the recently observed LHCb B-meson anomalies. Nevertheless, our classification encompasses a class of models featuring vector-like families with non-trivial Z'-couplings that can account for these effects. These models exhibit a universal nature of the Z' couplings to the first two families, with negligible contributions to $K_0 - \overline{K_0}$ oscillations. Their distinguishing feature lies in the $U(1)'$ charges of the vector-like fields, which differ from those of the first two generations, leading to non-trivial mixing effects. As an illustrative example, we briefly describe such a model, which includes a complete family of vector-like fields capable of explaining the observed LHCb B-meson anomalies through the mixing of these additional fermions with the three generations of the SM.

Chapter 5

In this chapter, we have built upon our prior research on F-theory motivated models, extending our exploration to encompass a comprehensive scan of all potential $SU(5) \times U(1)'$ semi-local constructions that predict a full family of vector-like exotic particles. Our approach leverages $U(1)'$ hypercharge flux to facilitate the symmetry breaking of the non-abelian sector, coupled with a Z_2 monodromy mechanism ensuring the presence of a tree-level top Yukawa coupling.

Moreover, we've imposed stringent phenomenological constraints on the various flux parameters, a crucial step in achieving a model that predicts precisely three chiral generations alongside a complete family of vector-like quarks and leptons. By rigorously enforcing anomaly cancellation requirements, we've unveiled a fascinating result: the existence of 192 distinct models where the $U(1)'$ charges are universal for the MSSM families but non-universal for the vector-like states.

These 192 models naturally fall into five well-defined classes, denoted as $A, B, C, D, andE$ in our analysis. For each class, we've presented one illustrative model, providing a detailed exploration of their fundamental characteristics. This exploration encompasses computations of superpotential terms and the construction of fermion mass matrices.

Notably, we've delved into the potential of class A models to explain the observed R_K anomalies. We've showcased how these models achieve this feat through the mixing of vector-like states while simultaneously avoiding violations of other flavor observables. This is made possible by the universal nature of the three Standard Model families within this class.

Furthermore, we've discussed the presence of R-parity violating (RPV) couplings in these models and their potential contributions to observed experimental deviations from Standard Model predictions. It's worth noting that due to the inherent flux restrictions and symmetries of the theory, only a limited set of possible RPV terms appear in these models. This selective inclusion allows us to interpret deviation effects while sidestepping significant contributions to potentially problematic proton decay effects.

In sum, our research represents a comprehensive exploration of F-theory models within the $SU(5) \times U(1)'$ framework, offering a valuable and structured perspective on potential extensions to the Standard Model and their implications for particle physics phenomenology.

Conclusions

We have embarked on an extensive journey through the fascinating realm of unified theoretical frameworks, both within the realm of particle physics and cosmology. We began our exploration by delving into Grand Unified Models with $SO(10)$ gauge symmetry, highlighting their intriguing features and their extensive study in both field theory and string theory contexts. The development of a simplified $SO(10)$ model, featuring lower-dimensional matter and Higgs fields, served as a foundation for our analysis. Through this model, we unveiled profound implications, both in the realm of particle physics and cosmology.

Our examination of the $SO(10)$ model revealed the intricate process of spontaneous symmetry breaking within the $SO(10)$ gauge group, culminating in the emergence of the Standard Model. We explored the role of Higgs fields, specifically those residing in $\underline{16}_H + \overline{16}_H$ and two Adjoints $\underline{45}_H, \underline{45'}_H$, and their vital contributions to this symmetry-breaking mechanism. Additionally, we uncovered how a pair of tenplets $\underline{10}_h + \underline{10}'_h$ played a pivotal role in conferring masses to fermions and generating the CKM mixing, ultimately leading to the realization of the minimal supersymmetric standard model in the low-energy effective theory.

Our foray into cosmological implications guided us through the complexities of primordial inflation. Employing the canonical form of the Kähler potential, we derived the effective scalar potential governing the dynamics of inflation. The compatibility of our findings with observed data showcased the richness of our model's predictions.

Expanding our horizons, we delved into a broader perspective, where the effective potential emerged as a function of an $SO(10)$ singlet S and the Higgs field ϕ. This perspective led us to scenarios where inflation was driven by specific fields, prompting a transition from $SO(10)$ to $SU(5)$ and contributing to the generation of right-handed neutrino masses through non-renormalizable terms. Furthermore, we scrutinized the cosmological implications of our model, addressing critical aspects such as reheating and the observed baryon asymmetry, all while adhering to constraints such as those imposed by gravitinos.

In a broader context, our journey continued into the realm of string theory, where we explored the cosmological and low-energy supersymmetry implications of effective models originating from the intricate geometry of intersecting D7-brane stacks. Our analysis accounted for perturbative string loop corrections, D-terms, and the presence of ordinary matter contributions in the Kähler potential. We investigated the role of Higgs fields in shaping low-energy phenomenology and cosmological observables, including the predictions of the standard hybrid inflationary scenario.

As we ventured further, the decay of Kähler moduli, dark radiation production, and constraints on the reheating temperature became focal points of our inquiry. Theoretical predictions and bounds from ongoing experiments began to shape our understanding of these complex models.

Transitioning to F-theory models, we embarked on a comprehensive examination of the implications stemming from $SU(5) \times U(1)'$ GUT symmetry embedded within $SU(5) \times SU(5)' \supset SU(5) \times U(1)^4$. We uncovered the natural emergence of this gauge symmetry from geometric singularities, underscoring the profound interplay between mathematics and physics.

Our investigation led to the imposition of a Z_2 monodromy group, which played a pivotal role in achieving realistic fermion mass textures and a tree-level top quark Yukawa coupling. Anomaly cancellation conditions guided us in constructing various $U(1)'$ combinations, revealing the appearance of non-universal Z' couplings to quarks and leptons. We introduced fluxes and neutral singlet fields, which, together, shaped an array of effective models, each distinguished by its low-energy spectrum.

Our focus extended to the predictions regarding flavor-changing currents and other processes mediated by the Z' gauge boson. Bounds from ongoing experiments provided crucial insights, constraining various parameters and paving the way for future discoveries.

In the final phase of our journey, we embarked on an exhaustive scan of $SU(5) \times U(1)'$ semi-local constructions, predicting complete families of vector-like exotics. The interplay between $U(1)'$ hypercharge flux and a Z_2 monodromy mechanism was at the heart of our approach. Phenomenological constraints and anomaly cancellation criteria guided us in selecting models that exhibited precisely three chiral generations and a full complement of vector-like quarks and leptons.

Our analysis unveiled 192 distinct models falling into five distinct classes, each characterized by its $SU(5) \times U(1)'$ properties. For each class, we presented illustrative models, diving deep into their fundamental properties, superpotential terms, and fermion mass matrices. Class A models, in particular, held the potential to explain the observed R_K anomalies through the mixing of vector-like states, all while maintaining consistency with other flavor observables.

Intriguingly, we explored the presence of R-parity violating (RPV) couplings within these models and their potential impact on experimental deviations from Standard Model predictions. The selective inclusion of RPV terms, guided by the theory's inherent symmetries and constraints, offered a path to interpret deviation effects while avoiding contributions to proton decay.

In closing, our extensive journey through these unified models, string theory, and F-theory constructions has illuminated a diverse landscape of theoretical possibilities and their consequences. The intricate interplay between mathematics and physics has been a constant theme, and the pursuit of answers to fundamental questions in particle physics and cosmology continues unabated. Our exploration serves as a testament to the rich tapestry of ideas and concepts that drive the forefront of scientific research, and it is our hope that this work has contributed meaningfully to this ongoing intellectual journey.

A Cosmic Odyssey Complete

In closing, our cosmic odyssey through diverse GUT models and string theory-inspired frameworks has expanded our understanding of the fundamental forces that shape the universe. The symphonies of particle physics and cosmology resonate deeply within these cosmic narratives, offering pathways to uncharted realms and the promise of groundbreaking discoveries. As we conclude this cosmic odyssey, we stand on the precipice of new frontiers, ready to explore the mysteries that the universe has yet to reveal.

This concluding chapter synthesizes the essence of our journey, highlighting the pivotal discoveries and cosmic revelations made along the way. Each model we've explored has contributed to our understanding of the cosmos, and together, they form a rich tapestry of knowledge that propels us into a future filled with promise and discovery.

Appendices

Appendix A

Inflation

A.1 Energy-momentum Tensor

In the realm of General Relativity, a crucial aspect involves accurately portraying the uniform distribution of matter and energy on a large scale. This becomes clearer when we delve into the concept of the scale factor, denoted as $a(t)$, which governs the universe's evolution over time. It's worth noting that the scale factor is the sole component in the metric that depends on time and is derived from Einstein's equations. Consequently, the scale factor is intricately linked to the distribution of energy within the universe.

This representation can be achieved by assuming that all the matter within the universe behaves akin to particles within a perfect fluid. The initial formulation of this hypothesis dates back to 1923 when Herman Weyl was pioneering research in this field. In his investigations, he embraced the foundational tenets of the Cosmological Principle and introduced a perfect fluid characterized by its matter-energy density ρ and pressure p. This fluid was envisioned to move while preserving its uniformity. To make this concept applicable, it was necessary for the relative motions between particles to be negligible, and the fluid's motion could be characterized by a single velocity described by the four-vector v^μ. Interestingly, even though galaxies do not precisely conform to this model, the deviations from it proved to be quite minor.

In General Relativity, the distribution of matter and energy is described by a tensor. The simplest form of this tensor, which upholds the uniform motion of a perfect fluid within a curved gravitational framework, is as follows:

$$T_{\mu\nu} = (\rho + p)v_\mu v_\nu - p g_{\mu\nu}. \tag{A.1}$$

This expression finds extensive application in the field of Cosmology and is commonly referred to as the energy-momentum tensor. We can simplify this expression further by assuming that there is no preferred reference point within the universe. Consequently, we select a reference point situated on a particle within the fluid. This choice effectively immobilizes not only the particle but also the entire fluid in a spatial sense. Moreover, under this condition, only the time component of the four-vector velocity remains non-zero, and with a unit normalization, it adopts the following form: $v^\mu = (1, 0, 0, 0)$. Consequently, the energy-momentum tensor can be expressed as follows:

$$T_{\mu\nu} = (\rho + p)g_{\mu\rho}v^\rho g_{\nu\sigma}v^\sigma - p g_{\mu\nu} = (\rho + p)g_{\mu 0}g_{\nu 0} - p g_{\mu\nu}. \tag{A.2}$$

We can re-write the energy-momentum tensor in the form of a 4×4 matrix using the metric tensor :

$$T_{\mu\nu} = \begin{pmatrix} \rho & 0 & 0 & 0 \\ 0 & -g_{11}p & 0 & 0 \\ 0 & 0 & -g_{22}p & 0 \\ 0 & 0 & 0 & -g_{33}p \end{pmatrix} \tag{A.3}$$

The conservation of energy, momentum, and matter holds significant significance in theory. As anticipated, a conservation law, such as the conservation of energy, typically takes the following form:

$$\frac{\partial T_{\mu\nu}}{\partial x^{\nu}} = 0. \tag{A.4}$$

This concept is accurate in the context of flat space-time, but in the framework of General Relativity, which involves the study of curved space-time, a distinction arises. In general, when differentiating a vector in a non-flat space, it yields two components. One component arises from the vector's shift, and the other from the change in the coordinate system. Therefore, we introduce the concept of covariant derivative, which possesses this specific property, and we can express the conservation of energy as follows:

$$T^{\mu\nu}_{\ \ ;\nu} = 0. \tag{A.5}$$

We can write the expression (A.5) in detail and take :

$$\partial_\nu T^{\mu\nu} + \Gamma^{\mu}{}_{\alpha\mu} T^{\alpha\nu} + \Gamma^{\nu}{}_{\alpha\mu} T^{\alpha\mu} = 0. \tag{A.6}$$

Here, it's important to emphasize that Equation (A.6) does not represent a conservation law. We can refer to it as a form of local conservation, but it doesn't hold universally. Locally, nearly all the Christoffel symbols are close to zero, allowing us to approximate it as a conservation law. However, in the context of General Relativity, conservation doesn't hold as a general rule.

A.1.1 Riemann Tensor

The second covariant derivative of a scalar can be written straightly as :

$$\phi_{;\mu\nu} \equiv (\phi_{;\mu})_{;\nu} = \partial_\nu \phi_{;\mu} - \Gamma^{\alpha}_{\ \nu\mu} \phi_{;\alpha} = \partial_\mu \partial_\nu \phi - \Gamma^{\alpha}_{\ \nu\mu} \partial_\alpha \phi. \tag{A.7}$$

The presence of the $\mathbf{\Gamma}$ term arises because the first derivative is a vector. When dealing with the second covariant derivative of a scalar, it exhibits symmetry when each term to the right of Equation (A.7) remains unchanged, alternating between μ and ν. However, when calculating the second covariant derivative of a vector, the situation becomes more complex : $\alpha_{\mu;\rho\sigma} \equiv (\alpha_{\mu;\rho})_{;\sigma} =$

$$= \partial_\sigma(\partial_\rho \alpha_\mu - \Gamma^{\lambda}_{\ \rho\mu}\alpha_\lambda) - \Gamma^{\beta}_{\ \sigma\rho}(\partial_\beta \alpha_\mu - \Gamma^{\lambda}_{\ \beta\mu}\alpha_\lambda) - \Gamma^{\beta}_{\ \sigma\mu}(\partial_\rho \alpha_\beta - \Gamma^{\lambda}_{\ \rho\beta}\alpha_\lambda)$$

$$= (\text{symmetric terms in } \rho \text{ and } \sigma) - \alpha_\lambda \partial_\sigma \Gamma^{\lambda}_{\ \rho\mu} + \Gamma^{\beta}_{\ \sigma\mu}\Gamma^{\lambda}_{\ \rho\beta}\alpha_\lambda.$$

In this scenario, the second covariant derivative need not be symmetric. The antisymmetric component arises from the difference between the two terms :

$$\alpha_{\mu;\rho\sigma} - \alpha_{\mu;\sigma\rho} = \alpha_\lambda R^{\lambda}_{\ \mu\rho\sigma}, \tag{A.8}$$

in which as we can see the **Riemann tensor** is involved :

$$R^{\lambda}_{\ \mu\rho\sigma} \equiv \partial_\rho \Gamma^{\lambda}_{\ \sigma\mu} - \partial_\sigma \Gamma^{\lambda}_{\ \rho\mu} + \Gamma^{\lambda}_{\ \rho\beta}\Gamma^{\beta}_{\ \sigma\mu} - \Gamma^{\lambda}_{\ \sigma\beta}\Gamma^{\beta}_{\ \rho\mu}. \tag{A.9}$$

The Riemann tensor requires careful attention. In flat space, the second covariant derivative must exhibit symmetry. Symmetry is an invariant characteristic that persists even when the coordinate system is altered. Therefore, whenever the Riemann tensor has a non-zero value, it signifies that space is not flat, and some information about its curvature is encoded within the non-zero Riemann tensor. Consequently, the Riemann tensor provides insights into the inherent curvature of space. Any additional curvatures resulting from the embedding of the system into a higher-dimensional space are considered and treated as extraneous and are disregarded by the Riemann tensor.

A.1.2 Ricci Tensor and Ricci Scalar

The contraction of Riemann tensor eq.(A.9) leads to a tensor of second order which is called **Ricci Tensor** :

$$R_{\alpha\beta} = R^{\lambda}_{\alpha\lambda\beta} = g^{\lambda\mu} R_{\lambda\alpha\mu\beta}. \tag{A.10}$$

Re-writing it in a more analytical form we take :

$$R_{\alpha\beta} = \partial_\mu \Gamma^{\mu}_{\ \alpha\beta} - \partial_\beta \Gamma^{\mu}_{\ \alpha\mu} + \Gamma^{\mu}_{\ \alpha\beta}\Gamma^{\nu}_{\ \nu\mu} - \Gamma^{\mu}_{\ \alpha\nu}\Gamma^{\nu}_{\ \beta\mu}. \tag{A.11}$$

Now if we apply one more contraction in the Ricci tensor, we take the **Ricci Scalar** :

$$R = R^{\alpha}_{\ \alpha} = g^{\alpha\beta} R_{\alpha\beta} = g^{\alpha\beta} g^{\mu\nu} R_{\mu\alpha\nu\beta}. \tag{A.12}$$

Einstein aimed to establish a connection between the geometry of space-time and the distribution of matter and energy within it. The equation he sought needed to involve tensors of the same order to maintain its invariance under arbitrary transformations, aligning with the expectations for any fundamental natural law.

Drawing inspiration from Newton's theory, which his theory should naturally reduce to in the limit of a very weak gravitational field, and also taking into account Poisson's law, represented as $\nabla^2\Phi = 4\pi G\rho$, Einstein formulated the fundamental concept of the **Einstein Tensor** :

$$G_{\mu\nu} = R_{\mu\nu} - \frac{1}{2} g_{\mu\nu} R. \tag{A.13}$$

Furthermore, he demonstrated that this tensor obeys an equation identical to the one satisfied by the energy-momentum tensor, namely $G^{\mu\nu}_{\ \ ;\nu} = 0$. Since this equation is a first-order differential equation, the two quantities are directly related to each other, ultimately leading to the final equation :

$$G_{\mu\nu} = R_{\mu\nu} - \frac{1}{2} g_{\mu\nu} R = 8\pi G T_{\mu\nu}. \tag{A.14}$$

These are the so-called Einstein's equations of the gravitational field.

A.2 Robertson-Walker space-time

The space-time of Robertson-Walker describes generally a homogeneous and isotropic universe in which the invariant interval has the form :

$$ds^2 = c^2dt^2 - \alpha^2(t)\left[\frac{dr^2}{1-kr^2} + r^2(d\theta^2 + sin^2\theta d\varphi^2)\right]. \tag{A.15}$$

The unknown time-dependent factor α(t) in the expression is referred to as the "scale factor" of the universe, and its precise form is derived from Einstein's equations. The parameter k plays a crucial role in determining the geometry of three-dimensional space. It can assume one of three possible values: $k = 0, -1, +1$, corresponding to three distinct types of three-dimensional space.

When $k = 0$, we are dealing with a flat space, and the measurement of distances within this space is described as follows :

$$ds^2 = dr^2 + r^2d\theta^2 + r^2sin^2\theta d\varphi^2. \tag{A.16}$$

The spatial coordinates take values $0 < r < \infty$, $0 < \theta < \pi$ and $0 < \varphi < 2\pi$, and the three-dimensional space is infinite.
For the case of $k = +1$, the three-dimensional space is characterized by positive curvature. Implementing a new coordinate $r = sin\chi$ the element length takes the form :

$$ds^2 = d\chi^2 + sin^2\chi(d\theta^2 + sin^2\theta d\varphi^2). \tag{A.17}$$

The spatial coordinate take values $0 < \chi$, $\theta < \pi$ and $0 < \varphi < 2\pi$, the three-dimensional space is finite and is called " closed ".
Finally, for the case of $k = -1$ space is characterized by negative curvature. Implementing a new coordinate $r = sinh\chi$ the element length takes the form :

$$ds^2 = d\chi^2 + sinh^2\chi(d\theta^2 + sin^2\theta d\varphi^2). \tag{A.18}$$

The spatial coordinates take values $0 < \chi < \infty$, $0 < \theta < \pi$ and $0 < \varphi < 2\pi$, the tree-dimensional space infinite and is called " open ".

A.3 The expanding universe-Friedmann equations

In this section, we will explore the scenario of an evolving universe over time. By beginning with Einstein's equations, we will derive the well-known **Friedmann Equations**, which govern the dynamic evolution of the universe through the solution for the scale factor α(t. We will specifically refer to the simple case of Robertson-Walker space-time, as the procedure remains the same in general.

To start, we will compute the nonzero elements of the metric tensor $g_{\mu\nu}$

$$g_{00}=1, \quad g_{11}=-\frac{\alpha^2}{1-kr^2}, \quad g_{22}=-\alpha^2r^2, \quad g_{33}=-\alpha^2r^2sin^2\theta, \tag{A.19}$$

as well as the inverse, $g^{\mu\nu}$:

$$g^{00}=1, \quad g^{11}=-\frac{1-kr^2}{\alpha^2}, \quad g^{22}=-\frac{1}{\alpha^2r^2}, \quad g^{33}=-\frac{1}{\alpha^2r^2sin^2\theta}. \tag{A.20}$$

Having calculated the elements of the metric tensor we are in the position to calculate the Cristoffel symbols, so we take :

$$\begin{gathered}\Gamma^0{}_{11}=\tfrac{\alpha\dot{\alpha}}{1-kr^2}, \quad \Gamma^0{}_{22}=\alpha\dot{\alpha}r^2, \quad \Gamma^0{}_{33}=\alpha\dot{\alpha}r^2sin^2\theta, \\ \Gamma^1{}_{11}=\tfrac{kr}{1-kr^2}, \quad \Gamma^1{}_{22}=-r(1-kr^2), \quad \Gamma^1{}_{33}=-r(1-kr^2)sin^2\theta, \\ \Gamma^1{}_{01}=\Gamma^2{}_{02}=\Gamma^3{}_{03}=\tfrac{\dot{\alpha}}{\alpha}, \quad \Gamma^2{}_{12}=\Gamma^3{}_{13}=\tfrac{1}{r}, \quad \Gamma^2{}_{33}=-sin\theta cos\theta, \quad \Gamma^3{}_{23}=\tfrac{cos\theta}{sin\theta}.\end{gathered} \tag{A.21}$$

Moreover, we calculate the non zero components of the Ricci tensor :

$$\begin{gathered}R_{00}=-3\tfrac{\ddot{\alpha}}{\alpha}, \quad R_{11}=\tfrac{\alpha\ddot{\alpha}+2\dot{\alpha}^2+2k}{1-kr^2}, \\ R_{22}=r^2(\alpha\ddot{\alpha}+2\dot{\alpha}^2+2k), \quad R_{33}=r^2(\alpha\ddot{\alpha}+2\dot{\alpha}^2+2k)sin^2\theta.\end{gathered} \tag{A.22}$$

and finally, we take the expression for the Ricci scalar :

$$R=g^{\mu\nu}R_{\mu\nu}=-6\left(\frac{\ddot{\alpha}}{\alpha}+\frac{\dot{\alpha}^2}{\alpha^2}+\frac{k}{\alpha^2}\right). \tag{A.23}$$

Now, we can utilize the findings we've discussed so far to compute the nonzero components of Einstein's equations based on the equation (A.14). Beginning with the (00)-component, we obtain :

$$\frac{\dot{\alpha}^2}{\alpha^2}+\frac{k}{\alpha^2}=\frac{8\pi G}{3}\rho, \tag{A.24}$$

while all the spatial components lead to the same equation :

$$\frac{2\ddot{\alpha}}{\alpha}+\frac{\dot{\alpha}^2}{\alpha^2}+\frac{k}{\alpha^2}=-8\pi Gp. \tag{A.25}$$

These two equations are the Friedmann equations of the universe. We can re-write the second equation substituting the first in it to eliminate the $\dot{\alpha}^2/\alpha^2$ term and take :

$$\frac{\ddot{\alpha}}{\alpha} = -\frac{4\pi G}{3}(\rho + 3p). \tag{A.26}$$

This is referred to as the **Raychaudhuri equation** or the acceleration equation. When examining these two equations, a challenge in solving them becomes apparent. We indeed require one more equation to resolve this issue. This problem can be addressed by incorporating the fluid equation, which can be readily derived from the energy conservation equation by setting $\mu = 0$ in equation (A.5) :

$$T^{0\nu}_{\ ;\nu} = 0 \Rightarrow$$

$$T^{0\nu}_{\ ;\nu} = \Gamma^0_{\ 00}T^{00} + \Gamma^0_{\ 11}T^{11} + \Gamma^0_{\ 22}T^{22} + \Gamma^0_{\ 33}T^{33} + T^{00}(\Gamma^1_{01} + \Gamma^2_{02} + \Gamma^3_{03})$$

$$\Rightarrow ... \Rightarrow$$

$$\dot{\rho} + 3\tfrac{\dot{\alpha}}{\alpha}(\rho + p) = 0. \tag{A.27}$$

Upon closer examination, it becomes evident that these three equations are not mutually independent. To resolve this issue, we can introduce one final equation that establishes a connection between the energy density and the pressure of the perfect fluid. This equation is known as the equation of state :

$$p = w\rho. \tag{A.28}$$

It's worth noting that in general, the proportionality factor, denoted as ω, can be a function of time. Utilizing the previous equation, we can express the conservation of energy in the following manner: :

$$\frac{\dot{\rho}}{\rho} = -3(1 + w)\frac{\dot{\alpha}}{\alpha}, \tag{A.29}$$

which lead to the solution :

$$\rho(t) = \frac{\rho_0}{\alpha^{3(1+w)}}, \tag{A.30}$$

where ρ_0 is an integration constant. Continuing a little more our thinking, we introduce the **Hubble parameter** :

$$H = \frac{\dot{a}}{a} \tag{A.31}$$

which determines the expansion rate of the universe. Also, we take the time derivative of the Hubble parameter and write it as the quantity ε :

$$\epsilon = -\frac{\dot{H}}{H^2} \tag{A.32}$$

We can deduce certain characteristics from this equation. If $\epsilon < 1$, it signifies that the universe's expansion rate is accelerating. Conversely, if $\epsilon > 1$, then the expansion rate diminishes, resulting in a decelerating universe expansion. Additionally, we can express Einstein's equations (A.24) and (A.25) in terms of H^2 by utilizing equation (A.32) and assuming $k = 0$ (representing flat space): :

$$H^2 = \frac{8\pi G}{3}\rho \tag{A.33}$$

and

$$(1-\epsilon)H^2 = -\frac{4\pi G}{3}(\rho + 3p) \tag{A.34}$$

Now, we substitute eq.(A.30) in eq.(A.33) and we take :

$$\tfrac{\dot{a}^2}{a^2} = \tfrac{8\pi G}{3}\tfrac{\rho_0}{a^{3(1+w)}} \Rightarrow \tfrac{\dot{a}^2}{a^2}a^{3(1+w)} = \tfrac{8\pi G}{3}\rho_0 \Rightarrow$$

$$\tfrac{\dot{a}}{a}a^{\frac{3}{2}(1+w)} = \sqrt{\tfrac{8\pi G}{3}\rho_0} \Rightarrow \tfrac{da}{dt}\tfrac{1}{a}a^{\frac{3}{2}(1+w)} = \sqrt{\tfrac{8\pi G}{3}\rho_0} \Rightarrow$$

$$\tfrac{da}{a}a^{\frac{3}{2}(1+w)} = \sqrt{\tfrac{8\pi G}{3}\rho_0}dt$$

After integration, we obtain :

$$a^{\frac{3}{2}(1+w)} = \tfrac{3}{2}(1+w)\sqrt{\tfrac{8\pi G}{3}\rho_0}t$$

So

$$a \sim t^{\frac{2}{3(1+w)}} \tag{A.35}$$

If we plug this equation into eq.(A.32), we see that ϵ is a constant :

$$\epsilon = \tfrac{3}{2}(1+w) \tag{A.36}$$

We can derive the following conclusions from this equation: In the case of a universe dominated by radiation ($w = \frac{1}{3}$), $\epsilon = 2$.
In the case of a universe dominated by matter ($w = 0$), $\epsilon = \frac{3}{2}$.
In both of these scenarios, the expansion of the universe is decelerating. For a more general case, such as an inflationary universe, where $\omega \simeq -1$ and $\epsilon \ll 1$, we can solve eq.(A.32) for $H(t)$ and $a(t)$ to obtain:

$$\boxed{H(t) = \frac{H_0}{1 + \epsilon H_0 t}} \quad \text{and} \quad \boxed{a(t) = (1 + \epsilon H_0 t)^{\frac{1}{\epsilon}}} \tag{A.37}$$

where $a(t = 0)$ is chosen to be $a_0 = 1$ and $H_0 = H(t = 0)$.

Now, let's examine the form of these equations when we work with conformal time. To make this transition, we can substitute $dt = a(\eta)d\eta$ into our metric ($ds^2 = g_{\mu\nu}dx^\mu dx^\nu$). This gives us $ds^2 = a^2(\eta)\eta_{\mu\nu}dx^\mu dx^\nu$, where η is the conformal time, and $\eta_{\mu\nu} = (-1, 1, 1, 1)$ represents the Minkowski metric. Using these transformations, we can easily derive the solutions for the scale factor and the Hubble rate in conformal time while considering a constant ϵ. Keeping in mind the relations $\dot{a} = \frac{a'}{a}$, $H(\eta) = \frac{a'}{a^2}$, and $H = \frac{H'}{a}$, where the prime denotes differentiation with respect to η, we obtain the following differential equation for $a(\eta)$:

$$\epsilon = -\frac{a''a}{(a')^2} + 2 \tag{A.38}$$

By following the same procedure as before and applying the boundary conditions $a(\eta_0) = 1$ and $H(\eta_0) = H_0$, we arrive at the following equations :

$$\boxed{a(\eta) = \frac{1}{[-(1-\epsilon)H_0\eta]^{\frac{1}{1-\epsilon}}}}, \quad \boxed{H(\eta) = \frac{H_0}{[-(1-\epsilon)H_0\eta]^{\frac{-\epsilon}{1-\epsilon}}}} \tag{A.39}$$

We can observe that the universe is expanding either when $\epsilon < 1$ and $-\infty < \eta < 0$ or when $\epsilon > 1$ and $0 < \eta < \infty$, with both a and H being positive. Additionally, when $\epsilon = 0$, the equations simplify to $H(\eta) = H_0$ and $a(\eta) = -\frac{1}{H_0\eta}$, representing the conformal scale factor in de Sitter space. Finally, we can utilize the following relation :

$$H(\eta)a(\eta) = -\frac{1}{(1-\epsilon)\eta}, \tag{A.40}$$

to write the expression :

$$a(\eta) = -\frac{1}{H\eta(1-\epsilon)} \tag{A.41}$$

regarding the scale factor. It's worth mentioning that when ϵ is significantly smaller than 1, we find ourselves in a scenario known as quasi de Sitter space. Furthermore, if we approach the limit of $\epsilon \to 0$, we transition into de Sitter space.

A.4 Equations from Action

In this section, we will derive Einstein's filed equations from an action. First, we take the Einstein-Hilbert action :

$$S_{EH} = \int d^D x \sqrt{-g} \frac{R}{16\pi G_N}, \tag{A.42}$$

where R is the Ricci scalar, and g=det($g_{\mu\nu}$).Let's now perform the variation of this action with respect to the metric $g_{\mu\nu}$. To do this, we need to carry out some calculations. First, let's consider the quantity δg, which can be expressed as :

$$\boxed{\delta g = \delta(det(g^{\mu\nu})) = g g^{\mu\nu} \delta g_{\mu\nu}} \tag{A.43}$$

and

$$\delta\sqrt{-g} = -\frac{1}{2\sqrt{-g}}\delta g = \frac{\sqrt{-g}}{2\cancel{g}}\cancel{g} g^{\mu\nu}\delta g_{\mu\nu} \Rightarrow$$

$$\boxed{\delta\sqrt{-g} = \frac{1}{2}\sqrt{-g} g^{\mu\nu}\delta g_{\mu\nu}} \tag{A.44}$$

We know that $g_{\mu\kappa}g^{\kappa\nu} = \delta^{\nu}{}_{\mu}$ so :

$$(\delta g_{\mu\kappa})g^{\kappa\nu} + g_{\mu\kappa}(\delta g^{\kappa\nu}) = 0 \Rightarrow (\delta g_{\mu\nu})g^{\kappa\nu} = -g_{\mu\kappa}(\delta g^{\kappa\nu}) \Rightarrow$$

$$\delta g^{\kappa\nu} = -g^{\mu\kappa}(\delta g_{\mu\nu})g^{\kappa\nu} \Rightarrow$$

$$\boxed{\delta g^{\mu\nu} = -g^{\mu\alpha}(\delta g_{\alpha\beta})g^{\beta\nu}} \tag{A.43}$$

and :

$$g_{\mu\nu}\delta g^{\mu\nu} = -g_{\mu\nu}g^{\mu\alpha}(\delta g_{\alpha\beta})g^{\beta\nu} = -\delta^{\alpha}{}_{\nu}(\delta g_{\alpha\beta})g^{\beta\nu} = -(\delta g_{\beta\nu})g^{\beta\nu} \Rightarrow$$

$$\boxed{g_{\mu\nu}\delta g^{\mu\nu} = -g^{\mu\nu}\delta g_{\mu\nu}} \tag{A.44}$$

So equation (A.44) from (A.44) becomes :

$$\boxed{\delta\sqrt{-g} = \frac{1}{2}\sqrt{-g}(g^{\mu\nu}\delta g_{\mu\nu}) = -\frac{1}{2}\sqrt{-g}(g_{\mu\nu}\delta g^{\mu\nu})} \tag{A.45}$$

Now for our variations, we will need the following relations :

$$\boxed{\nabla_l A_{ik} = A_{ik,l} - A_{mk}\Gamma^m_{il} - A_{im}\Gamma^m_{kl}}$$

$$\boxed{\nabla_l A^{ik} = A^{ik}_{,l} + \Gamma^i{}_{ml}A^{mk} + \Gamma^k{}_{ml}A^{im}}$$

So, from the above relations, we obtain :

$$\boxed{\nabla_\lambda(\delta\Gamma^\rho{}_{\nu\mu}) = \partial_\lambda\delta\Gamma^\rho{}_{\nu\mu} + \Gamma^\rho{}_{\sigma\lambda}\Gamma^\sigma{}_{\nu\mu} - \Gamma^\sigma{}_{\nu\lambda}\delta\Gamma^\rho{}_{\sigma\mu} - \Gamma^\sigma{}_{\mu\lambda}\delta\Gamma^\rho{}_{\nu\beta}} \tag{A.46}$$

We have the definition of the Riemann curvature tensor :

$$\boxed{R^\rho{}_{\sigma\mu\nu} = \partial_\mu\Gamma^\rho{}_{\nu\sigma} - \partial_\nu\Gamma^\rho{}_{\mu\sigma} + \Gamma^\rho{}_{\mu\lambda}\Gamma^\lambda{}_{\nu\sigma} - \Gamma^\rho{}_{\nu\lambda}\Gamma^\lambda{}_{\mu\sigma}} \tag{A.47}$$

and from the above equation, we take the variation of the Riemann tensor :

$$\delta R^\rho{}_{\sigma\mu\nu} = \partial_\mu\delta\Gamma^\rho{}_{\nu\sigma} - \partial_\nu\delta\Gamma^\rho{}_{\mu\sigma} + \delta\Gamma^\rho{}_{\mu\lambda}\Gamma^\lambda{}_{\nu\sigma} + \Gamma^\rho{}_{\mu\lambda}\delta\Gamma^\lambda{}_{\nu\sigma} - \delta\Gamma^\rho{}_{\nu\lambda}\Gamma^\lambda{}_{\mu\sigma} - \Gamma^\rho{}_{\nu\lambda}\delta\Gamma^\lambda{}_{\mu\sigma} \tag{A.48}$$

At this point, we calculate the quantities :

$$\nabla_\mu(\delta\Gamma^\rho{}_{\nu\sigma}) = \partial_\mu(\delta\Gamma^\rho{}_{\nu\sigma}) + \Gamma^\rho{}_{\lambda\mu}\delta\Gamma^\lambda{}_{\nu\sigma} - \Gamma^\lambda{}_{\nu\mu}\delta\Gamma^\rho{}_{\lambda\sigma} - \Gamma^\lambda{}_{\sigma\mu}\delta\Gamma^\rho{}_{\nu\lambda} \tag{A.49}$$

and

$$\nabla_\nu(\delta\Gamma^\rho{}_{\mu\sigma}) = \partial_\nu(\delta\Gamma^\rho{}_{\mu\sigma}) + \Gamma^\rho{}_{\lambda\nu}\delta\Gamma^\lambda{}_{\mu\sigma} - \Gamma^\lambda{}_{\mu\nu}\delta\Gamma^\rho{}_{\lambda\sigma} - \Gamma^\lambda{}_{\sigma\nu}\delta\Gamma^\rho{}_{\mu\lambda} \tag{A.50}$$

We take equation (A.49) minus equation (A.50) and we obtain :

$$\partial_\mu(\delta\Gamma^\rho{}_{\nu\sigma}) + \Gamma^\rho{}_{\lambda\mu}\delta\Gamma^\lambda{}_{\nu\sigma} - \cancel{\Gamma^\lambda{}_{\nu\mu}\delta\Gamma^\rho{}_{\lambda\sigma}} - \Gamma^\lambda{}_{\sigma\mu}\delta\Gamma^\rho{}_{\nu\lambda} - \partial_\nu(\delta\Gamma^\rho{}_{\mu\sigma}) - \Gamma^\rho{}_{\lambda\nu}\delta\Gamma^\lambda{}_{\mu\sigma} + \cancel{\Gamma^\lambda{}_{\mu\nu}\delta\Gamma^\rho{}_{\lambda\sigma}} + \Gamma^\lambda{}_{\sigma\nu}\delta\Gamma^\rho{}_{\mu\lambda}$$

This result we can see that it is equal to the $\delta R^\rho{}_{\sigma\mu\nu}$ from equation (A.48), so :

$$\boxed{\delta R^\rho{}_{\sigma\mu\nu} = \nabla_\mu(\delta\Gamma^\rho{}_{\nu\sigma}) - \nabla_\nu(\delta\Gamma^\rho{}_{\mu\sigma})} \tag{A.51}$$

We continue with the variation of the Ricci curvature tensor. To do this we contract two indices of the variation of the Riemann tensor :

$$\delta R_{\mu\nu} = \delta R^\rho{}_{\sigma\rho\nu} = \delta R^\rho{}_{\mu\rho\nu} \Rightarrow$$

and we obtain :

$$\boxed{\delta R_{\mu\nu} = \nabla_\rho(\delta\Gamma^\rho{}_{\nu\mu}) - \nabla_\nu(\delta\Gamma^\rho{}_{\rho\mu})} \tag{A.52}$$

Now we take the variation of the Ricci scalar $R = g^{\mu\nu}R_{\mu\nu}$:

$$\delta R = \delta(g^{\mu\nu}R_{\mu\nu}) = (\delta g^{\mu\nu})R_{\mu\nu} + g^{\mu\nu}\delta R_{\mu\nu} =$$

$$R_{\mu\nu}(\delta g^{\mu\nu}) + g^{\mu\nu}\left[\nabla_\rho(\delta\Gamma^\rho{}_{\nu\mu}) - \nabla_\nu(\delta\Gamma^\rho{}_{\rho\mu})\right] =$$

$$R_{\mu\nu}(\delta g^{\mu\nu}) + \nabla_\rho(g^{\mu\nu}\delta\Gamma^\rho{}_{\nu\mu}) - \nabla_\nu(g^{\mu\nu}\delta\Gamma^\rho{}_{\rho\mu}) =$$

$$R_{\mu\nu}(\delta g^{\mu\nu}) + \nabla_\rho(g^{\mu\nu}\delta\Gamma^\rho{}_{\nu\mu}) - \nabla_\rho(g^{\mu\rho}\delta\Gamma^\nu{}_{\nu\mu}) \Rightarrow$$

$$\boxed{\delta R = R_{\mu\nu}(\delta g^{\mu\nu}) + \nabla_\rho\left[g^{\mu\nu}\delta\Gamma^\rho{}_{\nu\mu} - g^{\mu\rho}\delta\Gamma^\sigma{}_{\sigma\mu}\right]} \tag{A.53}$$

where we used the property : $\nabla_\sigma g^{\mu\nu} = 0$.
For the Christoffel symbols first, we use the equation :

$$\boxed{\nabla_\gamma(\delta_{\alpha\beta}) = \partial_\gamma \delta g_{\alpha\beta} - \Gamma^\sigma{}_{\gamma\alpha}\delta g_{\sigma\beta} - \Gamma^\sigma{}_{\gamma\beta}\delta g_{\alpha\beta}} \tag{A.54}$$

and from the definition of the Christoffel symbols :

$$\boxed{\Gamma^\sigma{}_{\beta\alpha} = \frac{1}{2}g^{\sigma\gamma}\left(\partial_\beta g_{\gamma\alpha} + \partial_\alpha g_{\gamma\beta} - \partial_\gamma g_{\beta\alpha}\right)} \tag{A.55}$$

we take the variation which is :

$$\delta\Gamma^\sigma{}_{\beta\alpha} = \frac{1}{2}(\delta g^{\sigma\gamma})(\partial_\beta g_{\gamma\alpha} + \partial_\alpha g_{\gamma\beta} - \partial_\gamma g_{\beta\alpha}) + \frac{1}{2}g^{\sigma\gamma}\left[\partial_\beta(\delta g_{\gamma\alpha}) + \partial_\alpha(\delta g_{\gamma\beta}) - \partial_\gamma(\delta g_{\beta\alpha})\right] \tag{A.56}$$

We calculate the identities :

$$\boxed{\nabla_\beta(\delta g_{\gamma\alpha}) = \partial_\beta(\delta g_{\gamma\alpha}) - \Gamma^\sigma{}_{\beta\gamma}\delta g_{\sigma\alpha} - \Gamma^\sigma{}_{\beta\alpha}\delta g_{\gamma\beta}} \tag{A.57}$$

$$\boxed{\nabla_\alpha(\delta g_{\gamma\beta}) = \partial_\alpha(\delta g_{\gamma\beta}) - \Gamma^\sigma{}_{\alpha\gamma}\delta g_{\sigma\beta} - \Gamma^\sigma{}_{\alpha\beta}\delta g_{\gamma\sigma}} \tag{A.58}$$

$$\boxed{\nabla_\gamma(\delta g_{\beta\alpha}) = \partial_\gamma(\delta g_{\beta\alpha}) - \Gamma^\sigma{}_{\gamma\beta}\delta g_{\sigma\alpha} - \Gamma^\sigma{}_{\gamma\alpha}\delta g_{\beta\sigma}} \tag{A.59}$$

The second term of equation (A.56) from equations (A.57)-(A.59), becomes :

$$\frac{1}{2}g^{\sigma\gamma}[\nabla_\beta(\delta g_{\gamma\alpha}) + \cancel{\Gamma^\sigma{}_{\beta\gamma}\delta g_{\sigma\alpha}} + \Gamma^\sigma{}_{\beta\alpha}\delta g_{\gamma\beta} + \nabla_\alpha(\delta g_{\gamma\beta}) + \cancel{\Gamma^\sigma{}_{\alpha\gamma}\delta g_{\sigma\beta}} +$$

$$\Gamma^\sigma{}_{\alpha\beta}\delta g_{\gamma\sigma} - \nabla_\gamma(\delta g_{\beta\alpha}) - \cancel{\Gamma^\sigma{}_{\gamma\beta}\delta g_{\sigma\alpha}} - \cancel{\Gamma^\sigma{}_{\gamma\alpha}\delta g_{\beta\sigma}}] =$$

$$= \frac{1}{2}g^{\sigma\gamma}[\nabla_\beta(\delta g_{\gamma\alpha}) + \nabla_\alpha(\delta g_{\gamma\beta}) - \nabla_\gamma(\delta g_{\beta\alpha}) + 2\Gamma^\sigma{}_{\alpha\beta}\delta g_{\gamma\sigma}] =$$

$$= \frac{1}{2}g^{\sigma\gamma}[\nabla_\beta(\delta g_{\gamma\alpha}) + \nabla_\alpha(\delta g_{\gamma\beta}) - \nabla_\gamma(\delta g_{\beta\alpha})] + g^{\sigma\gamma}\Gamma^\sigma_{\alpha\beta}\delta g_{\gamma\sigma}$$

Eventually equation (A.56) becomes :

$$\delta\Gamma^{\sigma}{}_{\beta\alpha} = \frac{1}{\cancel{2}}(\delta g^{\mu\gamma})\cancel{2}g_{\mu\gamma}\Gamma^{\mu}{}_{\beta\alpha} + g^{\sigma\gamma}(\delta g_{\gamma\beta})\Gamma^{\sigma}{}_{\alpha\beta} + \frac{1}{2}g^{\sigma\gamma}[\nabla_{\beta}(\delta g_{\gamma\alpha}) + \nabla_{\alpha}(\delta g_{\gamma\beta}) - \nabla_{\gamma}(\delta g_{\beta\alpha})] \Rightarrow$$

$$\delta\Gamma^{\sigma}{}_{\beta\alpha} = (\delta g^{\mu\nu})g_{\mu\nu}\Gamma^{\mu}{}_{\beta\alpha} + g^{\sigma\gamma}(-g_{\gamma\mu}g_{\nu\sigma}\delta g^{\mu\nu})\Gamma^{\sigma}{}_{\alpha\beta} + \frac{1}{2}g^{\sigma\gamma}[\nabla_{\beta}(\delta g_{\gamma\alpha}) + \nabla_{\alpha}(\delta g_{\gamma\beta}) - \nabla_{\gamma}(\delta g_{\beta\alpha})] =$$

$$= (\delta g^{\mu\nu})g_{\mu\nu}\Gamma^{\mu}{}_{\beta\alpha} - \delta^{\sigma}_{\mu}g_{\nu\sigma}(\delta g^{\mu\nu}) + \frac{1}{2}g^{\sigma\gamma}[\nabla_{\beta}(\delta g_{\gamma\alpha}) + \nabla_{\alpha}(\delta g_{\gamma\beta}) - \nabla_{\gamma}(\delta g_{\beta\alpha})] =$$

$$= \cancel{(\delta g^{\mu\nu})g_{\mu\nu}\Gamma^{\mu}{}_{\beta\alpha}} - \cancel{g_{\mu\nu}(\delta g^{\mu\nu})\Gamma^{\mu}{}_{\alpha\beta}} + \frac{1}{2}g^{\sigma\gamma}[\nabla_{\beta}(\delta g_{\gamma\alpha}) + \nabla_{\alpha}(\delta g_{\gamma\beta}) - \nabla_{\gamma}(\delta g_{\beta\alpha})] \Rightarrow$$

$$\boxed{\delta\Gamma^{\sigma}{}_{\beta\alpha} = \frac{1}{2}g^{\sigma\gamma}[\nabla_{\beta}(\delta g_{\gamma\alpha}) + \nabla_{\alpha}(\delta g_{\gamma\beta}) - \nabla_{\gamma}(\delta g_{\beta\alpha})]} \tag{A.60}$$

Furthermore, easily we can show that :

$$\delta\Gamma^{\gamma}{}_{\alpha\gamma} = \frac{1}{2}g^{\sigma\gamma}[\nabla_{\alpha}(\delta g_{\sigma\gamma}) + \cancel{\nabla_{\gamma}(\delta g_{\sigma\alpha})} - \cancel{\nabla_{\sigma}(\delta g_{\sigma\alpha})}] \Rightarrow$$

$$\boxed{\delta\Gamma^{\gamma}{}_{\alpha\gamma} = \frac{1}{2}g^{\sigma\gamma}\nabla_{\alpha}(\delta g_{\sigma\gamma})} \tag{A.61}$$

We can write the above equation (A.60) as :

$$\begin{aligned}
\delta\Gamma^{\sigma}_{\beta\alpha} &= \frac{1}{2}g^{\sigma\gamma}\left[\nabla_{\beta}\left(-g_{\gamma\mu}g_{\nu\alpha}\delta g^{\mu\nu}\right) + \nabla_{\alpha}\left(-g_{\gamma\mu}g_{\nu\beta}\delta g^{\mu\nu}\right) - \nabla_{\gamma}\left(-g_{\beta\mu}g_{\nu\alpha}\delta g^{\mu\nu}\right)\right] \\
&= \frac{1}{2}g^{\sigma\gamma}\left[-g_{\gamma\mu}g_{\nu\alpha}\nabla_{\beta}\left(\delta g^{\mu\nu}\right) - g_{\gamma\mu}g_{\nu\beta}\nabla_{\alpha}\left(\delta g^{\mu\nu}\right) + g_{\beta\mu}g_{\nu\alpha}\nabla_{\gamma}\left(\delta g^{\mu\nu}\right)\right] \\
&= -\frac{1}{2}\left[\delta^{\sigma}_{\mu}g_{\nu\alpha}\nabla_{\beta}\left(\delta g^{\mu\nu}\right) + \delta^{\sigma}_{\mu}g_{\nu\beta}\nabla_{\alpha}\left(\delta g^{\mu\nu}\right) - g_{\beta\mu}g_{\nu\alpha}g^{\sigma\gamma}\nabla_{\gamma}\left(\delta g^{\mu\nu}\right)\right] \\
&= -\frac{1}{2}\left[g_{\nu\alpha}\nabla_{\beta}\left(\delta g^{\sigma\nu}\right) + g_{\nu\beta}\nabla_{\alpha}\left(\delta g^{\sigma\nu}\right) - g_{\beta\mu}g_{\nu\alpha}\nabla^{\sigma}\left(\delta g^{\mu\nu}\right)\right]
\end{aligned} \tag{A.62}$$

At this point, we will calculate the identities :

$$g^{\alpha\beta}(\delta\Gamma^{\sigma}_{\beta\alpha}) \quad \text{and} \quad g^{\alpha\beta}(\delta\Gamma^{\gamma}_{\alpha\gamma})$$

Using eq.(A.61) and eq.(A.62) we obtain :

$$g^{\alpha\beta}(\delta\Gamma^{\sigma}_{\beta\alpha}) = g^{\alpha\beta}\left\{-\frac{1}{2}\left[g_{\nu\alpha}\nabla_{\beta}\left(\delta g^{\sigma\nu}\right) + g_{\nu\beta}\nabla_{\alpha}\left(\delta g^{\sigma\nu}\right) - g_{\beta\mu}g_{\nu\alpha}\nabla^{\sigma}\left(\delta g^{\mu\nu}\right)\right]\right\}$$

$$-\frac{1}{2}\left[g^{\alpha\beta}g_{\nu\alpha}\nabla_{\beta}\left(\delta g^{\sigma\nu}\right) + g^{\alpha\beta}g_{\nu\beta}\nabla_{\alpha}\left(\delta g^{\sigma\nu}\right) - g^{\alpha\beta}g_{\beta\mu}g_{\nu\alpha}\nabla^{\sigma}\left(\delta g^{\mu\nu}\right)\right]$$

$$-\frac{1}{2}\left[\delta^{\beta}_{\nu}\nabla_{\beta}\left(\delta g^{\sigma\nu}\right) + \delta^{\alpha}_{\nu}\nabla_{\alpha}\left(\delta g^{\sigma\nu}\right) - \delta^{\alpha}_{\mu}g_{\nu\alpha}\nabla^{\sigma}\left(\delta g^{\mu\nu}\right)\right]$$

$$-\frac{1}{2}\left[\nabla_{\nu}\left(\delta g^{\sigma\nu}\right) + \nabla_{\nu}\left(\delta g^{\sigma\nu}\right) - g_{\mu\nu}\nabla^{\sigma}\left(\delta g^{\mu\nu}\right)\right]$$

$$-\frac{1}{2}\left[2\nabla_{\nu}\left(\delta g^{\sigma\nu}\right) - g_{\mu\nu}\nabla^{\sigma}\left(\delta g^{\mu\nu}\right)\right] \tag{A.63}$$

and

$$g^{\alpha\sigma}(\delta\Gamma^{\gamma}_{\alpha\gamma}) = -\frac{1}{2}g^{\alpha\sigma}g_{\mu\nu}\nabla_{\alpha}(\delta g^{\mu\nu}) = -\frac{1}{2}g_{\mu\nu}\nabla^{\sigma}(\delta g^{\mu\nu}) \tag{A.64}$$

Now we compute the relation (A.63)-(A.64) :

$$g^{\alpha\beta}(\delta\Gamma^{\sigma}_{\beta\alpha}) - g^{\alpha\sigma}(\delta\Gamma^{\gamma}_{\alpha\gamma}) =$$

$$= -\frac{1}{2}[2\nabla_{\nu}(\delta g^{\sigma\nu}) - g_{\mu\nu}\nabla^{\sigma}(\delta g^{\mu\nu}) - g_{\mu\nu}\nabla^{\sigma}(\delta g^{\mu\nu})] =$$

$$= -\frac{1}{2}[2\nabla_{\nu}(\delta g^{\sigma\nu}) - 2g_{\mu\nu}\nabla^{\sigma}(\delta g^{\mu\nu})]$$

So the variation of the Ricci scalar becomes :

$$\delta R = R_{\mu\nu}\delta g^{\mu\nu} + \nabla_{\sigma}[g^{\alpha\beta}(\delta\Gamma^{\sigma}_{\beta\alpha} - g^{\alpha\sigma}(\delta\Gamma^{\gamma}_{\alpha\gamma})] =$$

$$= R_{\mu\nu}\delta g^{\mu\nu} + \nabla_{\sigma}\left\{-\frac{1}{2}[2\nabla_{\nu}(\delta g^{\sigma\nu}) - 2g_{\mu\nu}\nabla^{\sigma}(\delta g^{\mu\nu})]\right\}$$

$$= R_{\mu\nu}\delta g^{\mu\nu} + [-\nabla_{\sigma}\nabla_{\nu}(\delta g^{\sigma\nu}) + g_{\mu\nu}\nabla_{\rho}\nabla^{\sigma}(\delta g^{\mu\nu})] \Longrightarrow$$

$$\Longrightarrow \boxed{\delta R = R_{\mu\nu}\delta g^{\mu\nu} - \nabla_{\mu}\nabla_{\nu}\delta g^{\mu\nu} + g_{\mu\nu}\nabla_{\sigma}\nabla^{\sigma}(\delta g^{\mu\nu})} \tag{A.65}$$

It's worth noting that there are no fields coupled to R in the action, which means that the covariant derivatives vanish. Consequently, we arrive at the following expression :

$$\delta S_{EH} = \frac{1}{16\pi G_N}\int d^D x\sqrt{-g}(R_{\mu\nu} - \frac{1}{2}Rg_{\mu\nu})\delta g^{\mu\nu}. \tag{A.66}$$

Thus, we obtain :

$$\frac{16\pi G_N}{\sqrt{-g}}\frac{\delta S_{EH}}{\delta g^{\mu\nu}} = R_{\mu\nu} - \frac{1}{2}Rg_{\mu\nu} = 0. \tag{A.67}$$

These equations are essentially the vacuum Einstein equations. Our next step is to incorporate matter into these equations. This can be achieved by introducing matter fields into the action, like so :

$$S = S_{EH} + S_M, \tag{A.68}$$

where S_M is the action for the matter :

$$S_M = \int d^D x\sqrt{-g}\mathscr{L}_M, \tag{A.69}$$

and $\mathscr{L}$ represents the Lagrangian density for matter, which encompasses the matter fields. When we vary the matter action with respect to the metric, we obtain the following result :

$$\begin{aligned}\delta S_M &= \int d^4 x\frac{\delta(\sqrt{-g}\mathscr{L}_M)}{\delta g^{\mu\nu}}\delta g^{\mu\nu}\\ &= \int d^4 x\sqrt{-g}\frac{1}{\sqrt{-g}}\frac{\delta(\sqrt{-g}\mathscr{L}_M)}{\delta g^{\mu\nu}}\delta g^{\mu\nu}\end{aligned} \tag{A.70}$$

At this point if we set :

$$T_{\mu\nu} = -\frac{2}{\sqrt{-g}}\frac{\delta(\sqrt{-g}\mathscr{L}_M)}{\delta g^{\mu\nu}} \tag{A.71}$$

We obtain

$$\delta S_M = -\frac{1}{2}\int d^4 x\sqrt{-g}T_{\mu\nu}\delta g^{\mu\nu} \tag{A.72}$$

So from eq.(A.68), combining eq.(A.66) and eq.(A.72) we take

$$\delta S = 0 \Rightarrow \int d^4 x\sqrt{-g}\left[-\frac{1}{2}T_{\mu\nu} + \frac{1}{16\pi G_N}\left(R_{\mu\nu} - \frac{1}{2}Rg_{\mu\nu}\right)\right]\delta g^{\mu\nu}$$

$$\boxed{8\pi G_N T_{\mu\nu} = R_{\mu\nu} - \frac{1}{2}Rg_{\mu\nu}} \tag{A.73}$$

These correspond to the Einstein equations (A.14). In the present low-energy state of the universe, the matter action corresponds to the Standard Model action. However, in the early universe with its extreme conditions, this is not the case. The matter action serves as an effective matter action at low temperatures, and the complete action is expected to differ significantly from our Standard Model description.

Now, let's provide a straightforward example of an action involving a real scalar field $\phi(x)$ to facilitate our discussion. The action takes the following form :

$$S_M = \int d^4x\sqrt{-g}\mathscr{L}_M = \int d^4x\sqrt{-g}\left(\frac{1}{2}g^{\mu\nu}(\partial_\mu\phi)(\partial_\nu\phi) - V(\phi)\right). \tag{A.74}$$

We note that our metric sign convention is $(+,-,-,-)$. First, we write the Lagrangian density

$$\mathscr{L} = \tfrac{1}{2}\partial_\mu\phi\partial^\mu\phi - V(\phi) = \tfrac{1}{2}\partial_\mu\phi g^{\mu\nu}\partial_\nu\phi - V(\phi) \tag{A.75}$$

Our Lagrangian then is:

$$L = \sqrt{-g}\mathscr{L} = \tfrac{1}{2}\sqrt{-g}\partial_\mu\phi\partial^\mu\phi - \sqrt{-g}V(\phi)$$

We assume a Robertson$-$Walker metric so we have:

$$g_{\mu\nu} = \begin{pmatrix} -1 & 0 & 0 & 0 \\ 0 & \frac{a^2}{1-kr^2} & 0 & 0 \\ 0 & 0 & r^2a^2 & 0 \\ 0 & 0 & 0 & r^2a^2\sin^2\theta \end{pmatrix} \tag{A.76}$$

The determinant of this matrix is:

$$det(g_{\mu\nu}) = -\frac{r^4a^6\sin^2\theta}{1-kr^2}$$

and so we have:

$$\boxed{\sqrt{-g} = \frac{r^4a^6\sin^2\theta}{1-kr^2}}$$

Now we obtain the field equation using the Euler$-$Lagrange equation:

$$\frac{\partial\mathscr{L}}{\partial\phi} = \partial_\mu\left(\frac{\partial\mathscr{L}}{\partial(\partial_\mu\phi)}\right)$$

The LHS is:

$$\frac{\partial L}{\partial\phi} = -\frac{dV(\phi)}{dt}\sqrt{-g}$$

and for the RHS we have:

$$\partial_\mu\Big\{\tfrac{1}{2}\sqrt{-g}\left[g^{\mu\nu}\partial_\nu\phi+\partial_\mu\phi g^{\mu\nu}\delta^\mu{}_\nu\right]\Big\}\Longrightarrow$$

$$\partial_\mu\Big\{\tfrac{1}{2}\sqrt{-g}\left[2g^{\mu\nu}\partial_\mu\phi\right]\Big\}=$$

$$\partial_\mu\Big\{\sqrt{-g}g^{\mu\nu}\partial_\mu\phi\Big\}=$$

$$\left(\partial_\mu\sqrt{-g}\right)g^{\mu\nu}\partial_\mu\phi+\sqrt{-g}g^{\mu\nu}\partial_\mu\partial_\nu\phi=$$

$$\left(\partial_0\sqrt{-g}\right)g^{00}\partial_0\phi+\sqrt{-g}g^{00}\partial_0\partial_0\phi=$$

$$\left(\partial_0\sqrt{-g}\right)\dot{\phi}+\sqrt{-g}\ddot{\phi}$$

From Mathematica, we find:

$$\partial_0\sqrt{-g}=\frac{3r^4a^5\sin^2\theta\dot{a}}{(1-kr^2)\sqrt{-g}}$$

Finally, we have:

$$\frac{3r^4a^5\sin^2\theta\dot{a}}{(1-kr^2)\sqrt{-g}}\dot{\phi}+\sqrt{-g}\ddot{\phi}=-\frac{dV(\phi)}{d\phi}\sqrt{-g}\Rightarrow$$

$$\frac{3r^4a^5\sin^2\theta\dot{a}}{(1-kr^2)(-g)}\dot{\phi}+\ddot{\phi}=-\frac{dV(\phi)}{d\phi}\Rightarrow$$

$$\boxed{3\frac{\dot{a}}{a}\dot{\phi}+\ddot{\phi}=-\frac{dV}{d\phi}}\Rightarrow$$

$$\boxed{\ddot{\phi}+3H\dot{\phi}=-\frac{dV}{d\phi}} \tag{A.77}$$

where we have set H=$\frac{\dot{a}}{a}$.

At this point, we take the stress−energy tensor for this scalar field:

$$\boxed{T^{\mu\nu}=\partial^\mu\phi\partial^\nu\phi+\mathscr{L}g^{\mu\nu}} \tag{A.78}$$

First, we obtain the energy density ρ:

$$-T^0{}_0 = T^{00} = \rho \Rightarrow$$

$$\partial^0\phi\partial^0\phi + \left[\frac{1}{2}\partial_0\phi\partial^0\phi - V(\phi)\right] g^{00} = \rho \Rightarrow$$

$$\rho = \dot{\phi}^2 - \frac{1}{2}\dot{\phi}^2 + V(\phi) \Rightarrow$$

$$\boxed{\rho = \frac{1}{2}\dot{\phi}^2 + V(\phi)} \tag{A.79}$$

and then, the pressure p:

$$p = T^i{}_i(\text{ no sum}) \Rightarrow$$

$$p = g_{11}T^{11} \quad \text{or} \quad g_{22}T^{22} \quad \text{or} \quad g_{33}T^{33}$$

So we have:

$$p = g_{11}T^{11} = g_{11}\partial^1\phi\partial^1\phi - g_{11}\mathscr{L}g^{11} \Rightarrow$$

$$\boxed{p = \mathscr{L} = \frac{1}{2}\dot{\phi}^2 - V(\phi)} \tag{A.80}$$

and the resulting equation of state is :

$$\omega = \frac{p}{\rho} = \frac{\frac{1}{2}\dot{\phi}^2 - V}{\frac{1}{2}\dot{\phi}^2 + V} \tag{A.81}$$

This equation reveals that a scalar field with a value of $\omega < 0$ (indicating negative pressure) can result in an accelerated expansion if the kinetic energy $\frac{1}{2}\dot{\phi}^2$ is less than the potential energy V.

By combining equations (A.77) and (A.79), we arrive at the continuity equation :

$$\frac{d\rho}{dt} = \dot{\phi}\ddot{\phi} + \frac{dV}{dt}\dot{\phi} \Rightarrow$$

$$\frac{d\rho}{dt} = \dot{\phi}\ddot{\phi} + (-\ddot{\phi} - 3H\dot{\phi})\dot{\phi} \Rightarrow$$

$$\boxed{\frac{d\rho}{dt} = -3H\dot{\phi}^2}. \tag{A.82}$$

There are three equations in total: two are obtained by varying the action with respect to the metric $g^{\mu\nu}$, and the third is the equation of motion for ϕ. It's worth noting that the equation of motion connects the other two equations, making only two of them independent. We will utilize this insight in a subsequent chapter when we tackle the field equations for a specific matter action.

In a more comprehensive theory where multiple types of matter may exist (such as photons, baryons, neutrinos, dark energy, etc.), and these components make significant contributions to both the energy density ρ and the pressure p, we consider the summation of all these components: :

$$\rho \equiv \sum_i \rho_i \quad , \quad p \equiv \sum_i p_i. \tag{A.83}$$

For each component denoted as 'i,' we introduce the quantity Ω_i, representing the current ratio of energy density to the critical energy density, defined as $\rho_{crit} = 3H_0^2$:

$$\Omega_i \equiv \frac{\rho_0^i}{\rho_{crit}}, \tag{A.84}$$

and also we write the corresponding equations of state for each component :

$$\omega_i \equiv \frac{p_i}{\rho_i}. \tag{A.85}$$

We should take note that the subscript '0' indicates the evaluation of a quantity at the present time, denoted as t_0. Utilizing this information and the scale factor's normalization, which is $a_0 = a(t_0) \equiv 1$, we can express the Friedmann equation (A.24) as follows :

$$\frac{H^2}{\rho_{crit}} + \frac{k}{a^2\rho_{crit}} = \frac{8\pi G}{3}\sum_i \Omega_i a^{-3(1+\omega_i)} \Longrightarrow$$
$$\frac{H^2}{3H_0^2} + \frac{k}{a^2 3H_0^2} = \frac{8\pi G}{3}\sum_i \Omega_i a^{-3(1+\omega_i)}$$

We set $8\pi G = 1$ and we obtain :

$$\frac{H^2}{H_0^2} + \frac{k}{a^2 H_0^2} = \sum_i \Omega_i a^{-3(1+\omega_i)} \Longrightarrow$$
$$\left(\frac{H}{H_0}\right)^2 = \sum_i \Omega_i a^{-3(1+\omega_i)} + \Omega_k a^{-2}. \tag{A.86}$$

Here, we define the parameters as follows: $H \equiv \frac{\dot{a}}{a}$ and $\Omega_k \equiv -\frac{k}{a_0^2 H_0^2}$ to parameterize curvature. When we evaluate eq(A.86) at the present time, we obtain the consistency relation::

$$\sum_i \Omega_i + \Omega_k = 1. \tag{A.87}$$

From the second Friedmann equation (A.26) we obtain at $t = t_0$:

$$\frac{1}{a_0}\frac{d^2 a_0}{dt^2} = -\frac{4\pi G}{3}\Omega_i \rho_{crit}(1+3\omega_i) \Longrightarrow$$

$$\frac{1}{a_0 H_0^2}\frac{d^2 a_0}{dt^2} = -4\pi G \Omega_i \rho_{crit}(1+3\omega_i) \Longrightarrow$$

$$\frac{1}{a_0 H_0^2}\frac{d^2 a_0}{dt^2} = -\frac{1}{2}\Omega_i(1+3\omega_i) \tag{A.88}$$

Appendix B

Soft Terms and CW Corrections

B.1 Soft Term Potential

In general, the soft term scalar Lagrangian can be written as

$$\mathscr{L} \supset m_\alpha^2 C^\alpha \overline{C}^{\bar{\alpha}} \tag{B.1}$$

where the soft mass m_α^2 of the field C defined as

$$m_\alpha^2 = (m_{3/2}^2 + V_0) - F^{\bar{m}} F^n \partial_{\bar{m}} \partial_n \log \tilde{K}_\alpha. \tag{B.2}$$

Here, $F^{\bar{m}}$ is defined as $F^{\bar{m}} = e^{G/2} K^{\bar{m}n} \partial G / \partial n$. Utilizing the superpotential and Kähler metric as given in Eq.(2.4) and Eq.(2.9), we find that the soft mass of the canonically normalized field s is

$$m_s^2 \sim (m_{3/2}^2 + V_0) - \frac{2}{3\mathscr{V}_o^2} W_o^2 + \cdots \tag{B.3}$$

where V_0 represents the minima of the potential. Hence the soft-term potential is

$$\Delta V_{soft} = m_S^2 S^2 = \left[(m_{3/2}^2 + V_0) - \frac{2}{3\mathscr{V}_o^2} W_o^2 + \cdots \right] S^2. \tag{B.4}$$

Taking into account the relation $s^2 = \frac{(3a\gamma)}{\mathscr{V}_0^{2/3}} S^2$ between canonically normalized field s and non-canonically normalized field S we have

$$\Delta V_{soft} = \left[(m_{3/2}^2 + V_0) - \frac{2}{3\mathscr{V}_o^2} W_o^2 + \cdots \right] \frac{\mathscr{V}_0^{2/3}}{(3a\gamma)} s^2. \tag{B.5}$$

If we further define the ratio $y = s/M$, then B.1 takes the form

$$\Delta V_{\text{soft}} = \left[(m_{3/2}^2 + V_0) - \frac{2}{3\mathscr{V}_o^2} W_o^2 + \cdots \right] M^2 y^2 \frac{\mathscr{V}_o^{2/3}}{3a\gamma} = M_{s_c}^2 y^2 \ , \tag{B.6}$$

where

$$M_{s_c} = \left[(m_{3/2}^2 + V_0) - \frac{2}{3\mathscr{V}_o^2} W_o^2 + \cdots \right] M^2 \frac{\mathscr{V}_o^{2/3}}{3a\gamma} \ .$$

B.2 Coleman-Weinberg Corrections

In this Appendix we present analytically the computation of the CW corrections. Using the effective potential

$$V_{\text{eff}} = \frac{\kappa^2\alpha \mid \left(M^2 - \Phi_1\Phi_2\right) \mid^2 + 2\gamma\kappa^2 S^2(\alpha\Phi_1\Phi_1^\dagger + \beta\Phi_2\Phi_2^\dagger)}{3a\alpha\beta\gamma\mathcal{V}^{4/3}} + \frac{3W_0^2(2\eta_0\log(\mathcal{V}) - 8\eta_0 + \xi_0)}{2\mathcal{V}^3} + \frac{d}{\mathcal{V}^2}, \tag{B.7}$$

the scalar mass matrix along the inflationary track read as,

$$M_S^2 = \begin{pmatrix} \frac{\kappa^2 S^2}{6a\beta\mathcal{V}^{4/3}} & 0 & -\frac{\kappa^2 M^2}{3a\gamma\mathcal{V}^{4/3}} & 0 & 0 & 0 & 0 \\ 0 & \frac{\kappa^2 S^2}{6a\beta\mathcal{V}^{4/3}} & 0 & \frac{\kappa^2 M^2}{3a\gamma\mathcal{V}^{4/3}} & 0 & 0 & 0 \\ -\frac{\kappa^2 M^2}{3a\gamma\mathcal{V}^{4/3}} & 0 & \frac{\kappa^2 S^2}{6a\alpha\mathcal{V}^{4/3}} & 0 & 0 & 0 & 0 \\ 0 & \frac{\kappa^2 M^2}{3a\gamma\mathcal{V}^{4/3}} & 0 & \frac{\kappa^2 S^2}{6a\alpha\mathcal{V}^{4/3}} & 0 & 0 & 0 \\ 0 & 0 & 0 & 0 & 0 & 0 & 0 \\ 0 & 0 & 0 & 0 & 0 & 0 & 0 \\ 0 & 0 & 0 & 0 & 0 & 0 & \frac{28\kappa^2 M^4}{27a\gamma\mathcal{V}^{\frac{10}{3}}} + \cdots \end{pmatrix} \tag{B.8}$$

After diagonalization and choosing $\alpha = \beta$ the scalar mass spectrum is

$$M_S^2 = \left[0, 0, \frac{\kappa^2 M^2\left(y^2 - \frac{2\alpha}{\gamma}\right)}{6a\mathcal{V}^{4/3}\alpha}, \frac{\kappa^2 M^2\left(y^2 - \frac{2\alpha}{\gamma}\right)}{6a\mathcal{V}^{4/3}\alpha}, \frac{\kappa^2 M^2\left(y^2 + \frac{2\alpha}{\gamma}\right)}{6a\mathcal{V}^{4/3}\alpha}, \frac{\kappa^2 M^2\left(y^2 + \frac{2\alpha}{\gamma}\right)}{6a\mathcal{V}^{4/3}\alpha}, \quad \frac{28\kappa^2 M^4}{27a\gamma\mathcal{V}^{10/3}} + \cdots\right] \tag{B.9}$$

where $y^2 = s^2/M^2$. Similarly, the generic fermionic mass matrix is defined as

$$M_{F_{ij}} = e^{\mathcal{K}/2}\left(W_{ij} + \mathcal{K}_{ij}W + \mathcal{K}_i W_j + \mathcal{K}_j W_i + \mathcal{K}_i\mathcal{K}_j W - \mathcal{K}^{k\bar{l}}\mathcal{K}_{ij\bar{l}}D_k W\right). \tag{B.10}$$

Using the superpotential (3.2) and the Kähler potential in (3.2) we obtain

$$M_{F_{ij}} = \begin{pmatrix} -\frac{6a\gamma\kappa M^2 S}{\mathcal{V}^{2/3}} + \frac{9a^2\gamma^2 S^2}{\mathcal{V}^{4/3}} + \cdots & 0 & 0 & \frac{2kM^2}{\mathcal{V}} + \frac{2a\gamma S\left(kM^2 S - 4\right)}{\mathcal{V}^{5/3}} + \cdots \\ 0 & 0 & \kappa S & 0 \\ 0 & \kappa S & 0 & 0 \\ \frac{2\kappa M^2}{\mathcal{V}} + \frac{2a\gamma S\left(\kappa M^2 S - 4\right)}{\mathcal{V}^{5/3}} + \cdots & 0 & 0 & \frac{6}{\mathcal{V}^2} + \frac{34}{3}a\gamma S^2\left(\frac{1}{\mathcal{V}}\right)^{8/3} + \cdots \end{pmatrix}. \tag{B.11}$$

After diagonalization, the fermionic masses are

$$M_{F_{ij}}^2 = \left[\kappa^2 M^2 y^2, \kappa^2 M^2 y^2, \frac{36a^2\kappa^2 M^6 y^2\gamma^2}{\mathcal{V}^{4/3}} + \cdots, \frac{36a^2\kappa^2 M^6 y^2\gamma^2}{\mathcal{V}^{4/3}} + \cdots\right]. \tag{B.12}$$

The fermionic mass $\frac{36a^2\kappa^2 M^6 y^2\gamma^2}{\mathcal{V}^{4/3}}$ and the bosonic mass $\frac{28\kappa^2 M^4}{27a\gamma\mathcal{V}^{10/3}}$ are small compared to other masses, so their contribution to the Coleman-Weinberg potential is suppressed. Additionally, we focus on the region where $(y^2 \gg 2\alpha/\gamma)$. The relation between canonically and non-canonically normalised field is $s = S\sqrt{3a\gamma}/V_0^{1/3}$. The effective contribution of the one-loop radiative corrections can be calculated using the Coleman-Weinberg formula

$$\Delta V_{\text{1-loop}} = \frac{1}{64\pi^2}\left[M_S^4\log\left(\frac{M_S^2}{Q^2}\right) - 2M_F^4\log\left(\frac{M_F^2}{Q^2}\right) - \frac{3}{2}\left(M_S^4 - 2M_F^4\right)\right] \tag{B.13}$$

$$\Delta V_{\text{1-loop}} = \frac{\kappa^4 M^4 y^4}{144\pi^2 a^2 \gamma^2 \mathscr{V}_o^{4/3}} \left[F(y) - \left(\frac{1}{54 a^2 \alpha^2 \gamma^2} - \frac{3}{2} \mathscr{V}_o^{8/3} \right) \right], \tag{B.14}$$

where

$$F(y) = \frac{1}{81 a^2 \alpha^2 \gamma^2} \log \left(\frac{\kappa^2 M^2 y^2}{27 a^2 \alpha \gamma^2 Q^2 \mathscr{V}_o^{2/3}} \right) - \mathscr{V}_o^{8/3} \log \left(\frac{\kappa^2 M^2 y^2 \mathscr{V}_o^{2/3}}{3 a \gamma Q^2} \right) . \tag{B.15}$$

Appendix C

Beta functions

C.1 Beta functions and GRE's

C.1.1 SU(5) case

The whole idea behind RGE's is that the renormalization scale M in the theories is arbitrary, so we don't want the physical quantities to depend on it. The first step to achieve this is by taking into consideration the Callan-Symanzik equation which states that if we shift M in a theory then we should also shift the coupling constant g and the scalar field in a way that the bare n-point function $G^n(x_1, ..., x_n)$ remains fixed. So, we take :

$$\left[M\frac{\partial}{\partial M} + \beta\frac{\partial}{\partial g} + n\gamma\right] G^n(x_1, ..., x_n, M, g) = 0. \tag{C.1}$$

where β and γ are

$$\beta \equiv \frac{M}{\delta M}\delta g, \quad \gamma \equiv -\frac{M}{\delta M}\delta\eta. \tag{C.2}$$

From this point, we can easily end up with the renormalization equation :

$$M\frac{\partial g_i}{\partial M} = \beta_i(g). \tag{C.3}$$

It is straightforward from this equation that once we have the tree beta functions (for SU(5)) in hand, we can then solve the renormalization equation to find the tree running coupling constants $g_i(M)$. In the limit $d \to 4$ after some work we obtain :

$$\beta_i = -\frac{g_i^3}{16\pi^2}b_i \tag{C.4}$$

so our results can be summarized as follows:

$$b_1 = -\frac{2}{3}\sum_f \frac{3}{5}Y_f^2 - \frac{1}{3}\sum_b \frac{3}{5}Y_b^2 \tag{C.5}$$

$$b_{2,3} = \frac{11}{3}C_2(G) - \frac{2}{3}\sum_f C(r_f) - \frac{1}{3}\sum_b C(r_b). \tag{C.6}$$

Analytical Calculations :
• For b_1 we have ($n_g = 3$,$n_h = 1$) :

$$b_1 = -\frac{2}{5}\left[\underbrace{2\times 3\times\left(\frac{1}{6}\right)^2}_{Q}+\underbrace{3\times\left(-\frac{1}{3}\right)^2}_{d^c}+\underbrace{3\times\left(\frac{2}{3}\right)^2}_{u^c}+\underbrace{2\times\left(-\frac{1}{2}\right)^2}_{L}+\underbrace{1}_{e^c}\right]\times n_g - \underbrace{\frac{1}{5}\times 2\times\left(\frac{1}{2}\right)^2}_{H}\times n_h$$

$$= -\frac{2}{5}\left(\frac{1}{6}+\frac{1}{3}+\frac{4}{3}+\frac{1}{2}+1\right)n_g - \frac{1}{10} \Rightarrow$$

$$\boxed{b_1 = -\frac{4}{3}\times n_g - \frac{1}{10} = -\frac{41}{10}} \tag{C.7}$$

• For b_2 we have ($n_g = 3$,$n_h = 1$) :

$$b_2 = \frac{11}{3}\times 2 - \frac{2}{3}\left[\frac{1}{2}\times 3+\frac{1}{2}\right]\times n_g - \frac{1}{6}\times n_h = \frac{22}{3} - \frac{4}{3}\times n_g - \frac{1}{6}\times n_h \Rightarrow$$

$$\boxed{b_2 = -\frac{19}{6}} \tag{C.8}$$

• For b_3 we have ($n_g = 3$,$n_h = 1$) :

$$b_3 = \frac{11}{3}\times 3 - \frac{2}{3}\left[\frac{1}{2}\times 2+\frac{1}{2}+\frac{1}{2}\right]\times n_g = 11 - \frac{4}{3}\times n_g \Rightarrow$$

$$\boxed{b_3 = 7} \tag{C.9}$$

Threshold effects : When we make these calculations it is crucial to realize that below M_{top} the top quark does not contribute to the various sums of the above expressions as Higgs boson below M_{Higgs} (in this case at 120 GeV). Having said that, the various calculations are modified to be consistent with our statement, so we obtain:
• For $b_1^{'}$ we have ($n_g = 3$,$n_h = 1$ and $n_g^{'} = 2$) and $M_{Higgs} < M < M_{top}$:

$$b_1^{'} = -\frac{2}{5}\left[2\times 3\times\left(\frac{1}{6}\right)^2\times n_g^{'} + 3\times\left(-\frac{1}{3}\right)^2\times n_g + 3\times\left(\frac{2}{3}\right)^2\times n_g^{'} + 2\times\left(-\frac{1}{2}\right)^2\times n_g\right.$$
$$\left.+n_g + 3\times\left(\frac{1}{6}\right)^2\right] - \frac{1}{10}$$
$$= -\frac{2}{5}\left(\frac{1}{3}+1+\frac{8}{3}+\frac{3}{2}+3+\frac{1}{12}\right) - \frac{1}{10} \Rightarrow$$

$$\boxed{b_1^{'} = -\frac{106}{30} = -\frac{53}{15}} \tag{C.10}$$

• For $b_2^{'}$ we have ($n_g = 3$,$n_h = 1$ and $n_g^{'} = 2$) and $M_{Higgs} < M < M_{top}$:

$$b_2^{'} = \frac{11}{3} \times 2 - \frac{2}{3}\left[\frac{1}{2} \times 3 \times n_g^{'} + \frac{1}{2}n_g + \frac{1}{2} \times 3 \times \frac{1}{2}\right] - \frac{1}{6} \Rightarrow$$

$$\boxed{b_2^{'} = \frac{11}{3}} \tag{C.11}$$

• For $b_3^{'}$ we have ($n_g = 3$ and $n_g^{'} = 2$) and $M_{Higgs} < M < M_{top}$:

$$b_3^{'} = 11 - \frac{2}{3}\left[\frac{1}{2} \times 2 \times n_g^{'} + \frac{1}{2} \times n_g + \frac{1}{2} \times n_g\right] \Rightarrow$$

$$\boxed{b_3^{'} = \frac{23}{3}} \tag{C.12}$$

Finally, in the range $M_Z < M < M_{Higgs}$ where we have $n_h = 0$ we obtain :

$$\boxed{b_1^{''} = -\frac{103}{30}} \ , \ \boxed{b_2^{''} = \frac{23}{6}} \ , \ \boxed{b_3^{''} = \frac{23}{3}} \tag{C.13}$$

C.1.2 MSSM case

In the MSSM case we will see those sparticles in the supersymmetric model contribute significantly to the beta functions which in turn dictate the running of the couplings constants.
Analytical Calculations :
• For b_1 we have ($n_g = 3$,$n_h = 2$) :

$$b_1 = -\frac{2}{5}\left[\underbrace{\frac{20}{6} \times n_g}_{SM\ fermionic\ fields} + \underbrace{2 \times \left(\frac{1}{2}\right)^2 \times n_h}_{Higginos}\right] - \frac{1}{5}\left[2 \times \left(\frac{1}{2}\right)^2 \times n_h + \underbrace{\frac{20}{6} \times n_g}_{sfermions}\right] \Rightarrow$$

$$\boxed{b_1 = -\frac{33}{5}} \tag{C.14}$$

• For b_2 we have ($n_g = 3$,$n_h = 2$)[1] :

$$b_2 = \frac{22}{3} - \frac{2}{3}\left[\underbrace{4 \times \frac{1}{2} \times n_g}_{SM\ part} + \underbrace{\frac{1}{2} \times n_h}_{Higgsinos} + \underbrace{2}_{gauginos}\right] - \frac{1}{3}\left[\underbrace{4 \times \frac{1}{2} \times n_g}_{sfermions} + \frac{1}{2} \times n_h\right] \Rightarrow$$

$$\boxed{b_2 = -1} \tag{C.15}$$

[1]we note that gauginos are in the adjoint representation so $C = N$ which in this case is 2. The gauginos here are Winos and Zino.

• For b_3 we have $(n_g = 3)$:

$$b_3 = \frac{11}{3}\times 3 - \frac{2}{3}\left[\underbrace{4\times\frac{1}{2}\times n_g}_{SM\ part} + \underbrace{3}_{gluino\ contribution}\right] - \frac{1}{3}\left[\underbrace{4\times\frac{1}{2}\times n_g}_{sfermion\ contribution}\right] \Rightarrow$$

$$\boxed{b_3 = 3} \tag{C.16}$$

<u>Threshold effects</u> :
We have to take the supersymmetric approach to consider the threshold effects of this tie. The beta functions are unchanged above the universal sfermion mass (4500 GeV). In the rage $M_{700\ GeV} < M < M_{uni}$ we rule out the sfermionic contributions from the beta functions. In the range $M_{200\ GeV} < M < M_{700\ GeV}$ we freeze out the contribution of the second Higgs boson doublet and finally in the range $M < M_{200\ GeV}$ we rule out the contributions of gauginos and Higgsinos leading us this way to the SM beta functions. So, analytically we have:
<u>Range $M_{700\ GeV} < M < M_{uni}$</u> :
• For $b_1^{'}$ we have $(n_g = 3, n_h = 2)$:

$$b_1^{'} = -\frac{2}{5}\left[\underbrace{\frac{20}{6}\times n_g}_{SM\ fermionic\ fields} \underbrace{+2\times\left(\frac{1}{2}\right)^2\times n_h}_{Higginos}\right] - \frac{1}{5}\left[2\times\left(\frac{1}{2}\right)^2\times n_h\right] \Rightarrow$$

$$\boxed{b_1^{'} = -\frac{23}{5}} \tag{C.17}$$

• For $b_2^{'}$ we have $(n_g = 3, n_h = 2)$:

$$b_2^{'} = \frac{22}{3} - \frac{2}{3}\left[\underbrace{4\times\frac{1}{2}\times n_g}_{SM\ part} + \underbrace{\frac{1}{2}\times n_h}_{Higgsinos} + \underbrace{2}_{gauginos}\right] - \frac{1}{3}\left[\frac{1}{2}\times n_h\right] \Rightarrow$$

$$\boxed{b_2^{'} = \frac{7}{6}} \tag{C.18}$$

• For $b_3^{'}$ we have $(n_g = 3)$:

$$b_3^{'} = \frac{11}{3}\times 3 - \frac{2}{3}\left[\underbrace{4\times\frac{1}{2}\times n_g}_{SM\ part} + \underbrace{3}_{gluino\ contribution}\right] \Rightarrow$$

$$\boxed{b_3^{'} = 5} \tag{C.19}$$

Range $M_{200\ GeV} < M < M_{700\ GeV}$:
• For $b_1^{''}$ we have ($n_g = 3$,$n_h = 1$) :

$$b_1^{''} = -\frac{2}{5}\left[\underbrace{\frac{20}{6}\times n_g}_{SM\ fermionic\ fields} \underbrace{+2\times\left(\frac{1}{2}\right)^2\times n_h}_{Higginos}\right] - \frac{1}{5}\left[2\times\left(\frac{1}{2}\right)^2\times n_h\right] \Rightarrow$$

$$\boxed{b_1^{'} = -\frac{43}{10}} \tag{C.20}$$

• For $b_2^{''}$ we have ($n_g = 3$,$n_h = 1$) :

$$b_2^{'} = \frac{22}{3} - \frac{2}{3}\left[\underbrace{4\times\frac{1}{2}\times n_g}_{SM\ part} + \underbrace{\frac{1}{2}\times n_h}_{Higgsinos} + \underbrace{2}_{gauginos}\right] - \frac{1}{3}\left[\frac{1}{2}\times n_h\right] \Rightarrow$$

$$\boxed{b_2^{'} = \frac{3}{2}} \tag{C.21}$$

• For $b_3^{''}$ we have ($n_g = 3$) :

$$\boxed{b_3^{''} = b_3^{'}} \tag{C.22}$$

C.1.2.1 Extensions of the MSSM

In this section, we will extend the MSSM spectrum by introducing extra vector-like pairs (VP) like $\mathbf{5}-\bar{\mathbf{5}}$'s. We already know that a $\bar{\mathbf{5}}$ contains (d^c, L) or (if it's a Higgs $\bar{\mathbf{5}}$ then $(\bar{D}, H_d)$) and the $\mathbf{5}$ contains $(d, \bar{L})$ or (if it's a Higgs $\mathbf{5}$ then (D, H_u). Our work is to find how these VP contribute to the beta functions. Let us first consider the scenario of an extra $\mathbf{5_H}$:
• For b_1 we have :

$$b_1 = b_1^{MSSM} - \underbrace{-\frac{2}{5}\left[3\times\left(\frac{1}{3}\right)^2\times n_{D'} + 2\times\left(\frac{1}{2}\right)^2\times n_{h'}\right]}_{fermionic\ cotribution} \underbrace{-\frac{1}{5}\left[3\times\left(\frac{1}{3}\right)^2\times n_{D'} + 2\times\left(\frac{1}{2}\right)^2\times n_{h'}\right]}_{bosonic\ cotribution} \Rightarrow$$

$$b_1 = b_1^{MSSM} - \frac{3}{5}\left(\frac{1}{3}\times n_{D'} + \frac{1}{2}\times n_{h'}\right) \tag{C.23}$$

and for complete $\mathbf{5}$'s we have $n_{h'} = n_{D'} = n_5$, so we obtain :

$$\boxed{b_1 = b_1^{MSSM} + \frac{n_5}{2}} \tag{C.24}$$

Similarly for the rest beta functions we obtain the:

$$\boxed{b_2 = b_2^{MSSM} + \frac{n_5}{2}} \tag{C.25}$$

and

$$\boxed{b_3 = b_3^{MSSM} + \frac{n_5}{2}} \tag{C.26}$$

Now, we consider the contribution from the $\bar{\mathbf{5}}$. We easily can see that it contributes to each beta function a term $\dfrac{n_{\bar{5}}}{2}$. So, in the case of one VP, we take :

$$\boxed{b_1 = b_1^{MSSM} + 1} \quad \boxed{b_2 = b_2^{MSSM} + 1} \quad \boxed{b_3 = b_3^{MSSM} + 1} \tag{C.27}$$

In this point we generalize:
When we have complete $\mathbf{5}$ and $\bar{\mathbf{5}}$'s in vector pairs, the beta coefficients receive a common shift

$$b_i = b_i^{MSSM} + n_v \tag{C.28}$$

where n_v is the number of extra vector pairs.
An interesting case occurs when we consider 3 VP. Using the above relations we obtain :

$$b_1 = -\frac{33}{5} - 3 = -\frac{48}{5}, \quad b_2 = -1 - 3 = -4, \quad b_3 = 3 - 3 = 0. \tag{C.29}$$

We notice that b_3 vanish!.

C.2 Yukawa couplings

First, we write down the fields of the theory, so we have :

$$H = \begin{pmatrix} h^0 \\ h^+ \end{pmatrix} \ , \ Q = \begin{pmatrix} u_1 & d_1 \\ u_2 & d_2 \\ u_3 & d_3 \end{pmatrix} \ , \ \bar{H} = \begin{pmatrix} \bar{h}^- \\ \bar{h}^0 \end{pmatrix} \ , \ L = \begin{pmatrix} \nu \\ e \end{pmatrix}$$

$$u^c_{\underbrace{1,2,3}_{color}} \ , \ d^c_{\underbrace{1,2,3}_{color}} \ , \ e^c \ , \ S \tag{C.30}$$

Let us now write the invariant terms of the Lagrangian with the Yukawa couplings. We have :

$$\lambda_t H^a Q^{bi} u_i^c \to \lambda_t \left(h^0 u_i u_i^c \ , \ h^+ d_i u_i^c\right)$$

$$\lambda_b \bar{H}^a Q^{bi} d_i^c \to \lambda_b \left(\bar{h}^0 d_i d_i^c \ , \ \bar{h}^- u_i d_i^c\right)$$

$$\lambda_\tau \bar{H}^a L^b e^c \to \lambda_\tau \left(\bar{h}^0 e e^c \ , \ \bar{h}^- \nu e^c\right)$$

$$\lambda_s S \bar{H} H \to \lambda_s \left(S h^0 \bar{h}^0 \ , \ S h^+ h^-\right) \tag{C.31}$$

To keep up with the calculations we number all the fields, so we obtain :

$$\underbrace{\underbrace{h^0, h^+}_{(1,2)}, \underbrace{h^-, \bar{h}^0}_{(3,4)}, \underbrace{u_1, u_2, u_3}_{(5,6,7)}, \underbrace{d_1, d_2, d_3}_{(8,9,10)}, \underbrace{u^c_{1,2,3}}_{(11,12,13)} \ , \ \underbrace{d^c_{1,2,3}}_{(14,15,16)} \ , \underbrace{\nu}_{(17)}, \underbrace{e}_{(18)}, \underbrace{e^c}_{(19)}, \underbrace{S}_{(20)}}_{\phi^i}$$

The potential is of the form :

$$\boxed{W \sim \lambda_{i\,j\,k}\phi^i\phi^j\phi^k} \tag{C.32}$$

and we have the relation :

$$\Lambda^n_m = \lambda^{nij}\lambda_{mij} \to \lambda_{nij}\lambda_{mij} \tag{C.33}$$

Having said this, we take the equation for the calculation of the Yukawa couplings :

$$\frac{d}{dt}\lambda_{ijk} = \frac{1}{32\pi^2}\left\{\left(\Lambda_i^{i'}\lambda_{i'jk} + \Lambda_j^{j'}\lambda_{ij'k} + \Lambda_k^{k'}\lambda_{ijk'}\right) - \lambda_{ijk}\,(\text{Gauge Part})\right\} \tag{C.34}$$

We write down all the possible terms for λ's :

$$\lambda_t \to \lambda_{1,5,11}|\lambda_{1,6,12}|\lambda_{1,7,13}|\lambda_{2,8,11}|\lambda_{2,9,12}|\lambda_{2,10,13} \tag{C.35}$$

$$\lambda_b \to \lambda_{3,8,14}|\lambda_{3,9,15}|\lambda_{3,10,16}|\lambda_{4,5,14}|\lambda_{4,6,15}|\lambda_{4,7,16} \tag{C.36}$$

$$\lambda_\tau \to \lambda_{3,18,19}|\lambda_{4,17,19} \tag{C.37}$$

$$\lambda_S \to \lambda_{1,3,20}|\lambda_{2,4,20} \tag{C.38}$$

- For the top Yukawa we have :

$$\frac{d\lambda_t}{dt} = \frac{1}{32\pi^2}\left\{\left(\Lambda^1{}_1\lambda_{1\,j\,k} + \Lambda^5{}_5\lambda_{i\,5\,k} + \Lambda^{11}{}_{11}\lambda_{i\,j\,11}\right)\right\}$$

We calculate each term individual :

$$\Lambda^1{}_1 = \lambda_{1\,j\,k}\lambda_{1\,j\,k} = (\lambda_{1\,5\,11})^2 + (\lambda_{1\,6\,12})^2 + (\lambda_{1\,7\,13})^2 + (\lambda_{1\,3\,10})^2 = 3\lambda_t^2 + \lambda_S^2$$

$$\Lambda^5{}_5 = \lambda_{i\,5\,k}\lambda_{i\,5\,k} = (\lambda_{1\,5\,11})^2 + (\lambda_{4\,5\,14})^2 = \lambda_t^2 + \lambda_b^2$$

$$\Lambda^{11}{}_{11} = \lambda_{i\,j\,11}\lambda_{i\,j\,11} = (\lambda_{1\,5\,11})^2 + (\lambda_{2\,8\,11})^2 = 2\lambda_t^2$$

So

$$\frac{d\lambda_t}{dt} \propto \left(6\lambda_t^2 + \lambda_S^2 + \lambda_b^2 + \text{Gauge Part}\right)\lambda_t \tag{C.39}$$

- For the bottom Yukawa we have :

$$\frac{d\lambda_b}{dt} = \frac{1}{32\pi^2}\left\{\left(\Lambda^3{}_3\lambda_{3\,j\,k} + \Lambda^8{}_8\lambda_{i\,8\,k} + \Lambda^{14}{}_{14}\lambda_{i\,j\,14}\right)\right\}$$

We calculate each term individually:

$$\Lambda^3{}_3 = \lambda_{3\,j\,k}\lambda_{3\,j\,k} = (\lambda_{3\,9\,15})^2 + (\lambda_{3\,10\,16})^2 + (\lambda_{3\,18\,19})^2 + (\lambda_{1\,3\,20})^2 = 3\lambda_b^2 + \lambda_\tau^2 + \lambda_S^2$$

$$\Lambda^8{}_8 = \lambda_{i\,8\,k}\lambda_{i\,8\,k} = (\lambda_{2\,8\,11})^2 + (\lambda_{3\,8\,14})^2 = \lambda_t^2 + \lambda_b^2$$

$$\Lambda^{14}{}_{14} = \lambda_{i\,j\,14}\lambda_{i\,j\,14} = (\lambda_{3\,8\,14})^2 + (\lambda_{4\,5\,14})^2 = 2\lambda_b^2$$

So

$$\frac{d\lambda_b}{dt} \propto \left(6\lambda_b^2 + \lambda_t^2 + \lambda_\tau^2 + \lambda_S^2 + \text{Gauge Part}\right)\lambda_b \tag{C.40}$$

• For the tau Yukawa we have :

$$\frac{\tau\lambda_b}{dt} = \frac{1}{32\pi^2}\left\{\left(\Lambda^3{}_3\lambda_{3\,j\,k} + \Lambda^{18}{}_{18}\lambda_{i\,18\,k} + \Lambda^{19}{}_{19}\lambda_{i\,j\,19}\right)\right\}$$

We calculate each term individual :

$$\Lambda^3{}_3 = 3\lambda_b^2 + \lambda_\tau^2 + \lambda_S^2$$

$$\Lambda^{18}{}_{18} = \lambda_{i\,18\,k}\lambda_{i\,18\,k} = (\lambda_{3\,18\,19})^2 = \lambda_\tau^2$$

$$\Lambda^{19}{}_{19} = \lambda_{i\,j\,19}\lambda_{i\,j\,19} = (\lambda_{3\,18\,19})^2 + (\lambda_{4\,17\,19})^2 = 2\lambda_\tau^2$$

So

$$\frac{d\lambda_\tau}{dt} \propto \left(4\lambda_\tau^2 + 3\lambda_b^2 + \lambda_S^2 + \text{Gauge Part}\right)\lambda_\tau \tag{C.41}$$

• For the S Yukawa we have :

$$\frac{d\lambda_b}{dt} = \frac{1}{32\pi^2}\left\{\left(\Lambda^1{}_1\lambda_{1\,j\,k} + \Lambda^3{}_3\lambda_{i\,3\,k} + \Lambda^{20}{}_{20}\lambda_{i\,j\,20}\right)\right\}$$

We calculate each term individual :

$$\Lambda^1{}_1 = 3\lambda_t^2 + \lambda_S^2$$

$$\Lambda^3{}_3 = 3\lambda_b^2 + \lambda_\tau^2 + \lambda_S^2$$

$$\Lambda^{20}{}_{20} = \lambda_{i\,j\,20}\lambda_{i\,j\,20} = (\lambda_{1\,3\,20})^2 + (\lambda_{2\,4\,20})^2 = 2\lambda_S^2$$

So

$$\frac{d\lambda_S}{dt} \propto \left(4\lambda_S^2 + 3\lambda_b^2 + 3\lambda_t^2 + \lambda_\tau^2 + \text{Gauge Part}\right)\lambda_S \tag{C.42}$$

For the sake of completeness, we should also include the contributions from D,$\bar{D}$ and L,$\bar{L}$ fields. To do so, we first need to know the couplings. For the term $\lambda_D S D\bar{D}$ we have :

$$S(D_i\bar{D}_i)_{i=1,2,3} \to S(D_1\bar{D}_1 + D_2\bar{D}_2 + D_3\bar{D}_3)$$

and for L,$\bar{L}$ we have $\lambda_L SL$ and $\lambda_L S\bar{L}$ respectively. We note that these fields are numbered as follows:

$$\underbrace{D_{1,2,3}}_{(21,22,23)} \quad , \quad \underbrace{\bar{D}_{1,2,3}}_{(24,25,26)} \quad , \underbrace{L \to (\nu_L, e_L)}_{(27,28)} \text{ and } \underbrace{\bar{L} \to \bar{\nu}_L, \bar{e}_L}_{(29,30)}$$

Having said these, we take all the possible terms for the D and $\bar{D}$:

$$\lambda_{20,21,24}|\lambda_{20,22,25}|\lambda_{20,23,26} \tag{C.43}$$

and for the L and $\bar{L}$:

$$\lambda_{20,27,28}|\lambda_{20,29,30} \tag{C.44}$$

• For the D Yukawa we have :

$$\frac{d\lambda_D}{dt} = \frac{1}{32\pi^2}\left\{\left(\Lambda^{20}{}_{20}\lambda_{20\;j\;k} + \Lambda^{21}{}_{21}\lambda_{i\;21\;k} + \Lambda^{24}{}_{24}\lambda_{i\;j\;24}\right)\right\}$$

We calculate each term individual :

$$\Lambda^{20}{}_{20} = \lambda_{20\;j\;k}\lambda_{20\;j\;k} = (\lambda_{20\;21\;24})^2 + (\lambda_{20\;22\;25})^2 + (\lambda_{20\;23\;26})^2 + (\lambda_{20\;1\;3})^2 + (\lambda_{20\;2\;4})^2 \\ +(\lambda_{20\;27\;28})^2 + (\lambda_{20\;29\;30})^2 = 3\lambda_D^2 + 2\lambda_S^2 + 2\lambda_L^2$$

$$\Lambda^{21}{}_{21} = \lambda_{i\;21\;k}\lambda_{i\;21\;k} = (\lambda_{20\;21\;24})^2 = \lambda_D^2$$

$$\Lambda^{24}{}_{24} = \lambda_{i\;j\;24}\lambda_{i\;j\;24} = (\lambda_{20\;21\;24})^2 = \lambda_D^2$$

So

$$\frac{d\lambda_D}{dt} \propto \left(5\lambda_D^2 + 2\lambda_S^2 + 2\lambda_L^2 + \text{Gauge Part}\right)\lambda_D \tag{C.45}$$

• Finally for the L Yukawa we have :

$$\frac{d\lambda_L}{dt} = \frac{1}{32\pi^2}\left\{\left(\Lambda^{20}{}_{20}\lambda_{20\;j\;k} + \Lambda^{27}{}_{27}\lambda_{i\;27\;k} + \Lambda^{28}{}_{28}\lambda_{i\;j\;28}\right)\right\}$$

We calculate each term individual :

$$\Lambda^{20}{}_{20} = \lambda_{20\;j\;k}\lambda_{20\;j\;k} = (\lambda_{20\;21\;24})^2 + (\lambda_{20\;22\;25})^2 + (\lambda_{20\;23\;26})^2 + (\lambda_{20\;1\;3})^2 + (\lambda_{20\;2\;4})^2 \\ +(\lambda_{20\;27\;28})^2 + (\lambda_{20\;29\;30})^2 = 3\lambda_D^2 + 2\lambda_S^2 + 2\lambda_L^2$$

$$\Lambda^{27}{}_{27} = \lambda_{i\;27\;k}\lambda_{i\;27\;k} = (\lambda_{20\;27\;28})^2 = \lambda_L^2$$

$$\Lambda^{28}{}_{28} = \lambda_{i\;j\;28}\lambda_{i\;j\;28} = (\lambda_{20\;27\;28})^2 = \lambda_L^2$$

So

$$\frac{d\lambda_L}{dt} \propto \left(3\lambda_D^2 + 2\lambda_S^2 + 4\lambda_L^2 + \text{Gauge Part}\right)\lambda_L \tag{C.46}$$

C.2.1 Gauge Part for the Top Yukawa

When we plot the RGE's we are also interested to see the running of the top Yukawa since it has the biggest contribution among the other Yukawas. Having said these we write down the general equations for the gauge part of the beta functions in the MSSM case :

$$\text{Gauge Part} = -4g_\alpha^2 C_\alpha(i)\delta_j^i \tag{C.47}$$

where

$$C_3(i) = \begin{cases} 4/3 & \text{for } \Phi_i = \mathrm{Q}, u^c, d^c \\ 0 & \text{for } \Phi_i = \mathrm{L}, e^c, H_u, H_d \end{cases} \tag{C.48}$$

$$C_2(i) = \begin{cases} 3/4 & \text{for } \Phi_i = \mathrm{Q}, \mathrm{L}, H_u, H_d \\ 0 & \text{for } \Phi_i = u^c, d^c, e^c \end{cases} \tag{C.49}$$

$$C_1(i) = 3Y_i^2/5 \;\; \text{for each } \Phi_i \text{ with weak hypercharge } Y_i. \tag{C.50}$$

Using the above we obtain the Gauge Part for the top Yukawa in the MSSM :

$$\frac{1}{32\pi^2}\left[-4g_\alpha^2 C_\alpha(i)\delta_j^i\right] =$$

$$\frac{1}{32\pi^2}\left\{-4g_3^2C_3(Q) - 4g_3^2C_3(u^c) - 4g_2^2C_2(Q) - 4g_2^2C_2(H_u) - 4g_1^2\frac{3}{5}\left[\underbrace{\left(\frac{1}{6}\right)^2}_{Y_u^2} + \underbrace{\left(\frac{1}{2}\right)^2}_{Y_{Hu}^2} + \underbrace{\left(\frac{2}{3}\right)^2}_{Y_{u^c}^2}\right]\right\} =$$

$$\frac{1}{32\pi^2}\left(-\frac{32}{3}g_3^2 - 6g_2^2 - \frac{26}{15}g_1^2\right)$$

Taking in account these results we have the final form of the top Yukawa in 1-loop in the MSSM case :

$$\frac{d\lambda_t}{dt} = \frac{1}{32\pi^2}\left(6\lambda_t^2 + \lambda_S^2 + \lambda_b^2 - \frac{32}{3}g_3^2 - 6g_2^2 - \frac{26}{15}g_1^2\right)\lambda_t \tag{C.51}$$

C.3 NMSSM case-Plots

Making use of the Mathematica package we obtained the various plots for the case of the NMSSM. First, we run the RGE's in the range ($m_t = 173,34$ GeV -1 TeV) :

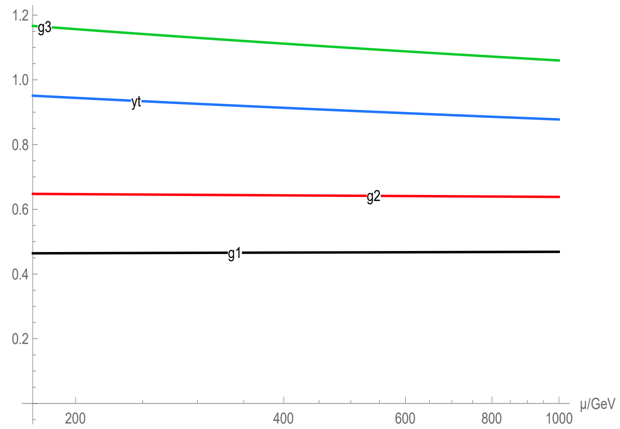

and then we plot them in the range (1 TeV - $M_{GUT} \sim 1 \times 10^{16}$), so we obtain :

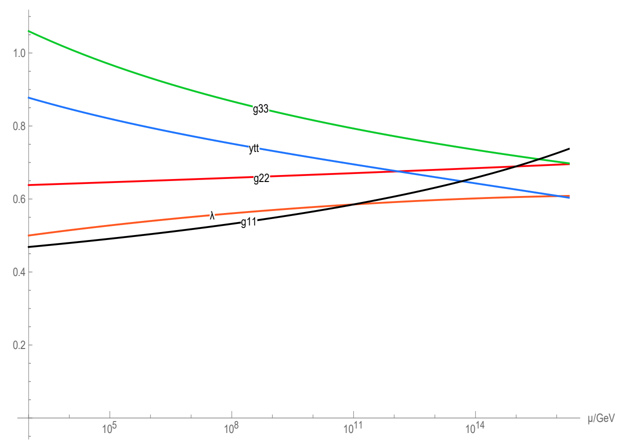

Finally, we can merge the two plots to have the whole picture of the running of the couplings in the NMSSM case. The graph takes the final form :

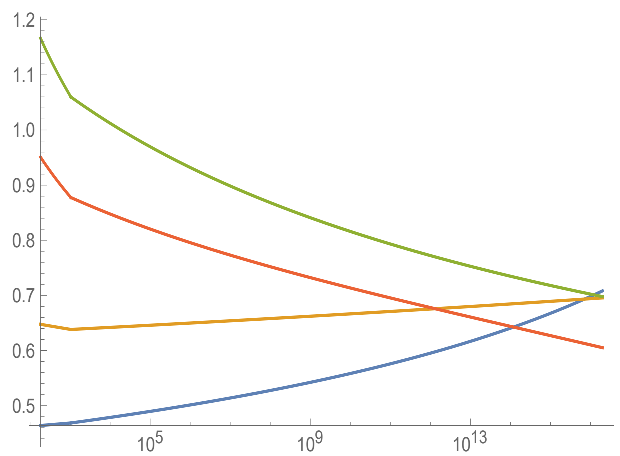

C.4 The Case of SU(5)× U(1)

The spectrum of the model is defined as :

$$16_1 \to \underbrace{10_{-1}}_{Q,u^c,e^c} + \underbrace{\bar{5}_3}_{d^c,L} + \underbrace{1_{-5}}_{\nu^c}$$

$$10_{-2} \to \underbrace{5_2 + \bar{5}_{-2}}_{2\ Higgs}$$

$$1_4 \to \underbrace{24_0}_{\Sigma} \tag{C.52}$$

Plus, we have a pair of ϕ,$\bar{\phi}$ coming from the 126,$\overline{126}$ representations of SO(10).
For the RGEs of the model, we have :

$$\underbrace{SU(5)}_{b_1,b_2,b_3} \times \underbrace{U(1)_\chi}_{b_\chi}$$

where b_1, b_2, b_3 are the usual RGE's of SM and b_χ is an extra RGE which we have to calculate. First, we make use of the relation :

$$\mathrm{Tr}\left(Q_\chi^2\right) = 3 \tag{C.53}$$

combined with the relation :

$$Q_\chi = c\widetilde{Q_\chi} \tag{C.54}$$

to find the renormalization constant c. Having said these, we obtain :

$$c^2\left[10 \times (-1)^2 + 5 \times 3^2 + 1 \times (-5)^2 + 5 \times 2^2 + 5 \times (-2)^2 + 0\right] = 3 \Rightarrow$$

$$c^2 120 = 3 \Rightarrow$$

$$\boxed{c = \frac{1}{\sqrt{40}}} \tag{C.55}$$

So, the beta function of χ is :

$$b_\chi = c^2 Y_\chi^2 = c^2 \left\{ \left[\underbrace{2 \times 3 \times (-1)^2}_{Q} + \underbrace{3 \times (3)^2}_{d^c} + \underbrace{3 \times (-1)^2}_{u^c} + \underbrace{2 \times (3)^2}_{L} + \underbrace{1 \times (-5)^2}_{\nu^c} + \underbrace{1 \times (-1)^2}_{e^c} \right] \times 3 \right.$$

$$\left. \underbrace{2 \times (2)^2 + 2 \times (-2)^2}_{2\ Higgs} + \underbrace{2 \times (10)^2}_{\phi,\bar{\phi}} \right\} \Rightarrow$$

$$b_\chi = \frac{1}{40} 456 \Rightarrow$$

$$\boxed{b_\chi = \frac{57}{5}} \tag{C.56}$$

To run the plots we have to take into consideration 2 regions. In the first region $GUT - M_{neutrino}$[2] the beta functions are unchanged. In the region M_{neut}-$M_{SUSY} \simeq 1$TeV b_χ is changed in a way :

$$b'_\chi = \frac{57}{5} - \frac{3\times 25}{40} - \frac{200}{40} = \frac{57}{5} - \frac{275}{40} \Rightarrow$$

$$\boxed{b'\chi = \frac{35}{8}} \tag{C.57}$$

For the top Yukawa we have also a contribution coming from the $U(1)_\chi$. So, equation (C.51) takes the form :

$$\frac{d\lambda_t}{dt} = \frac{1}{32\pi^2}\left(6\lambda_t^2 + \lambda_S^2 + \lambda_b^2 - \frac{32}{3}g_3^2 - 6g_2^2 - \frac{26}{15}g_1^2 - \frac{72}{5}g_\chi^2\right)\lambda_t \tag{C.58}$$

Now, we run in Mathematica the Plot of RGE's for the various regions and we obtain:
In the range M_{GUT}-M_{neut} :

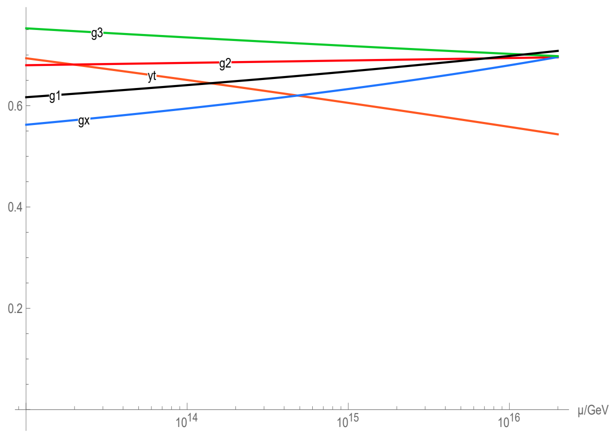

and then we plot them in the range M_{neut}-M_{SUSY}, so we obtain :

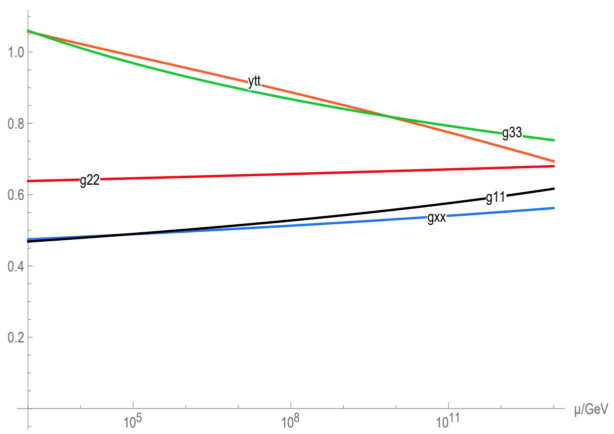

[2] $M_{neutrino} \simeq 1\times 10^{13}$ is the energy scale where we throw out the neutrinos and the ϕ and $\bar{\phi}$

Finally, we can merge the two plots to have the whole picture of the running of the couplings in the NMSSM case. The graph takes the final form :

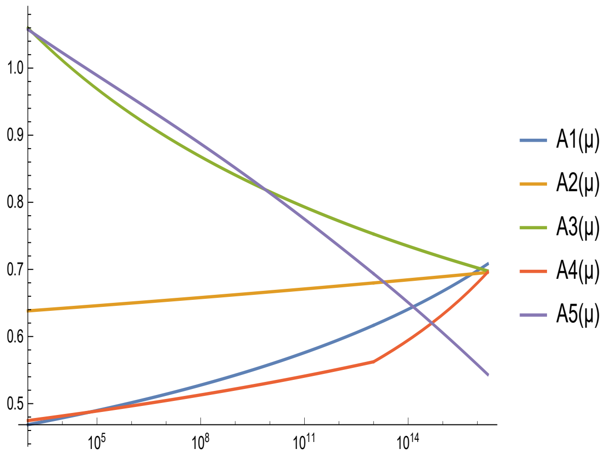

Appendix D

Model Building

D.1 Anomaly Conditions: Analytic expressions

Regarding the overall factors, in our calculations, we find that $\mathscr{A}_{221} = \mathscr{A}_{331} = \mathscr{A}_{YY1} \equiv \mathscr{A}$.

$$\begin{aligned}
\mathscr{A} &= \left(30\sqrt{3}c_1 + 15\sqrt{6}c_2 + 9\sqrt{10}c_3\right) m_1 + \left(-60\sqrt{3}c_1 + 15\sqrt{6}c_2 + 9\sqrt{10}c_3\right) m_2 + \left(9\sqrt{10}c_3 - 45\sqrt{6}c_2\right) m_3 \\
&- 36\sqrt{10}c_3 m_4 + \left(-20\sqrt{3}c_1 - 10\sqrt{6}c_2 - 6\sqrt{10}c_3\right) M_1 + \left(10\sqrt{3}c_1 - 10\sqrt{6}c_2 - 6\sqrt{10}c_3\right) M_2 \\
&+ \left(-10\sqrt{3}c_1 + 10\sqrt{6}c_2 - 6\sqrt{10}c_3\right) M_3 + \left(-10\sqrt{3}c_1 - 5\sqrt{6}c_2 + 9\sqrt{10}c_3\right) M_4 \\
&+ \left(20\sqrt{3}c_1 + 10\sqrt{6}c_2 - 6\sqrt{10}c_3\right) M_5 + \left(20\sqrt{3}c_1 - 5\sqrt{6}c_2 + 9\sqrt{10}c_3\right) M_6 + \left(15\sqrt{6}c_2 + 9\sqrt{10}c_3\right) M_7 \\
&+ 30\sqrt{3}c_1 N_7 + \left(10\sqrt{3}c_1 + 20\sqrt{6}c_2\right) N_8 + \left(10\sqrt{3}c_1 + 5\sqrt{6}c_2 + 15\sqrt{10}c_3\right) N_9 \, .
\end{aligned} \tag{D.1}$$

Regarding the mixed $\mathscr{A}_{Y11}$ anomaly, we can express it as follows:

$$\begin{aligned}
\mathscr{A}_{Y11} &= \frac{3}{2}\sqrt{\frac{3}{5}} c_1^2 N_7 + \frac{1}{30}\left(\sqrt{15}c_1^2 + 4\sqrt{30}c_2 c_1 + 8\sqrt{15}c_2^2\right) N_8 \\
&+ \frac{1}{60}\left(2\sqrt{15}c_1^2 + 2\sqrt{30}c_2 c_1 + 30\sqrt{2}c_3 c_1 + \sqrt{15}c_2^2 + 15\sqrt{15}c_3^2 + 30 c_2 c_3\right) N_9
\end{aligned}$$

The expression arising from the $U(1)'$-gravity anomaly is as follows:

$$\begin{aligned}
\mathscr{A}_G &= \left(20\sqrt{3}c_1 + 10\sqrt{6}c_2 + 6\sqrt{10}c_3\right) m_1 + \left(-40\sqrt{3}c_1 + 10\sqrt{6}c_2 + 6\sqrt{10}c_3\right) m_2 + \left(6\sqrt{10}c_3 - 30\sqrt{6}c_2\right) m_3 \\
&- 24\sqrt{10}c_3 m_4 + \left(-20\sqrt{3}c_1 - 10\sqrt{6}c_2 - 6\sqrt{10}c_3\right) M_1 + \left(10\sqrt{3}c_1 - 10\sqrt{6}c_2 - 6\sqrt{10}c_3\right) M_2 \\
&+ \left(-10\sqrt{3}c_1 + 10\sqrt{6}c_2 - 6\sqrt{10}c_3\right) M_3 + \left(-10\sqrt{3}c_1 - 5\sqrt{6}c_2 + 9\sqrt{10}c_3\right) M_4 \\
&+ \left(20\sqrt{3}c_1 + 10\sqrt{6}c_2 - 6\sqrt{10}c_3\right) M_5 + \left(20\sqrt{3}c_1 - 5\sqrt{6}c_2 + 9\sqrt{10}c_3\right) M_6 + \left(15\sqrt{6}c_2 + 9\sqrt{10}c_3\right) M_7 \\
&+ 24\sqrt{3}c_1 N_7 + \left(8\sqrt{3}c_1 + 16\sqrt{6}c_2\right) N_8 + \left(8\sqrt{3}c_1 + 4\sqrt{6}c_2 + 12\sqrt{10}c_3\right) N_9 + \sum_{i\neq j} M_{ij} Q'_{ij} \, .
\end{aligned} \tag{D.2}$$

and the pure cubic $U(1)'$ anomaly is:

$$
\begin{aligned}
\mathscr{A}_{111} \;=\;& \left(20\sqrt{3}c_1^3+6\left(5\sqrt{6}c_2+3\sqrt{10}c_3\right)c_1^2+6\left(5\sqrt{3}c_2^2+6\sqrt{5}c_3c_2+3\sqrt{3}c_3^2\right)c_1\right.\\
+\;& \left.5\sqrt{6}c_2^3+9\sqrt{\frac{2}{5}}c_3^3+9\sqrt{6}c_2c_3^2+9\sqrt{10}c_2^2c_3\right)m_1\\
+\;& \left(-160\sqrt{3}c_1^3+24\left(5\sqrt{6}c_2+3\sqrt{10}c_3\right)c_1^2-12\left(5\sqrt{3}c_2^2+6\sqrt{5}c_3c_2+3\sqrt{3}c_3^2\right)c_1\right.\\
+\;& \left.5\sqrt{6}c_2^3+9\sqrt{\frac{2}{5}}c_3^3+9\sqrt{6}c_2c_3^2+9\sqrt{10}c_2^2c_3\right)m_2\\
-\;& 9\left(15\sqrt{6}c_2^3-9\sqrt{10}c_3c_2^2+3\sqrt{6}c_3^2c_2-\sqrt{\frac{2}{5}}c_3^3\right)m_3-576\sqrt{\frac{2}{5}}c_3^2m_4\\
-\;& \left(80\sqrt{3}c_1^3+24\left(5\sqrt{6}c_2+3\sqrt{10}c_3\right)c_1^2+24\left(5\sqrt{3}c_2^2+6\sqrt{5}c_3c_2+3\sqrt{3}c_3^2\right)c_1\right.\\
+\;& \left.20\sqrt{6}c_2^3+9\sqrt{10}c_3^3+36\sqrt{6}c_2c_3^2+36\sqrt{10}c_2^2c_3\right)M_0\\
+\;& \left(10\sqrt{3}c_1^3-6\left(5\sqrt{6}c_2+3\sqrt{10}c_3\right)c_1^2+12\left(5\sqrt{3}c_2^2+6\sqrt{5}c_3c_2+3\sqrt{3}c_3^2\right)c_1\right.\\
-\;& \left.20\sqrt{6}c_2^3-36\sqrt{10}c_3c_2^2-36\sqrt{6}c_3^2c_2-36\sqrt{\frac{2}{5}}c_3^3\right)M_1\\
-\;& \left(10\sqrt{3}c_1^3+6\left(5\sqrt{6}c_2-3\sqrt{10}c_3\right)c_1^2-12\left(5\sqrt{3}c_2^2-6\sqrt{5}c_3c_2+3\sqrt{3}c_3^2\right)c_1\right.\\
+\;& \left.20\sqrt{6}c_2^3-36\sqrt{\frac{2}{5}}c_3^3+36\sqrt{6}c_2c_3^2-36\sqrt{10}c_2^2c_3\right)M_2\\
-\;& \left(10\sqrt{3}c_1^3-3\left(5\sqrt{6}c_2-9\sqrt{10}c_3\right)c_1^2-3\left(5\sqrt{3}c_2^2-18\sqrt{5}c_3c_2+27\sqrt{3}c_3^2\right)c_1\right.\\
-\;& \left.5\sqrt{\frac{3}{2}}c_2^3+\frac{243c_3^3}{\sqrt{10}}-81\sqrt{\frac{3}{2}}c_2c_3^2+27\sqrt{\frac{5}{2}}c_2^2c_3\right)M_3\\
+\;& \left(80\sqrt{3}c_1^3+20\sqrt{6}c_2^3-36\sqrt{\frac{2}{5}}c_3^3+36\sqrt{6}c_2c_3^2-36\sqrt{10}c_2^2c_3\right.\\
+\;& \left.24\left(5\sqrt{6}c_2-3\sqrt{10}c_3\right)c_1^2+24\left(5\sqrt{3}c_2^2-6\sqrt{5}c_3c_2+3\sqrt{3}c_3^2\right)c_1\right)M_4\\
+\;& \left(80\sqrt{3}c_1^3-12\left(5\sqrt{6}c_2-9\sqrt{10}c_3\right)c_1^2+6\left(5\sqrt{3}c_2^2-18\sqrt{5}c_3c_2+27\sqrt{3}c_3^2\right)c_1\right.\\
-\;& \left.5\sqrt{\frac{3}{2}}c_2^3+\frac{243c_3^3}{\sqrt{10}}-81\sqrt{\frac{3}{2}}c_2c_3^2+27\sqrt{\frac{5}{2}}c_2^2c_3\right)M_5\\
+\;& \frac{27}{10}\left(25\sqrt{6}c_2^3+45\sqrt{10}c_3c_2^2+45\sqrt{6}c_3^2c_2+9\sqrt{10}c_3^3\right)M_6+\sum_{i\neq j}M_{ij}Q'^{\,3}_{ij}
\end{aligned}
\tag{D.3}
$$

The sums in (D.2) and (D.3) represents the contribution from the singlets.

D.2 List of models

In this appendix, we provide an overview of all the flux solutions that meet the criteria for an MSSM spectrum, including the corresponding $U(1)'$ charges and information about the singlet spectrum.

For each presented solution with a specific value of c_i, there is a corresponding solution obtained by replacing c_i with $-c_i$ while maintaining the anomaly cancellation conditions. Therefore, there are also models with charges that undergo $Q' \rightarrow -Q'$.

As mentioned in the main text, there are a total of fifty-four solutions, categorized into four classes: Class A, B, C, and D.

Class A

This class encompasses six models, and the flux data solutions, along with the resulting c_i coefficients, are detailed in Table 4.5 in the main text. The corresponding models defined by these solutions, along with their $U(1)'$ charges, are provided in Table 4.6.

In this section, we exclusively present the singlet spectrum for Class A models. It is noteworthy that in this particular class, singlets are arranged in pairs, meaning that $M_{ij} = M_{ji}$. Consequently, a minimal singlet spectrum scenario implies $M_{ij} = M_{ji} = 1$. The singlet charges Q'_{ij} for each model can be found in Table D.1 below.

Class A	Charges					
Models	Q'_{13}	Q'_{14}	Q'_{15}	Q'_{34}	Q'_{35}	Q'_{45}
A1, **A6**	0	$\frac{1}{2}$	$-\frac{1}{2}$	$\frac{1}{2}$	$-\frac{1}{2}$	-1
A2, **A5**	$\frac{1}{2}$	0	$-\frac{1}{2}$	$-\frac{1}{2}$	-1	$-\frac{1}{2}$
A3, **A4**	$-\frac{1}{2}$	$\frac{1}{2}$	0	1	$\frac{1}{2}$	$-\frac{1}{2}$

Table D.1: Singlets charges of Class A models.

Class B

This Class of models consists of twenty-four solutions. All the relevant data characterized the models organized in three tables. In particular, Table D.2 contains the flux data of the models along with the corresponding c_i-solutions, as those have been extracted from the solution of the anomaly cancellation conditions. In Table D.3, the $U(1)'$ charges of the matter curves are given. Finally, details about the singlet spectrum are presented in Table D.4.

Class B	Flux data														c_i coefficients		
Model	m_1	m_2	m_3	m_4	M_1	M_2	M_3	M_4	M_5	M_6	M_7	N_7	N_8	N_9	c_1	c_2	c_3
B1	1	0	1	1	0	-1	0	0	0	-1	-1	0	0	1	$-\frac{\sqrt{5}}{3}$	$-\frac{\sqrt{\frac{5}{2}}}{3}$	$\frac{1}{\sqrt{6}}$
B2	1	0	1	1	0	0	-1	0	0	-1	-1	0	0	1	$-\frac{\sqrt{5}}{3}$	$-\frac{\sqrt{\frac{5}{2}}}{3}$	$\frac{1}{\sqrt{6}}$
B3	1	0	1	1	0	0	0	-1	-1	0	-1	0	1	0	$\frac{\sqrt{5}}{3}$	$-\frac{\sqrt{\frac{5}{2}}}{6}$	$\frac{\sqrt{\frac{3}{2}}}{2}$
B4	1	0	1	1	0	0	0	0	-2	0	-1	0	1	0	$\frac{\sqrt{5}}{3}$	$-\frac{\sqrt{\frac{5}{2}}}{6}$	$\frac{\sqrt{\frac{3}{2}}}{2}$
B5	1	0	1	1	0	0	0	0	-1	0	-2	0	1	0	$\frac{\sqrt{5}}{3}$	$-\frac{\sqrt{\frac{5}{2}}}{6}$	$\frac{\sqrt{\frac{3}{2}}}{2}$
B6	1	0	1	1	0	0	0	0	0	-2	-1	0	0	1	$-\frac{\sqrt{5}}{3}$	$-\frac{\sqrt{\frac{5}{2}}}{3}$	$\frac{1}{\sqrt{6}}$
B7	1	0	1	1	0	-1	0	0	-1	0	-1	0	1	0	$\frac{\sqrt{5}}{3}$	$-\frac{\sqrt{\frac{5}{2}}}{6}$	$\frac{\sqrt{\frac{3}{2}}}{2}$
B8	1	0	1	1	0	0	0	0	0	-1	-2	0	0	1	$-\frac{\sqrt{5}}{3}$	$-\frac{\sqrt{\frac{5}{2}}}{3}$	$\frac{1}{\sqrt{6}}$
B9	1	1	0	1	0	-1	0	0	0	-1	-1	0	0	1	$-\frac{\sqrt{5}}{3}$	$-\frac{\sqrt{\frac{5}{2}}}{3}$	$\frac{1}{\sqrt{6}}$
B10	1	1	0	1	0	0	-1	0	-1	-1	0	1	0	0	0	$-\frac{\sqrt{\frac{5}{2}}}{2}$	$-\frac{\sqrt{\frac{3}{2}}}{2}$
B11	1	1	0	1	0	0	-1	0	0	-1	-1	0	0	1	$-\frac{\sqrt{5}}{3}$	$-\frac{\sqrt{\frac{5}{2}}}{3}$	$\frac{1}{\sqrt{6}}$
B12	1	1	0	1	0	0	0	-1	-1	-1	0	1	0	0	0	$-\frac{\sqrt{\frac{5}{2}}}{2}$	$-\frac{\sqrt{\frac{3}{2}}}{2}$
B13	1	1	0	1	0	0	0	0	-2	-1	0	1	0	0	0	$-\frac{\sqrt{\frac{5}{2}}}{2}$	$-\frac{\sqrt{\frac{3}{2}}}{2}$
B14	1	1	0	1	0	0	0	0	-1	-2	0	1	0	0	0	$-\frac{\sqrt{\frac{5}{2}}}{2}$	$-\frac{\sqrt{\frac{3}{2}}}{2}$
B15	1	1	0	1	0	0	0	0	0	-2	-1	0	0	1	$-\frac{\sqrt{5}}{3}$	$-\frac{\sqrt{\frac{5}{2}}}{3}$	$\frac{1}{\sqrt{6}}$
B16	1	1	0	1	0	0	0	0	0	-1	-2	0	0	1	$-\frac{\sqrt{5}}{3}$	$-\frac{\sqrt{\frac{5}{2}}}{3}$	$\frac{1}{\sqrt{6}}$
B17	1	1	1	0	0	-1	0	0	-1	0	-1	0	1	0	$\frac{\sqrt{5}}{3}$	$-\frac{\sqrt{\frac{5}{2}}}{6}$	$\frac{\sqrt{\frac{3}{2}}}{2}$
B18	1	1	1	0	0	0	-1	0	-1	-1	0	1	0	0	0	$-\frac{\sqrt{\frac{5}{2}}}{2}$	$-\frac{\sqrt{\frac{3}{2}}}{2}$
B19	1	1	1	0	0	0	0	-1	-1	-1	0	1	0	0	0	$-\frac{\sqrt{\frac{5}{2}}}{2}$	$-\frac{\sqrt{\frac{3}{2}}}{2}$
B20	1	1	1	0	0	0	0	-1	-1	0	-1	0	1	0	$\frac{\sqrt{5}}{3}$	$-\frac{\sqrt{\frac{5}{2}}}{6}$	$\frac{\sqrt{\frac{3}{2}}}{2}$
B21	1	1	1	0	0	0	0	0	-2	-1	0	1	0	0	0	$-\frac{\sqrt{\frac{5}{2}}}{2}$	$-\frac{\sqrt{\frac{3}{2}}}{2}$
B22	1	1	1	0	0	0	0	0	-2	0	-1	0	1	0	$\frac{\sqrt{5}}{3}$	$-\frac{\sqrt{\frac{5}{2}}}{6}$	$\frac{\sqrt{\frac{3}{2}}}{2}$
B23	1	1	1	0	0	0	0	0	-1	-2	0	1	0	0	0	$-\frac{\sqrt{\frac{5}{2}}}{2}$	$-\frac{\sqrt{\frac{3}{2}}}{2}$
B24	1	1	1	0	0	0	0	0	-1	0	-2	0	1	0	$\frac{\sqrt{5}}{3}$	$-\frac{\sqrt{\frac{5}{2}}}{6}$	$\frac{\sqrt{\frac{3}{2}}}{2}$

Table D.2: Class B models, flux data and the corresponding c_i-solutions.

Class B	Charges$\times\sqrt{15}$										
Models	Q'_{10_1}	Q'_{10_2}	Q'_{10_3}	Q'_{10_4}	Q'_{5_1}	Q'_{5_2}	Q'_{5_3}	Q'_{5_4}	Q'_{5_5}	Q'_{5_6}	Q'_{5_7}
B1, **B2**, **B6**, **B8**, **B9**, **B11**, **B15**, **B16**	-1	3/2	3/2	-1	2	-1/2	-1/2	2	-3	-1/2	-1/2
B3, **B4**, **B5**, **B7**, **B17**, **B20**, **B22**, **B24**	1	-3/2	1	-3/2	-2	1/2	-2	1/2	1/2	3	1/2
B10, **B12**, **B13**, **B14**, **B18**, **B19**, **B21**, **B23**	-1	-1	3/2	3/2	2	2	-1/2	-1/2	-1/2	-1/2	-3

Table D.3: $U(1)'$ charges of Class B models.

Class B	Multiplicities												Charges$\times\sqrt{15}$					
Models	M_{13}	M_{14}	M_{15}	M_{34}	M_{35}	M_{45}	M_{31}	M_{41}	M_{51}	M_{43}	M_{53}	M_{54}	Q'_{13}	Q'_{14}	Q'_{15}	Q'_{34}	Q'_{35}	Q'_{45}
B1, **B2**, **B6**, **B8**, **B9**, **B11**, **B15**, **B16**	1	2	2	1	1	1	1	1	1	1	1	1	$-\frac{5}{2}$	$-\frac{5}{2}$	0	0	$\frac{5}{2}$	$\frac{5}{2}$
B3, **B4**, **B5**, **B7**, **B17**, **B20**, **B22**, **B24**	1	2	2	1	1	1	1	1	1	1	1	1	$\frac{5}{2}$	0	$\frac{5}{2}$	$-\frac{5}{2}$	0	$\frac{5}{2}$
B10, **B12**, **B13**, **B14**, **B18**, **B19**, **B21**, **B23**	1	2	2	1	1	1	1	1	1	1	1	1	0	$-\frac{5}{2}$	$-\frac{5}{2}$	$-\frac{5}{2}$	$-\frac{5}{2}$	0

Table D.4: Singlets spectrum of Class B models.

Class C

This class is defined by twelve models, each with specific gauge anomaly cancellation solutions detailed in Table D.5. Additionally, the $U(1)'$ charges of the matter curves for these models are provided in Table D.6. Further information about the singlet spectrum properties can be found in Table D.7.

Class C	Flux data														c_i coefficients		
Model	m_1	m_2	m_3	m_4	M_1	M_2	M_3	M_4	M_5	M_6	M_7	N_7	N_8	N_9	c_1	c_2	c_3
C1	1	0	0	2	0	-1	0	0	0	-1	-1	0	0	1	$-\frac{\sqrt{5}}{3}$	$\frac{5\sqrt{\frac{5}{2}}}{12}$	$\frac{1}{4\sqrt{6}}$
C2	1	0	0	2	0	0	0	0	0	-2	-1	0	0	1	$-\frac{\sqrt{5}}{3}$	$\frac{5\sqrt{\frac{5}{2}}}{12}$	$\frac{1}{4\sqrt{6}}$
C3	1	0	0	2	0	0	0	0	0	-1	-2	0	0	1	$-\frac{\sqrt{5}}{6}$	$\frac{7\sqrt{\frac{5}{2}}}{12}$	$-\frac{1}{4\sqrt{6}}$
C4	1	0	2	0	0	-1	0	0	-1	0	-1	0	1	0	$\frac{\sqrt{5}}{3}$	$-\frac{\sqrt{\frac{5}{2}}}{6}$	$-\frac{\sqrt{\frac{3}{2}}}{2}$
C5	1	0	2	0	0	0	0	-1	-1	0	-1	0	1	0	$\frac{\sqrt{5}}{6}$	$-\frac{\sqrt{\frac{5}{2}}}{12}$	$-\frac{3\sqrt{\frac{3}{2}}}{4}$
C6	1	0	2	0	0	0	0	0	-2	0	-1	0	1	0	$\frac{\sqrt{5}}{3}$	$-\frac{\sqrt{\frac{5}{2}}}{6}$	$-\frac{\sqrt{\frac{3}{2}}}{2}$
C7	1	0	2	0	0	0	0	0	-1	0	-2	0	1	0	$\frac{\sqrt{5}}{6}$	$-\frac{\sqrt{\frac{5}{2}}}{12}$	$-\frac{3\sqrt{\frac{3}{2}}}{4}$
C8	1	0	0	2	0	0	-1	0	0	-1	-1	0	0	1	$-\frac{\sqrt{5}}{6}$	$\frac{7\sqrt{\frac{5}{2}}}{12}$	$-\frac{1}{4\sqrt{6}}$
C9	1	2	0	0	0	0	-1	0	-1	-1	0	1	0	0	0	$\frac{\sqrt{\frac{5}{2}}}{2}$	$-\frac{\sqrt{\frac{3}{2}}}{2}$
C10	1	2	0	0	0	0	0	-1	-1	-1	0	1	0	0	0	$\frac{\sqrt{\frac{5}{2}}}{4}$	$-\frac{3\sqrt{\frac{3}{2}}}{4}$
C11	1	2	0	0	0	0	0	0	-2	-1	0	1	0	0	0	$\frac{\sqrt{\frac{5}{2}}}{2}$	$-\frac{\sqrt{\frac{3}{2}}}{2}$
C12	1	2	0	0	0	0	0	0	-1	-2	0	1	0	0	0	$\frac{\sqrt{\frac{5}{2}}}{4}$	$-\frac{3\sqrt{\frac{3}{2}}}{4}$

Table D.5: Class C models, flux data along with the corresponding c_i-coefficients.

Class C	Charges×$\sqrt{15}$										
Models	Q'_{10_1}	Q'_{10_2}	Q'_{10_3}	Q'_{10_4}	Q'_{5_1}	Q'_{5_2}	Q'_{5_3}	Q'_{5_4}	Q'_{5_5}	Q'_{5_6}	Q'_{5_7}
C1, **C2**	-1/4	9/4	-3/2	-1/4	1/2	-2	7/4	1/2	-3/4	-2	7/4
C3, **C8**	1/4	3/2	-9/4	1/4	-1/2	-7/4	2	-1/2	3/4	-7/4	2
C4, **C6**	1/4	-9/4	1/4	3/2	-1/2	2	-1/2	-7/4	2	3/4	-7/4
C5, **C7**	-1/4	-3/2	-1/4	9/4	1/2	7/4	1/2	-2	7/4	-3/4	-2
C9, **C11**	1/4	1/4	-9/4	3/2	-1/2	-1/2	2	-7/4	2	-7/4	3/4
C10, **C12**	-1/4	-1/4	-3/2	9/4	1/2	1/2	7/4	-2	7/4	-2	-3/4

Table D.6: $U(1)'$ charges of Class C models. The charges are multiplied with $\sqrt{15}$.

Class C	Multiplicities												Charges×$\sqrt{15}$					
Models	M_{13}	M_{14}	M_{15}	M_{34}	M_{35}	M_{45}	M_{31}	M_{41}	M_{51}	M_{43}	M_{53}	M_{54}	Q'_{13}	Q'_{14}	Q'_{15}	Q'_{34}	Q'_{35}	Q'_{45}
C1, **C2**	1	1	1	1	1	1	1	1	1	2	1	1	$-\frac{5}{2}$	$\frac{5}{4}$	0	$\frac{15}{4}$	$\frac{5}{2}$	$-\frac{5}{4}$
C3, **C8**	1	1	1	2	1	1	1	1	1	1	1	1	$-\frac{5}{4}$	$\frac{5}{2}$	0	$\frac{15}{4}$	$\frac{5}{4}$	$-\frac{5}{2}$
C4, **C6**	1	1	1	1	1	1	1	1	1	1	2	1	$\frac{5}{2}$	0	$-\frac{5}{4}$	$-\frac{5}{2}$	$-\frac{15}{4}$	$-\frac{5}{4}$
C5, **C7**	1	1	1	1	2	1	1	1	1	1	1	1	$\frac{5}{4}$	0	$-\frac{5}{2}$	$-\frac{5}{4}$	$-\frac{15}{4}$	$-\frac{5}{2}$
C9, **C11**	1	1	1	1	1	1	1	1	1	1	1	2	0	$\frac{5}{2}$	$-\frac{5}{4}$	$\frac{5}{2}$	$-\frac{5}{4}$	$-\frac{15}{4}$
C10, **C12**	1	1	1	1	1	2	1	1	1	1	1	1	0	$\frac{5}{4}$	$-\frac{5}{2}$	$\frac{5}{4}$	$-\frac{5}{2}$	$-\frac{15}{4}$

Table D.7: Singlets spectrum of Class C models.

Class D

Within this class, twelve distinct models are identified. The flux data, including the corresponding c_i-coefficients solutions, can be found in Table D.8. Table D.9 provides information about the $U(1)'$ charges associated with the matter curves in these models. For details regarding the singlet spectrum, including multiplicities and Q'_{ij} charges, please refer to Table D.10.

Class D	Flux data														c_i coefficients		
Model	m_1	m_2	m_3	m_4	M_1	M_2	M_3	M_4	M_5	M_6	M_7	N_7	N_8	N_9	c_1	c_2	c_3
D1	1	0	1	1	0	0	-1	0	-1	0	-1	0	1	0	$\frac{\sqrt{\frac{5}{6}}}{2}$	$-\frac{\sqrt{\frac{5}{3}}}{8}$	$\frac{7}{8}$
D2	1	0	1	1	0	0	0	-1	0	-1	-1	0	0	1	$\frac{\sqrt{\frac{5}{6}}}{2}$	$\frac{5\sqrt{\frac{5}{3}}}{8}$	$-\frac{3}{8}$
D3	1	0	1	1	0	0	0	0	-1	-1	-1	0	0	1	$-\sqrt{\frac{5}{6}}$	$-\frac{\sqrt{\frac{5}{3}}}{8}$	$\frac{3}{8}$
D4	1	0	1	1	0	0	0	0	-1	-1	-1	0	1	0	$\sqrt{\frac{5}{6}}$	$-\frac{\sqrt{\frac{5}{3}}}{4}$	$\frac{1}{4}$
D5	1	1	0	1	0	-1	0	0	-1	-1	0	1	0	0	0	$-\frac{\sqrt{15}}{8}$	$-\frac{7}{8}$
D6	1	1	0	1	0	0	0	-1	0	-1	-1	0	0	1	$-\sqrt{\frac{5}{6}}$	$-\frac{\sqrt{\frac{5}{3}}}{8}$	$\frac{3}{8}$
D7	1	1	0	1	0	0	0	0	-1	-1	-1	1	0	0	0	$-\frac{\sqrt{15}}{4}$	$-\frac{1}{4}$
D8	1	1	1	0	0	-1	0	0	-1	-1	0	1	0	0	0	$-\frac{\sqrt{15}}{4}$	$-\frac{1}{4}$
D9	1	1	0	1	0	0	0	0	-1	-1	-1	0	0	1	$\frac{\sqrt{\frac{5}{6}}}{2}$	$\frac{5\sqrt{\frac{5}{3}}}{8}$	$-\frac{3}{8}$
D10	1	1	1	0	0	0	-1	0	-1	0	-1	0	1	0	$\sqrt{\frac{5}{6}}$	$-\frac{\sqrt{\frac{5}{3}}}{4}$	$\frac{1}{4}$
D11	1	1	1	0	0	0	0	0	-1	-1	-1	0	1	0	$\frac{\sqrt{\frac{5}{6}}}{2}$	$-\frac{\sqrt{\frac{5}{3}}}{8}$	$\frac{7}{8}$
D12	1	1	1	0	0	0	0	0	-1	-1	-1	1	0	0	0	$-\frac{\sqrt{15}}{8}$	$-\frac{7}{8}$

Table D.8: Class D models flux data.

Class D	Charges$\times\sqrt{10}$										
Models	Q'_{10_1}	Q'_{10_2}	Q'_{10_3}	Q'_{10_4}	Q'_{5_1}	Q'_{5_2}	Q'_{5_3}	Q'_{5_4}	Q'_{5_5}	Q'_{5_6}	Q'_{5_7}
D1, **D11**	3/4	-1/2	3/4	-7/4	-3/2	-1/4	-3/2	1	-1/4	9/4	1
D2, **D9**	3/4	-1/2	-7/4	3/4	-3/2	-1/4	1	-3/2	9/4	-1/4	1
D3, **D6**	-3/4	7/4	1/2	-3/4	3/2	-1	1/4	3/2	-9/4	-1	1/4
D4, **D10**	3/4	-7/4	3/4	-1/2	-3/2	1	-3/2	-1/4	1	9/4	-1/4
D5, **D12**	-3/4	-3/4	1/2	7/4	3/2	3/2	1/4	-1	1/4	-1	-9/4
D7, **D8**	-3/4	-3/4	7/4	1/2	3/2	3/2	-1	1/4	-1	1/4	-9/4

Table D.9: $U(1)'$ charges of Class D models.

Class D	Multiplicities												Charges$\times\sqrt{10}$					
Models	M_{13}	M_{14}	M_{15}	M_{34}	M_{35}	M_{45}	M_{31}	M_{41}	M_{51}	M_{43}	M_{53}	M_{54}	Q'_{13}	Q'_{14}	Q'_{15}	Q'_{34}	Q'_{35}	Q'_{45}
D1, **D11**	1	1	3	4	1	2	2	2	1	1	4	1	$\frac{5}{4}$	0	$\frac{5}{2}$	$-\frac{5}{4}$	$\frac{5}{4}$	$\frac{5}{2}$
D2, **D9**	1	1	1	1	4	1	3	1	2	3	1	4	$\frac{5}{4}$	$-\frac{5}{2}$	0	$\frac{5}{4}$	$-\frac{5}{4}$	$-\frac{5}{2}$
D3, **D6**	3	1	1	3	1	3	1	1	1	1	3	1	$-\frac{5}{2}$	$-\frac{5}{4}$	0	$\frac{5}{4}$	$\frac{5}{2}$	$\frac{5}{4}$
D4, **D10**	3	1	1	1	3	1	1	1	1	3	1	3	$\frac{5}{2}$	0	$\frac{5}{4}$	$-\frac{5}{2}$	$-\frac{5}{4}$	$\frac{5}{4}$
D5, **D12**	1	1	2	1	3	1	1	4	1	3	1	3	0	$-\frac{5}{4}$	$-\frac{5}{2}$	$-\frac{5}{4}$	$-\frac{5}{2}$	$-\frac{5}{4}$
D7, **D8**	1	2	1	2	1	4	3	1	3	1	3	1	0	$-\frac{5}{2}$	$-\frac{5}{4}$	$-\frac{5}{2}$	$-\frac{5}{4}$	$\frac{5}{4}$

Table D.10: Singlets spectrum of Class D models.

The main body of this text already contains a detailed phenomenological analysis of Model D9. Concerning the singlet sector of these models, their superpotential takes the following form:

$$W \supset \mu_{ij}^{\alpha\beta}\theta_{ij}^{\alpha}\theta_{ji}^{\beta} + \lambda_{ijk}^{\alpha\beta\gamma}\theta_{ij}^{\alpha}\theta_{kj}^{\beta}\theta_{ki}^{\gamma}. \tag{D.4}$$

In the above expression, $\mu_{ij}^{\alpha\beta}$ represents the mass parameters, and $\lambda_{ijk}^{\alpha\beta\gamma}$ stands for dimensionless coupling constants. The Greek indices span from 1 to the multiplicity denoted as M_{ij} for the respective singlet. The minimization of the superpotential, achieved by setting $\partial W/\partial\theta_{ij}^{\alpha}$ equal to zero, results in the F-flatness conditions.

D.3 Flavour violation bounds for the various models

In the main text, we extensively examined the low-energy implications of Model D9. A similar comprehensive analysis was conducted for all the MSSM spectrum models discussed previously. Due to the numerous models, we won't delve into the detailed analysis of each one here. Instead, we will focus on the main results concerning flavor violation for the four classes of MSSM models introduced in the preceding sections.

Models within the same class share common $U(1)'$ properties, resulting in quite similar phenomenological analyses. Below, we discuss the fundamental flavor violation constraints for each class of models, with the primary outcomes summarized in Table D.11.

Class A: Class A comprises six models, characterized by very similar $U(1)'$ charges. Specifically, they exhibit only two possible values for the absolute values of Q' charges: 0 and $1/2$. The matter fields stemming from the $SU(5)$ tenplets have zero charge, leading to significantly suppressed flavor violation processes. While the Q' charges exhibit some (semi) non-universality in the lepton sector, the corresponding LFV processes remain notably suppressed when compared to experimental results. In summary, flavor violation processes in Class A models appear highly suppressed, making it challenging to extract meaningful $M_{Z'}$ bounds for this class.

Class B: Out of the twenty-four models in this class, we analyzed eighteen in detail. Specifically, models B4, B5, B8, B13, B15, and B16 exhibited improper mass hierarchies and were subsequently excluded from further analysis. For the remaining viable models, the dominant constraints emanate from the Kaon oscillation system. Approximately, the Z' contribution to the $K^0-\overline{K^0}$ mass difference is estimated as:

$$\Delta M_K^{Z'} \simeq \frac{10^{-13} g'^2}{M_{Z'}^2} \tag{D.5}$$

Comparing this with experimental bounds, for $g' = 0.5$, we obtain the constraint: $M_{Z'} \gtrsim 190$ TeV.

Class C: In this class of models, the flux integers (as presented in Table D.5) lead to identical $U(1)'$ charges for all matter fields stemming from the $SU(5)$ tenplets. Consequently, flavor violation processes such as semi-leptonic meson decays and meson mixing effects are heavily suppressed. However, in the lepton sector, $U(1)'$ charges are non-universal, leading to lepton flavor violation phenomena at low energies. The dominant constraint arises from the three-body decay $\mu^- \to e^- e^- e^+$. Approximately for all Class C models, we find that the Z' contribution to the branching ratio of this decay is:

$$Br(\mu^- \to e^- e^- e^+) \simeq 7.2 \times 10^{-6} \left(\frac{g' \;\; \text{TeV}}{M_{Z'}}\right)^4$$

Comparing this with the current experimental bound implies that $M_{Z'} \gtrsim (51.8 \times g')$ TeV, where g' is the $U(1)'$ gauge coupling. In the absence of any signal in future $\mu^- \to e^- e^- e^+$ searches, this bound is expected to increase by an order of magnitude to $M_{Z'} \gtrsim (518 \times g')$ TeV.

Class D: For models in this class, the dominant constraints stem from the Kaon system. In some cases, strong bounds will also be imposed by future $\mu^- \to e^- e^- e^+$ searches. Specifically, for models D1, D2, D5, D6, D8, and D10, the constraints from Z' contributions to the $K^0 - \overline{K^0}$ mass difference are as follows: $M_{Z'} \gtrsim (475 \times g')$ TeV. For the remaining D-models (D3, D4, D7, D9, D11, D12), the results are similar to those of model D9, which was thoroughly analyzed in the main body of this text.

Models	**Dominant Process**	$(M_{Z'}/g')$ **bound** (TeV)
Class-B (excluded: B4, B5, B8, B13, B15, B16)	$K^0 - \overline{K^0}$ mixing	$M_{Z'}/g' \gtrsim 380$
Class-C	$\mu^- \to e^- e^- e^+$	$M_{Z'}/g' \gtrsim 51.8$
	Future $\mu^- \to e^- e^- e^+$ searches	$M_{Z'}/g' \gtrsim 518$
D1, D2, D5, D6, D8, D10	$K^0 - \overline{K^0}$ mixing	$M_{Z'}/g' \gtrsim 475$
D3, D4, D7, D9, D11, D12	$K^0 - \overline{K^0}$ mixing	$M_{Z'}/g' \gtrsim 238$
	Future $\mu^- \to e^- e^- e^+$ searches	$M_{Z'}/g' \gtrsim 420$

Table D.11: Dominant flavour violation process for each model along with the corresponding bounds on the mass of the flavour mixing Z' boson.

Bibliography

[1] A. Karozas, G. K. Leontaris, I. Tavellaris and N. D. Vlachos, "On the LHC signatures of $SU(5) \times U(1)'$ F-theory motivated models," Eur. Phys. J. C **81** (2021) no.1, 35 doi:10.1140/epjc/s10052-020-08794-y [arXiv:2007.05936 [hep-ph]].

[2] A. Karozas, G. K. Leontaris and I. Tavellaris, "SU(5)×U(1)' Models with a Vector-Like Fermion Family," Universe **7** (2021) no.10, 356 doi:10.3390/universe7100356 [arXiv:2108.10989 [hep-ph]].

[3] A. Karozas, G. K. Leontaris, I. Tavellaris and N. D. Vlachos, "Flavor and Lepton Universality Violation Phenomena in F-Theory Inspired GUTs," doi:10.31526/ACP.BSM-2021.13

[4] W. Ahmed, A. Karozas, G. K. Leontaris and I. Tavellaris, "Hybrid inflation, reheating and dark radiation in a IIB perturbative moduli stabilization scenario," JHEP **07** (2024), 282 doi:10.1007/JHEP07(2024)282 [arXiv:2301.00329 [hep-ph]].

[5] S. Weinberg, "A model of leptons," Phys. Rev. Lett. **19** (1967), 1264-1266 doi:10.1103/PhysRevLett.19.1264

[6] A. Salam, "Weak and Electromagnetic Interactions," Conf. Proc. C **680519** (1968), 367-377 doi:10.1142/9789812795915_0034

[7] D. J. Gross and F. Wilczek, "Ultraviolet behavior of non-abelian gauge theories," Phys. Rev. Lett. **30** (1973), 1343-1346 doi:10.1103/PhysRevLett.30.1343

[8] H. D. Politzer, "Reliable perturbative results for strong interactions?," Phys. Rev. Lett. **30** (1973), 1346-1349 doi:10.1103/PhysRevLett.30.1346

[9] S. L. Glashow, "Partial Symmetries of Weak Interactions," Nucl. Phys. **22** (1961), 579-588 doi:10.1016/0029-5582(61)90469-2

[10] P. W. Higgs, "Broken symmetries, massless particles and gauge fields," Phys. Lett. **12** (1964), 132-133 doi:10.1016/0031-9163(64)91136-9

[11] P. W. Higgs, "Broken Symmetries and the Masses of Gauge Bosons," Phys. Rev. Lett. **13** (1964), 508-509 doi:10.1103/PhysRevLett.13.508

[12] F. Englert and R. Brout, "Broken Symmetry and the Mass of Gauge Vector Mesons," Phys. Rev. Lett. **13** (1964), 321-323 doi:10.1103/PhysRevLett.13.321

[13] G. S. Guralnik, C. R. Hagen and T. W. B. Kibble, "Global Conservation Laws and Massless Particles," Phys. Rev. Lett. **13** (1964), 585-587 doi:10.1103/PhysRevLett.13.585

[14] J. Goldstone, “Field Theories with Superconductor Solutions,” Nuovo Cim. **19** (1961), 154-164 doi:10.1007/BF02812722

[15] J. Goldstone, A. Salam and S. Weinberg, “Broken Symmetries,” Phys. Rev. **127** (1962), 965-970 doi:10.1103/PhysRev.127.965

[16] Y. Nambu, “Quasi-Particles and Gauge Invariance in the Theory of Superconductivity,” Phys. Rev. **117** (1960), 648-663 doi:10.1103/PhysRev.117.648

[17] N. Cabibbo, “Unitary Symmetry and Leptonic Decays,” Phys. Rev. Lett. **10** (1963), 531-533 doi:10.1103/PhysRevLett.10.531

[18] M. Kobayashi and T. Maskawa, “CP Violation in the Renormalizable Theory of Weak Interaction,” Prog. Theor. Phys. **49** (1973), 652-657 doi:10.1143/PTP.49.652

[19] L. Wolfenstein, “Parametrization of the Kobayashi-Maskawa Matrix,” Phys. Rev. Lett. **51** (1983), 1945 doi:10.1103/PhysRevLett.51.1945

[20] Y. Fukuda *et al.* [Super-Kamiokande], “Evidence for oscillation of atmospheric neutrinos,” Phys. Rev. Lett. **81** (1998), 1562-1567 doi:10.1103/PhysRevLett.81.1562 [arXiv:hep-ex/9807003 [hep-ex]].

[21] F. Boehm *et al.* [Palo Verde], “Final results from the Palo Verde neutrino oscillation experiment,” Phys. Rev. D **64** (2001), 112001 doi:10.1103/PhysRevD.64.112001 [arXiv:hep-ex/0107009 [hep-ex]].

[22] A.A. Aguilar-Arevalo *et al.* [LSND], “Evidence for neutrino oscillations from the observation of $\bar{\nu}e$ appearance in a $\bar{\nu}\mu$ beam,” Phys. Rev. D **64** (2001), 112007 doi:10.1103/PhysRevD.64.112007 [arXiv:hep-ex/0104049 [hep-ex]].

[23] M.H. Ahn *et al.* [K2K], “Indications of neutrino oscillation in a 250 km long-baseline experiment,” Phys. Rev. Lett. **90** (2003), 041801 doi:10.1103/PhysRevLett.90.041801 [arXiv:hep-ex/0212007 [hep-ex]].

[24] Y. Ashie *et al.* [Super-Kamiokande], “Evidence for an oscillatory signature in atmospheric neutrino oscillation,” Phys. Rev. Lett. **93** (2004), 101801 doi:10.1103/PhysRevLett.93.101801 [arXiv:hep-ex/0404034 [hep-ex]].

[25] T. Araki *et al.* [KamLAND], “Measurement of neutrino oscillation with KamLAND: Evidence of spectral distortion,” Phys.Rev.Lett., volume=94, pages=081801, year=2005, doi=10.1103/PhysRevLett.94.081801, eprint=hep-ex/0406035

[26] E. Aliu *et al.* [K2K], “Evidence for muon neutrino oscillation in an accelerator-based experiment,” Phys.Rev.Lett., volume=94, pages=081802, year=2005, doi=10.1103/PhysRevLett.94.081802, eprint=hep-ex/0411038

[27] Z. Maki, M. Nakagawa and S. Sakata, “Remarks on the unified model of elementary particles,” Prog. Theor. Phys. **28** (1962), 870-880 doi:10.1143/PTP.28.870 [arXiv:hep-ph/0607084 [hep-ph]].

[28] I. Esteban, M. C. Gonzalez-Garcia, M. Maltoni, T. Schwetz and A. Zhou, JHEP **09** (2020), 178 doi:10.1007/JHEP09(2020)178 [arXiv:2007.14792 [hep-ph]].

[29] Planck Collaboration, “Planck 2018 results. VI. Cosmological parameters,” [arXiv:1807.06209 [astro-ph.CO]].

[30] M. Gell-Mann, P. Ramond and R. Slansky, “Complex Spinors and Unified Theories,” Conf. Proc. C **790927** (1979), 315-321 [arXiv:1306.4669 [hep-th]].

[31] T. Yanagida, “Horizontal gauge symmetry and masses of neutrinos,” Conf. Proc. C **7902131** (1979), 95-99

[32] R.N. Mohapatra and G. Senjanovic, “Neutrino Mass and Spontaneous Parity Nonconservation,” Phys. Rev. Lett. **44** (1980), 912 doi:10.1103/PhysRevLett.44.912

[33] F. Zwicky, “Die Rotverschiebung von extragalaktischen Nebeln,” Helvetica Physica Acta **6**, 110 (1933).

[34] V. C. Rubin and W. K. Ford Jr., “Rotation of the Andromeda Nebula from a Spectroscopic Survey of Emission Regions,” Astrophysical Journal **159**, 379 (1970). doi:10.1086/150317

[35] R. D. Peccei and H. R. Quinn, “CP Conservation in the Presence of Instantons,” Physical Review Letters **38**, 1440 (1977). doi:10.1103/PhysRevLett.38.1440

[36] J. R. Ellis, J. S. Hagelin, D. V. Nanopoulos, K. A. Olive and M. Srednicki, “Supersymmetric Relics from the Big Bang,” Nuclear Physics B **238**, 453 (1984). doi:10.1016/0550-3213(84)90461-9

[37] G. Steigman and M. S. Turner, “Cosmological Constraints on the Properties of Weakly Interacting Massive Particles,” Nuclear Physics B **253**, 375 (1985). doi:10.1016/0550-3213(85)90537-1

[38] R. Massey, T. Kitching and J. Richard, “The dark matter of gravitational lensing,” Rept. Prog. Phys. **73**, 086901 (2010) doi:10.1088/0034-4885/73/8/086901 [arXiv:1001.1739 [astro-ph.CO]].

[39] D. Clowe, A. Gonzalez and M. Markevitch, “Weak lensing mass reconstruction of the interacting cluster 1E0657-558: Direct evidence for the existence of dark matter,” Astrophys. J. **604**, 596 (2004) doi:10.1086/381970 [astro-ph/0312273].

[40] D. Clowe, M. Bradac, A. H. Gonzalez, M. Markevitch, S. W. Randall, C. Jones and D. Zaritsky, “A direct empirical proof of the existence of dark matter,” Astrophys. J. **648**, L109 (2006) doi:10.1086/508162 [astro-ph/0608407].

[41] R. D. Peccei and H. R. Quinn, “Constraints Imposed by CP Conservation in the Presence of Instantons,” Physical Review D **16**, 1791 (1977). doi:10.1103/PhysRevD.16.1791

[42] S. Weinberg, “The Problem of Mass,” Transactions of The New York Academy of Sciences **38**, 185 (1980). doi:10.1111/j.2164-0947.1980.tb02734.x

[43] F. Wilczek, "Problem of Strong p and t Invariance in the Presence of Instantons," Physical Review Letters **40**, 279 (1978). doi:10.1103/PhysRevLett.40.279

[44] S. Weinberg, "Implications of Dynamical Symmetry Breaking," Phys. Rev. D **13**, 974 (1976) [Addendum: Phys.Rev.D **19**, 1277 (1979)]. doi:10.1103/PhysRevD.13.974

[45] L. Susskind, "Dynamics of Spontaneous Symmetry Breaking in the Weinberg-Salam Theory," Phys. Rev. D **20**, 2619 (1979). doi:10.1103/PhysRevD.20.2619

[46] G. 't Hooft, "Naturalness, chiral symmetry, and spontaneous chiral symmetry breaking," NATO Sci. Ser. B **59**, 135 (1980).

[47] H. Georgi and S. L. Glashow, "Mass Matrices for Quarks and Leptons," Phys. Lett. B **86**, 297 (1979). doi:10.1016/0370-2693(79)90895-4

[48] C. D. Froggatt and H. B. Nielsen, "Hierarchy of Quark Masses, Cabibbo Angles and CP Violation," Nucl. Phys. B **147**, 277 (1979). doi:10.1016/0550-3213(79)90316-X

[49] A. D. Sakharov, "Violation of CP Invariance, C asymmetry, and baryon asymmetry of the universe," Pisma Zh. Eksp. Teor. Fiz. **5**, 32 (1967) [JETP Lett. **5**, 24 (1967)] [Sov. Phys. Usp. **34**, no.5, 392 (1991)] [Usp. Fiz. Nauk **161**, no.5, 61 (1991)]. doi:10.1070/PU1991v034n05ABEH002497

[50] R. Foot, H. Lew and R. R. Volkas, "Electric charge quantization," Mod. Phys. Lett. A **8**, 1859 (1993) doi:10.1142/S0217732393001730 [hep-ph/9305275].

[51] J. A. Harvey and M. S. Turner, "Charge quantization is a mystery," Phys. Rev. D **42**, 3344 (1990). doi:10.1103/PhysRevD.42.3344

[52] T. Banks, Y. Nir and N. Seiberg, "Charge quantization from a number operator," Phys. Lett. B **340**, 393 (1994) doi:10.1016/0370-2693(94)01321-2 [hep-th/9408097].

[53] S. Weinberg, "The Cosmological Constant Problem," Rev. Mod. Phys. **61**, 1 (1989). doi:10.1103/RevModPhys.61.1

[54] P. J. E. Peebles and B. Ratra, "The Cosmological constant and dark energy," Rev. Mod. Phys. **75**, 559 (2003) doi:10.1103/RevModPhys.75.559 [astro-ph/0207347].

[55] T. Padmanabhan, "Cosmological constant: The Weight of the vacuum," Phys. Rept. **380**, 235 (2003) doi:10.1016/S0370-1573(03)00120-0 [hep-th/0212290].

[56] Y. A. Golfand and E. P. Likhtman, "Extension of the Algebra of Poincare Group Generators and Violation of p Invariance," JETP Lett. **13**, 323 (1971) [Pisma Zh. Eksp. Teor. Fiz. **13**, 452 (1971)].

[57] J. Wess and B. Zumino, "Supergauge Transformations in Four-Dimensions," Nucl. Phys. B **70**, 39 (1974). doi:10.1016/0550-3213(74)90355-1

[58] S. Ferrara, J. Wess and B. Zumino, "Supergauge Multiplets and Superfields," Phys. Lett. B **51**, 239 (1974). doi:10.1016/0370-2693(74)90281-9

[59] H. Miyazawa, "Baryon Number Changing Currents," Prog. Theor. Phys. **36**, 1266 (1966). doi:10.1143/PTP.36.1266

[60] S. R. Coleman and J. Mandula, "All Possible Symmetries of the S Matrix," Phys. Rev. **159**, 1251 (1967). doi:10.1103/PhysRev.159.1251

[61] A. Neveu and J. H. Schwarz, "Factorizable dual model of pions," Nucl. Phys. B **31**, 86 (1971). doi:10.1016/0550-3213(71)90448-2

[62] P. Ramond, "Dual Theory for Free Fermions," Phys. Rev. D **3**, 2415 (1971). doi:10.1103/PhysRevD.3.2415

[63] J. L. Gervais and B. Sakita, "Field theory interpretation of supergauges in dual models," Nucl. Phys. B **34**, 632 (1971). doi:10.1016/0550-3213(71)90351-8

[64] D. Volkov and V. P. Akulov, "Is the Neutrino a Goldstone Particle?," JETP Lett. **16**, 438 (1972) [Pisma Zh. Eksp. Teor. Fiz.**16**, 621 (1972)].

[65] R. Haag, J. T. Lopuszanski and M. Sohnius, "All Possible Generators of Supersymmetries of the s Matrix," Nucl. Phys.**B88**, 257 (1975). doi:10.1016/0550-3213(75)90279-5

[66] R. N. Mohapatra, Int. J. Mod. Phys. A **30**, no.28n29, 1545001 (2015) doi:10.1142/S0217751X1545001X [arXiv:1506.06788 [hep-ph]].

[67] E. Ma, "R-Parity in Supersymmetric Left-Right Models," Phys. Lett. B **649**, 287 (2007) doi:10.1016/j.physletb.2007.04.019 [arXiv:hep-ph/0701014 [hep-ph]].

[68] R. Barbier et al., "R-parity violating supersymmetry," Phys. Rept. **420**, 1 (2005) doi:10.1016/j.physrep.2005.08.006 [arXiv:hep-ph/0406039 [hep-ph]].

[69] H. K. Dreiner, M. Krämer and J. Tattersall, "R-parity Violation at the LHC," Eur. Phys. J. C **73**, no.9, 2558 (2013) doi:10.1140/epjc/s10052-013-2558-0 [arXiv:1209.5988 [hep-ph]].

[70] C. Csaki, "The Minimal supersymmetric standard model (MSSM)," Mod. Phys. Lett. A **11**, 599 (1996) doi:10.1142/S0217732396000628 [hep-ph/9606414].

[71] P. Fayet and S. Ferrara, "Supersymmetry," Phys. Rept. **32**, 249 (1977). doi:10.1016/0370-1573(77)90066-7

[72] S. P. Martin, "A Supersymmetry primer," Adv. Ser. Direct. High Energy Phys. **21**, 1 (2010) [Adv. Ser. Direct. High Energy Phys. **18**, 1 (1998)] doi:10.1142/97898128396570001, 10.1142/97898143075050001 [arXiv:hep-ph/9709356 [hep-ph]].

[73] A. Djouadi, "The Anatomy of electro-weak symmetry breaking. II. The Higgs bosons in the minimal supersymmetric model," Phys. Rept. **459**, 1 (2008) doi:10.1016/j.physrep.2007.10.005 [arXiv:hep-ph/0503173 [hep-ph]].

[74] P. Fayet, "Supergauge Invariant Extension of the Higgs Mechanism and a Model for the electron and Its Neutrino," Nucl. Phys. B **90**, 104 (1975). doi:10.1016/0550-3213(75)90636-7

[75] S. Dimopoulos and H. Georgi, "Supersymmetry and the Hierarchy Problem," Phys. Lett. B **117**, 287 (1982). doi:10.1016/0370-2693(82)90619-0

[76] E. Witten, "Supersymmetry and Dimensional Transmutation," Nucl. Phys. B **202**, 253 (1982). doi:10.1016/0550-3213(82)90071-2

[77] N. Arkani-Hamed, S. Dimopoulos and G. Dvali, "The Hierarchy problem and new dimensions at a millimeter," Phys. Lett. B **429**, 263 (1998) doi:10.1016/S0370-2693(98)00466-3 [arXiv:hep-ph/9803315 [hep-ph]].

[78] S. Dimopoulos and H. Georgi, "Softly Broken Supersymmetry and SU(5)," Nucl. Phys. B **193**, 150 (1981). doi:10.1016/0550-3213(81)90522-8

[79] H. P. Nilles, "Supersymmetry, Supergravity and Particle Physics," Phys. Rept. **110**, 1 (1984). doi:10.1016/0370-1573(84)90008-5

[80] J. R. Ellis, S. Kelley and D. V. Nanopoulos, "Probing the desert using gauge coupling unification," Phys. Lett. B **260**, 131-137 (1991) doi:10.1016/0370-2693(91)90980-5

[81] P. Langacker and M.-x. Luo, "Implications of precision electroweak experiments for M(t), rho(0), sin**2-Theta(W) and grand unification," Phys. Rev. D **44**, 817-822 (1991) doi:10.1103/PhysRevD.44.817

[82] P. Langacker and N. Polonsky, "Gauge coupling unification in minimal supersymmetric SU(5)," Phys. Rev. D **47**, 4028-4045 (1993) doi:10.1103/PhysRevD.47.4028 [arXiv:hep-ph/9210235]

[83] N. Arkani-Hamed and S. Dimopoulos, "Supersymmetric unification without low energy supersymmetry and signatures for fine-tuning at the LHC," JHEP **06**, 073 (2005) doi:10.1088/1126-6708/2005/06/073 [arXiv:hep-th/0405159]

[84] J. E. Kim and H. P. Nilles, "The Mu Problem and the Strong CP Problem," Phys. Lett. B **138**, 150-154 (1984) doi:10.1016/0370-2693(84)91890-2

[85] G. F. Giudice and A. Masiero, "A Natural Solution to the mu Problem in Supergravity Theories," Phys. Lett. B **206**, 480-484 (1988) doi:10.1016/0370-2693(88)91613-9

[86] J. A. Casas and C. Munoz, "A Natural solution to the mu problem," Phys. Lett. B **306**, 288-294 (1993) doi:10.1016/0370-2693(93)90146-J [arXiv:hep-ph/9302227]

[87] P. Fayet, "Supergauge Invariant Extension of the Higgs Mechanism and a Model for the electron and Its Neutrino," Nucl. Phys. B **90**, 104-124 (1975) doi:10.1016/0550-3213(75)90636-7

[88] H. P. Nilles, M. Srednicki and D. Wyler, "Weak Interaction Breakdown Induced by Supergravity," Phys. Lett. B **120**, 346-348 (1983) doi:10.1016/0370-2693(83)90460-4

[89] J. R. Ellis, J. F. Gunion, H. E. Haber, L. Roszkowski and F. Zwirner, "Higgs Bosons in a Nonminimal Supersymmetric Model," Phys. Rev. D **39**, 844-869 (1989) doi:10.1103/PhysRevD.39.844

[90] C. Panagiotakopoulos and K. Tamvakis, “New minimal extension of MSSM,” Phys. Lett. B **469**, 145-150 (1999) doi:10.1016/S0370-2693(99)01247-2 [arXiv:hep-ph/9908351]

[91] U. Ellwanger, C. Hugonie and A. M. Teixeira, “The Next-to-Minimal Supersymmetric Standard Model,” Phys. Rept. **496**, 1-77 (2010) doi:10.1016/j.physrep.2010.07.001 [arXiv:0910.1785 [hep-ph]]

[92] S. Weinberg, “Supersymmetry at Ordinary Energies. 1. Masses and Conservation Laws,” Phys. Rev. D **26**, 287-302 (1982) doi:10.1103/PhysRevD.26.287

[93] L. J. Hall and M. Suzuki, “Explicit R-Parity Breaking in Supersymmetric Models,” Nucl. Phys. B **231**, 419-463 (1984) doi:10.1016/0550-3213(84)90513-3

[94] S. Dawson, “R-Parity Breaking in Supersymmetric Theories,” Nucl. Phys. B **261**, 297-324 (1985) doi:10.1016/0550-3213(85)90550-9

[95] H. K. Dreiner, “An Introduction to explicit R-parity violation,” Adv. Ser. Direct. High Energy Phys. **21**, 565-583 (2010) doi:10.1142/97898143075050017 [arXiv:hep-ph/9707435]

[96] H. Georgi and S. L. Glashow, “Unity of All Elementary-Particle Forces,” Phys. Rev. Lett. **32**, 438-441 (1974) doi:10.1103/PhysRevLett.32.438

[97] H. Fritzsch and P. Minkowski, “Unified Interactions of Leptons and Hadrons,” Annals Phys. **93**, 193-266 (1975) doi:10.1016/0003-4916(75)90211-0

[98] H. Georgi, “Towards a Grand Unified Theory of Flavor,” Nucl. Phys. B **156**, 126-134 (1979) doi:10.1016/0550-3213(79)90122-6

[99] J. C. Pati and A. Salam, “Lepton Number as the Fourth Color,” Phys. Rev. D **10**, 275-289 (1974) doi:10.1103/PhysRevD.10.275

[100] N. Sakai and T. Yanagida, “Proton Decay in a Class of Supersymmetric Grand Unified Models,” Nucl. Phys. B **197**, 533-542 (1982) doi:10.1016/0550-3213(82)90402-0

[101] J. Hisano, H. Murayama and T. Yanagida, “Nucleon decay in the minimal supersymmetric SU(5) grand unification,” Nucl. Phys. B **402**, 46-84 (1993) doi:10.1016/0550-3213(93)90636-4 [arXiv:hep-ph/9207279]

[102] P. Langacker, “Grand Unified Theories and Proton Decay,” Phys. Rept. **72**, 185-385 (1981) doi:10.1016/0370-1573(81)90059-4

[103] G. Senjanovic, “Proton decay and grand unification,” AIP Conf. Proc. **1200**, 131-140 (2010) doi:10.1063/1.3327552 [arXiv:0912.5375 [hep-ph]]

[104] T. Goto and T. Nihei, “Effect of RRRR dimension five operator on the proton decay in the minimal SU(5) SUGRA GUT model,” Phys. Rev. D **59**, 115009 (1999) doi:10.1103/PhysRevD.59.115009 [arXiv:hep-ph/9808255]

[105] B. Bajc, P. Fileviez Perez and G. Senjanovic, “Minimal supersymmetric SU(5) theory and proton decay: Where do we stand?,” [arXiv:hep-ph/0210374]

[106] A. Zee, "A Theory of Lepton Number Violation, Neutrino Majorana Mass, and Oscillation," Phys. Lett. B **93**, 389-393 (1980) doi:10.1016/0370-2693(80)90349-4 [Erratum: Phys. Lett. B **95**, 461 (1980)]

[107] E. Ma, "Pathways to naturally small neutrino masses," Phys. Rev. Lett. **81**, 1171-1174 (1998) doi:10.1103/PhysRevLett.81.1171 [arXiv:hep-ph/9805219]

[108] M. Paraskevas and K. Tamvakis, "Hierarchical neutrino masses and mixing in non minimal-SU(5)," Phys. Rev. D **84**, 013010 (2011) doi:10.1103/PhysRevD.84.013010 [arXiv:1104.1901 [hep-ph]]

[109] K.S. Babu, J.C. Pati and F. Wilczek, "Renormalizable SO(10) grand unified theory with suppressed dimension-5 proton decays," Prog. Theor. Exp. Phys. **2021**, 043B01 (2021) doi:10.1093/ptep/ptab027 [arXiv:2007.03928 [hep-ph]]

[110] S.F. King, "Phenomenology of SO(10) Grand Unified Theories," PhD thesis, University of Southampton, 1990

[111] T. Fukuyama, "SO(10) GUT in Four and Five Dimensions: A Review," Int. J. Mod. Phys. A **28**, 1330008 (2013) doi:10.1142/S0217751X13300081 [arXiv:1212.3407 [hep-ph]]

[112] S.F. King, "SO(10) Grand Unified Theories," in Grand Unified Theories: Current Status and Future Prospects, edited by S.F. King and C.H. Llewellyn Smith, World Scientific, Singapore, 2019 doi:10.1142/9789811202495-0004

[113] I. de Medeiros Varzielas and G.G. Ross, "SO(10) models with flavour symmetries: classification and examples," Nucl. Phys. B **733**, 31-65 (2006) doi:10.1016/j.nuclphysb.2005.11.001 [hep-ph/0507176]

[114] S.M. Barr, "A New Horizontal Symmetry for Quark and Lepton Masses," Phys. Rev. Lett. **49**, 448-451 (1982) doi:10.1103/PhysRevLett.49.448

[115] I. Antoniadis, J.R. Ellis, J.S. Hagelin and D.V. Nanopoulos, "Flipped SU(5) from Manifold Compactification of the 10D Heterotic String," Phys. Lett. B **194**, 231-235 (1987) doi:10.1016/0370-2693(87)90533-8

[116] I. Antoniadis, J.R. Ellis, J.S. Hagelin and D.V. Nanopoulos, "Flipped SU(5) × U(1) from Four-Dimensional String," Phys. Lett. B **205**, 459-464 (1988) doi:10.1016/0370-2693(88)91659-4

[117] J.P. Derendinger, J.E. Kim and D.V. Nanopoulos, "Anti-SU(5)," Phys. Lett. B **139**, 170-174 (1984) doi:10.1016/0370-2693(84)91238-3

[118] K.S. Babu and R.N. Mohapatra, "Yukawa coupling unification in SO(10) with a unified Higgs sector," Phys. Rev. D **48**, 5354-5361 (1993) doi:10.1103/PhysRevD.48.R5354 [hep-ph/9207249]

[119] L.J. Hall, R. Rattazzi and U. Sarid, "Yukawa coupling unification in supersymmetric SO(10) models," Phys. Rev. D **50**, 7048-7065 (1994) doi:10.1103/PhysRevD.50.7048 [hep-ph/9306309]

[120] B. Ananthanarayan, G. Lazarides and Q. Sha, "Top mass prediction from supersymmetric guts," Phys. Rev. D **44**, 1613-1616 (1991) doi:10.1103/PhysRevD.44.1613

[121] I. Gogoladze, Q. Sha and C.S. Un, “SO(10) Yukawa unification with ¡ 0,” Phys. Lett. B **704**, 201-206 (2011) doi:10.1016/j.physletb.2011.09.006 [arXiv:1107.1228 [hep-ph]]

[122] M. Badziak, M. Olechowski and S. Pokorski, “Yukawa unification in SO(10) with light sparticle spectrum,” JHEP **08**, 147 (2011) doi:10.1007/JHEP08(2011)147 [arXiv:1107.2764 [hep-ph]]

[123] M. Badziak, “Yukawa unification in SUSY SO(10) in light of the LHC Higgs data,” Mod. Phys. Lett. A **27**, 1230020 (2012) doi:10.1142/S0217732312300200 [arXiv:1205.6232 [hep-ph]]

[124] A. Anandakrishnan, B.C. Bryant, S. Raby and A. Wingerter, “LHC Phenomenology of SO(10) Models with Yukawa Unification,” Phys. Rev. D **88**, 075002 (2013) doi:10.1103/PhysRevD.88.075002 [arXiv:1307.7723 [hep-ph]]

[125] Z. Poh and S. Raby, “Yukawa Unification in an SO(10) SUSY GUT: SUSY on the Edge,” Phys. Rev. D **92**, no.1, 015017 (2015) doi:10.1103/PhysRevD.92.015017 [arXiv:1505.00264 [hep-ph]]

[126] H. Freudenthal, “Lie groups in the foundations of geometry,” Adv. Math. **1**, 145-190 (1964) doi:10.1016/0001-8708(64)90011-0

[127] E. Cremmer and B. Julia, “The SO(8) supergravity,” Nucl. Phys. B **159**, 141-212 (1979) doi:10.1016/0550-3213(79)90331-6

[128] F. Gursey and P. Sikivie, “E6 as a flavor group,” Mod. Phys. Lett. A **3**, 697-703 (1988) doi:10.1142/S0217732388000827

[129] Y. Achiman and B. Stech, “Quark Lepton Symmetry and Mass Scales in an E6 Unified Gauge Model,” Phys. Lett. B **77**, 389-392 (1978) doi:10.1016/0370-2693(78)90584-1

[130] Q. Sha, “E(6) as a Unifying Gauge Symmetry,” Phys. Lett. B **79**, 301-304 (1978) doi:10.1016/0370-2693(78)90248-4

[131] S.P. Martin, “Extra vector-like matter and the lightest Higgs scalar boson mass in low-energy supersymmetry,” Phys. Rev. D **81**, 035004 (2010) doi:10.1103/PhysRevD.81.035004 [arXiv:0910.2732 [hep-ph]]

[132] J.L. Hewett and T.G. Rizzo, “Low-Energy Phenomenology of Superstring Inspired E6 Models,” Phys. Rept. **183**, 193-381 (1989) doi:10.1016/0370-1573(89)90071-9

[133] M. Cvetic and P. Langacker, “New Gauge Bosons from String Models,” Mod. Phys. Lett. A **11**, 1247-1262 (1996) doi:10.1142/S0217732396001248 [hep-ph/9511428]

[134] S.F. King and S. Moretti, “Gauge Coupling Unification in the Exceptional Supersymmetric Standard Model,” Phys. Lett. B **634**, 278-284 (2006) doi:10.1016/j.physletb.2006.01.048 [hep-ph/0511256]

[135] P. Langacker, “The Physics of Heavy Z’ Gauge Bosons,” Rev. Mod. Phys. **81**, 1199-1228 (2009) doi:10.1103/RevModPhys.81.1199 [arXiv:0801.1345 [hep-ph]]

[136] C. Vafa, “Evidence for F-theory,” Nucl. Phys. B **469**, 403-418 (1996) doi:10.1016/0550-3213(96)00172-1 [hep-th/9602022]

[137] D.R. Morrison and C. Vafa, "Compactifications of F-theory on Calabi-Yau threefolds. 1," Nucl. Phys. B **473**, 74-92 (1996) doi:10.1016/0550-3213(96)00242-8 [hep-th/9602114]

[138] D.R. Morrison and C. Vafa, "Compactifications of F-theory on Calabi-Yau threefolds. 2.," Nucl. Phys. B **476**, 437-469 (1996) doi:10.1016/0550-3213(96)00369-0 [hep-th/9603161]

[139] C. Beasley, J. J. Heckman and C. Vafa, "GUTs and Exceptional Branes in F-theory - I," JHEP **01**, 058 (2009) doi:10.1088/1126-6708/2009/01/058 [arXiv:0802.3391 [hep-th]].

[140] C. Beasley, J. J. Heckman and C. Vafa, "GUTs and Exceptional Branes in F-theory - II: Experimental Predictions," JHEP **01**, 059 (2009) doi:10.1088/1126-6708/2009/01/059 [arXiv:0806.0102 [hep-th]].

[141] R. Donagi and M. Wijnholt, "Breaking GUT Groups in F-Theory," [arXiv:0808.2223 [hep-th]].

[142] R. Donagi and M. Wijnholt, "Higgs Bundles and UV Completion in F-Theory," Commun. Math. Phys. **326**, 287-327 (2014) doi:10.1007/s00220-013-1864-5 [arXiv:0904.1218 [hep-th]].

[143] F. Denef, "Les Houches Lectures on Constructing String Vacua," [arXiv:0803.1194 [hep-th]].

[144] J. J. Heckman, "Particle Physics Implications of F-theory," Ann. Rev. Nucl. Part. Sci. **60**, 237-265 (2010) doi:10.1146/annurev.nucl.012809.104532 [arXiv:1001.0577 [hep-th]].

[145] T. Weigand, "Lectures on F-theory compactifications and model building," Class. Quant. Grav. **27**, 214004 (2010) doi:10.1088/0264-9381/27/21/214004 [arXiv:1009.3497 [hep-th]].

[146] G. K. Leontaris, "Aspects of F-Theory GUTs," PoS **CORFU2011**, 095 (2011) doi:10.22323/1.155.0095 [arXiv:1203.6277 [hep-th]].

[147] A. Maharana and E. Palti, "Models of Particle Physics from Type IIB String Theory and F-theory: A Review," Int. J. Mod. Phys. A **28**, 1330005 (2013) doi:10.1142/S0217751X13300056 [arXiv:1212.0555 [hep-th]].

[148] G. K. Leontaris, "F-Theory GUTs," PoS **CORFU2014**, 046 (2015) doi:10.22323/1.231.0046

[149] T. Weigand, "F-theory," PoS **TASI2017**, 016 (2018) doi:10.22323/1.305.0016

[150] M. Bershadsky, K. A. Intriligator, S. Kachru, D. R. Morrison, V. Sadov and C. Vafa, "Geometric singularities and enhanced gauge symmetries," Nucl. Phys. B **481**, 215-252 (1996) doi:10.1016/S0550-3213(96)90131-5 [arXiv:hep-th/9605200 [hep-th]].

[151] D. R. Morrison and W. Taylor, "Matter and singularities," JHEP **01**, 022 (2012) doi:10.1007/JHEP01(2012)022 [arXiv:1106.3563 [hep-th]].

[152] R. Blumenhagen, T. W. Grimm, B. Jurke and T. Weigand, "Global F-theory GUTs," Nucl. Phys. B **829**, 325-369 (2010) doi:10.1016/j.nuclphysb.2009.12.013 [arXiv:0908.1784 [hep-th]].

[153] M. Esole and S. T. Yau, "Small resolutions of SU(5)-models in F-theory," [arXiv:1107.0733 [hep-th]].

[154] G. R. Dvali, Q. Shafi and R. K. Schaefer, "Large scale structure and supersymmetric inflation without fine-tuning," Phys. Rev. Lett. **73** (1994) 1886 [hep-ph/9406319].

[155] E. J. Copeland, A. R. Liddle, D. H. Lyth, E. D. Stewart and D. Wands, “False vacuum inflation with Einstein gravity,” Phys. Rev. D **49** (1994) 6410 [astro-ph/9401011].

[156] A. D. Linde and A. Riotto, “Hybrid inflation in supergravity,” Phys. Rev. D **56** (1997) R1841 [hep-ph/9703209].

[157] V. N. Senoguz and Q. Shafi, “Testing supersymmetric grand unified models of inflation,” Phys. Lett. B **567** (2003) 79 [hep-ph/0305089].

[158] V. N. Senoguz and Q. Shafi, “Reheat temperature in supersymmetric hybrid inflation models,” Phys. Rev. D **71** (2005) 043514 [hep-ph/0412102].

[159] M. U. Rehman, Q. Shafi and J. R. Wickman, “Supersymmetric Hybrid Inflation Redux,” Phys. Lett. B **683** (2010) 191 [arXiv:0908.3896 [hep-ph]].

[160] G. K. Leontaris, N. Okada and Q. Shafi, “Non-minimal quartic inflation in supersymmetric $SO(10)$,” Phys. Lett. B **765** (2017) 256 [arXiv:1611.10196 [hep-ph]].

[161] J. Polchinski, “Dirichlet Branes and Ramond-Ramond Charges,” Phys. Rev. Lett. **75**, 4724-4727 (1995) doi:10.1103/PhysRevLett.75.4724 [arXiv:hep-th/9510017 [hep-th]].

[162] E. Bergshoeff, B. Janssen and T. Ortin, “Solution generating transformations and the string effective action,” Class. Quant. Grav. **13**, 321-343 (1996) doi:10.1088/0264-9381/13/3/006 [arXiv:hep-th/9506156 [hep-th]].

[163] S. F. Hassan, “T duality, space-time spinors and R-R fields in curved backgrounds,” Nucl. Phys. B **568**, 145-161 (2000) doi:10.1016/S0550-3213(99)00617-0 [arXiv:hep-th/9907152 [hep-th]].

[164] K. Becker, M. Becker and J. H. Schwarz, “String Theory and M-Theory: A Modern Introduction,” Cambridge University Press (2007).

[165] J. Tate, “Algorithm for determining the type of a singular fiber in an elliptic pencil,” Modular functions of one variable, IV (Proc. Internat. Summer School, Univ. Antwerp, Antwerp, 1972), pp. 33-52. Lecture Notes in Math., Vol. 476, Springer, Berlin, 1975.

[166] R. Donagi and M. Wijnholt, “Model Building with F-Theory,” Adv. Theor. Math. Phys. **15**, 1237-1317 (2011) doi:10.4310/ATMP.2011.v15.n5.a2 [arXiv:0802.2969 [hep-th]].

[167] E. Dudas and E. Palti, “On hypercharge flux and exotics in F-theory GUTs,” JHEP **09**, 013 (2010) doi:10.1007/JHEP09(2010)013 [arXiv:1007.1297 [hep-th]]

[168] G. K. Leontaris, “Aspects of F-Theory GUTs,” PoS **CORFU2011** (2011), 095 doi:10.22323/1.155.0095 [arXiv:1203.6277 [hep-th]].

[169] A. H. Guth, “The Inflationary Universe: A Possible Solution to the Horizon and Flatness Problems,” Phys. Rev. D **23**, 347 (1981) doi:10.1103/PhysRevD.23.347

[170] A. D. Linde, “A New Inflationary Universe Scenario: A Possible Solution of the Horizon, Flatness, Homogeneity, Isotropy and Primordial Monopole Problems,” Phys. Lett. **108B**, 389 (1982) doi:10.1016/0370-2693(82)91219-9

[171] A. D. Linde, "Scalar Field Fluctuations in Expanding Universe and the New Inflationary Universe Scenario," Phys. Lett. **116B**, 335 (1982) doi:10.1016/0370-2693(82)90293-3

[172] A. Albrecht and P. J. Steinhardt, "Cosmology for Grand Unified Theories with Radiatively Induced Symmetry Breaking," Phys. Rev. Lett. **48**, 1220 (1982) doi:10.1103/PhysRevLett.48.1220

[173] V. F. Mukhanov and G. V. Chibisov, "Quantum Fluctuation and Nonsingular Universe," JETP Lett. **33**, 532 (1981) [Pisma Zh. Eksp. Teor. Fiz. **33**, 549 (1981)]

[174] G. V. Chibisov and A. D. Linde, "On the Production of Entropy in the Early Universe," Preprint ITP-78-37P, Institute of Theoretical Physics, Lebedev Physical Institute, Moscow (1978)

[175] A. A. Starobinsky, "A New Type of Isotropic Cosmological Models Without Singularity," Phys. Lett. B **91**, 99 (1980) doi:10.1016/0370-2693(80)90670-X

[176] A. D. Linde, "Chaotic Inflation," Phys. Lett. B **129**, 177 (1983) doi:10.1016/0370-2693(83)90837-7

[177] H. Weyl, "Zur allgemeinen Relativitätstheorie," Phys. Z. **24**, 230 (1923)

[178] A. Friedmann, "Über die Möglichkeit einer Welt mit konstanter negativer Krümmung des Raumes," Z. Phys. **10**, 377 (1922) doi:10.1007/BF01332580

[179] A. G. Riess *et al.* [Supernova Search Team], "Observational evidence from supernovae for an accelerating universe and a cosmological constant," Astron. J. **116**, 1009 (1998) doi:10.1086/300499 [astro-ph/9805201]

[180] S. Perlmutter *et al.* [Supernova Cosmology Project], "Measurements of Omega and Lambda from 42 high redshift supernovae," Astrophys. J. **517**, 565 (1999) doi:10.1086/307221 [astro-ph/9812133]

[181] D. N. Spergel *et al.* [WMAP], "First year Wilkinson Microwave Anisotropy Probe (WMAP) observations: Determination of cosmological parameters," Astrophys. J. Suppl. **148**, 175 (2003) doi:10.1086/377226 [astro-ph/0302209]

[182] A. Albrecht, P. J. Steinhardt, M. S. Turner and F. Wilczek, "Reheating an Inflationary Universe," Phys. Rev. Lett. **48**, 1437-1440 (1982) doi:10.1103/PhysRevLett.48.1437

[183] R. Allahverdi, R. Brandenberger, F. Y. Cyr-Racine and A. Mazumdar, "Reheating in Inflationary Cosmology: Theory and Applications," Annu. Rev. Nucl. Part. Sci. **60**, 27-51 (2010) doi:10.1146/annurev.nucl.012809.104511 [arXiv:1001.2600 [hep-th]].

[184] M. Amin, M. P. Hertzberg, D. I. Kaiser and J. Karouby, "Nonperturbative Dynamics Of Reheating After Inflation: A Review," Int. J. Mod. Phys.**D24**, no.01, 1530003 (2014) doi:10.1142/S0218271815300037 [arXiv:1410.3808 [hep-ph]].

[185] D. V. Volkov and V. A. Soroka, "Higgs effect for Goldstone particles with spin 1/2," JETP Lett. **18**, 312-314 (1973)

[186] D. Z. Freedman, P. van Nieuwenhuizen and S. Ferrara, "Progress Toward a Theory of Supergravity," Phys. Rev. D **13**, 3214-3218 (1976) doi:10.1103/PhysRevD.13.3214

[187] P. Nath and R. L. Arnowitt, "Gauge Symmetry Breaking by Supergravity," Phys. Lett. B **56**, 177-181 (1975) doi:10.1016/0370-2693(75)90353-8

[188] H. Nastase, "Introduction to supergravity," [arXiv:1112.3502 [hep-th]].

[189] D. Z. Freedman and A. Van Proeyen, "Supergravity," Cambridge University Press, Cambridge, UK, (2012) doi:10.1017/CBO9781139026833

[190] J. Wess and J. Bagger, "Supersymmetry and supergravity," Princeton University Press, Princeton, USA, (1992)

[191] G. R. Dvali, G. Lazarides and Q. Shafi, "Mu problem and hybrid inflation in supersymmetric SU(2)-L x SU(2)-R x U(1)-(B-L)," Phys. Lett. B **424** (1998) 259 [hep-ph/9710314].

[192] R. Jeannerot, S. Khalil, G. Lazarides and Q. Shafi, "Inflation and monopoles in supersymmetric SU(4)C x SU(2)(L) x SU(2)(R)," JHEP **0010** (2000) 012 [hep-ph/0002151].

[193] M. U. Rehman, Q. Shafi and J. R. Wickman, "Minimal Supersymmetric Hybrid Inflation, Flipped SU(5) and Proton Decay," Phys. Lett. B **688** (2010) 75 [arXiv:0912.4737 [hep-ph]].

[194] S. Khalil, M. U. Rehman, Q. Shafi and E. A. Zaakouk, "Inflation in Supersymmetric SU(5)," Phys. Rev. D **83** (2011) 063522 [arXiv:1010.3657 [hep-ph]].

[195] M. Arai, S. Kawai and N. Okada, "Higgs inflation in minimal supersymmetric SU(5) GUT," Phys. Rev. D **84** (2011) 123515 [arXiv:1107.4767 [hep-ph]].

[196] C. Pallis and N. Toumbas, "Non-Minimal Higgs Inflation and non-Thermal Leptogenesis in A Supersymmetric Pati-Salam Model," JCAP **1112** (2011) 002 [arXiv:1108.1771 [hep-ph]]; C. Pallis and N. Toumbas, arXiv:1207.3730 [hep-ph].

[197] B. C. Bryant and S. Raby, "Pati-Salam version of subcritical hybrid inflation," Phys. Rev. D **93** (2016) no.9, 095003 [arXiv:1601.03749 [hep-ph]].

[198] J. Ellis, H. J. He and Z. Z. Xianyu, "New Higgs Inflation in a No-Scale Supersymmetric SU(5) GUT," Phys. Rev. D **91** (2015) no.2, 021302 [arXiv:1411.5537 [hep-ph]].

[199] I. Garg and S. Mohanty, "No scale SUGRA SO(10) derived Starobinsky Model of Inflation," Phys. Lett. B **751** (2015) 7 [arXiv:1504.07725 [hep-ph]].

[200] J. Ellis, H. J. He and Z. Z. Xianyu, "Higgs Inflation, Reheating and Gravitino Production in No-Scale Supersymmetric GUTs," JCAP **1608** (2016) no.08, 068 [arXiv:1606.02202 [hep-ph]].

[201] J. Ellis, M. A. G. Garcia, N. Nagata, D. V. Nanopoulos and K. A. Olive, "Starobinsky-Like Inflation and Neutrino Masses in a No-Scale SO(10) Model," JCAP **1611** (2016) no.11, 018 [arXiv:1609.05849 [hep-ph]].

[202] J. Ellis, M. A. G. Garcia, N. Nagata, D. V. Nanopoulos and K. A. Olive, "Starobinsky-like Inflation, Supercosmology and Neutrino Masses in No-Scale Flipped SU(5)," JCAP **1707** (2017) no.07, 006 [arXiv:1704.07331 [hep-ph]].

[203] L. Wu, S. Hu and T. Li, "No-Scale μ-Term Hybrid Inflation," Eur. Phys. J. C **77** (2017) no.3, 168 [arXiv:1605.00735 [hep-ph]].

[204] M. U. Rehman, Q. Shafi and U. Zubair, "Gravity waves and proton decay in a flipped SU(5) hybrid inflation model," Phys. Rev. D **97** (2018) no.12, 123522 [arXiv:1804.02493 [hep-ph]].

[205] W. Ahmed and A. Karozas, "Inflation from a no-scale supersymmetric $SU(4)_c \times SU(2)_L \times SU(2)_R$ model," Phys. Rev. D **98** (2018) no.2, 023538 [arXiv:1804.04822 [hep-ph]].

[206] M. A. Masoud, M. U. Rehman and M. M. A. Abid, "Nonminimal inflation in supersymmetric GUTs with $U(1)_R \times Z_n$ symmetry," Int. J. Mod. Phys. D **28** (2019) no.16, 2040015 doi:10.1142/S0218271820400155 [arXiv:1910.10519 [hep-ph]].

[207] J. Ellis, M. A. G. Garcia, N. Nagata, D. V. Nanopoulos and K. A. Olive, "Symmetry Breaking and Reheating after Inflation in No-Scale Flipped SU(5)," JCAP **1904** (2019) no.04, 009 [arXiv:1812.08184 [hep-ph]].

[208] J. Ellis, M. A. G. Garcia, N. Nagata, N. D. V., K. A. Olive and S. Verner, "Building Models of Inflation in No-Scale Supergravity," [arXiv:2009.01709 [hep-ph]].

[209] M. Fukugita and T. Yanagida, "Baryogenesis Without Grand Unification," Phys. Lett. B **174** (1986) 45.

[210] G. Lazarides and Q. Shafi, "Origin of matter in the inflationary cosmology," Phys. Lett. B **258** (1991) 305.

[211] K. S. Babu and S. M. Barr, "Natural gauge hierarchy in SO(10)," Phys. Rev. D **50** (1994) 3529 [hep-ph/9402291].

[212] K. S. Babu and S. M. Barr, "Natural suppression of Higgsino mediated proton decay in supersymmetric SO(10)," Phys. Rev. D **48** (1993) 5354 [hep-ph/9306242].

[213] K. S. Babu, J. C. Pati and F. Wilczek, "Fermion masses, neutrino oscillations, and proton decay in the light of Super-Kamiokande," Nucl. Phys. B **566** (2000) 33 [hep-ph/9812538].

[214] M. Adeel Ajaib, I. Gogoladze, Q. Shafi and C. S. Un, "A Predictive Yukawa Unified SO(10) Model: Higgs and Sparticle Masses," JHEP **1307** (2013) 139 [arXiv:1303.6964 [hep-ph]].

[215] M. Badziak, "Yukawa unification in SUSY SO(10) in light of the LHC Higgs data," Mod. Phys. Lett. A **27** (2012) 1230020 [arXiv:1205.6232 [hep-ph]].

[216] D. Chang, T. Fukuyama, Y. Y. Keum, T. Kikuchi and N. Okada, "Perturbative SO(10) grand unification," Phys. Rev. D **71** (2005) 095002 [hep-ph/0412011].

[217] I. Esteban, M. C. Gonzalez-Garcia, A. Hernandez-Cabezudo, M. Maltoni and T. Schwetz, "Global analysis of three-flavour neutrino oscillations: synergies and tensions in the determination of θ_{23}, δ_{CP}, and the mass ordering," JHEP **1901** (2019) 106 [arXiv:1811.05487 [hep-ph]].

[218] S. Ferrara, R. Kallosh, A. Linde, A. Marrani and A. Van Proeyen, "Jordan Frame Supergravity and Inflation in NMSSM," Phys. Rev. D **82** (2010) 045003 [arXiv:1004.0712 [hep-th]]; "Superconformal Symmetry, NMSSM, and Inflation," Phys. Rev. D **83** (2011) 025008 [arXiv:1008.2942 [hep-th]].

[219] N. Aghanim *et al.* [Planck Collaboration], "Planck 2018 results. VI. Cosmological parameters," arXiv:1807.06209 [astro-ph.CO].

[220] A. De Simone, M. P. Hertzberg and F. Wilczek, "Running Inflation in the Standard Model," Phys. Lett. B **678** (2009) 1 [arXiv:0812.4946 [hep-ph]].

[221] N. Okada, M. U. Rehman and Q. Shafi, "Tensor to Scalar Ratio in Non-Minimal ϕ^4 Inflation," Phys. Rev. D **82** (2010) 043502 [arXiv:1005.5161 [hep-ph]].

[222] E. W. Kolb and M. S. Turner, "The Early Universe," Front. Phys. **69** (1990) 1.

[223] M. Y. Khlopov and A. D. Linde, "Is It Easy to Save the Gravitino?" Phys. Lett. **138B** (1984) 265.

[224] J. R. Ellis, J. E. Kim and D. V. Nanopoulos, "Cosmological Gravitino Regeneration and Decay," Phys. Lett. **145B** (1984) 181.

[225] M. Kawasaki, K. Kohri, T. Moroi and A. Yotsuyanagi, "Big-Bang Nucleosynthesis and Gravitino," Phys. Rev. D **78** (2008) 065011 [arXiv:0804.3745 [hep-ph]].

[226] V. N. Senoguz and Q. Shafi, Phys. Lett. B **582** (2004) 6 [hep-ph/0309134].

[227] S. Y. Khlebnikov and M. E. Shaposhnikov, Nucl. Phys. B **308** (1988) 885. J. A. Harvey and M. S. Turner, Phys. Rev. D **42** (1990) 3344. doi:10.1103/PhysRevD.42.3344

[228] L. E. Ibanez and F. Quevedo, Phys. Lett. B **283** (1992) 261 [hep-ph/9204205].

[229] D. Buttazzo, G. Degrassi, P. P. Giardino, G. F. Giudice, F. Sala, A. Salvio and A. Strumia, JHEP **1312** (2013) 089 doi:10.1007/JHEP12(2013)089 [arXiv:1307.3536 [hep-ph]].

[230] E. Palti, "The Swampland: Introduction and Review," Fortsch. Phys. **67** (2019) no.6, 1900037 doi:10.1002/prop.201900037 [arXiv:1903.06239 [hep-th]].

[231] N. B. Agmon, A. Bedroya, M. J. Kang and C. Vafa, "Lectures on the string landscape and the Swampland," [arXiv:2212.06187 [hep-th]].

[232] T. Van Riet and G. Zoccarato, "Beginners lectures on flux compactifications and related Swampland topics," [arXiv:2305.01722 [hep-th]].

[233] E. Palti, "The Swampland: Introduction and Review," Fortsch. Phys. **67** (2019) no.6, 1900037 [arXiv:1903.06239 [hep-th]].

[234] N. B. Agmon, A. Bedroya, M. J. Kang and C. Vafa, "Lectures on the string landscape and the Swampland," [arXiv:2212.06187 [hep-th]].

[235] T. Van Riet and G. Zoccarato, "Beginners lectures on flux compactifications and related Swampland topics," [arXiv:2305.01722 [hep-th]].

[236] V. Balasubramanian, P. Berglund, J. P. Conlon and F. Quevedo, "Systematics of moduli stabilization in Calabi-Yau flux compactifications," JHEP **03** (2005), 007 [arXiv:hep-th/0502058 [hep-th]].

[237] M. Berg, M. Haack and E. Pajer, "Jumping Through Loops: On Soft Terms from Large Volume Compactifications," JHEP **09** (2007), 031 [arXiv:0704.0737 [hep-th]].

[238] M. Reece and W. Xue, "SUSY's Ladder: reframing sequestering at Large Volume," JHEP **04** (2016), 045 [arXiv:1512.04941 [hep-ph]].

[239] M. Cicoli, I. Garcìa-Etxebarria, C. Mayrhofer, F. Quevedo, P. Shukla and R. Valandro, "Global Orientifolded Quivers with Inflation," JHEP **11** (2017), 134 [arXiv:1706.06128 [hep-th]].

[240] M. Cicoli, I. G. Etxebarria, F. Quevedo, A. Schachner, P. Shukla and R. Valandro, "The Standard Model quiver in de Sitter string compactifications," JHEP **08** (2021), 109 [arXiv:2106.11964 [hep-th]].

[241] X. Gao, A. Hebecker, S. Schreyer and G. Venken, "The LVS parametric tadpole constraint," JHEP **07** (2022), 056 [arXiv:2202.04087 [hep-th]].

[242] I. Antoniadis, Y. Chen and G. K. Leontaris, "Perturbative moduli stabilization in type IIB/F-theory framework," Eur. Phys. J. C **78** (2018) no.9, 766 [arXiv:1803.08941 [hep-th]].

[243] I. Antoniadis, Y. Chen and G. K. Leontaris, "Logarithmic loop corrections, moduli stabilization and de Sitter vacua in string theory," JHEP **01**, 149 (2020) [arXiv:1909.10525 [hep-th]].

[244] V. Basiouris and G. K. Leontaris, "Note on de Sitter vacua from perturbative and non-perturbative dynamics in type IIB/F-theory compactifications," Phys. Lett. B **810** (2020), 135809 [arXiv:2007.15423 [hep-th]].

[245] V. Basiouris and G. K. Leontaris, "Remarks on the Effects of Quantum Corrections on Moduli Stabilization and de Sitter Vacua in Type IIB String Theory," Fortsch. Phys. **70** (2022) no.2-3, 2100181 [arXiv:2109.08421 [hep-th]].

[246] M. Cicoli, J. P. Conlon, A. Maharana, S. Parameswaran, F. Quevedo and I. Zavala, "String cosmology: From the early universe to today," Phys. Rept. **1059** (2024), 1-155 [arXiv:2303.04819 [hep-th]].

[247] G. K. Leontaris and P. Shukla, "Seeking de Sitter vacua in the string landscape," PoS **CORFU2022** (2023), 058 [arXiv:2303.16689 [hep-th]].

[248] C. P. Burgess, R. Kallosh and F. Quevedo, "De Sitter string vacua from supersymmetric D terms," JHEP **10**, 056 (2003) [arXiv:hep-th/0309187 [hep-th]].

[249] I. Antoniadis, O. Lacombe and G. K. Leontaris, "Hybrid inflation and waterfall field in string theory from D7-branes," JHEP **01** (2022), 011 [arXiv:2109.03243 [hep-th]].

[250] I. Antoniadis, O. Lacombe and G. K. Leontaris, "Type IIB moduli stabilization, inflation, and waterfall fields," Int. J. Mod. Phys. A **37** (2022) no.34, 2244001

[251] A. D. Linde, "Hybrid inflation," Phys. Rev. D **49** (1994), 748-754 [arXiv:astro-ph/9307002].

[252] G. Lazarides and C. Panagiotakopoulos, "Smooth hybrid inflation," Phys. Rev. D **52** (1995), R559-R563 [arXiv:hep-ph/9506325 [hep-ph]].

[253] S. Gukov, C. Vafa and E. Witten, "CFT's from Calabi-Yau four folds," Nucl. Phys. B **584** (2000), 69-108 [arXiv:hep-th/9906070 [hep-th]].

[254] I. Antoniadis, Y. Chen and G. K. Leontaris, "Moduli stabilization and inflation in type IIB/F-theory," PoS **CORFU2018** (2019), 068 [arXiv:1901.05075 [hep-th]].

[255] G. K. Leontaris and P. Shukla, "Stabilising all Kähler moduli in perturbative LVS," JHEP **07** (2022), 047 [arXiv:2203.03362 [hep-th]].

[256] M. Kreuzer and H. Skarke, "Complete classification of reflexive polyhedra in four-dimensions," Adv. Theor. Math. Phys. **4** (2000), 1209-1230 [arXiv:hep-th/0002240 [hep-th]].

[257] R. Altman, J. Gray, Y. H. He, V. Jejjala and B. D. Nelson, "A Calabi-Yau Database: Three-folds Constructed from the Kreuzer-Skarke List," JHEP **02** (2015), 158 [arXiv:1411.1418 [hep-th]].

[258] R. Blumenhagen, J. P. Conlon, S. Krippendorf, S. Moster and F. Quevedo, "SUSY Breaking in Local String/F-Theory Models," JHEP **09** (2009), 007 doi:10.1088/1126-6708/2009/09/007 [arXiv:0906.3297 [hep-th]].

[259] L. Aparicio, D. G. Cerdeno and L. E. Ibanez, "Modulus-dominated SUSY-breaking soft terms in F-theory and their test at LHC," JHEP **07** (2008), 099 doi:10.1088/1126-6708/2008/07/099 [arXiv:0805.2943 [hep-ph]].

[260] D. Lüst, S. Reffert and S. Stieberger, "Flux-induced soft supersymmetry breaking in chiral type IIB orientifolds with D3 / D7-branes," Nucl. Phys. B **706** (2005), 3-52 [arXiv:hep-th/0406092 [hep-th]].

[261] K. Becker, M. Becker, M. Haack and J. Louis, "Supersymmetry breaking and alpha-prime corrections to flux induced potentials," JHEP **06**, 060 (2002) [arXiv:hep-th/0204254 [hep-th]].

[262] A. Hebecker, P. Mangat, F. Rompineve and L. T. Witkowski, "Dark Radiation predictions from general Large Volume Scenarios," JHEP **09** (2014), 140 doi:10.1007/JHEP09(2014)140 [arXiv:1403.6810 [hep-ph]].

[263] J. P. Conlon, D. Cremades and F. Quevedo, "Kahler potentials of chiral matter fields for Calabi-Yau string compactifications," JHEP **01** (2007), 022 [arXiv:hep-th/0609180 [hep-th]].

[264] M. Haack, D. Krefl, D. Lüst, A. Van Proeyen and M. Zagermann, "Gaugino Condensates and D-terms from D7-branes," JHEP **01** (2007), 078 [arXiv:hep-th/0609211 [hep-th]].

[265] S. Kachru, R. Kallosh, A. Linde and S. P. Trivedi, "de Sitter vacua in string theory," Phys. Rev. D **68**, 046005 (2003) [arXiv:hep-th/0301240 [hep-th]].

[266] A. Achucarro, B. de Carlos, J. A. Casas and L. Doplicher, "De Sitter vacua from uplifting D-terms in effective supergravities from realistic strings," JHEP **06** (2006), 014 [arXiv:hep-th/0601190 [hep-th]].

[267] I. Antoniadis, O. Lacombe and G. K. Leontaris, "Inflation near a metastable de Sitter vacuum from moduli stabilization," Eur. Phys. J. C **80**, no.11, 1014 (2020) [arXiv:2007.10362 [hep-th]].

[268] A. Brignole, L. E. Ibanez and C. Munoz, "Towards a theory of soft terms for the supersymmetric Standard Model," Nucl. Phys. B **422**, 125-171 (1994) [erratum: Nucl. Phys. B **436**, 747-748 (1995)] [arXiv:hep-ph/9308271 [hep-ph]].

[269] J. P. Conlon, S. S. Abdussalam, F. Quevedo and K. Suruliz, "Soft SUSY Breaking Terms for Chiral Matter in IIB String Compactifications," JHEP **01**, 032 (2007) [arXiv:hep-th/0610129 [hep-th]].

[270] M. Demirtas, M. Kim, L. McAllister and J. Moritz, "Conifold Vacua with Small Flux Superpotential," Fortsch. Phys. **68** (2020), 2000085 [arXiv:2009.03312 [hep-th]].

[271] S.R. Coleman and E.J. Weinberg, "Radiative Corrections as the Origin of Spontaneous Symmetry Breaking," Phys. Rev. D **7**, 1888 (1973) [arXiv:hep-ph/].

[272] I. Antoniadis, Y. Chen and G. K. Leontaris, Int. J. Mod. Phys. A **34** (2019) no.08, 1950042 doi:10.1142/S0217751X19500428 [arXiv:1810.05060 [hep-th]].

[273] Y. Akrami *et al.* [Planck], "Planck 2018 results. X. Constraints on inflation," Astron. Astrophys. **641** (2020), A10 [arXiv:1807.06211 [astro-ph.CO]].

[274] M. Cicoli, K. Sinha and R. Wiley Deal, "The dark universe after reheating in string inflation," JHEP **12** (2022), 068 [arXiv:2208.01017 [hep-th]].

[275] M. Cicoli, C. P. Burgess and F. Quevedo, "Anisotropic Modulus Stabilisation: Strings at LHC Scales with Micron-sized Extra Dimensions," JHEP **10**, 119 (2011) [arXiv:1105.2107 [hep-th]].

[276] G. F. Giudice and A. Masiero, "A Natural Solution to the mu Problem in Supergravity Theories," Phys. Lett. B **206** (1988), 480-484

[277] S. Angus, J. P. Conlon, U. Haisch and A. J. Powell, "Loop corrections to ΔN_{eff} in large volume models," JHEP **12** (2013), 061 [arXiv:1305.4128 [hep-ph]].

[278] S. Böser, C. Buck, C. Giunti, J. Lesgourgues, L. Ludhova, S. Mertens, A. Schukraft and M. Wurm, Status of Light Sterile Neutrino Searches, *Prog. Part. Nucl. Phys.* **111** (2020), 103736

[279] A. Boyarsky, M. Drewes, T. Lasserre, S. Mertens and O. Ruchayskiy, "Sterile Neutrino Dark Matter," Prog. Part. Nucl. Phys. **104** (2019) 1 [arXiv:1807.07938 [hep-ph]].

[280] C. Beasley, J. J. Heckman and C. Vafa, "GUTs and Exceptional Branes in F-theory - II: Experimental Predictions," JHEP **0901** (2009) 059 [arXiv:0806.0102 [hep-th]].

[281] D. R. Morrison and D. S. Park, JHEP **10** (2012), 128 [arXiv:1208.2695 [hep-th]].

[282] M. Del Zotto, J. J. Heckman, D. R. Morrison and D. S. Park, JHEP **06** (2015), 158 [arXiv:1412.6526 [hep-th]].

[283] D. R. Morrison, D. S. Park and W. Taylor, Adv. Theor. Math. Phys. **22** (2018), 177-245 [arXiv:1610.06929 [hep-th]].

[284] F. Baume, M. Cvetic, C. Lawrie and L. Lin, JHEP **03** (2018), 069 [arXiv:1709.07453 [hep-th]].

[285] N. Raghuram, JHEP **05** (2018), 050 [arXiv:1711.03210 [hep-th]].

[286] Y. Kimura, JHEP **03** (2020), 153 [arXiv:1908.06621 [hep-th]].

[287] M. Crispim Romão, S. F. King and G. K. Leontaris, "Non-universal Z' from fluxed GUTs," Phys. Lett. B **782** (2018) 353 [arXiv:1710.02349].

[288] J. Ellis, M. Fairbairn and P. Tunney, Eur. Phys. J. C **78** (2018) no.3, 238 [arXiv:1705.03447 [hep-ph]].

[289] B. C. Allanach, J. Davighi and S. Melville, JHEP **1902** (2019) 082 Erratum: [JHEP **1908** (2019) 064] [arXiv:1812.04602 [hep-ph]].

[290] R. Aaij *et al.* [LHCb Collaboration], "Test of lepton universality using $B^+ \to K^+\ell^+\ell^-$ decays," Phys. Rev. Lett. **113** (2014) 151601 [arXiv:1406.6482 [hep-ex]].

[291] R. Aaij *et al.* [LHCb Collaboration], "Test of lepton universality with $B^0 \to K^{*0}\ell^+\ell^-$ decays," JHEP **1708** (2017) 055 [arXiv:1705.05802 [hep-ex]].

[292] R. Aaij *et al.* [LHCb Collaboration], Phys. Rev. Lett. **122** (2019) no.19, 191801 [arXiv:1903.09252 [hep-ex]].

[293] P. Langacker and M. Plumacher, "Flavor changing effects in theories with a heavy Z' boson with family non-universal couplings," Phys. Rev. D **62** (2000) 013006 [hep-ph/0001204].

[294] J. P. Lees *et al.* [BaBar Collaboration], Phys. Rev. D **93** (2016) no.5, 052015 [arXiv:1508.07960 [hep-ex]].

[295] R. Aaij *et al.* [LHCb Collaboration], JHEP **1602** (2016) 104 doi:10.1007/JHEP02(2016)104 [arXiv:1512.04442 [hep-ex]].

[296] V. Khachatryan *et al.* [CMS Collaboration], Phys. Lett. B **753** (2016) 424 doi:10.1016/j.physletb.2015.12.020 [arXiv:1507.08126 [hep-ex]].

[297] W. Altmannshofer and D. M. Straub, "New Physics in $B \to K^*\mu\mu$?," Eur. Phys. J. C **73** (2013) 2646 [arXiv:1308.1501 [hep-ph]].

[298] J. Aebischer, W. Altmannshofer, D. Guadagnoli, M. Reboud, P. Stangl and D. M. Straub, "B-decay discrepancies after Moriond 2019," arXiv:1903.10434 [hep-ph].

[299] A. K. Alok, A. Dighe, S. Gangal and D. Kumar, "Continuing search for new physics in $b \to s\mu\mu$ decays: two operators at a time," JHEP **1906** (2019) 089 doi:10.1007/JHEP06(2019)089 [arXiv:1903.09617 [hep-ph]].

[300] M. Algueró, B. Capdevila, A. Crivellin, S. Descotes-Genon, P. Masjuan, J. Matias and J. Virto, "Emerging patterns of New Physics with and without Lepton Flavour Universal contributions," Eur. Phys. J. C **79** (2019) no.8, 714 doi:10.1140/epjc/s10052-019-7216-3 [arXiv:1903.09578 [hep-ph]].

[301] K. Kowalska, D. Kumar and E. M. Sessolo, "Implications for new physics in $b \to s\mu\mu$ transitions after recent measurements by Belle and LHCb," Eur. Phys. J. C **79** (2019) no.10, 840 doi:10.1140/epjc/s10052-019-7330-2 [arXiv:1903.10932 [hep-ph]].

[302] A. Arbey, T. Hurth, F. Mahmoudi, D. M. Santos and S. Neshatpour, Phys. Rev. D **100** (2019) no.1, 015045 doi:10.1103/PhysRevD.100.015045 [arXiv:1904.08399 [hep-ph]].

[303] L. Di Luzio, M. Kirk and A. Lenz, Phys. Rev. D **97** (2018) no.9, 095035 doi:10.1103/PhysRevD.97.095035 [arXiv:1712.06572 [hep-ph]].

[304] A. J. Buras, M. Misiak and J. Urban, Nucl. Phys. B **586** (2000) 397 doi:10.1016/S0550-3213(00)00437-5 [hep-ph/0005183].

[305] D. King, A. Lenz and T. Rauh, JHEP **1905** (2019) 034 doi:10.1007/JHEP05(2019)034 [arXiv:1904.00940 [hep-ph]].

[306] M. Tanabashi *et al.* [Particle Data Group], "Review of Particle Physics," Phys. Rev. D **98** (2018) no.3, 030001. doi:10.1103/PhysRevD.98.030001

[307] A. J. Buras, J. M. Gérard and W. A. Bardeen, Eur. Phys. J. C **74** (2014) 2871 doi:10.1140/epjc/s10052-014-2871-x [arXiv:1401.1385 [hep-ph]].

[308] C. H. Chen and T. Nomura, JHEP **1903** (2019) 009 doi:10.1007/JHEP03(2019)009 [arXiv:1808.04097 [hep-ph]].

[309] Y. Amhis *et al.* [HFLAV Collaboration], Eur. Phys. J. C **77** (2017) no.12, 895 doi:10.1140/epjc/s10052-017-5058-4 [arXiv:1612.07233 [hep-ex]].

[310] S. Glashow, J. Iliopoulos and L. Maiani, "Weak Interactions with Lepton-Hadron Symmetry," Phys. Rev. D **2** (1970), 1285-1292 doi:10.1103/PhysRevD.2.1285

[311] F. Jegerlehner and A. Nyffeler, "The Muon g-2," Phys. Rept. **477** (2009) 1 doi:10.1016/j.physrep.2009.04.003 [arXiv:0902.3360 [hep-ph]].

[312] L. Lavoura, Eur. Phys. J. C **29** (2003) 191 doi:10.1140/epjc/s2003-01212-7 [hep-ph/0302221].

[313] Y. Okada, K. i. Okumura and Y. Shimizu, Phys. Rev. D **61** (2000) 094001 doi:10.1103/PhysRevD.61.094001 [hep-ph/9906446].

[314] U. Bellgardt *et al.* [SINDRUM], Nucl. Phys. B **299** (1988), 1-6 doi:10.1016/0550-3213(88)90462-2

[315] S. Cecotti, C. Cordova, J. J. Heckman and C. Vafa, "T-Branes and Monodromy," JHEP **1107** (2011) 030 doi:10.1007/JHEP07(2011)030 [arXiv:1010.5780 [hep-th]].

[316] J. Marsano, Phys. Rev. Lett. **106** (2011) 081601 doi:10.1103/PhysRevLett.106.081601 [arXiv:1011.2212 [hep-th]].

[317] E. Palti, Phys. Rev. D **87** (2013) no.8, 085036 doi:10.1103/PhysRevD.87.085036 [arXiv:1209.4421 [hep-th]].

[318] S. Cecotti, M. C. N. Cheng, J. J. Heckman and C. Vafa, arXiv:0910.0477 [hep-th].

[319] L. Aparicio, A. Font, L. E. Ibanez and F. Marchesano, JHEP **1108** (2011) 152 doi:10.1007/JHEP08(2011)152 [arXiv:1104.2609 [hep-th]].

[320] F. Marchesano, D. Regalado and G. Zoccarato, JHEP **1504** (2015) 179 doi:10.1007/JHEP04(2015)179 [arXiv:1503.02683 [hep-th]].

[321] I. Antoniadis and G. K. Leontaris, "Neutrino mass textures from F-theory," Eur. Phys. J. C **73** (2013) 2670 doi:10.1140/epjc/s10052-013-2670-9 [arXiv:1308.1581 [hep-th]].

[322] G. Ross and M. Serna, "Unification and fermion mass structure," Phys. Lett. B **664** (2008) 97 doi:10.1016/j.physletb.2008.05.014 [arXiv:0704.1248 [hep-ph]].

[323] I. Antoniadis and G. K. Leontaris, "Building SO(10) models from F-theory," JHEP **1208** (2012) 001 [arXiv:1205.6930 [hep-th]].

[324] A. Karozas, S. F. King, G. K. Leontaris and A. K. Meadowcroft, "Phenomenological implications of a minimal F-theory GUT with discrete symmetry," JHEP **1510** (2015) 041 doi:10.1007/JHEP10(2015)041 [arXiv:1505.00937 [hep-ph]].

[325] J. C. Callaghan and S. F. King, "E6 Models from F-theory," JHEP **1304** (2013) 034 doi:10.1007/JHEP04(2013)034 [arXiv:1210.6913 [hep-ph]].

[326] M. Crispim Romão, A. Karozas, S. F. King, G. K. Leontaris and A. K. Meadowcroft, "MSSM from F-theory SU(5) with Klein Monodromy," Phys. Rev. D **93** (2016) no.12, 126007 doi:10.1103/PhysRevD.93.126007 [arXiv:1512.09148 [hep-ph]].

[327] M. Crispim Romão, A. Karozas, S. F. King, G. K. Leontaris and A. K. Meadowcroft, JHEP **1611** (2016) 081 doi:10.1007/JHEP11(2016)081 [arXiv:1608.04746 [hep-ph]].

[328] A. de Gouvea, S. Lola and K. Tobe, "Lepton flavor violation in supersymmetric models with trilinear R-parity violation," Phys. Rev. D **63** (2001) 035004 doi:10.1103/PhysRevD.63.035004 [hep-ph/0008085].

[329] F. Domingo, H. K. Dreiner, J. S. Kim, M. E. Krauss, M. Lozano and Z. S. Wang, "Updating Bounds on R-Parity Violating Supersymmetry from Meson Oscillation Data," JHEP **1902** (2019) 066 doi:10.1007/JHEP02(2019)066 [arXiv:1810.08228 [hep-ph]].

[330] K. Earl and T. Gregoire, "Contributions to $b \to s\ell\ell$ Anomalies from R-Parity Violating Interactions," JHEP **1808** (2018) 201 doi:10.1007/JHEP08(2018)201 [arXiv:1806.01343 [hep-ph]].

[331] Q. Y. Hu, Y. D. Yang and M. D. Zheng, "Revisiting the B-physics anomalies in R-parity violating MSSM," Eur. Phys. J. C **80** (2020) no.5, 365 doi:10.1140/epjc/s10052-020-7940-8 [arXiv:2002.09875 [hep-ph]].

[332] W. Altmannshofer, P. S. B. Dev, A. Soni and Y. Sui, "Addressing $R_{D^{(*)}}$, $R_{K^{(*)}}$, muon $g-2$ and ANITA anomalies in a minimal R-parity violating supersymmetric framework," arXiv:2002.12910 [hep-ph].

[333] M. D. Zheng and H. H. Zhang, Phys. Rev. D **104** (2021) no.11, 115023 doi:10.1103/PhysRevD.104.115023 [arXiv:2105.06954 [hep-ph]].

[334] M. Aaboud *et al.* [ATLAS Collaboration], Phys. Rev. D **99** (2019) no.9, 092004 doi:10.1103/PhysRevD.99.092004 [arXiv:1902.10077 [hep-ex]].

[335] G. Aad *et al.* [ATLAS Collaboration], Phys. Lett. B **796** (2019) 68 doi:10.1016/j.physletb.2019.07.016 [arXiv:1903.06248 [hep-ex]].

[336] CMS Collaboration [CMS Collaboration], CMS-PAS-EXO-19-019.

[337] S. Aoki *et al.* [Flavour Lattice Averaging Group], Eur. Phys. J. C **80** (2020) no.2, 113 doi:10.1140/epjc/s10052-019-7354-7 [arXiv:1902.08191 [hep-lat]].

[338] F. Renga, "Experimental searches for muon decays beyond the Standard Model," Rev. Phys. **4** (2019), 100029 doi:10.1016/j.revip.2019.100029 [arXiv:1902.06291 [hep-ex]].

[339] A. Blondel, A. Bravar, M. Pohl, S. Bachmann, N. Berger, M. Kiehn, A. Schoning, D. Wiedner, B. Windelband, P. Eckert, H. Schultz-Coulon, W. Shen, P. Fischer, I. Peric, M. Hildebrandt, P. Kettle, A. Papa, S. Ritt, A. Stoykov, G. Dissertori, C. Grab, R. Wallny, R. Gredig, P. Robmann and U. Straumann, "Research Proposal for an Experiment to Search for the Decay $\mu \to eee$," [arXiv:1301.6113 [physics.ins-det]].

[340] B. Allanach, F. S. Queiroz, A. Strumia and S. Sun, "Z' models for the LHCb and $g-2$ muon anomalies," Phys. Rev. D **93** (2016) no.5, 055045 doi:10.1103/PhysRevD.93.055045 [arXiv:1511.07447 [hep-ph]].

[341] S. F. King, "Flavourful Z$'$ models for $R_{K^{(*)}}$," JHEP **08** (2017), 019 doi:10.1007/JHEP08(2017)019 [arXiv:1706.06100 [hep-ph]].

[342] S. Antusch, C. Hohl, S. F. King and V. Susic, "Non-universal Z' from SO(10) GUTs with vector-like family and the origin of neutrino masses," Nucl. Phys. B **934** (2018), 578-605 doi:10.1016/j.nuclphysb.2018.07.022 [arXiv:1712.05366 [hep-ph]].

[343] A. Falkowski, S. F. King, E. Perdomo and M. Pierre, "Flavourful Z' portal for vector-like neutrino Dark Matter and $R_{K^{(*)}}$," JHEP **08** (2018), 061 doi:10.1007/JHEP08(2018)061 [arXiv:1803.04430 [hep-ph]].

[344] S. F. King, "$R_{K^{(*)}}$ and the origin of Yukawa couplings," JHEP **09** (2018), 069 doi:10.1007/JHEP09(2018)069 [arXiv:1806.06780 [hep-ph]].

[345] C. Hernández, A.E., S. King, H. Lee and S. Rowley, "Is it possible to explain the muon and electron $g-2$ in a Z' model?," Phys. Rev. D **101** (2020) no.11, 11 [arXiv:1910.10734 [hep-ph]].

[346] S. Raby and A. Trautner, "Vectorlike chiral fourth family to explain muon anomalies," Phys. Rev. D **97** (2018) no.9, 095006 [arXiv:1712.09360 [hep-ph]].

[347] J. Kawamura, S. Raby and A. Trautner, "Complete vectorlike fourth family and new U(1)' for muon anomalies," Phys. Rev. D **100** (2019) no.5, 055030 [arXiv:1906.11297 [hep-ph]].

[348] J. Kawamura, S. Raby and A. Trautner, "Complete vectorlike fourth family with U(1)' : A global analysis," Phys. Rev. D **101** (2020) no.3, 035026 [arXiv:1911.11075 [hep-ph]].

[349] R. Aaij *et al.* [LHCb], [arXiv:2103.11769 [hep-ex]].

[350] G. D'Amico, M. Nardecchia, P. Panci, F. Sannino, A. Strumia, R. Torre and A. Urbano, "Flavour anomalies after the R_{K^*} measurement," JHEP **09** (2017), 010 [arXiv:1704.05438 [hep-ph]].

[351] S. Bifani, S. Descotes-Genon, A. Romero Vidal and M. H. Schune, "Review of Lepton Universality tests in B decays," J. Phys. G **46** (2019) no.2, 023001 [arXiv:1809.06229 [hep-ex]].

[352] A. Cerri, V. V. Gligorov, S. Malvezzi, J. Martin Camalich, J. Zupan, S. Akar, J. Alimena, B. C. Allanach, W. Altmannshofer and L. Anderlini, *et al.* "Report from Working Group 4: Opportunities in Flavour Physics at the HL-LHC and HE-LHC," CERN Yellow Rep. Monogr. **7** (2019), 867-1158 [arXiv:1812.07638 [hep-ph]].

[353] A. Crivellin, G. D'Ambrosio and J. Heeck, "Explaining $h \to \mu^\pm\tau^\mp$, $B \to K^*\mu^+\mu^-$ and $B \to K\mu^+\mu^-/B \to Ke^+e^-$ in a two-Higgs-doublet model with gauged $L_\mu - L_\tau$," Phys. Rev. Lett. **114** (2015), 151801 [arXiv:1501.00993 [hep-ph]].; A. Crivellin, C. A. Manzari, M. Alguero and J. Matias, Phys. Rev. Lett. **127** (2021) no.1, 011801 [arXiv:2010.14504 [hep-ph]].

[354] A. Crivellin, C. A. Manzari, M. Alguero and J. Matias, "Combined Explanation of the Z→bb$^-$ Forward-Backward Asymmetry, the Cabibbo Angle Anomaly, and $\tau\to\mu\nu\nu$ and b→sℓ+ℓ- Data," Phys. Rev. Lett. **127** (2021) no.1, 011801 doi:10.1103/PhysRevLett.127.011801 [arXiv:2010.14504 [hep-ph]].

[355] A. Karozas, G. K. Leontaris, I. Tavellaris and N. D. Vlachos, "On the LHC signatures of $SU(5) \times U(1)'$ F-theory motivated models," Eur. Phys. J. C **81** (2021) no.1, 35 [arXiv:2007.05936 [hep-ph]].

[356] P. A. Zyla *et al.* [Particle Data Group], "Review of Particle Physics," PTEP **2020** (2020) no.8, 083C01

[357] P. Arnan, A. Crivellin, M. Fedele and F. Mescia, "Generic Loop Effects of New Scalars and Fermions in $b \to s\ell^+\ell^-$, $(g-2)_\mu$ and a Vector-like 4$^{\text{th}}$ Generation," JHEP **06** (2019), 118 [arXiv:1904.05890 [hep-ph]].

[358] F. F. Freitas, J. Gonçalves, A. P. Morais and R. Pasechnik, "Phenomenology of vector-like leptons with Deep Learning at the Large Hadron Collider," JHEP **01** (2021), 076 [arXiv:2010.01307 [hep-ph]].

[359] S. F. King, G. K. Leontaris and G. G. Ross, "Family symmetries in F-theory GUTs," Nucl. Phys. B **838** (2010), 119-135 [arXiv:1005.1025 [hep-ph]].

[360] G. K. Leontaris and G. G. Ross, "Yukawa couplings and fermion mass structure in F-theory GUTs," JHEP **02** (2011), 108 [arXiv:1009.6000 [hep-th]].

[361] A. Carvunis, F. Dettori, S. Gangal, D. Guadagnoli and C. Normand, "On the effective lifetime of B$_s$→ $\mu\mu\gamma$," JHEP **12** (2021), 078 doi:10.1007/JHEP12(2021)078 [arXiv:2102.13390 [hep-ph]].

[362] M. Algueró, B. Capdevila, S. Descotes-Genon, J. Matias and M. Novoa-Brunet, "$\boldsymbol{b \to s\ell\ell}$ global fits after Moriond 2021 results," [arXiv:2104.08921 [hep-ph]].

[363] S. Dwivedi, D. Kumar Ghosh, A. Falkowski and N. Ghosh, "Associated Z' production in the flavorful $U(1)$ scenario for $R_{K^{(*)}}$," Eur. Phys. J. C **80** (2020) no.3, 263 [arXiv:1908.03031 [hep-ph]].

[364] W. Huang and Y. L. Tang, "Flavor anomalies at the LHC and the R-parity violating supersymmetric model extended with vectorlike particles," Phys. Rev. D **92** (2015) no.9, 094015 [arXiv:1509.08599 [hep-ph]].

[365] S. Trifinopoulos, "Revisiting R-parity violating interactions as an explanation of the B-physics anomalies," Eur. Phys. J. C **78** (2018) no.10, 803 [arXiv:1807.01638 [hep-ph]].

[366] D. Bardhan, D. Ghosh and D. Sachdeva, "$R_{K^{(*)}}$ from RPV-SUSY sneutrinos," [arXiv:2107.10163 [hep-ph]].

[367] H. Hayashi, T. Kawano, Y. Tsuchiya and T. Watari, "Flavor Structure in F-theory Compactifications," JHEP **08** (2010), 036 [arXiv:0910.2762 [hep-th]].

[368] C. M. Chen, J. Knapp, M. Kreuzer and C. Mayrhofer, "Global SO(10) F-theory GUTs," JHEP **10** (2010), 057 [arXiv:1005.5735 [hep-th]].